



HAL
open science

Acoustic-gravity waves in free-surface flows: modeling, analysis and simulation towards tsunami early-warning systems

Juliette Dubois

► **To cite this version:**

Juliette Dubois. Acoustic-gravity waves in free-surface flows: modeling, analysis and simulation towards tsunami early-warning systems. Modeling and Simulation. Sorbonne Université, 2023. English. NNT: 2023SORUS561 . tel-04531035

HAL Id: tel-04531035

<https://theses.hal.science/tel-04531035>

Submitted on 3 Apr 2024

HAL is a multi-disciplinary open access archive for the deposit and dissemination of scientific research documents, whether they are published or not. The documents may come from teaching and research institutions in France or abroad, or from public or private research centers.

L'archive ouverte pluridisciplinaire **HAL**, est destinée au dépôt et à la diffusion de documents scientifiques de niveau recherche, publiés ou non, émanant des établissements d'enseignement et de recherche français ou étrangers, des laboratoires publics ou privés.



Sorbonne Université

Ecole doctorale **École Doctorale Sciences Mathématiques de Paris Centre**

Unité de recherche **Laboratoire Jacques-Louis Lions, Inria Paris équipe ANGE**

Thèse présentée par **Juliette Dubois**

Soutenue le 21 décembre 2023

En vue de l'obtention du grade de docteur de Sorbonne Université

Discipline **Mathématiques appliquées**

Vagues et ondes hydro-acoustiques pour l'alerte précoce de tsunami : modélisation, analyse et simulation

Thèse dirigée par Jacques SAINTE-MARIE
Sébastien IMPERIALE

Composition du jury

<i>Rapporteurs</i>	Eric BLAYO Frédéric DIAS	Université Grenoble Alpes University College Dublin	
<i>Examineurs</i>	Anne-Sophie BONNET BEN DHIA Anne-Laure DALIBARD Aline LEFEBVRE-LEPOT Agnès MAUREL	CNRS, ENSTA Sorbonne Université CNRS, CentraleSupélec Institut Langevin	Présidente du jury



Sorbonne Université

Doctoral school **École Doctorale Sciences Mathématiques de Paris Centre**

Research unit **Laboratoire Jacques-Louis Lions, Inria Paris ANGE team**

Thesis presented by **Juliette Dubois**

Defended on December 21, 2023

In order to become Doctor from Sorbonne Université

Academic field **Applied Mathematics**

Acoustic-gravity waves in free-surface flows: modeling, analysis and simulation towards tsunami early-warning systems

Thesis supervised by Jacques SAINTE-MARIE
Sébastien IMPERIALE

Committee members

<i>Referees</i>	Eric BLAYO Frédéric DIAS	Université Grenoble Alpes University College Dublin	
<i>Examiners</i>	Anne-Sophie BONNET BEN DHIA Anne-Laure DALIBARD Aline LEFEBVRE-LEPOT Agnès MAUREL	CNRS, ENSTA Sorbonne Université CNRS, CentraleSupélec Institut Langevin	Committee President

Mots clés : Modélisation, analyse, simulation, fluide à surface libre, ondes acoustiques
Keywords: Modeling, analysis, simulation, free-surface flow, acoustic waves

This thesis has been prepared at the following research units:

[Laboratoire Jacques-Louis Lions](#)

Sorbonne Université
Campus Pierre et Marie Curie
4 place Jussieu
75005 Paris
France



[Inria Paris, ANGE team](#)

2 Rue Simone Iff
75012 Paris
France



Vagues et ondes hydro-acoustiques pour l'alerte précoce de tsunami : modélisation, analyse et simulation

Résumé

L'objectif de cette thèse est de proposer des modèles décrivant la génération et la propagation des ondes acoustiques et des ondes de tsunami générées par les mouvements du fond marin. Lors d'un tremblement de terre sous-marin générant un tsunami, les ondes acoustiques qui se propagent dans l'eau peuvent être considérées comme un précurseur du tsunami. L'étude de ces ondes acoustiques peut donc permettre d'améliorer les systèmes d'alerte précoce aux tsunamis. Nous commençons par un chapitre introductif décrivant l'état de l'art sur le sujet, ainsi que les principales notions qui seront abordées. Nous présentons ensuite un modèle permettant de décrire la propagation des ondes acoustiques et des ondes de gravité dans un fluide à surface libre. Les propriétés mathématiques du modèle sont ensuite étudiées, et une discrétisation par la méthode des éléments finis spectraux est proposée. En particulier, nous montrons que le même modèle physique peut être décrit à l'aide d'un autre système d'équations portant sur une nouvelle variable. Afin de mieux décrire les interactions des ondes avec le fond marin, le modèle est ensuite étendu pour étudier un système fluide-solide. Pour cette extension, nous présentons son étude mathématique ainsi qu'une simulation. Enfin, nous utilisons les équations développées au cours des précédents chapitres pour simuler des cas-tests appliqués à la géophysique.

Mots clés : Modélisation, analyse, simulation, fluide à surface libre, ondes acoustiques

Acoustic-gravity waves in free-surface flows: modeling, analysis and simulation towards tsunami early-warning systems

Abstract

The aim of the present thesis is to propose models describing the generation and propagation of acoustic and tsunami waves generated by movements of the seabed. In the event of an underwater earthquake generating a tsunami, acoustic waves propagating in water can be seen as a precursor of the tsunami wave. The study of these acoustic waves can therefore lead to improvements of tsunami early-warning systems. We start with an introductory chapter describing the state of the art on the subject, as well as the main concepts to be covered. Then, we present a model describing the propagation of acoustic-gravity waves in a free-surface flow. The mathematical properties of the model are then studied, and a discretization based on the spectral finite elements method is proposed. In particular, we show that the same physical model can be described by an alternative system of equations written for a new variable. In order to describe more accurately the ocean interaction with the seabed, the model is then extended so as to study a fluid-solid system. We present the mathematical study and the discretization of this new model. Finally, the equations that were introduced throughout the previous chapters are used to simulate test-cases with application to geophysics.

Keywords: Modeling, analysis, simulation, free-surface flow, acoustic waves

Remerciements

Ce manuscrit présente mes travaux de thèse réalisés au Laboratoire Jacques-Louis Lions, à l'Inria Paris et parfois à l'Inria Saclay. Je voudrais prendre quelques instants pour remercier les personnes qui ont rendu ce travail possible, et même agréable. J'espère que cela vous occupera un peu pendant la soutenance !

Tout d'abord je souhaite remercier mes deux directeurs de thèse, Jacques Sainte-Marie et Sébastien Imperiale. On dit souvent que le bon déroulement d'une thèse dépend plus de la qualité de l'encadrement que du choix du sujet, et j'ai eu beaucoup de chance de vous avoir comme encadrant. Vous m'avez donné une très grande liberté dans l'organisation de mon travail, tout en me guidant à chaque fois que j'en avais besoin. Jacques, merci pour les discussions toujours très intéressantes et les conseils à chaque étape de ma thèse. Malgré tes nombreuses responsabilités tu as toujours su te rendre disponible et tu m'as aidé à garder la motivation tout au long de ces trois ans. Sébastien, merci d'avoir consacré autant d'énergie, de nouvelles idées, de calculs au tableau et de lignes de code à ce travail de thèse ! Tu m'as énormément appris, toujours avec patience et pédagogie. C'était un vrai plaisir de travailler avec toi.

Je suis reconnaissante à Anne Mangeney, qui a été mon premier contact pour commencer cette thèse et avec qui j'ai eu la chance de travailler par la suite. Nos échanges sont toujours très enrichissants et très inspirants pour moi.

Merci Eric Blayo et Frédéric Dias pour leur relecture attentive du manuscrit. Vos remarques ont beaucoup contribué à son amélioration. Je remercie vivement Anne-Sophie Bonnet Ben Dhia, Anne-Laure Dalibard, Aline Lefebvre-Lepot et Agnès Maurel d'avoir accepté de participer à mon jury de thèse.

Michel Kern et Muriel Boulakia ont été mon comité de suivi, je les remercie pour leur implication. Un grand merci à Julien Guieu et à Corentin Lacombe pour avoir répondu à mes (nombreuses) questions administratives, toujours avec efficacité et rapidité. I would like to thank Maria Westdickenberg and Sebastian Noelle for hiring me as a postdoc in the Eddy research group. Thanks for the warm welcome in your team!

J'ai beaucoup apprécié de travailler au sein de l'équipe ANGE. Merci à Nina, Julien S, Julien G, Bernard, Edwige, Marie-Odile, Yohann pour les réunions d'équipe chaleureuses et pour les crêperies. Merci en particulier à Emmanuel Audusse pour m'avoir aidé dans ma recherche de post-doc.

Les trois années passées entre les murs du LJLL et de l'Inria Paris n'auraient pas eu la même saveur sans les nombreux camarades de thèse (et assimilé). Dans un ordre à peu près par ancienneté mais tout de même très arbitraire, je vais tenter de me souvenir de tous ceux avec qui j'ai eu le plaisir d'échanger. Je m'excuse par avance d'en oublier ! Merci aux anciens : Apolline, Emma, Jesus, Jules, Lise, Matthias, Matthieu R, Niels, Ramon, Rémi, Ypeng pour la vie que vous avez

apportée au bureau. J'ai une pensée particulière pour Liu-Di, qui m'a souhaité la bienvenue lors de mes premiers jours de thèse, commencée en télétravail pendant le Covid. Merci aux contemporains et aux nouveaux (les années se mélangent un peu) : Agustin, Antoine, Charles, Daniel, Djahou, Edouard, Elena, Haibo, Jean-Guillaume, Liangfei, Lucas J, Lucas P et Lucas E, Ludovic, Matthieu, Nga, Nicolai, Pierre, Rui, Robin, Siwar, Thomas, Yvonne, et bien d'autres. J'ai passé de très bons moments avec vous au Crous de 11h45 et à celui de 12h30 (plus rare), à la cantine de Bercy, aux Sciences et aux différents événements du laboratoire. Chourouk, merci de m'avoir expliqué les nombreuses démarches de fin de thèse, de la rédaction du manuscrit à l'organisation de la soutenance ! Je souhaite également remercier toute l'équipe M3DISIM, en particulier les doctorants qui m'ont accueillie à plusieurs reprises dans leur open space : Alice, André, Jessica, Gaël, Giulia, Matthieu B, Tiphaine et Zineb.

Mille mercis à mes amis de Paris, pour leur présence inestimable, les après-midi jeux, les discussions et les sorties : Adrien, Alexandre, Agnès, Elias, Etienne, Yusra, Hugo, Lucas, Louis, Guilhem, Fabienne, Julien A. Le début de la thèse a marqué la fin d'une période difficile pour moi et vous m'avez beaucoup aidée. Merci à mon colocataire et ami Julien G, qui m'a supportée pendant ces trois ans de cohabitation. Merci aussi à Léopold qui a pris le temps de répondre sur Ariane à mes questions de maths mal formulées et peu claires.

Je souhaite également adresser un mot à Marion, Mathilde et Camille, Pierre et Rachel, Jean-Marc et Marie-Pierre pour les bons moments (principalement culinaires) passés ensemble. Merci en particulier à Michel et Catherine pour leur gentillesse et leur générosité, et pour m'avoir accueillie chez eux pendant la rédaction de ma thèse.

Merci à ma famille, mes parents Christian et Sara, mon frère Antoine et ma soeur Clémence pour leur soutien inconditionnel. Je n'en serais certainement pas là sans vous. Et pour Manu : merci pour ta présence, tes conseils, ton soutien, et tous les moments passés avec toi.

Résumé long en Français

Dans cette thèse, nous étudions des modèles linéaires décrivant la propagation des ondes acoustiques et des ondes de gravité pour un fluide à surface libre. Lors d'un tremblement de terre sous-marin générant un tsunami, les ondes acoustiques qui se propagent dans l'eau peuvent être considérées comme un précurseur du tsunami. L'étude de ces ondes acoustiques peut donc permettre d'améliorer les systèmes d'alerte précoce aux tsunamis.

La thèse est divisée en cinq chapitres :

Le premier chapitre présente un état de l'art sur la modélisation des ondes acoustiques dans le contexte de tsunamis générés par des tremblements de terre. Nous commençons par décrire plusieurs modèles de tsunami et d'ondes acoustiques à différents niveaux de complexité. Un modèle pour la propagation des ondes acoustiques dans un flot moyen est ensuite présenté, car son formalisme sera utilisé dans le reste de la thèse. Nous décrivons ensuite d'autres modèles de tsunamis, pour lesquels une importance particulière est accordée à l'interaction avec le fond marin. Enfin, nous expliquons les effets de la stratification de l'océan sur la propagation des ondes acoustiques ; en effet, l'une des nouveautés du modèle développé dans la thèse est qu'il prend en compte cette stratification.

Le deuxième chapitre reproduit un article publié (Dubois et al., 2023). Dans cet article, nous dérivons un modèle pour les ondes acoustiques et les ondes de gravité dans un fluide stratifié à surface libre. Nous montrons comment plusieurs modèles de la littérature, qui ont été présentés dans le Chapitre 1, peuvent être considérés comme des cas simplifiés ou des cas limites de ce modèle plus complexe. Nous écrivons également la relation de dispersion associée à ce modèle. La relation de dispersion est un outil utile pour étudier les différents phénomènes physiques pris en compte dans le modèle, comme par exemple la stratification verticale de l'océan et en particulier les variations verticales de la vitesse du son.

Le troisième chapitre a pour objet l'analyse et la simulation du modèle présenté dans le Chapitre 2. Nous montrons que le modèle physique peut être décrit par une formulation alternative, utilisant une nouvelle variable. Cette nouvelle formulation présente plusieurs avantages, tant du point de vue mathématique et que pour la simulation numérique. La nouvelle variable peut être vue comme un "potentiel généralisé", au sens où elle correspond au potentiel de vitesse dans le cas d'un flot irrotationnel. Nous prouvons que la formulation originale et la nouvelle formulation sont toutes les

deux bien posées, et qu'elles sont équivalentes. Nous décrivons également la discrétisation des deux formulations, et donnons un exemple numérique pour illustrer leur équivalence, obtenu avec une discrétisation par éléments finis spectraux en espace et par différences finies en temps.

Le quatrième chapitre propose une extension du modèle présenté dans le Chapitre 2, permettant de prendre en compte l'interaction avec le fond marin. L'hypothèse d'un sol rigide est remplacée par celle d'un solide élastique, qui s'étend sous la couche de fluide. Le domaine fluide-solide est modélisé comme un seul domaine élastique, avec des paramètres constitutifs différents pour chaque sous-domaine. Un système linéaire décrivant le mouvement joint du fluide et du solide est ainsi déduit. Nous montrons que ce système est bien posé, et nous présentons une illustration numérique obtenue par la méthode des éléments finis spectraux.

Le cinquième chapitre s'appuie en partie sur une communication présentée à l'assemblée générale de l'EGU ¹. Dans ce chapitre, nous présentons des simulations numériques obtenues avec les formulations présentées dans le Chapitre 3. Nous nous intéressons à deux cas de propagation d'onde dans l'océan. Le premier cas est une figure d'interférence observée pour des ondes acoustiques générées par un glissement de terrain. Le deuxième cas est une illustration du guidage d'onde des ondes acoustiques, que l'on observe pour certains profils de la vitesse du son.

¹<https://meetingorganizer.copernicus.org/EGU23/EGU23-15937.html>

Contents

Abstract	i
Remerciements	iii
Résumé long en Français	v
Table of contents	ix
List of figures	xii
Context	1
1 Introduction	5
1.1 Hydro-acoustic waves for tsunami early-warning systems	6
1.1.1 The Euler equations for a free-surface flow	6
1.1.2 Classical models for tsunami	7
1.1.3 Acoustic waves in water	8
1.1.4 Models for tsunami in compressible water	9
1.1.5 A model for acoustic waves in a flow: the Galbrun equation	12
1.2 Coupling with the earth and the gravito-elastic models	13
1.2.1 Generation of a tsunami: the passive approach	14
1.2.2 Models with partial coupling	14
1.2.3 The fully coupled elastic-acoustic-gravity model	16
1.3 Water stratification, the SOFAR channel, and T-waves	17
1.4 Contributions of the thesis	19
1.4.1 A model for hydro-acoustic and gravity waves in a stratified free-surface flow	19
1.4.2 Mathematical analysis and numerical approximation of the model.	22
1.4.3 Gravito-elastic equations	25
1.4.4 Preliminary results for geophysical applications	27

2	Modelling of acoustic and surface gravity waves in a stratified ocean	29
2.1	Introduction	30
2.2	Linearization of compressible Euler equations in Lagrangian coordinates	32
2.2.1	Euler equations in Eulerian coordinates	32
2.2.2	Lagrangian description	35
2.2.3	Linearization and wave equation	37
2.3	Derivation of simplified models	40
2.3.1	The barotropic case	40
2.3.2	Two asymptotic regimes of the system	42
2.4	The model in Eulerian coordinates	49
2.4.1	General method	49
2.4.2	The model in Eulerian coordinates	51
2.5	Dispersion relation	53
2.6	Conclusion and future work	57
	Appendix	57
	A Derivation of the energy equation	57
	B From the Lagrangian to the Eulerian coordinates	59
3	Mathematical analysis and numerical approximation of the model	61
3.1	Introduction	62
3.2	Preliminary definitions	65
3.3	Analysis of the potential-based formulation	69
3.3.1	Variational formulation	69
3.3.2	Existence and uniqueness results	70
3.3.3	Energy identity	71
3.4	Analysis of the velocity-based formulation	72
3.4.1	Variational formulation and uniqueness result	72
3.4.2	Existence results	74
3.5	Equivalence of the velocity and the potential formulations	78
3.5.1	Equivalence for the relaxed problem	78
3.5.2	The equivalence for the non-relaxed formulations	81
3.6	Numerical illustration	82
3.6.1	Discretization	83
3.6.2	Numerical example: tsunami and hydro-acoustic waves generation	86
3.7	Conclusion and future work	89
4	Coupling with the earth: the gravito-elastic equations	93
4.1	Introduction	94
4.2	The equations for linear elasticity with a prestress	95
4.2.1	The equations in Eulerian coordinates	95
4.2.2	The equations in Lagrangian coordinates	96
4.2.3	Linearization around the equilibrium state	98
4.2.4	The linear equations for the fluid-solid system	99
4.3	Mathematical analysis	100
4.3.1	A first variational formulation	101
4.3.2	The modified variational formulation	102
4.3.3	Mathematical analysis of the modified formulation	107

4.3.4	Energy estimates	110
4.4	Numerical illustration	112
4.5	Conclusion and future work	115
Appendix	115
A	The bilinear form in the fluid domain	115
B	An expression for the extended density	116
5	Preliminary results for geophysical applications	119
5.1	Simulation of acoustic waves generated by landslides	119
5.1.1	Detecting an underwater landslide from interference patterns: the Lloyd mirror	120
5.1.2	Reproducing the Lloyd mirror with static emitters	122
5.1.3	Perspectives	123
5.2	Wave trapping in the SOFAR channel	123
5.2.1	Simulation of trapped waves	127
5.2.2	T-wave propagation from a beam located near the seabed	129
5.2.3	Perspectives	130
5.3	Conclusion and future work	130
	Perspectives	131
	Bibliography	133

List of Figures

1	Two of the deadliest tsunamis in recent history. (a): The Sumatra tsunami in 2004; (b): the Tohoku-Oki tsunami in 2011.	1
1.1	The domain $\Omega(t)$	6
1.2	A typical profile for the temperature T_0	18
1.3	(a) A typical profile for the sound speed. (b) Ray path. Picture taken from Williams et al. (2006)	18
1.4	The domain Ω , made of two layers: the fluid layer Ω^F and the solid layer Ω^S . The boundary of the domain is Γ	25
2.1	The domain $\Omega(t)$: (2.1a) for time $t = 0$; (2.1b) for time $t > 0$. In panel (2.1a), typical profiles for the temperature and the density at rest are drawn.	33
2.2	The mapping ϕ_t between the reference domain $\hat{\Omega} = \Omega(0)$ and the domain $\Omega(t)$	36
2.3	Temperature, density and sound speed profiles used for the computation of the dispersion relation where $\xi_3 = 0$ is the seafloor and $\xi_3 = 4000$ m is the ocean surface: 2.3a temperature profile ; 2.3b density profile and 2.3c sound speed profile.	55
2.4	Contour of the vertical wavenumber as a function of the horizontal wavenumber δ_x and the angular frequency δ_ω , at different depths ξ_3 : 2.4a $\xi_3 = 2000$ m; 2.4b $\xi_3 = 3600$ m; 2.4c $\xi_3 = 4000$ m.	56
3.1	The domain Ω	65
3.2	Vertical displacement at $x = 50$ km for the velocity formulation at different elements orders.	87
3.3	Vertical displacement at $x = 50$ km for the potential formulation at different elements orders.	88
3.4	Vertical displacement at $x = 50$ km for the potential formulation at different elements orders.	88
3.5	Vertical displacement at $x = 50$ km, computed from the velocity-based (blue) and the potential-based (orange) formulations.	90
3.6	Vertical displacement at $x = 50$ km, by Sammarco et al. (2013).	90

3.7	Vertical displacement at $x = 50$ km from the velocity-based and the potential-based formulations, and absolute error.	91
3.8	Snapshots of the displacement obtained with the potential formulation, for the times $t = 49.0$ s, $t = 147.1$ s, $t = 343.3$ s, $t = 833.8$ s.	92
4.1	The domain $\Omega(t)$	96
4.2	The domain Ω with a fluid layer Ω^F and a solid layer Ω^{FS}	99
4.3	The decomposition of the domain Ω	104
4.4	The functions $\tilde{\rho}_0$ and \tilde{p}_0	105
4.5	Snapshots of the horizontal (figures a) and vertical displacement (figures b) field. Figures 1a, 1b: $t = 10$ s, Figures 2a, 2b: $t = 50$ s, Figures 3a, 3b: $t = 80$ s.	114
5.1	The direct path (in red) and the reflected path (in blue) connecting the source S to a point P . The location of the reflection (point R) is deduced from the image source S' . The declination angle θ is also indicated.	120
5.2	Interference pattern obtained from Equation (5.3) for $k = 66.7$ m ⁻¹ , $z_s = 0.5$ km. The modulus $ \rho(x, z) $ is plotted in log scale.	121
5.3	The source term	123
5.4	Spectrograms for the emitter and for each receiver. The coordinates for each receiver are, in km: R1=(5,0.3) ; R2=(8,0.3) ; R3=(5,1.35) ; R4=(8,1.35).	124
5.5	Background quantities for a variable temperature: (a) temperature; (b): density; (c): sound speed profiles. In panel (c), the Munk profile is in dashed line, the profile obtained from Equation (5.14) is in continuous line, and the constant profile is in dotted line. Here the vertical axis is oriented upwards, hence 5 km corresponds to the surface, and 0 km to the seabed.	126
5.6	Logarithm of the acoustic energy $\log_{10} \mathcal{E}_p$ for different sound speed profiles: (a) with the Munk profile; (b) with the profile $c(p, T)$; (c) with the constant profile $c \equiv 1500$ ms ⁻¹	128
5.7	Data for the second simulation: (a) the domain; (b) the Munk sound speed profile, obtained from Equation (5.16). In panel (a), the cross indicates the center of the source.	129
5.8	Acoustic energy density.	129

Context of the thesis

Tsunamis are devastating natural hazards, and early warning against potential arrivals remains the most efficient way to reduce damage. However, they are also quite difficult to detect during their early stage. Most tsunamis are generated by seabed movements, such as underwater earthquakes or landslides. While traveling the ocean, a tsunami is usually a wave less than a meter high, with a very long wavelength and propagating at a high speed; only when it reaches a coast does it becomes a wave of significant height. Because tsunami waves are not very tall during their propagation, detecting them visually or with sea-level measurements remains a challenge. In order to alert the populations at risk, faster signals must be used to forecast the arrival time of a tsunami wave on a coast. This is the purpose of early-warning systems.



(a) A village near the coast of Sumatra after the Tsunami that struck South East Asia. (Source: Navy Visual News Service)



(b) Tsunami from the Tohoku-Pacific Ocean Earthquake. (Source: Miyako, Iwate Prefecture, Japan).

Figure 1: Two of the deadliest tsunamis in recent history. (a): The Sumatra tsunami in 2004; (b): the Tohoku-Oki tsunami in 2011.

Current early-warning systems rely exclusively on monitoring seismic waves. However, in the last decade, several studies have confirmed that acoustic waves propagating in water, also called hydro-acoustic waves, carry valuable information about both earthquakes and tsunamis, and that

they could improve current tsunamis early-warning systems (Nosov and Kolesov, 2007; Yamamoto, 1982). The increased availability of hydro-acoustic recordings related to seismic and landslide events (Matsumoto et al., 2012; Caplan-Auerbach et al., 2001, 2014) makes it possible to compare theory and data and brings us closer to practical applications.

In this context, the aim of the present thesis is to

Develop a linear model describing the generation and propagation of acoustic and surface gravity waves generated by movements of the seabed.

The model is formulated along with a dedicated mathematical framework, allowing us to prove its well-posedness and solve it numerically using a spectral element method. The obtained model is used to provide simulations for some geophysical applications. Another aspect that we will investigate is the modeling of the ocean-earth interaction. The effect of such an interaction on the waves' generation and propagation is the subject of ongoing research. To contribute to a better understanding of this topic, the model is extended to include seabed interactions. We present the mathematical analysis and a numerical approximation for this extended model.

This PhD thesis has been prepared in the ANGE team at Inria Paris and Sorbonne Université, funded by a fellowship from Région Ile-de-France (DIM MathInnov), and under the supervision of Jacques Sainte-Marie (Inria Paris, Ange team) and Sébastien Imperiale (Inria Saclay, MΞdisim team). The interdisciplinary nature of both the ANGE team and this topic offered the opportunity to directly work with experienced geophysicists. Several results presented in this thesis have been obtained in collaboration with Anne Mangeney (Institut de Physique du Globe de Paris).

The thesis is divided into five chapters.

The first chapter gives a state of the art on the modeling of acoustic waves in the context of tsunami and underwater earthquakes. We first introduce several models describing the tsunami and the acoustic waves with different level of complexity. A model for acoustic propagation in a mean flow is also presented, since its formalism will be used in the remaining of the thesis. Then, we introduce some models focusing on the earth-ocean interaction. We also describe the effect of the ocean stratification on the acoustic wave propagation, since one novelty of the model developed in this thesis is to take the ocean stratification into account. Finally, we present the contributions of the thesis and relate them to the literature.

The second chapter reproduces a published paper (Dubois et al., 2023), where we derive a model for acoustic and gravity waves in a stratified, free-surface flow. We show that models from the literature, which were presented in Chapter 1, can be seen as simplified or limit cases of this more complex model. We also derive the dispersion relation of the model, reflecting the different physical processes involved, such as the ocean stratification and the sound speed's dependency on depth.

The third chapter focuses on the analysis and numerical approximation of the model presented in Chapter 2. An alternative, more advantageous formulation based on a new variable is introduced. The new variable can be understood as a "generalized potential", in the sense that the new variable corresponds to the fluid potential in the particular case of an irrotational flow. We prove the well-posedness of both formulations, and show that they are equivalent. We also present the discretization of both formulations and numerically illustrate the equivalence. The results presented

in this chapter will be submitted as a paper.

The fourth chapter is an ongoing work, where the model presented in Chapter 2 is extended by taking into account the interaction with the seabed. Instead of assuming a rigid-body seabed, we consider it an elastic domain below the fluid layer. The fluid-solid system is modeled as one elastic domain, with different parameters for the fluid and solid sub-domains. We derive a linear system describing the coupled motion of the fluid and the solid. We show the well-posedness of the obtained formulation and present a numerical illustration.

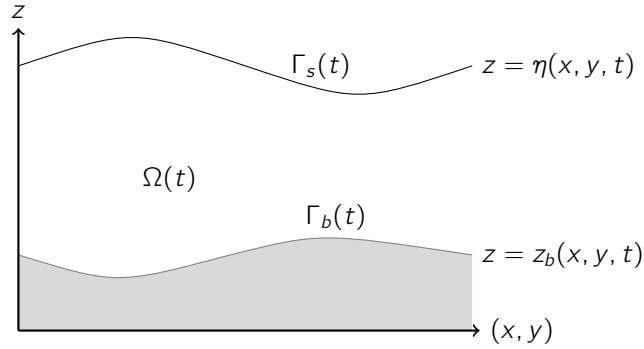
The fifth chapter is based, in part, on a communication presented in the European Geoscience Union General Assembly². We show numerical simulations obtained with the formulations presented in Chapters 2 and 3. We consider two different cases of wave propagation in the ocean, and discuss the insight obtained from these preliminary results. The first simulation reproduces an interference pattern observed for acoustic waves generated by a landslide. The second simulation illustrates the trapping of acoustic waves in the so-called SOFAR channel, an open waveguide forming in the presence of specific underwater sound speed profiles.

²<https://meetingorganizer.copernicus.org/EGU23/EGU23-15937.html>

Contents

1.1 Hydro-acoustic waves for tsunami early-warning systems	6
1.1.1 The Euler equations for a free-surface flow	6
1.1.2 Classical models for tsunami	7
1.1.3 Acoustic waves in water	8
1.1.4 Models for tsunami in compressible water	9
1.1.5 A model for acoustic waves in a flow: the Galbrun equation	12
1.2 Coupling with the earth and the gravito-elastic models	13
1.2.1 Generation of a tsunami: the passive approach	14
1.2.2 Models with partial coupling	14
1.2.3 The fully coupled elastic-acoustic-gravity model	16
1.3 Water stratification, the SOFAR channel, and T-waves	17
1.4 Contributions of the thesis	19
1.4.1 A model for hydro-acoustic and gravity waves in a stratified free-surface flow	19
1.4.2 Mathematical analysis and numerical approximation of the model. . .	22
1.4.3 Gravito-elastic equations	25
1.4.4 Preliminary results for geophysical applications	27

In this chapter, we present the state of the art for the physical systems studied in the thesis, and summarize the contribution made in each chapter. Section 1.1 presents models from the literature for the propagation of tsunami waves and acoustic waves. In Chapter 2, the model developed in the thesis will be compared to those models. We also introduce so-called Galbrun equation, which describes the propagation of acoustic wave in a mean flow, written in Lagrangian coordinates. The Galbrun equation is closely related to the model developed in this thesis. In Section 1.2, we present the state of the art on the earth-ocean coupling for the tsunami generation and propagation. The mathematical analysis of such models is still an open question, and we present in Chapter 4 the analysis for the fully-coupled model. In Section 1.3, we describe the effect of the ocean stratification on the acoustic wave propagation, since one novelty of the model developed in this thesis is to take the ocean stratification into account. Finally, Section 1.4 summarizes the contributions of the thesis.

Figure 1.1: The domain $\Omega(t)$

1.1 Hydro-acoustic waves for tsunami early-warning systems

In this section, we introduce the various models describing the tsunamis and the acoustic waves. Since all of the models in this section are derived from the Euler equations with free surface, we begin with a reminder on this topic. Both tsunami models and underwater acoustics are subjects too broad to be discussed here in detail, so the introduction that we give here aims only to write the main equations and giving some notations. We briefly present two tsunami models that are mainly used in the early-warning system literature, and give some fundamentals on the acoustic equation in the ocean. We then present three models coupling the two acoustic and gravity waves in the ocean, and we conclude by a short introduction to the Galbrun equation, which describes the propagation of acoustic waves in a flow.

1.1.1 The Euler equations for a free-surface flow

In the ocean, the viscosity is generally assumed negligible (Gill, 1982), hence the system is described by the Euler equations. We consider a portion of the ocean, denoted $\Omega(t)$. The portion is assumed small enough to neglect the curvature of the Earth and consider the ocean far away from the coast. Hence $\Omega(t)$ is infinite in the horizontal direction. It is bounded in the vertical direction by the free surface, denoted Γ_s , and by the seabed, denoted Γ_b . We assume that the surface and the seabed can be described as graph of functions, namely the free surface $\eta(x, y, t)$ and the topography $z_b(x, y, t)$. In the following, we will only consider linear models, so that this assumption is not problematic. The domain is then described by

$$\Omega(t) = \{(x, y, z) \in \mathbb{R}^3 \mid z_b(x, y, t) < z < \eta(x, y, t)\}. \quad (1.1)$$

The boundaries of the domain Γ_s and Γ_b are respectively described by

$$\Gamma_s(t) = \{(x, y, z) \in \mathbb{R}^3 \mid z = \eta(x, y, t)\}, \quad (1.2)$$

and

$$\Gamma_b(t) = \{(x, y, z) \in \mathbb{R}^3 \mid z = z_b(x, y, t)\}. \quad (1.3)$$

The domain as well as its boundary are represented on Figure 1.1.

The Euler equations state the conservation of mass, momentum and energy for a non-viscous fluid in the time-dependant domain $\Omega(t)$. The unknowns are the fluid velocity \mathbf{U} with components

$\mathbf{U} = (u \ v \ w)^t$, its density ρ , its pressure p , its temperature T , its internal energy e and its entropy s .

$$\begin{cases} \frac{\partial \rho}{\partial t} + \nabla \cdot (\rho \mathbf{U}) = 0, & (1.4) \end{cases}$$

$$\begin{cases} \frac{\partial}{\partial t} (\rho \mathbf{U}) + \nabla \cdot (\rho \mathbf{U} \otimes \mathbf{U}) + \nabla p = \rho \mathbf{g}, & (1.5) \end{cases}$$

$$\begin{cases} \frac{\partial}{\partial t} \left(\rho \frac{|\mathbf{U}|^2}{2} + \rho e \right) + \nabla \cdot \left(\left(\rho \frac{|\mathbf{U}|^2}{2} + \rho e + p \right) \mathbf{U} \right) = \rho \mathbf{g} \cdot \mathbf{U}. & (1.6) \end{cases}$$

Among the five variables p, ρ, T, e, s , only three are independent. Indeed, those variables are related by the Gibbs law (Gill, 1982)

$$de = T ds + \frac{p}{\rho} d\rho, \quad (1.7)$$

and by an equation of state of the form

$$f(\rho, T, p) = 0. \quad (1.8)$$

Initial and boundary conditions must also be prescribed. Since the initial condition will depend on the considered case we do not give them here. The boundary conditions describe the continuity of pressure on the surface and the continuity of normal velocity on the seabed. The pressure above the ocean is assumed equal to the atmospheric pressure $p^a(x, y, z, t)$. The seabed is moving with a prescribed normal velocity $u_b = \partial_t z_b$, and we denote by \mathbf{n}_b the unit vector normal to Γ_b . The boundary conditions read then

$$\begin{cases} \mathbf{U} \cdot \mathbf{n}_b = u_b & \text{on } \Gamma_b(t), \\ p = p^a & \text{on } \Gamma_s(t). \end{cases} \quad (1.9)$$

$$(1.10)$$

Because of the free surface and the moving seabed, the domain $\Omega(t)$ changes with time. Its boundary are described with the kinematic boundary conditions,

$$\frac{\partial \eta}{\partial t} + \mathbf{U} \cdot \begin{pmatrix} \partial_x \eta \\ \partial_y \eta \\ -1 \end{pmatrix} = 0 \text{ on } \Gamma_s(t), \quad \frac{\partial z_b}{\partial t} + \mathbf{U} \cdot \begin{pmatrix} \partial_x z_b \\ \partial_y z_b \\ -1 \end{pmatrix} = 0 \text{ on } \Gamma_b(t). \quad (1.11)$$

An equation for the pressure can be derived from the system (1.4)-(1.8). We denote by c the sound speed, defined by

$$c^2 = \left(\frac{\partial p}{\partial \rho} \right)_s, \quad (1.12)$$

and the equation for pressure reads (Gill, 1982)

$$\frac{\partial p}{\partial t} + \mathbf{U} \cdot \nabla p + \rho c^2 \nabla \cdot \mathbf{U} = 0, \quad (1.13)$$

1.1.2 Classical models for tsunami

We present two models used for tsunami propagation. Classically, models for tsunami propagation are obtained from the system (1.4)-(1.11) by assuming that the flow is incompressible and irrotational. An incompressible fluid is the limit case where the sound speed c goes to infinity. From Equation (1.13), we have that the assumption $c \rightarrow \infty$ implies $\nabla \cdot \mathbf{U} = 0$. An irrotational flow satisfies $\nabla \times \mathbf{U} = 0$, which implies that \mathbf{U} can be written as the gradient of some potential

ϕ . This is expressed as $\mathbf{U} = \nabla\phi$. The bottom displacement is considered as a perturbation to a time-independant topography, hence the total topography is decomposed as $z_b(x, y) + b(x, y, t)$.

As explained before, tsunami are a small perturbation of water depth compared to the total ocean depth, and have a long wavelength. Typically, the total ocean height is of the order of a few kilometers, whereas the raising above the mean sea level is a few dozen centimeters, and the wavelength is hundreds of kilometers. The first model, used by Saito (2019) and Dutykh and Dias (2007), uses the small raising assumption to linearize the boundary conditions (1.11). Using the fact that the flow is irrotational and incompressible, the mass conservation (1.4) becomes a Laplace equation for the fluid potential. For a flat bottom ($z_b \equiv 0$) and a water height at rest denoted H , the model reads

$$\Delta\phi = 0 \text{ in } \Omega, \quad \frac{\partial^2\phi}{\partial t^2} + g\frac{\partial\phi}{\partial z} = 0, \quad \text{on } z = H, \quad \frac{\partial\phi}{\partial z} = \frac{\partial b}{\partial t}, \quad \text{on } z = 0. \quad (1.14)$$

The second model used for geophysical flows is the shallow water model. This model makes use of the assumption that the wavelength of the surface waves is much larger than the total water depth. Additionnally, the vertical acceleration of the fluid is neglected. With those two assumptions, one can derive the following non-linear shallow water equations,

$$\left\{ \begin{array}{l} \frac{\partial H}{\partial t} + \nabla_{x,y} \cdot (H\bar{\mathbf{U}}) = 0, \end{array} \right. \quad (1.15)$$

$$\left\{ \begin{array}{l} \frac{\partial(H\bar{\mathbf{U}})}{\partial t} + \nabla_{x,y} \cdot (H\bar{\mathbf{U}} \otimes \bar{\mathbf{U}}) + \frac{g}{2}\nabla(H^2) = -H\nabla_{x,y}p^a - gh\nabla_{x,y}z_b, \end{array} \right. \quad (1.16)$$

with $\nabla_{x,y} = (\partial_x \partial_y)^t$. The unknowns are the water height $H(x, y, t) = \eta(x, y, t) - z_b(x, y) - b(x, y, t)$ and the vertical average of the horizontal velocity $\bar{\mathbf{U}}$,

$$\bar{\mathbf{U}} = \begin{pmatrix} \bar{u} \\ \bar{v} \end{pmatrix}, \quad \bar{u} = \frac{1}{H} \int_{z_b+b}^{\eta} u(x, y, z, t) dz, \quad \bar{v} = \frac{1}{H} \int_{z_b+b}^{\eta} v(x, y, z, t) dz. \quad (1.17)$$

A great variety of shallow water models can be obtained, for example to include dispersive effects (Aïssiouene et al., 2020). For more details on the shallow water approximation, see Lannes (2013) and Gerbeau and Perthame (2001).

Either model is used depending on the most significant hypothesis, namely the small perturbation or the long wave assumption. The potential model (1.14) is a linear model, whereas the shallow-water model (1.15)-(1.16) is nonlinear. On the other hand, the shallow-water model is depth-averaged, whereas the potential model describes the fluid is every space dimension.

1.1.3 Acoustic waves in water

In tsunami models, the water is assumed incompressible and the effect of gravity is non negligible. On the contrary, the usual models for the propagation of acoustic waves in water take the water compressibility into account and neglect the effects of gravity. Without gravity, the water surface can deform but there is no surface wave propagation because of the lack of restoring force. The most simple model for the propagation of acoustic waves is a linear wave equation for the velocity potential ϕ (Jensen et al., 2011). It is obtained by the linearization of the system (1.4)-(1.11) around a state at rest, with no gravity and a homogeneous background density. The sound speed c defined by Equation (1.12) is assumed constant in time. The flow is assumed irrotational and the perturbations in pressure, density are assumed small. Then the system (1.4)-(1.6) simplifies to a linear wave equation for ϕ ,

$$\frac{\partial^2\phi}{\partial t^2} - c^2\Delta\phi = 0, \quad (1.18)$$

and the pressure is related to the fluid potential by

$$p = -\rho \frac{\partial \phi}{\partial t}. \quad (1.19)$$

For an ocean with a free-surface and a rigid seabed, the linearized boundary conditions yield

$$p = 0, \quad \text{on } z = H, \quad \nabla \phi \cdot \mathbf{n} = 0, \quad \text{on } z = z_b. \quad (1.20)$$

The dispersion relation for a simple ocean model. Each model presented in this thesis is classically studied through its dispersion relation. Dispersion relations are very useful tools for wave equations, which help gain insight on some characteristics of the model without solving the entire system of partial differential equations. Even if we have not used them in the thesis (a dispersion relation is derived in Chapter 2 but it is not thoroughly analyzed), for completeness we show how they are derived in simple cases. We show first how the dispersion relation is obtained for the acoustic model in the 2D case (x, z) . We consider the equation (1.18) and the boundary conditions (1.20). Using the relation (1.19) between the pressure and the potential, and assuming a flat bottom, the boundary conditions read for the potential

$$\phi = 0, \quad \text{on } z = H, \quad \frac{\partial \phi}{\partial z} = 0, \quad \text{on } z = 0. \quad (1.21)$$

If we assume for ϕ a progressive wave of the form

$$\phi = \tilde{\phi}(z) e^{i(k_x x - \omega t)}, \quad (1.22)$$

substituting in the equation (1.18) and introducing $k_z^2 = \omega^2/c^2 - k_x^2$ yields

$$\frac{d^2 \tilde{\phi}}{dz^2} + k_z^2 \tilde{\phi} = 0, \quad k_z^2 = \frac{\omega^2}{c^2} - k_x^2. \quad (1.23)$$

For $k_z^2 \leq 0$, the only solution satisfying the boundary conditions is the trivial solution $\tilde{\phi} = 0$. For $k_z^2 > 0$ the solution has the form $\tilde{\phi} = A \cos(k_z z) + B \sin(k_z z)$. With the boundary conditions we obtain that the solution reads $\tilde{\phi} = A \cos(k_z z)$, and that k_z must satisfy $\cos(k_z H) = 0$, hence

$$k_z = \frac{(2m-1)\pi}{2H}, \quad k_x^2 = \frac{\omega^2}{c^2} - \frac{(2m-1)^2 \pi^2}{4H^2}, \quad m \in \mathbb{N}^*. \quad (1.24)$$

When $\omega < c(2m-1)\pi/(2H)$, the solution is an evanescent wave of the form $\tilde{\phi}(z) e^{-k_x x} e^{-i\omega t}$. The minimal frequency at which acoustic waves can propagate, or cut-off frequency, is obtained for $m = 1$. It reads $\omega_0 = c\pi/(2H)$. Such cut-off frequency will also be present in the models introduced below.

1.1.4 Models for tsunami in compressible water

In the literature, we can distinguish three models for the propagation of tsunami in a compressible ocean. We describe how each model was obtained and write their corresponding dispersion relations.

Model 1. The first model, and by far the most used, consists in the acoustic equation for the fluid potential

$$\frac{\partial^2 \phi}{\partial t^2} - c^2 \Delta \phi = 0 \quad (1.25)$$

coupled with the boundary conditions representing a free-surface and a rigid bottom,

$$\frac{\partial^2 \phi}{\partial t^2} + g \frac{\partial \phi}{\partial z} = 0, \quad \text{on } z = H, \quad \nabla \phi \cdot \mathbf{n} = \frac{\partial b}{\partial t}, \quad \text{on } z = z_b. \quad (1.26)$$

It can be seen as the coupling of the acoustic equation (1.18) with the free-surface condition (1.14) of an incompressible fluid subject to gravity. One of the earliest work using this model in the frame of tsunami propagation was done by Ewing et al. (1950). The coupled acoustic and gravity waves described with this model are called acoustic-gravity waves. This coupling has been considered as the standard model to study the applicability of hydro-acoustic waves for tsunami early-warning systems. Semi-analytical solutions were proposed by Nosov (1999), Nosov and Kolesov (2007) and Stiassnie (2010). Correlations between the hydro-acoustic signal and some characteristics of the tsunami, such as its height or its phase velocity, are studied by Yamamoto (1982), Chierici et al. (2010) and Watada (2013). A depth-integrated version is proposed by Sammarco et al. (2013) to reduce the computational costs. This approach has been developed in a series of papers (Cecioni et al., 2014; Abdolali et al., 2015; Gomez and Kadri, 2021).

To write the dispersion relation associated to the model (1.25)-(1.26) in the 2D case (x, z) , we assume a solution of the form of a plane wave $\phi(x, z, t) = \tilde{\phi}(z)e^{i(k_x x - \omega t)}$. We obtain the same equation for $\tilde{\phi}$ as for the purely acoustic case,

$$\frac{d^2 \tilde{\phi}}{dz^2} + k_z^2 \tilde{\phi} = 0, \quad k_z^2 = \frac{\omega^2}{c^2} - k_x^2, \quad (1.27)$$

but with different boundary conditions. The boundary conditions for a flat bottom ($z_b \equiv 0$) yield

$$-\omega^2 \tilde{\phi}(H) + g \tilde{\phi}'(H) = 0, \quad \tilde{\phi}'(0) = 0. \quad (1.28)$$

If $k_z^2 < 0$, then it holds $k_z = i\mu$ for some $\mu > 0$, and the solution has the form $\tilde{\phi} = Ae^{\mu z} + Be^{-\mu z}$. With the boundary conditions we obtain

$$\mu(A - B) = 0, \quad -\omega^2 \cosh(\mu H) + g\mu \sinh(\mu H) = 0. \quad (1.29)$$

If $k_z^2 > 0$, the solution has the form $\tilde{\phi} = A \cos(k_z z) + B \sin(k_z z)$ and the boundary conditions yield

$$Bk_z = 0, \quad \omega^2 \cos(k_z H) + gk_z \sin(k_z H) = 0. \quad (1.30)$$

Since neither case $\sinh(\mu H) = 0$ or $\sin(k_z H) = 0$ are solutions, we can express the equations (1.29) and (1.30) as equations respectively on μ and k_z ,

$$\begin{cases} \omega^2 = g\mu \tanh(\mu H), & (1.31) \\ \omega^2 = -gk_z \tan(k_z H). & (1.32) \end{cases}$$

For a fixed ω^2 , the equation (1.31) has two solutions $\pm\mu_0(\omega)$, with $\mu_0 > 0$. Similarly, for a fixed ω^2 , the equation (1.32) has infinitely many solutions $\pm k_{zm}(\omega)$, with $m \in \mathbb{N}^*$ and $k_{zm} \in (m\pi - \pi/2, m\pi)$.

The horizontal wavenumbers are then deduced,

$$\left\{ \begin{array}{l} k_{x0} = \sqrt{\frac{\omega^2}{c^2} + \mu_0^2}, \end{array} \right. \quad (1.33)$$

$$\left\{ \begin{array}{l} k_{xm} = \sqrt{\frac{\omega^2}{c^2} - k_{zm}^2}, \quad \frac{\omega^2}{c^2} \geq k_{zm}^2, \quad m \in \mathbb{N}^*, \end{array} \right. \quad (1.34)$$

$$\left\{ \begin{array}{l} \tilde{k}_{xm} = \sqrt{k_{zm}^2 - \frac{\omega^2}{c^2}}, \quad \frac{\omega^2}{c^2} \leq k_{zm}^2, \quad m \in \mathbb{N}^*. \end{array} \right. \quad (1.35)$$

The wavenumbers k_{x0} and k_{xm} represent propagating modes, and the wavenumbers \tilde{k}_{xm} are evanescent modes. The modes k_{xm} are the same as the ones obtained for the acoustic equation and are called acoustic modes. The new mode k_{x0} , due to the surface conditions of gravity waves, is called the gravity mode (Yamamoto, 1982).

Model 2. Another model is proposed by Longuet-Higgins (1950), where the equation is still on the fluid potential, but includes a gravity term,

$$\frac{\partial^2 \phi}{\partial t^2} - c^2 \Delta \phi + g \frac{\partial \phi}{\partial z} = 0, \quad (1.36)$$

with the boundary conditions (1.26). This model is obtained by an asymptotic expansion of the system (1.4)-(1.6) around a state at rest. The derivation is done in the same way as for the models (1.14), (1.18), but this time neither the compressibility nor the gravity are neglected. In Longuet-Higgins (1950), an asymptotic development is written to the second order. The first order corresponds to the linear model (1.36), and only few studies have used it in the context of tsunami early-warning systems (see for example Abdolali et al., 2019). The second order is a nonlinear model, and it is the starting point of an extensive work to describe the nonlinear interactions between acoustic and gravity waves (Stutzmann et al., 2012; Kadri and Stiassnie, 2013; Noguier et al., 2015).

The dispersion relation is obtained in the same way as for the previous models. In the 2D case, it reads (Longuet-Higgins, 1950)

$$k_z H \coth(k_z H) - \frac{g}{H\omega^2} (k_z H)^2 - \frac{g}{2c^2} H \left(1 - \frac{g^2}{2\omega^2 c^2} \right) = 0, \quad k_z^2 = \frac{\omega^2}{c^2} - k_x^2 - \frac{g}{2c^2}. \quad (1.37)$$

The above equation can be written

$$f_\omega(\mu H) = 0, \quad \mu^2 = -k_z^2. \quad (1.38)$$

It can be shown that for a fixed ω , the function f_ω has one real positive zero μ_0 , infinitely many imaginary zeros μ_n , and no complex zero. We have then $k_{z0} = \pm i\mu_0$ and $k_{zn} = \pm\mu_n$, and the horizontal wavenumbers read

$$\left\{ \begin{array}{l} k_{x0} = \sqrt{\frac{\omega^2}{c^2} + \mu_0^2 - \frac{g}{2c^2}}, \end{array} \right. \quad (1.39)$$

$$\left\{ \begin{array}{l} k_{xm} = \sqrt{\frac{\omega^2}{c^2} - k_{zm}^2 - \frac{g}{2c^2}}, \quad \frac{\omega^2}{c^2} \geq k_{zm}^2 + \frac{g}{2c^2}, \quad m \in \mathbb{N}^*, \end{array} \right. \quad (1.40)$$

$$\left\{ \begin{array}{l} \tilde{k}_{xm} = \sqrt{k_{zm}^2 - \frac{\omega^2}{c^2} + \frac{g}{2c^2}}, \quad \frac{\omega^2}{c^2} \leq k_{zm}^2 + \frac{g}{2c^2}, \quad m \in \mathbb{N}^*. \end{array} \right. \quad (1.41)$$

A more complete study of the dispersion relation (1.37) can be found in Abdolali et al. (2019).

Model 3. The last model, and the most recent one, has been derived in several papers (Dukowicz, 2013; Smith, 2015; Auclair et al., 2021). It consists in a system of first-order equations for the fluid velocity, and first-order approximations for the density and the pressure. More precisely, the density is of the form $\rho = \hat{\rho}_h + \rho'$ and $p = \hat{p}_h + p'$, where $\hat{\rho}_h, \hat{p}_h$ are reference profiles depending on z only, and ρ', p' are the small increments due to the perturbation. The model is derived from a linearization around a reference state. The reference state is described by the reference profiles $\hat{\rho}_h, \hat{p}_h$, and by a vanishing velocity. The obtained system reads

$$\begin{cases} \frac{\partial \hat{\rho}_h \mathbf{U}}{\partial t} + \nabla p = -\rho g \mathbf{e}_3, & (1.42) \end{cases}$$

$$\begin{cases} \frac{\partial \rho}{\partial t} + \nabla \cdot (\hat{\rho}_h \mathbf{U}) = 0, & (1.43) \end{cases}$$

$$\begin{cases} \frac{\partial p}{\partial t} + c^2 \nabla \cdot (\hat{\rho}_h \mathbf{U}) - \frac{c^2 N^2}{g} \mathbf{U} \cdot \mathbf{e}_3 = 0, & (1.44) \end{cases}$$

where N is the buoyancy frequency (Gill, 1982), defined by

$$N^2 = - \left(\frac{g^2}{c^2} + \frac{g}{\hat{\rho}_h} \frac{d\rho_h(z)}{dz} \right). \quad (1.45)$$

The system (1.42)-(1.44) is completed with the boundary conditions

$$\mathbf{U} \cdot \mathbf{n} = 0, \text{ on } z = z_b, \quad \frac{\partial p}{\partial t} = \rho_h g \mathbf{U} \cdot \mathbf{e}_3, \text{ on } z = 0. \quad (1.46)$$

The model (1.42)-(1.46) is significantly more complex than the models (1.25), (1.36), since it is written for five scalar unknowns \mathbf{U}, p, ρ , instead of one scalar unknown ϕ . On the other hand, this model is richer, as it includes the gravity and a vertical stratification for the background density and temperature. This generalisation allows to study the internal waves caused by the stratification of the fluid.

Inner and surface dispersion relations can be written for the system (1.42)-(1.46). Since the system is richer than the previous ones, the dispersion relations are more complex. The derivation and study of the dispersion relations for the three types of waves (acoustic, internal, surface) can be found in the paper by Auclair et al. (2021).

1.1.5 A model for acoustic waves in a flow: the Galbrun equation

The propagation of acoustic waves in a stratified flow can also be described with the Galbrun equation. It is obtained by the linearization of the system (1.4)-(1.11) written in Lagrangian coordinates. For its derivation, we refer to the very complete review from Maeder et al. (2020). The Galbrun equation is often written for the displacement, denoted \mathbf{d} , and reads (Maeder et al., 2020)

$$\rho_0 \frac{D^2 \mathbf{d}}{Dt^2} - \nabla p_0 \nabla^T \mathbf{d} + \nabla p_0 (\nabla \cdot \mathbf{d}) - \nabla (\rho_0 c_0^2 \nabla \cdot \mathbf{d}) = \mathbf{F},$$

where ρ_0 is the background density, p_0 is the background pressure, and \mathbf{F} is the source term. The derivative $D\mathbf{d}/Dt$ stands for

$$\frac{D\mathbf{d}}{Dt} = \frac{\partial \mathbf{d}}{\partial t} + (\nabla \mathbf{d}) \mathbf{U}_0. \quad (1.47)$$

The Galbrun usually arises in the modelling of acoustic waves in the air (Berriri, 2006; Legendre, 2003; Brazier, 2011) or in helioseismology (Chabassier and Duruflé, 2018). This equation is rarely

used for hydro-acoustic models, except in the work by Godin (2011). Most of the results are given for the harmonic problem, but there are also some studies focused on the evolution problem, such as the work by Bonnet-Bendhia et al. (2006) and Hägg and Berggren (2021). Bonnet-Bendhia et al. (2006) explain that because of the lack of a natural functional frame, one cannot directly show that the equation is well-posed. Instead, the mathematical analysis is done on a relaxed problem. A recent paper by Hägg and Berggren (2021) shows that the solutions to the Galbrun equation can be computed from the solution to another set of equations, called in their paper the linearized Euler's equations. They also show existence and uniqueness of solution to the linearized Euler's equations in the case of a mean flow tangential to the boundary.

1.2 Coupling with the earth and the gravito-elastic models

In this chapter, we present models from the literature describing the interaction between the earth and this ocean. The seabed is described by the equations of linear elasticity, that we briefly recall below. The various models differ mostly by the considered coupling between the fluid equations and the solid equations. The first model presented is the one commonly used for the tsunami generation, and is sometimes called passive approach or two-step method. We describe then models based on the two-step method, and extended to include more physical phenomenons. Fully coupled models, based on solving simultaneously the fluid and the solid equations, are then presented.

Context. The displacement of the seabed, for example an earthquake or a landslide, does not produce only surface waves and acoustic waves. Because the earth is not a rigid material, seismic waves are generated, and this affects both the propagation and generation of tsunami and hydro-acoustic waves.

The models (1.25), (1.36) and (1.42) for the propagation of hydro-acoustic and surface waves are all obtained with the assumption of a rigid seabed. However, it was shown by Nosov and Kolesov (2007) that the assumption of a rigid seabed creates, for the acoustic wavefield, significant differences with the field data. The models (1.14) and (1.15)-(1.16) describing the tsunami propagation are also derived with the assumption of a rigid seabed, and this assumption has some effect on the tsunami prediction (Richard et al., 2023; Abdolali et al., 2019), even if it is relatively small.

The generation of tsunami and acoustic waves are complex processes that are not well understood yet. Several studies (Dutykh and Dias, 2009; Abrahams et al., 2023) indicate that the shape and height of the tsunami wave near the tsunami source depend very much on the type of coupling considered with the earth. For the generation of hydro-acoustic waves it was noted by several authors (Krenz et al., 2021) that near the tsunami source it is very difficult to distinguish the acoustic and the seismic waves. To fully understand the generation mechanism, a description of the rupture in the earth is therefore needed (Lotto and Dunham, 2015).

The solid earth model. The earth is usually modelled as an elastic material (Dahlen and Tromp, 1998). The equations of linear elasticity for the velocity \mathbf{U} and the stress $\underline{\underline{\Sigma}}$ are

$$\begin{cases} \rho_0 \frac{\partial \mathbf{U}}{\partial t} - \nabla \cdot \underline{\underline{\Sigma}} = 0, & (1.48) \\ \frac{\partial \underline{\underline{\Sigma}}}{\partial t} = \lambda \operatorname{tr}(\underline{\underline{\epsilon}}(\mathbf{U})) \underline{\underline{I}} + 2\mu \underline{\underline{\epsilon}}(\mathbf{U}). & (1.49) \end{cases}$$

The tensor $\underline{\underline{\varepsilon}}$ is the linearized strain tensor,

$$\underline{\underline{\varepsilon}}(\mathbf{U}) = \frac{1}{2}(\nabla\mathbf{U} + \nabla\mathbf{U}^t).$$

The parameters λ and μ are the Lamé parameters. They are related to the pressure waves speed c_p and shear waves speed c_s by

$$\lambda = \rho_0(c_p^2 - c_s^2), \quad \mu = \rho_0 c_s^2. \quad (1.50)$$

When considering the coupling of the earth with the ocean, those equations are completed with coupling conditions stating that the normal velocity $\mathbf{U} \cdot \mathbf{n}$ and the traction $\boldsymbol{\tau} = \underline{\underline{\Sigma}} \cdot \mathbf{n}$ are continuous. We refer to Ciarlet (1988) and Dahlen and Tromp (1998) for the derivation of the equations (1.48)-(1.49). Note that those equations are written in Lagrangian coordinates, on the contrary to the Euler equations (1.4)-(1.6).

1.2.1 Generation of a tsunami: the passive approach

We start by giving a short description of the classical model used for the generation of a tsunami, sometimes called the "passive approach". An analysis of this model was made by Dutykh and Dias (2007) and Saito (2019). In the classical model, the earth model and the ocean model are solved separately.

In a first step, the deformation of the seabed is computed from models for the earth crust. The ocean is not taken into account here, hence the surface of the earth is considered as a free surface. The earthquake is modelled as a discontinuity of the velocity field along a surface or a line. The equations (1.48)-(1.49) together with the description of the discontinuity are solved. The seabed displacement is then deduced.

In a second step, the tsunami is computed. Either the seabed displacement is directly used as source term, or the free-surface displacement is computed from the seabed displacement and then used as a source term for computing the tsunami propagation (Kajiura, 1963).

With the passive approach, the model for the seabed and the model for the hydrodynamics are decoupled after the initial time. Moreover, this approach relies on the assumption that the seabed deformation is instantaneous. This is justified by the idea that in many cases, the rupture mechanism is very fast. However, it was suggested by several authors (Dutykh and Dias, 2009; Saito, 2019) that slower earthquakes can also generate tsunamis.

1.2.2 Models with partial coupling

We present three models extending the passive approach. The first one aims at taking into account the interaction with the earth during the tsunami propagation. The second one proposes a more precise description of the seabed deformation during the tsunami generation. The last model is an extension of the two-step approach to compute hydro-acoustic waves on the seabed.

Tsunami propagation over a porous layer. Some models propose to consider the seabed as a porous layer, to account for the damping caused by the earth. One of the early work on this subject was made by Chierici et al. (2010). By considering an incompressible layer made of sediments described with the Darcy equation, the authors show that the porous layer acts as a low-pass filter and modifies the spectral informations of the signal. The same approach is used in Abdolali et al.

(2015). The authors extend the depth-integrated model, originally derived by Sammarco et al. (2013) for a rigid bottom, to include the dissipation by a viscous compressible sediment layer. The obtained model is then used by Abdolali et al. (2017) to reproduce hydro-acoustic wavefields of the 2011 Tohoku-Oki tsunami.

Dynamical models for tsunami in incompressible water. Other models focus on the effect of the seabed change on the tsunami alone and neglect the water compressibility. Dutykh and Dias (2007, 2009) put the emphasis on the precise description of the source term. Instead of assuming that the seabed elevation is instantaneous as in the passive model, a dynamic process is considered. In their paper, Dutykh and Dias (2007) show that the dynamic approach and the passive approach predict different water levels and different shapes of the tsunami wave near the tsunami source. The seabed displacement b is given with the form

$$b(x, y, t) = b_0(x, y)g(t).$$

A semi-analytic expression for the static displacement b_0 is given and several time dependencies $g(t)$ are tested. The model for the fluid is the Laplace equation (1.14), which yields a semi-analytical expression for the free surface. The coupling of the earth and water models is done with the linearized kinematic condition on the seabed (1.14).

A more complex model is considered in the follow-up paper (Dutykh and Dias, 2009). Again, the coupling is done through the seabed displacement, but instead of an analytic expression, the displacement is deduced from an elastic earth model. The elastic equations are written as a second-order equation for the displacement,

$$\rho \frac{\partial^2 \mathbf{d}}{\partial t^2} - \nabla \cdot (\lambda(\nabla \cdot \mathbf{d})\underline{\underline{1}} + \mu\underline{\underline{\epsilon}}(\mathbf{d})) = 0. \quad (1.51)$$

The earthquake is generated by a discontinuity in displacement along a line for 2D problems, and on a surface for 3D problems. Similarly to the two-step approach, when computing the seabed displacement, the ocean is neglected and the seabed is assumed to be a free surface. The ocean is described with the non-linear shallow water model (1.15)-(1.16). The equations are solved numerically, with a finite element method for the earth, and a finite volume method for the water. Compared to the first paper (Dutykh and Dias, 2007), the seabed displacement generated by the earthquake is more accurate thanks to the elastic earth model.

Superposition method. Saito and Tsushima (2016) propose a method for synthesizing the ocean bottom pressure. Similarly to the passive approach, the method is divided into several steps. First the earthquake is simulated in the earth, using for example the elastic equations (1.48)-(1.49). The water layer is not taken into account for this step, and the earth surface is assumed free. In the second step, the tsunami is propagated by using the nonlinear shallow water equations. The seabed displacement is used as a source and the earth is assumed rigid in this step. Finally the results of the tsunami simulation and the seismic simulation are combined to compute the ocean bottom pressure p ,

$$p = p_{\text{static}} + p_{\text{dynamic}}, \quad p_{\text{static}} = \rho_0 g(\eta - u_z^{\text{bot}}), \quad p_{\text{dynamic}} = -\underline{\underline{\Sigma}}_{zz}^{\text{bot}}. \quad (1.52)$$

The static component p_{static} is computed from the sea surface height displacement η and the vertical sea bottom displacement u_z^{bot} . The dynamic component is computed from the stress tensor $\underline{\underline{\Sigma}}$. We refer to Saito (2019) for other related studies on the coupling between the hydro-acoustic waves, tsunami and seismic waves.

1.2.3 The fully coupled elastic-acoustic-gravity model

Thanks to increased computational resources, it is now possible to solve simultaneously the elastic equations in the earth and the gravito-acoustic equations in the ocean (Maeda and Furumura, 2013; Lotto and Dunham, 2015; Krenz et al., 2021; Lotto et al., 2019). Models coupling the hydro-acoustic waves and the elastic waves in the earth are already available and efficiently implemented (Komatitsch and Tromp, 1999). The main novelty of the models presented below is that they take the gravity into account, necessary to generate a tsunami.

A first model, proposed by Eyov et al. (2013) and further studied by Abdolali et al. (2019), is a system of linear wave equations for the fluid velocity potential and for the solid dilatation potential and rotation potential. By studying the associated dispersion relation, they show that the first acoustic-gravity mode is dominant.

This approach relies on the irrotationality assumption, and other models for more general velocity profiles were proposed. Maeda and Furumura (2013) assimilate the fluid-solid domain to an elastic medium with different Lamé coefficients λ, μ and different densities ρ in the fluid and the solid layer. In particular, $\mu = 0$ in the fluid layer. The free-surface displacement and the equilibrium with gravity at rest are explicitly added in the equations by introducing a quasi-static pressure. The equations of motions for the velocity \mathbf{U} and the stress tensor $\underline{\Sigma}$ read

$$\rho \frac{\partial \mathbf{U}}{\partial t} - \nabla \cdot \underline{\Sigma} = \rho_w g \begin{pmatrix} \partial_x \eta \\ \partial_y \eta \\ 0 \end{pmatrix}, \quad (1.53)$$

where ρ_w is the seawater density, assumed constant. Simulations in 2D and in 3D are presented for earthquakes with a slow rupture, that are good candidates to produce tsunamis. The simulations are also used to investigate whether the strength of the different waves are correlated to the source rupture time.

Another fully-coupled model is proposed by Lotto and Dunham (2015). The author extend the classical acoustic-elastic equations (Komatitsch and Tromp, 1999) to the tsunami generation by adding the surface equation for free-surface flows with gravity. In the earth, the equations for the elasticity are solved in the velocity-stress formulation (1.48)-(1.49). The ocean model consists in a linear system of equations for the velocity \mathbf{U} and the pressure p ,

$$\begin{cases} \rho \frac{\partial \mathbf{U}}{\partial t} + \nabla p = 0, & (1.54) \\ \frac{\partial p}{\partial t} + \rho c^2 \nabla \cdot \mathbf{U} = 0, & (1.55) \end{cases}$$

where c is the sound speed in water and ρ is the water density, both assumed constant. The earthquake is generated by a dislocation, namely a displacement discontinuity along a fault line. An energy equation and the dispersion relation for the fluid layer are given. The model is further studied by Krenz et al. (2021), which describes its implementation in the software SeisSol, a high-order earthquake simulation software based on a Discontinuous Galerkin method. The coupling between the elastic and the acoustic layers is ensured by the continuity of the normal velocity and the continuity of the traction.

In the study by Abrahams et al. (2023) four models are compared: the fully coupled model by Krenz et al. (2021), the passive approach, the dynamic approach, and the superposition method of Saito. The authors show formally that the superposition method is an approximation of the fully coupled model, with the simplifying assumptions that the water is incompressible and the pressure

change are hydrostatic and depth-independent. Then the four methods are compared numerically, with the implementation by Krenz et al. (2021) as the reference solution. They show that when assuming an elastic earth, the cutoff frequency that existed in the hydro-acoustic models vanishes.

A similar approach is proposed by Richard et al. (2023) to study the effect of the compressibility of the earth and of the ocean on the propagation of a tsunami. The earth is assimilated to a visco-elastic fluid with no gravity. For the ocean, a weakly compressible Boussinesq-type model is used. The authors show that the depth-integrated equations yield a hyperbolic system. They also study the energy equation and the dispersive effects of the system. Numerical approximations of the model show that taking the elasticity of the earth into account creates a delay and a distortion of the tsunami.

1.3 Water stratification, the SOFAR channel, and T-waves

Most of the models presented above, except for the model (1.42)-(1.46), do not consider in detail the stratification of the ocean at rest. We recall briefly the equations satisfied by a vertically stratified fluid at rest. The fluid is described by its density ρ_0 , its pressure p_0 and its temperature T_0 . The quantities are denoted with the subscript 0 to stress the fact that they are time-independent. Because of the effect of gravity, the fluid with density ρ_0 should have a pressure p_0 increasing with depth, such that

$$\nabla p_0 = -\rho_0 g \mathbf{e}_3.$$

Additionally, it is common in ocean models to consider a background temperature $T_0(z)$ varying with depth. The background density, temperature and pressure are also related by an equation of state of the form

$$f(\rho_0, \rho_0, T_0) = 0.$$

An equation of state for pure water is given as reference in IAPWS-SR7 (2009). It should be noted that for oceans the variations of salinity can also be included, which yields additional equations and a modified equation of state (Boittin, 2019). The speed of sound c_0 can be computed from the pressure, density and temperature profiles.

If the equation of state has the simpler form

$$f(\rho_0, \rho_0) = 0,$$

the fluid is said to be barotropic. For a barotropic fluid, the pressure is a function of the density only, or equivalently the variations of the temperature are neglected. The direct consequence of this assumption is that the sound speed is necessarily constant. We can note that most of the models presented above share the common assumption of a barotropic fluid. Even though the model (1.42)-(1.46) does not make this assumption, its study is done for a constant sound speed.

The variable sound speed and the SOFAR channel. In the ocean, the temperature varies with depth. The upper layers, heated by the sun, are generally warmer than the lower layers. A typical temperature profile in the ocean is shown in Figure 1.2. The combined effects of the temperature and pressure change yield a sound speed profile with a minimum around 1 km below the sea surface, see Figure 1.3-(a). Using ray theory, one can then show (Jensen et al., 2011) that there exists a layer around the depth of the sound speed minimum in which acoustic waves are trapped. If a ray enters this layer with a small incident angle, the change in velocity is such that the ray stays trapped

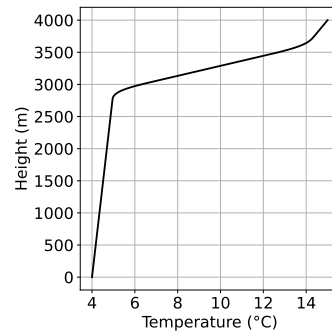


Figure 1.2: A typical profile for the temperature T_0

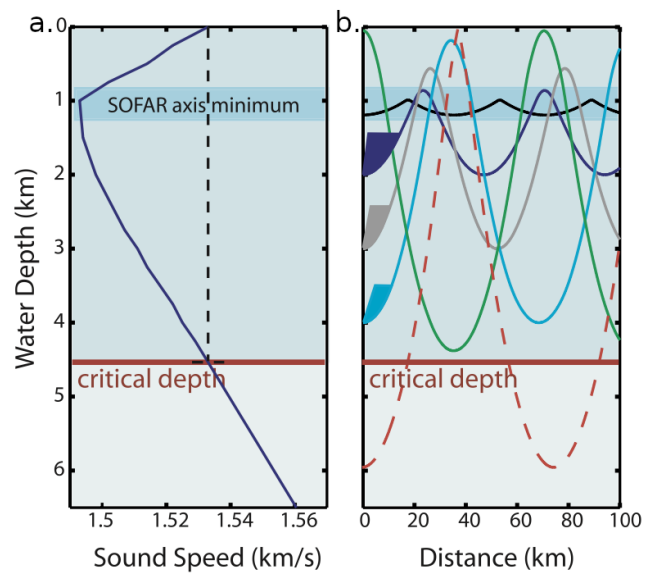


Figure 1.3: (a) A typical profile for the sound speed. (b) Ray path. Picture taken from Williams et al. (2006)

in the layer, see Figure 1.3-(b). The layer is called SOund Fixing And Ranging channel, or SOFAR channel.

The SOFAR channel acts as an open waveguide inside the ocean. When considering acoustic waves travelling over hundreds of kilometers, the reflexion on the sea surface and the seabed dissipates the energy. Since the waves trapped in the SOFAR channel never reach the surface of the seabed, they are much less dissipated than the waves outside of it. This mechanism is used by whales and submarine to propagate sound over very long distances. For the same reason, the hydro-acoustics sensors are sometimes located in the SOFAR channel (Caplan-Auerbach et al., 2001).

Possible application to tsunami early-warning system: the T-waves. A possible application of the SOFAR channel in the context of tsunami was investigated in studies by Ewing et al. (1950) and Okal et al. (2003). The application relies on the use of the tertiary waves, or T-waves. T-waves are the seismic waves converted into hydro-acoustic waves, and then propagated in the SOFAR channel. The generation mechanism of T-waves is an open question, and we refer to the thesis by Balanche (2010) for a description of the different proposed models. The main difficulty lies in the fact that waves can propagate in the SOFAR channel if they enter the channel with a relatively low angle (see Figure 1.3-(b)). This condition does not seem satisfied for acoustic waves coming from the seabed. The different models cited by Balanche (2010) give various explanations to solve this apparent contradiction.

1.4 Contributions of the thesis

The contributions of the thesis are organised in four chapters. We first present a model for the acoustic-gravity waves in a free-surface stratified ocean. Then, we prove that the model is well-posed, and introduce a potential-based formulation. We also present some numerical illustrations. The model is then extended in order to take interactions with the solid Earth into account. Finally, we present some preliminary work on numerical simulations for two geophysical applications, namely landslide-generated acoustic wavefields and wave trapping in the SOFAR channel.

1.4.1 A model for hydro-acoustic and gravity waves in a stratified free-surface flow

Chapter 2 reproduces a published paper (Dubois et al., 2023). In this chapter, we propose a model for the propagation of hydro-acoustic waves in a stratified, free-surface fluid. As mentioned earlier in this chapter, many models are already available in the literature. However, they all rely on some a priori modeling choices such as the irrotationality assumption or the barotropic assumption, and the validity of these assumptions is rarely addressed in the papers where they are used. To understand the consequences of some of these modeling choices, we intend on preserving as much of the physics as possible in the model we present.

We propose a method which consists in the linearization of the compressible Euler equations written in Lagrangian coordinates. The obtained equation is the Galbrun equation for a vanishing mean flow. One of the advantages of the Galbrun equation, compared to the linearized equations in Eulerian coordinates, is that the use of Lagrangian coordinates results in a more natural treatment of the boundary conditions. As a result, the continuity of displacement on the seabed and the description of the free-surface are obtained in a straightforward way.

The linearization is done around a state at equilibrium. The velocity, pressure, and density are respectively decomposed as $\mathbf{U}_0 + \mathbf{U}$, $p_0 + p$, and $\rho_0 + \rho$. In our case, the state at equilibrium has no mean flow hence $\mathbf{U}_0 = 0$. The state at equilibrium is described by a reference domain

$$\Omega(0) = \{(x, y, z) \in \mathbb{R}^3 \mid z_b(x, y) < z < H\}, \quad (1.56)$$

and the initial pressure, density and temperature satisfy

$$\nabla p_0 = \rho_0 \mathbf{g}, \quad \rho_0 = f_p(p_0, T_0), \quad \rho_0(H) = \rho^a, \quad (1.57)$$

where p^a is the constant atmospheric pressure. After linearization, we obtain the following system of equations written on the reference domain $\Omega(0)$,

$$\begin{cases} \rho_0 \frac{\partial \mathbf{U}}{\partial t} + \nabla p - (\nabla \mathbf{d})^T \nabla p_0 = \rho \mathbf{g}, & (1.58) \\ \frac{\partial \rho}{\partial t} + \rho_0 \nabla \cdot \mathbf{U} = 0, & (1.59) \\ \frac{\partial p}{\partial t} + \rho_0 c_0^2 \nabla \cdot \mathbf{U} = 0, & (1.60) \end{cases}$$

with the boundary conditions

$$\begin{cases} \mathbf{U} \cdot \mathbf{n}_b = u_b & \text{on } \Gamma_b, & (1.61) \\ p = 0 & \text{on } \Gamma_s. & (1.62) \end{cases}$$

The first boundary conditions is a non-penetration condition with a source term. It models the tsunami source as a displacement of the ocean bottom with velocity u_b . We denote by \mathbf{n}_b the unit vector normal to the bottom and oriented outwards. The second condition comes from dynamic condition, where we assume that the surface pressure $p_0 + p$ is at equilibrium with the atmospheric pressure p^a .

The problem (1.58)-(1.62) is formulated as a second-order system of equations,

$$\rho_0 \frac{\partial^2 \mathbf{U}}{\partial t^2} - \nabla (\rho_0 c_0^2 \nabla \cdot \mathbf{U} - \rho_0 g \mathbf{U} \cdot \mathbf{e}_3) - \nabla \cdot (\rho_0 g \mathbf{U}) \mathbf{e}_3 = 0, \quad \text{in } \Omega \times [0, T], \quad (1.63)$$

with boundary conditions

$$\mathbf{U} \cdot \mathbf{n}_b = u_b \quad \text{on } \Gamma_b \times [0, T], \quad \nabla \cdot \mathbf{U} = 0 \quad \text{on } \Gamma_s \times [0, T], \quad (1.64)$$

and vanishing initial conditions. This wave-like formulation gives a suitable framework for the mathematical analysis of the model, which we will present in Chapter 3. It also allows us to use numerical solvers dedicated to wave propagation problems. Finally, from the wave-like formulation (1.63)-(1.64), we deduce an energy equation associated to the system. We define the following quadratic functional,

$$\begin{aligned} \mathcal{E} = \int_{\Omega} \rho_0 \frac{1}{2} \left| \frac{\partial \mathbf{U}}{\partial t} \right|^2 dx + \frac{1}{2} \int_{\Omega} \rho_0 \left(c_0 \nabla \cdot \mathbf{U} - \frac{g}{c_0} \mathbf{U} \cdot \mathbf{e}_3 \right)^2 dx \\ + \frac{1}{2} \int_{\Omega} \rho_0 N_b (\mathbf{U} \cdot \mathbf{e}_3)^2 dx + \frac{1}{2} \int_{\Gamma_s} \rho_0 g (\mathbf{U} \cdot \mathbf{e}_3)^2 d\sigma, \end{aligned} \quad (1.65)$$

where the scalar N_b is defined by

$$N_b(z) = - \left(\frac{g^2}{c_0(z)^2} + g \frac{\rho_0'(z)}{\rho_0(z)} \right). \quad (1.66)$$

For physical reasons, the scalar N_b should be positive, which requires additional conditions on the choice of the initial conditions ρ_0, ρ_0 and T_0 . The square root of N_b , denoted N , is called the buoyancy frequency, or Brunt-Väisälä frequency. Then the functional \mathcal{E} is positive, and satisfies

$$\frac{d}{dt}\mathcal{E} = \text{source terms.} \quad (1.67)$$

We then show how the system (1.63)-(1.64) is related to other hydrodynamic and acoustic models. Let us first consider the barotropic assumption, namely the assumption that the pressure and the density are related by $p = c^2\rho$, where the sound speed c is constant. With this additional assumption, we show that the flow has a constant curl and that for irrotational initial data, the flow is irrotational. The flow is then described by the potential ψ such that $\mathbf{U} = \nabla\psi$. The wave equation reduces then to a scalar equation for the potential,

$$\begin{cases} \frac{\rho_0}{c_0^2} \frac{\partial^2 \psi}{\partial t^2} - \nabla \cdot (\rho_0 \nabla \psi) = 0, & \text{in } \Omega, & (1.68) \\ \nabla \psi \cdot \mathbf{n} = u_b & \text{on } \Gamma_b, & (1.69) \\ c_0^2 \Delta \psi = \frac{\partial^2 \psi}{\partial t^2} + g \frac{\partial \psi}{\partial z} = 0, & \text{on } \Gamma_s. & (1.70) \end{cases}$$

This system was studied by Longuet-Higgins (1950).

We now turn our attention to other types of simplified models, and consider two asymptotic regimes related to the low-Mach limit. The equation (1.63) is written in a non-dimensional form. First, by choosing characteristic scales adapted to the surface waves, we obtain the incompressible limit of the equation (1.63). Then, by repeating the process for acoustic waves, we obtain the acoustic limit. In the incompressible limit, the velocity \mathbf{U} is given by

$$\frac{\partial^2 \mathbf{U}}{\partial t^2} = -\frac{g}{\rho_0} \nabla \varphi,$$

and the function φ is solution to

$$\begin{cases} \Delta \varphi = 0, & \text{in } \Omega, & (1.71) \\ \nabla \varphi \cdot \mathbf{n} = -\rho_0 g u_b, & \text{on } \Gamma_b, & (1.72) \\ \frac{\partial^2 \varphi}{\partial t^2} + g \frac{\partial \varphi}{\partial z} = 0, & \text{on } \Gamma_s. & (1.73) \end{cases}$$

We recover the model (1.14), which is the classical description for irrotational free-surface flows.

In the acoustic limit, the velocity \mathbf{U} is given by $\mathbf{U} = \nabla\psi$, and the potential ψ is solution to

$$\begin{cases} \frac{\partial^2 \psi}{\partial t^2} - \rho_0 c_0^2 \nabla \cdot (\rho_0^{-1} \nabla \psi) = 0, & \text{in } \Omega, & (1.74) \\ \nabla \psi \cdot \mathbf{n} = u_{b,1}, & \text{on } \Gamma_b & (1.75) \\ \psi = 0, & \text{on } \Gamma_s. & (1.76) \end{cases}$$

We also give energy equations for each case. Another model for which a comparison is interesting is the current state-of-the-art model (1.25) for the propagation of hydro-acoustic waves. The model (1.25) can be seen as the acoustic limit (1.74), with an additional term of the form $g\partial_z\psi$ on the surface condition. This additional term is negligible when considering the acoustic limit, but is kept to couple the acoustic waves and the surface gravity waves.

Finally, we write the dispersion relation for the system, with depth-dependent temperature and sound speed profiles. The dispersion relation between the vertical wave-number k_z , the horizontal wave-number k_x and the frequency ω is

$$k_z^2 + k_x^2 \frac{N^2 - \omega^2}{\omega^2} + \frac{\omega^2}{c_0^2} - \frac{1 + 2D'}{4D^2} - \frac{1}{2}\omega^2 S' + S \left(\frac{g}{c_0^2} + \frac{N^2}{g} \frac{\omega^2}{\omega^2 - c_0^2 k_x^2} - \frac{\omega^2}{2D} - \frac{1}{4}\omega^4 S \right) = 0, \quad (1.77)$$

where $S = 2c_0'/c_0$ and $D = \rho_0'/\rho_0$ are length scales associated respectively to the variations of sound speed and background density. The equation (1.77) is a generalization of the dispersion relation obtained by Auclair et al. (2021) to the case of a non-constant sound speed. We numerically show that the stratification has an effect on the dispersion profiles.

In this chapter, we have derived a system describing the propagation of acoustic-gravity waves in a free-surface fluid. One of the main differences with the models available in the literature is the use of Lagrangian coordinates, which yields a correct description of the free-surface flow. Moreover, relatively few assumptions are being made, and some widespread hypotheses, e.g. the barotropic or irrotational character of the flow, were avoided. Thanks to this approach, many terms representing different physical phenomena are kept in the wave-like equation. This is well illustrated in the dispersion relation associated to the system. We also clearly identify the assumptions allowing us to deduce models well-established in the literature from the presented model. Finally, the wave-like formulation of the model makes studying its well-posedness convenient, as well as its discretization using a finite element method. This is the purpose of Chapter 3.

1.4.2 Mathematical analysis and numerical approximation of the model.

Chapter 3 presents the mathematical analysis of the model derived in Chapter 2. The model consists in a second-order wave-like equation for the velocity \mathbf{U} ,

$$\rho_0 \frac{\partial^2 \mathbf{U}}{\partial t^2} - \nabla \cdot (\rho_0 c_0^2 \nabla \cdot \mathbf{U} - \rho_0 g \mathbf{U} \cdot \mathbf{e}_3) - \nabla \cdot (\rho_0 g \mathbf{U}) \mathbf{e}_3 = 0, \quad \text{in } \Omega \times [0, T], \quad (1.78)$$

completed with the following boundary conditions

$$\mathbf{U} \cdot \mathbf{n}_b = u_b \quad \text{on } \Gamma_b \times [0, T], \quad \nabla \cdot \mathbf{U} = 0 \quad \text{on } \Gamma_s \times [0, T], \quad (1.79)$$

and vanishing initial conditions. This equation can be seen as a simplified case of the Galbrun equation, when the mean flow vanishes. From previous works on the Galbrun equation with a vanishing mean flow, we know that the natural space for the discretization is $H(\text{div}, \Omega)$, and that the problem is well-posed if the source term is located in the volume (Legendre, 2003; Berriri, 2006). In this case, the boundary conditions are homogeneous.

The first contribution of this chapter is the presentation of an equivalent "dual" formulation for the propagation of acoustic-gravity waves. To simplify the presentation here, we consider here volumic source terms. Formally, we call "primal" formulation, or velocity-based formulation, the Galbrun equation with no mean flow and written for the velocity \mathbf{U} ,

$$\frac{d^2 \mathbf{U}}{dt^2} + G^* G \mathbf{U} = \mathbf{F}_U. \quad (1.80)$$

Here, \mathbf{F}_U is a volume source term. The operator G is an unbounded operator with adjoint G^* . The operator G is defined by its domain $\mathcal{D}(G)$,

$$\mathcal{D}(G) = \{\mathbf{U} \in H(\operatorname{div}, \Omega), \mid \mathbf{U} \cdot \mathbf{n}_b = 0 \text{ on } \Gamma_b, \mathbf{U} \cdot \mathbf{n}_s \in L^2(\Gamma_s), \},$$

and by

$$\forall U \in \mathcal{D}(G), \quad G\mathbf{U} := \begin{pmatrix} c_0^2 \left(\nabla \cdot \mathbf{U} - \frac{g}{c_0^2} \mathbf{U} \cdot \mathbf{e}_z \right) \\ N\mathbf{U} \cdot \mathbf{e}_3 \\ -g\gamma_{1,s}(\mathbf{U}) \end{pmatrix}, \quad (1.81)$$

where $\gamma_{1,s}$ denotes the normal trace on the surface Γ_s . Similarly, we will use later $\gamma_{1,b}$, the normal trace on the bottom Γ_b . We show then that the adjoint G^* , with domain $\mathcal{D}(G^*)$, is defined by

$$\mathcal{D}(G^*) = \{\Phi = (\varphi, \psi, \gamma) \in H^1(\Omega) \times L^2(\Omega) \times L^2(\Gamma_s) \mid \nabla \varphi \cdot \mathbf{n}_b = 0 \text{ on } \Gamma_b, \varphi = \gamma \text{ on } \Gamma_s\},$$

and has the expression

$$\forall \Phi \in \mathcal{D}(G^*), \Phi = (\varphi, \psi, \gamma), \quad G^*\Phi = -\nabla \varphi + N \left(\psi + \frac{N}{g} \varphi \right) \mathbf{e}_z. \quad (1.82)$$

We call "dual formulation", or potential formulation, the following equation,

$$\frac{d^2 \Phi}{dt^2} + GG^*\Phi = \mathbf{F}_\Phi, \quad (1.83)$$

where \mathbf{F}_Φ is a source term. The two formulations are equivalent in the sense that if Φ is solution to (1.83), then $\mathbf{U} = G^*\Phi$ is solution to (1.80) for the source term $\mathbf{F}_U = G^*\mathbf{F}_\Phi$. The new variable Φ can be seen as a generalized potential for the velocity.

One of the advantages of the formulation (1.83) lies in the numerical approximation of the equations. Indeed, the natural space for \mathbf{U} is $H(\operatorname{div}, \Omega)$ with an homogeneous essential boundary condition. From a numerical perspective, the approximation of the velocity-based formulation requires to discretize the space $H(\operatorname{div}, \Omega)$, and to impose the essential boundary condition. On the other hand, the variable Φ is in $H^1(\Omega) \times L^2(\Omega)$, whose discretization is easier. Moreover, the boundary condition is of Neumann type, and is therefore naturally present in the variational formulation. Finally, the velocity-based formulation requires two (if $\Omega \subset \mathbb{R}^2$) or three (if $\Omega \subset \mathbb{R}^3$) unknowns, whereas Φ only requires two, since the last component is directly deduced from the first one.

The second contribution is related to the boundary conditions. The Galbrun equation is often studied with homogeneous boundary conditions; however, in our case, the relevant boundary condition is non-homogeneous, due to the source term. The weak formulation then reads:

$$\begin{cases} \frac{d^2}{dt^2} (\mathbf{U}, \tilde{\mathbf{U}})_{\mathcal{H}} + (\tilde{G}\mathbf{U}, G\tilde{\mathbf{U}})_{\mathcal{G}} = 0, & \forall \tilde{\mathbf{U}} \in \mathcal{D}(G), \quad \text{in } \mathcal{D}'(0, T), \\ \gamma_{1,s}(\mathbf{U}) = u_b, & \text{on } \Gamma_b \text{ in } \mathcal{D}'(0, T). \end{cases} \quad (1.84)$$

$$(1.85)$$

Here, $(\cdot, \cdot)_{\mathcal{H}}$ and $(\cdot, \cdot)_{\mathcal{G}}$ denote the scalar product on the Hilbert spaces \mathcal{H}, \mathcal{G} , defined by

$$\mathcal{H} = L^2(\Omega)^3, \quad \mathcal{G} = H^1(\Omega) \times L^2(\Omega) \times L^2(\Gamma_s), \quad (1.86)$$

respectively equipped with the weighted norms

$$\|\mathbf{U}\|_{\mathcal{H}} = \left(\int_{\Omega} \rho_0 |\mathbf{U}|^2 dx \right)^{1/2}, \quad (1.87)$$

$$\|\Phi\|_{\mathcal{G}} = \left(\int_{\Omega} \frac{\rho_0}{c_0^2} \varphi^2 dx + \int_{\Omega} \rho_0 \psi^2 dx + \int_{\Gamma_s} \frac{\rho_0}{g} \gamma^2 ds \right)^{1/2}, \quad \Phi = (\varphi, \psi, \gamma)^t. \quad (1.88)$$

We have also introduced the extension \tilde{G} of the operator G . The extension is defined on the domain

$$\mathcal{D}(\tilde{G}) = \{\mathbf{U} \in H(\operatorname{div}, \Omega), \mid \mathbf{U} \cdot \mathbf{n} \in L^2(\partial\Omega)\},$$

and has the same expression as G . To show the existence of solutions to (1.84)-(1.85), a first idea would consist in lifting the source term. However, finding a lifting operator is far from trivial. Instead, we introduce a relaxed problem for a new unknown. Assume that the solution \mathbf{U} to (1.80) exists and let \mathbf{U}_α be defined by

$$\mathbf{U}_\alpha(t) = e^{-\alpha t} \mathbf{U}(t).$$

The equation satisfied by \mathbf{U}_α reads then

$$\begin{cases} \frac{d^2}{dt^2}(\mathbf{U}_\alpha, \tilde{\mathbf{U}})_{\mathcal{H}} + 2\alpha \frac{d}{dt}(\mathbf{U}_\alpha, \tilde{\mathbf{U}})_{\mathcal{H}} + (\tilde{G}_\alpha \mathbf{U}_\alpha, G_\alpha \tilde{\mathbf{U}})_G = 0, & \forall \tilde{\mathbf{U}} \in \mathcal{D}(G), \quad \text{in } \mathcal{D}'([0, T]), \quad (1.89) \\ \gamma_{1,b}(\mathbf{U}_\alpha) = e^{-\alpha t} u_b, & \text{in } \mathcal{D}'([0, T]), \quad (1.90) \end{cases}$$

where the operator $G_\alpha : \mathcal{D}(G) \subset \mathcal{H} \rightarrow \mathcal{G} \times \mathcal{H}$ is defined by

$$\forall \mathbf{U} \in \mathcal{D}(G), \quad G_\alpha \mathbf{U} := \begin{pmatrix} G\mathbf{U} \\ \alpha \mathbf{U} \end{pmatrix}.$$

A lifting operator is defined for the new formulation (1.89)-(1.90). The lifting operator $L(u_b)$ of a function u_b defined on the boundary is

$$L_\alpha(u_b) = -G_\alpha^* \Phi_b,$$

where $\Phi_b \in \mathcal{D}(G_\alpha^*)$ is the solution to an elliptic problem, written with the new operator G_α^* , and dependent on u_b . Since the operator G_α^* has a closed range, showing the existence and uniqueness of solutions to the elliptic problem is rather direct. The solution to the problem (1.89)-(1.90) is then classically obtained by defining $\mathbf{U}_{\alpha,0}$ as the solution to the problem

$$\frac{d^2}{dt^2}(\mathbf{U}_{\alpha,0}, \tilde{\mathbf{U}})_{\mathcal{H}} + 2\alpha \frac{d}{dt}(\mathbf{U}_{\alpha,0}, \tilde{\mathbf{U}})_{\mathcal{H}} + (G_\alpha \mathbf{U}_{\alpha,0}, G_\alpha \tilde{\mathbf{U}})_G = e^{-\alpha t} \left(\frac{d^2}{dt^2} L_\alpha(u_b) - \alpha^2 L_\alpha(u_b), \tilde{\mathbf{U}} \right)_{\mathcal{H}}, \quad (1.91)$$

and by setting $\mathbf{U}_\alpha = \mathbf{U}_{\alpha,0} + G^* L_\alpha(u_b)$. The existence of a solution to the relaxed problem (1.89)-(1.90) implies the existence of a solution to (1.84)-(1.85).

The equivalence between the velocity formulation (1.80) and the potential formulation (1.83) is then shown. It is first proved for the relaxed formulations; then, for the non-relaxed formulations it is obtained by passing the relaxation parameter α to the limit $\alpha \rightarrow 0$. This last step requires the use of some energy estimates.

Finally, we show a numerical approximation for a simple test case in 2D in order to illustrate the equivalence between the two models. Convergence tests indicate that the potential formulation requires less degrees of freedom than the velocity formulation. This is an additional argument in favor of the potential-based formulation.

This chapter gives an adapted functional framework for the analysis of the model presented in Chapter 2. We also introduce a novel approach for the study of the Galbrun equation, in the particular case of a vanishing mean flow, by defining a potential-based formulation. This new formulation offers several advantages compared to the classical velocity-based model, both from a mathematical and a computational point of view. Additionally, the new variable Φ yields a natural decomposition for the velocity \mathbf{U} ,

$$\mathbf{U} = G^* \Phi = G^* \begin{pmatrix} \varphi \\ \psi \\ \gamma \end{pmatrix} = -\nabla \varphi + N \left(\psi + \frac{N}{g} \varphi \right) \mathbf{e}_3. \quad (1.92)$$

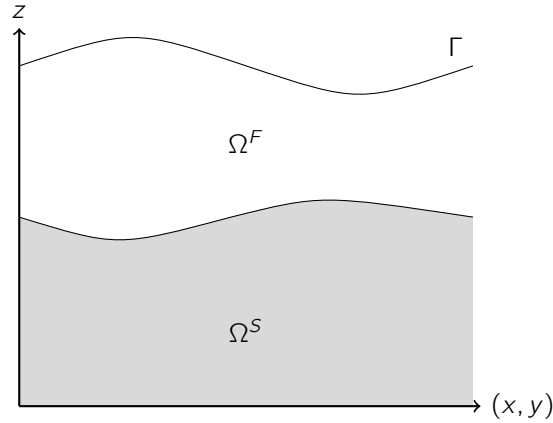


Figure 1.4: The domain Ω , made of two layers: the fluid layer Ω^F and the solid layer Ω^S . The boundary of the domain is Γ .

In this decomposition, $\nabla\varphi$ is the irrotational part of the velocity. The decomposition could be used to quantify the rotational part of the velocity, which is often neglected in hydro-acoustic models.

1.4.3 Gravito-elastic equations

The work presented in this chapter is ongoing. In the previous chapters, the seabed was assumed to be a rigid-body solid. In Chapter 4, we enrich the model by considering it an elastic half-plane representing the earth below the fluid layer, representing the ocean. As presented in the previous sections, such models exist in the literature, but have rarely been the subject of thorough mathematical analysis.

The main contribution of this chapter is the mathematical analysis of the fully coupled model with acoustic waves in water, seismic waves in the earth, and gravity. Realistic simulations have been presented in recent studies (see 1.2), but only rarely is a mathematical analysis presented alongside them. The mathematical analysis for the whole Earth with an arbitrary number of fluid and solid layers can be found in the paper by Valette (1986), and in the working paper by de Hoop et al. (2017). The studied model in both papers is very general, which makes it quite difficult to read.

We consider a simpler case with only one layer of fluid and one homogeneous layer of solid. Moreover, since we are interested in tsunamis generation and propagation, only a portion of the earth is considered, and is assumed small enough to neglect the earth curvature. With these simplifications, the system is an infinite fluid layer above an elastic half plane, with a topography between the two layers (see Figure 1.4). The fluid-solid system is modeled as one elastic domain, with different parameters for the fluid and solid layers. Starting from the equations of motions for a prestressed elastic domain, and using the same linearization method as in Chapter 2, we derive a linear system describing the coupled motion of the fluid and the solid. The effect of gravity induces a pre-stress, which makes the considered equation differ from the classical elastic-acoustic coupling. In this model, the velocity \mathbf{U} is solution to the system of second-order partial differential equations,

$$\rho_0 \frac{\partial^2 \mathbf{U}}{\partial t^2} - \nabla \cdot (\partial_t \underline{\underline{P}}) = \mathbf{F}, \quad (1.93)$$

where \mathbf{F} is a source term; and $\underline{\underline{P}}$ is the incremental first Piola-Kirchhoff stress tensor. It is explicitly written in terms of \mathbf{U} ,

$$\partial_t \underline{\underline{P}} = (\rho_0 c_0^2 \nabla \cdot \mathbf{U} - \rho_0 (\nabla \cdot \underline{\underline{U}}_l - \nabla \mathbf{U}^t)) \chi_F + (\underline{\underline{A}} : \underline{\underline{\varepsilon}}(\mathbf{U}) + \nabla \mathbf{U} \underline{\underline{P}}_0) \chi_S. \quad (1.94)$$

Here, ρ_0 is the background density, $\underline{\underline{P}}_0$ is the initial stress, also called static stress or prestress, and $\underline{\underline{\varepsilon}}(\mathbf{U}) = 1/2(\nabla \mathbf{U} + \nabla \mathbf{U}^t)$. In the fluid, the static stress reads $\underline{\underline{P}}_0 = -\rho_0 \underline{\underline{I}}$, where ρ_0 is the background fluid pressure. The background sound speed in the fluid is denoted c_0 , and can be depth-dependant. The fourth-order tensor $\underline{\underline{A}}$ acting on $\underline{\underline{\varepsilon}}$ is obtained from the linearization of the constitutive equation. The functions χ_F, χ_S are indicator functions, respectively for the fluid and the solid domain.

The system is completed with the boundary condition on the surface,

$$\partial_t \underline{\underline{P}} \cdot \mathbf{n} = 0 \quad \text{on } \Gamma, \quad (1.95)$$

where \mathbf{n} is the unit vector normal to the surface Γ . A first variational formulation is obtained by looking for a solution $\mathbf{U}(t) \in H^1(\Omega)$, and testing the system (1.93) against a function $\tilde{\mathbf{U}} \in H^1(\Omega)$. The variational formulation then reads: find $\mathbf{U}(t) \in H^1(\Omega)$ such that

$$\begin{aligned} (\rho_0 \partial_{tt}^2 \mathbf{U}(t), \tilde{\mathbf{U}})_{L^2(\Omega)^3} + \int_{\Omega^F} ((\rho_0 c_0^2 - \rho_0) \nabla \cdot \mathbf{U}(t) \underline{\underline{I}} + \rho_0 \nabla \mathbf{U}(t)^t) : \nabla \tilde{\mathbf{U}} \, dx \\ + \int_{\Omega^S} (\underline{\underline{A}} : \underline{\underline{\varepsilon}}(\mathbf{U}(t)) + \nabla \mathbf{U}(t) \underline{\underline{P}}_0) : \nabla \tilde{\mathbf{U}} \, dx = (\mathbf{F}, \tilde{\mathbf{U}})_{\mathcal{H}}. \quad \forall \tilde{\mathbf{U}} \in H^1(\Omega). \end{aligned} \quad (1.96)$$

Although the obtained variational formulation is convenient for numerical approximations, it is not clear whether it is adapted to show the existence and uniqueness of weak solutions. Indeed, the associated bilinear form is not coercive. We reformulate the problem by introducing a fictitious hydrostatic pressure in the solid near the fluid-solid interface. We also introduce the functional space

$$\mathcal{V} := \{\mathbf{U} \in H(\text{div}, \Omega) \mid \mathbf{U}|_{\Omega^S} \in H^1(\Omega^S), \gamma_1(\mathbf{U}) \in L^2(\Gamma)\}. \quad (1.97)$$

where γ_1 is the normal trace on the surface Γ . The variational formulation reads: find $\mathbf{U}_1 \in \mathcal{V}$ such that

$$\frac{d^2}{dt^2} (\rho_0 \mathbf{U}, \tilde{\mathbf{U}})_{L^2(\Omega)^3} + a(\mathbf{U}, \tilde{\mathbf{U}}) = (\mathbf{F}, \tilde{\mathbf{U}})_{L^2(\Omega)^3}, \quad \forall \tilde{\mathbf{U}} \in \mathcal{V}, \quad (1.98)$$

where a is a symmetric bilinear form satisfying the property

$$a(\mathbf{U}, \mathbf{U}) + \lambda \|\mathbf{U}\|_{L^2(\Omega)}^2 \geq \|\mathbf{U}\|_{\mathcal{V}}^2. \quad (1.99)$$

We show then that this second variational formulation is well-posed, provided that some conditions on the initial stress are met. Moreover, the energy equation

$$\frac{d}{dt} \left(\frac{1}{2} (a(\mathbf{U}, \mathbf{U}) + \|\partial_t \mathbf{U}\|_{L^2(\Omega)}^2 + \alpha \|\mathbf{U}\|_{L^2(\Omega)}^2) \right) = (\mathbf{F}, \partial_t \mathbf{U})_{L^2(\Omega)} + \frac{d}{dt} \left(\frac{\alpha}{2} \|\mathbf{U}\|_{L^2(\Omega)}^2 \right). \quad (1.100)$$

gives us a priori estimates for the solution.

We conclude this chapter with a numerical illustration, namely the simulation of a tsunami generated by a double couple source in the earth.

The model developed in this chapter is a new model for the coupled propagation of acoustic, gravity and seismic waves. The use of Lagrangian coordinates in the fluid layer ensures that the transmission condition between the fluid and the solid is preserved during the linearization. Taking

gravity into account induces a prestress, which makes the analysis more complex. We show that the model is well-posed and give a priori estimates. To our knowledge, this was not done for any other fully-coupled models. The numerical simulation serves as a preliminary validation of the model, by comparing it with simulations from the literature.

1.4.4 Preliminary results for geophysical applications

This chapter presents a preliminary work. The model developed in Chapter 2 is used to simulate two physical phenomena: the generation of acoustic waves by an underwater landslide, and the wave trapping SOFAR channel (described in Section 1.3). The literature on the numerical approximation for both applications is relatively scarce, in particular when one wants to consider the coupling with water waves.

For the first application, we partially reproduce experimental data studied by Caplan-Auerbach et al. (2014), namely the spectrogram of pressure fields recorded during a landslide. The spectrogram of the recorded pressure contains an interference pattern that is characteristic of those underwater landslides, caused by the sound reflecting on the surface. Preliminary simulations reproduce a similar interference pattern in a simplified case. This first result was presented in a talk at the European Geoscience Union General Assembly ¹.

The second application is the trapping of acoustic waves in the SOFAR channel. The SOFAR channel is an open waveguide which can be found in the ocean for particular sound speed profiles. To synthesize the corresponding pressure field, either the ray theory or the normal mode theory can be used. However, the first one is valid in high frequency approximations only, and the second one is generally used for point sources. We show here that the SOFAR channel can be reproduced with our model for various cases. The first case is a canonical example, where the source is located in the channel axis. The second case is a preliminary result, working towards the simulation of seismic waves first converted into hydro-acoustic waves at the solid-fluid interface, and then trapped in the SOFAR channel. In this preliminary simulation, we show that waves generated near the seabed, away from the channel axis, can be trapped in the SOFAR channel.

For both of the considered applications, there are, to our knowledge, either few or no simulations available in the literature. The simulations presented here can help provide a better representation of the acoustic waves propagation in a complex medium with a stratification and a topography.

¹<https://doi.org/10.5194/egusphere-egu23-15937>

Modelling of acoustic and surface gravity waves in a stratified ocean

Contents

2.1	Introduction	30
2.2	Linearization of compressible Euler equations in Lagrangian coordinates	32
2.2.1	Euler equations in Eulerian coordinates	32
2.2.2	Lagrangian description	35
2.2.3	Linearization and wave equation	37
2.3	Derivation of simplified models	40
2.3.1	The barotropic case	40
2.3.2	Two asymptotic regimes of the system	42
2.4	The model in Eulerian coordinates	49
2.4.1	General method	49
2.4.2	The model in Eulerian coordinates	51
2.5	Dispersion relation	53
2.6	Conclusion and future work	57
Appendix		57
A	Derivation of the energy equation	57
B	From the Lagrangian to the Eulerian coordinates	59

This chapter reproduces the following paper: J. Dubois, S. Imperiale, A. Mangeney, F. Bouchut, and J. Sainte-Marie. Acoustic and gravity waves in the ocean: a new derivation of a linear model from the compressible Euler equation. *Journal of Fluid Mechanics*, 970, 2023. doi: <https://doi.org/10.1017/jfm.2023.595>

Abstract: In this paper, we construct an accurate linear model describing the propagation of both acoustic and gravity waves in water. This original model is obtained by the linearization of the compressible Euler equations, written in Lagrangian coordinates. The system is studied in the isentropic case, with a free surface, an arbitrary bathymetry, and vertical variations of the background temperature and density. We show that our model is an extension of some models from the

literature to the case of a non-barotropic fluid with a variable sound speed. Other models from the literature are recovered from our model through two asymptotic analyses, one for the incompressible regime and one for the acoustic regime. We also propose a method to write the model in Eulerian coordinates. Our model includes many physical properties, such as the existence of internal gravity waves or the variation of the sound speed with depth.

2.1 Introduction

Several authors have proposed to use the propagation of acoustic waves in the ocean to detect tsunamis, as sound travels in water at approximately 1500 m s^{-1} and the velocity of a tsunami wave is approximately 300 m s^{-1} (Constantin, 2009). The existence of hydro-acoustic signals generated by tsunami sources such as earthquakes or landslides was shown by Tolstoy (1950). This motivates the mathematical modelling of the propagation of both surface waves – the tsunami – and underwater acoustic waves, also called hydroacoustic waves, in a compressible formulation.

The idea of using acoustic-gravity waves for tsunami early-warning systems dates back to 1950 (Ewing et al., 1950). A more recent study (Stiassnie, 2010) indicates that the pressure variations induced by the tsunami are significant enough to be used for the improvement of the tsunami early-warning systems.

For the description of the propagation of sound in water, the most common model is a linear wave equation for the fluid potential, i.e. for an irrotational flow (Jensen et al., 2011). When both surface and acoustic waves are considered, different types of models are available. In his work, Stiassnie (2010) studies the acoustic equation for the fluid potential coupled with a free-boundary condition. The three-dimensional acoustic equation is analysed by Nosov and Kolesov (2007) and a depth-integrated version is proposed by Sammarco et al. (2013) to reduce the computational costs. This approach was further developed in a series of papers (Cecioni et al., 2014; Abdolali et al., 2015; Gomez and Kadri, 2021).

Another approach was proposed by Longuet-Higgins (1950) where the equation is still on the fluid potential, but includes a gravity term. This equation, including second-order terms, made it possible for the first time to explain the seismic noise generated worldwide by wave interactions in the ocean Stutzmann et al. (2012). This model was also the starting point of an extensive work to describe the nonlinear interactions between acoustic and gravity waves (Kadri and Stiassnie, 2013). In other works, such as those of Smith (2015) and Auclair et al. (2021), the flow is not assumed irrotational, so that the equations are written for the fluid velocity. They include gravity terms and a vertical stratification for the background density, temperature and salinity. This generalization allows to study the internal waves caused by the stratification of the fluid, and dispersion relations for the three types of waves (acoustic, internal, surface) are obtained.

The above cited works share one or several of the following assumptions : irrotational flow, homogeneous background density or barotropic fluid, and a constant speed of sound. These modeling choices have a strong influence on the structure of the equations, resulting in a variety of tools for their analysis and their numerical approximation. For example, the irrotationality assumption allows to reduce the number of unknowns, but the validity of this assumption in the compressible case is not clear. Furthermore, in the models that do not assume irrotational flow, the bed is assumed to be flat, even though bed variations are a key element impacting tsunami and acoustic wave propagation (Caplan-Auerbach et al., 2014). In the ocean, the choice of a constant sound speed may be not appropriate since the variation of the sound speed creates the SOFAR channel, a horizontal

strip in which the acoustic waves propagate with very little energy loss. Quantifying the impact of these approximations requires the use of simulations based on a more complete model. Finally, the free-surface equation induces a strong nonlinearity in the system. Indeed, the domain on which the equations are written depends on the solution to the equations. The common approach for the linearization of the system consists in writing the linear equations on the unperturbed domain. However, by doing so, an approximation on the domain is made, in addition to the approximation made on the solution. It is not clear how to quantify the magnitude of the error made by the two combined approximations.

The aim of this work is to address these modelling choices by deriving an accurate linear model as rigorously as possible with only very few assumptions for hydro-acoustic, internal and surface waves propagating in a fluid over an arbitrary bathymetry. Salinity, thermal dissipation and viscosity are neglected, and to linearize the equations, we assume that the ocean is at equilibrium and at rest before the earthquake or landslide occurs, and that the tsunami source induces a small displacement of the water. In this model, the speed of sound results from the imposed background temperature profile, so that the effects of the SOFAR channel on the propagation of the hydroacoustic waves are naturally present. The obtained model is comparable to the model of Auclair et al. (2021); however, our model includes a bathymetry and a variable sound speed. Moreover, our approach differs on several aspects as follows.

- The problem is formulated as a second-order equation, which allows the use of numerical solver dedicated to wave propagation problem such as Specfem (Komatitsch and Tromp, 1999). Specfem uses spectral finite elements to compute acoustic and/or elastic wave propagations, and is widely used in the seismology community, for example, to simulate seismic waves generated by landslides (Kuehnert et al., 2020). In addition to the acoustic waves already modelled in Specfem, the model proposed in the present paper includes the linear water waves.
- The method used to write the linearization of a free-surface flow is generic and can be applied to extend the model. A possible extension would include second-order terms (a similar work was done by Longuet-Higgins (1950) in the barotropic case). Another possibility is to take into account the interaction with the Earth. In particular, one can consider the elastic deformations of the ocean bottom that are shown to impact the travel time of tsunami waves (Abdolali et al., 2019).

Another advantage of having a model with few assumptions is that a cascade of simplified systems can be obtained from it. We indeed show that with some simplifying assumptions, our model reduces to the models proposed in the literature. The analysis of these simplifications helps to understand the mathematical and physical choices made in these models. For example, the most common model for the propagation of hydro-acoustic waves (Stiassnie, 2010; Nosov and Kolesov, 2007; Sammarco et al., 2013) is recovered from the proposed model by assuming a barotropic fluid and a constant background density.

We also show that our model and the simplified models are energy-preserving. Our model is a linear version of the Euler equations, and the equation accounting for the energy conservation may be modified by the linearization. To ensure that the obtained model is physically relevant, we check that an equation for the energy conservation holds in the linear case. Beyond this aspect, the energy preservation allows to write stable numerical schemes (Allaire, 2015). Indeed, the properties of a numerical scheme are often related to the preservation of a discrete energy. For these reasons, the energy preservation is a key feature, both in the continuous and in the discrete level.

The paper is organized as follows. In Section 2.2, the compressible Euler equations for a free-surface flow are written, then the system is transformed in Lagrangian coordinates to keep an exact

description of the free surface. After linearization, a wave-like equation for the fluid velocity is obtained and we show that the energy of the system is preserved. In Section 2.3, we show that with additional assumptions, the model reduces to other linear models from the literature. The barotropic case is studied, then the incompressible limit and the acoustic limit of the wave equation are written. In Section 2.4, we present a method allowing to write the model in Eulerian coordinates. The obtained system can be linearized at the cost of an additional approximation, namely that the equations have to be restricted to a fixed domain, and we show how to obtain a linear free-surface condition. Finally, in Section 2.5, we obtain a dispersion relation which includes all of the physical effects mentioned above. In particular, it is a generalization of the dispersion relation studied in the work of Auclair et al. (2021) to the case of a varying sound speed.

2.2 Linearization of compressible Euler equations in Lagrangian coordinates

We derive here a linear model around a state at rest for the isentropic compressible Euler equation with a free surface and an arbitrary bathymetry, valid for a generic equation of state and a generic vertical temperature profile. We aim at deriving a model which is physically relevant in the sense that it preserves or dissipates energy. For this reason, we will analyse the energy equation associated with this system and show that preservation or dissipation of energy requires a condition on the fluid stratification that is related to the internal waves.

We consider a portion of the ocean away from the coast and at equilibrium: there is no mean current and the temperature varies only vertically. In this work, we do not take the presence of salinity into account; hence, the ocean is assimilated to pure water. The bottom and the surface of the domain are assumed to be parametrized as graphs, respectively the topography $z_b(x, y) \geq 0$ and the free-surface elevation $\eta(x, y, t)$. The reference level $z = 0$ is situated inside the earth at an arbitrary level. The ground displacement induced by an earthquake or landslide source is assumed to take place away from the coast, so that the domain is considered infinite in the (x, y) plane, see Figure 2.1. The domain is assumed to have the following description, for all time t ,

$$\Omega(t) = \{(x, y, z) \in \mathbb{R}^3 \mid z_b(x, y) < z < \eta(x, y, t)\}. \quad (2.1)$$

The boundaries of the domain are then defined by

$$\Gamma_s(t) = \{(x, y, z) \in \mathbb{R}^3 \mid z = \eta(x, y, t)\}, \quad (2.2)$$

and

$$\Gamma_b(t) = \{(x, y, z) \in \mathbb{R}^3 \mid z = z_b(x, y) - b(x, y, t)\}. \quad (2.3)$$

The function b is the source term, namely the normal displacement of the seabed. It can represent, for example, an earthquake or a landslide. It is assumed that this displacement starts at a time $t_0 > 0$, so that $b(x, y, 0) = 0$.

2.2.1 Euler equations in Eulerian coordinates

Equations in the volume

The unknowns are the fluid velocity \mathbf{U} , its density ρ , its pressure p , its temperature T , its internal energy e and its entropy s .

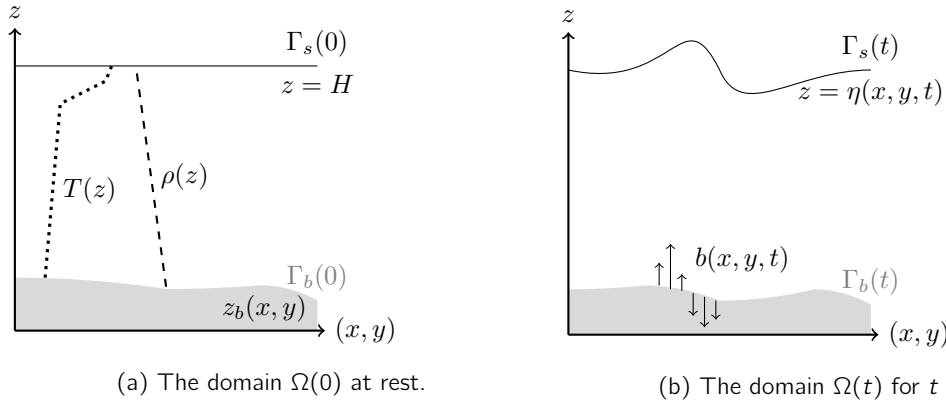


Figure 2.1: The domain $\Omega(t)$: (2.1a) for time $t = 0$; (2.1b) for time $t > 0$. In panel (2.1a), typical profiles for the temperature and the density at rest are drawn.

For future reference, the equations are written for a viscous fluid with thermal dissipation. The stress tensor of a Newtonian fluid \mathbf{T} has the form

$$\mathbf{T} = (-\rho + \lambda \nabla \cdot \mathbf{U}) \mathbf{I} + 2\mu \mathbf{D}(\mathbf{U}), \quad (2.4)$$

where $\mathbf{D}(\mathbf{U})$ is defined by $\mathbf{D}(\mathbf{U}) = (\frac{1}{2}(\partial_i \mathbf{U}^j + \partial_j \mathbf{U}^i))_{i,j=x,y,z}$ and \mathbf{I} is the identity matrix in \mathbb{R}^3 . The heat flux is denoted by \mathbf{q} and is a function of ρ and T .

The conservation of mass, momentum and energy of a Newtonian fluid read, in the domain $\Omega(t)$,

$$\left\{ \begin{array}{l} \frac{\partial \rho}{\partial t} + \nabla \cdot (\rho \mathbf{U}) = 0, \end{array} \right. \quad (2.5)$$

$$\left\{ \begin{array}{l} \frac{\partial}{\partial t} (\rho \mathbf{U}) + \nabla \cdot (\rho \mathbf{U} \otimes \mathbf{U}) + \nabla p = \rho \mathbf{g} + \nabla (\lambda \nabla \cdot \mathbf{U}) + \nabla \cdot (2\mu \mathbf{D}(\mathbf{U})), \end{array} \right. \quad (2.6)$$

$$\left\{ \begin{array}{l} \frac{\partial}{\partial t} \left(\rho \frac{|\mathbf{U}|^2}{2} + \rho e \right) + \nabla \cdot \left(\left(\rho \frac{|\mathbf{U}|^2}{2} + \rho e + p \right) \mathbf{U} \right) \\ = \rho \mathbf{g} \cdot \mathbf{U} + \nabla \cdot (\lambda \mathbf{U} \nabla \cdot \mathbf{U}) + \nabla \cdot (2\mu \mathbf{D}(\mathbf{U}) \cdot \mathbf{U}) - \nabla \cdot \mathbf{q}. \end{array} \right. \quad (2.7)$$

The acceleration of gravity is $\mathbf{g} = -g \mathbf{e}_3$ with $g > 0$ and \mathbf{e}_3 is the unit vector in the vertical direction, oriented upwards.

To describe the acoustic waves, we derive an equation for the pressure. Among (ρ, e, T, p, s) , only two variables are independent because of the Gibbs law and of the equation of state (Gill, 1982). When considering ρ and s as independent, it is natural to introduce the scalar functions f_e , f_p and f_T satisfying

$$e = f_e(\rho, s), \quad p = f_p(\rho, s), \quad T = f_T(\rho, s). \quad (2.8)$$

With the Gibbs law ($\partial f_e / \partial \rho = f_p / \rho^2$ and $\partial f_e / \partial s = f_T$), one has

$$\frac{\partial e}{\partial t} + \mathbf{U} \cdot \nabla e = \frac{f_p}{\rho^2} \left(\frac{\partial \rho}{\partial t} + \mathbf{U} \cdot \nabla \rho \right) + f_T \left(\frac{\partial s}{\partial t} + \mathbf{U} \cdot \nabla s \right). \quad (2.9)$$

Using (2.7) – $\mathbf{U} \cdot$ (2.6) and (2.9), one obtains as an intermediate step the evolution equation of the entropy,

$$\rho T \left(\frac{\partial s}{\partial t} + \mathbf{U} \cdot \nabla s \right) = \lambda (\nabla \cdot \mathbf{U})^2 + 2\mu \mathbf{D}(\mathbf{U}) : \mathbf{D}(\mathbf{U}) - \nabla \cdot \mathbf{q}. \quad (2.10)$$

Now, since $p = f_p(\rho, s)$ we have

$$\frac{\partial p}{\partial t} + \mathbf{U} \cdot \nabla p = \frac{\partial f_p}{\partial \rho} \left(\frac{\partial \rho}{\partial t} + \mathbf{U} \cdot \nabla \rho \right) + \frac{1}{T\rho} \frac{\partial f_p}{\partial s} \left(\frac{\partial s}{\partial t} + \mathbf{U} \cdot \nabla s \right), \quad (2.11)$$

hence using (2.5) and (2.10) one obtains

$$\frac{\partial p}{\partial t} + \mathbf{U} \cdot \nabla p = -\frac{\partial f_p}{\partial \rho} (\rho \nabla \cdot \mathbf{U}) + \frac{1}{T\rho} \frac{\partial f_p}{\partial s} (\lambda (\nabla \cdot \mathbf{U})^2 + 2\mu \mathbf{D}(\mathbf{U}) : \mathbf{D}(\mathbf{U}) - \nabla \cdot \mathbf{q}). \quad (2.12)$$

At this point, we use the common assumption that the viscous term and the thermal dissipation can be neglected compared with the advection term (see Lannes, 2013, Chap. 1). With (2.10), we see that this is equivalent to assuming that the flow is isentropic. Moreover, from physical considerations, the function f_p must satisfy $\partial_\rho f_p(\rho, s) \geq 0$, hence we can introduce the speed of sound c defined by

$$c^2 = \frac{\partial f_p}{\partial \rho}(\rho, s). \quad (2.13)$$

Equation (2.12) then reads

$$\frac{\partial p}{\partial t} + \mathbf{U} \cdot \nabla p + \rho c^2 \nabla \cdot \mathbf{U} = 0. \quad (2.14)$$

Equation (2.14) is used for the study of a compressible fluid in the isentropic case, see Gill (1982), Chap. 4. Note that the speed of sound c can also be viewed as a function of p and T , and in that case, we have

$$c^2(p, T) = \frac{\partial f_p}{\partial \rho}(f_p(p, T), f_s(p, T)). \quad (2.15)$$

In practice, we choose to work directly with the expression $c = c(p, T)$ tabulated by IAPWS-SR7 (2009). Note that here, the temperature intervenes as a side variable, because it is necessary to compute the speed of sound. However, we will see later that only the temperature profile of the state at rest is needed to close the system.

Boundary conditions

The following boundary conditions hold:

$$\begin{cases} \mathbf{U} \cdot \mathbf{n}_b = u_b = \partial_t b & \text{on } \Gamma_b, \\ \rho = p^a & \text{on } \Gamma_s. \end{cases} \quad (2.16)$$

$$(2.17)$$

The bottom boundary condition (2.16) is a non-penetration condition with a source term. It models the tsunami source as a displacement of the ocean bottom with velocity u_b . We denote by \mathbf{n}_b the unit vector normal to the bottom and oriented outwards. The second condition (2.17) is a dynamic condition, where we assume that the surface pressure is at equilibrium with a constant atmospheric pressure p^a . Note that the elevation η is a solution of the following kinematic equation:

$$\frac{\partial \eta}{\partial t} + \mathbf{U} \cdot \begin{pmatrix} \partial_x \eta \\ \partial_y \eta \\ -1 \end{pmatrix} = 0 \quad \text{on } \Gamma_s(t). \quad (2.18)$$

Initial conditions and equilibrium state

It is assumed that the initial state corresponds to the rest state, meaning that $\eta(x, y, 0) = H$ with the elevation at rest H being independent of space and $H > z_b(x, y)$; therefore

$$\Omega(0) = \{(x, y, z) \in \mathbb{R}^3 \mid z_b(x, y) < z < H\}. \quad (2.19)$$

We choose the following initial conditions for the velocity, the temperature, the density and the pressure:

$$\mathbf{U}(x, y, z, 0) = 0, \quad (2.20)$$

$$T(x, y, z, 0) = T_0(z), \quad \rho(x, y, z, 0) = \rho_0(z), \quad p(x, y, z, 0) = p_0(z), \quad (2.21)$$

where T_0, ρ_0, p_0 are functions defined on $(0, H)$ but because of the topography $z_b(x, y)$, the functions T, ρ, p need not to be defined from $z = 0$ for all (x, y) .

When the source term u_b vanishes, we have an equilibrium state around $\mathbf{U} \equiv 0$ if the functions T_0, ρ_0, p_0 satisfy

$$\nabla p_0 = \rho_0 \mathbf{g}, \quad \rho_0 = f_\rho(p_0, T_0), \quad p_0(H) = p^a. \quad (2.22)$$

Hence, if $T_0(z)$ is given, the system

$$\begin{cases} \frac{dp_0}{dz} = -gf_\rho(p_0, T_0), & z \in (0, H), \\ \rho_0 = f_\rho(p_0, T_0), & z = H \end{cases} \quad (2.23)$$

$$\rho_0 = p^a, \quad z = H \quad (2.24)$$

can be solved to compute p_0 , and then ρ_0 is computed with $\rho_0 = f_\rho(p_0, T_0)$. Note that, in the forthcoming section the system (2.5), (2.6), (2.14) with boundary conditions (2.16), (2.17) and initial conditions (2.20), (2.21) will be linearized around the previously defined equilibrium state.

2.2.2 Lagrangian description

Although most of the works on free-surface flows are done in Eulerian coordinates, the Lagrangian formalism is sometimes preferred, see for example the paper by Noguier et al. (2015) and the references therein, or the work of Godlewski et al. (1999) for a precise derivation of linear models. Here we choose the Lagrangian description to avoid any approximation on the shape of the domain when we linearize the equations. The usual approximation made on the surface for the linear models in Eulerian coordinates consists in evaluating the surface condition on pressure at a fixed height, rather than at the actual, time-dependant free surface. The kinematic boundary condition is also replaced by its linear approximation. For the derivation and justification of the approximation, see Lighthill (1978, Chap. 3).

Let $\hat{\Omega}$ be the domain of the ocean at a reference time, with its surface boundary $\hat{\Gamma}_s$ and bottom boundary $\hat{\Gamma}_b$. The reference time is chosen before the tsunami generation, so that the surface of the domain is horizontal. In fact, the following natural choice is made:

$$\hat{\Omega} = \Omega(0), \quad \hat{\Gamma}_s = \Gamma_s(0), \quad \hat{\Gamma}_b = \Gamma_b(0). \quad (2.25)$$

The position at the reference time of a fluid particle is denoted

$$\boldsymbol{\xi} = (\xi_1, \xi_2, \xi_3) \in \hat{\Omega}. \quad (2.26)$$

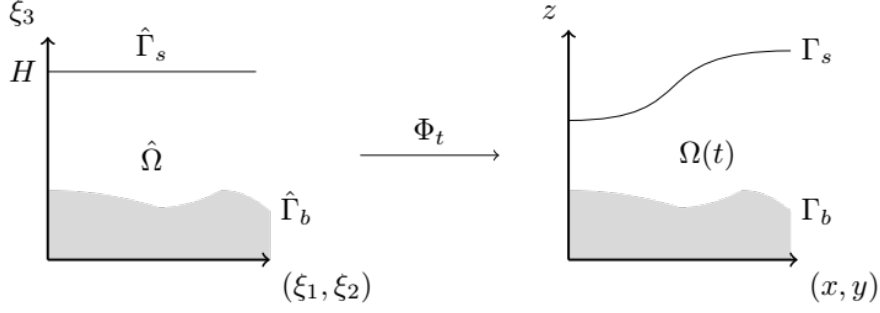


Figure 2.2: The mapping ϕ_t between the reference domain $\hat{\Omega} = \Omega(0)$ and the domain $\Omega(t)$.

At time t , the fluid has moved, the domain is $\Omega(t)$ and the new position of a fluid particle is $\mathbf{x} = (x(\boldsymbol{\xi}, t), y(\boldsymbol{\xi}, t), z(\boldsymbol{\xi}, t)) \in \Omega(t)$. We denote by $\boldsymbol{\phi}$ the transformation from $\hat{\Omega}$ to $\Omega(t)$ that maps each particle from its reference position $\boldsymbol{\xi}$ to its position \mathbf{x} at time t (see Figure 2.2):

$$\boldsymbol{\phi} : \begin{cases} \hat{\Omega} & \rightarrow \Omega(t) \\ \boldsymbol{\xi} & \mapsto \mathbf{x}(\boldsymbol{\xi}, t) \end{cases} \quad (2.27)$$

Hence, one has $\mathbf{x} = \boldsymbol{\phi}(\boldsymbol{\xi}, t)$. The transformation is assumed invertible, in particular, we do not consider the case of wave breaking. We also define the displacement of the fluid. For each fluid particle with initial position $\boldsymbol{\xi}$, its displacement is defined by

$$\mathbf{d}(\boldsymbol{\xi}, t) = \boldsymbol{\phi}(\boldsymbol{\xi}, t) - \boldsymbol{\xi}. \quad (2.28)$$

The gradient of $\boldsymbol{\phi}$ with respect to $\boldsymbol{\xi}$ is denoted \mathbf{F} ,

$$\mathbf{F} = \nabla_{\boldsymbol{\xi}} \boldsymbol{\phi}, \quad (2.29)$$

and its determinant is denoted J . Both \mathbf{F} and J can be expressed as functions of the displacement,

$$\mathbf{F} = \mathbf{I} + \nabla_{\boldsymbol{\xi}} \mathbf{d}, \quad J = \det \mathbf{F}, \quad (2.30)$$

where $\nabla_{\boldsymbol{\xi}}$ is the gradient with respect to the coordinate system $\boldsymbol{\xi}$. For a function $X(\mathbf{x}, t)$ defined on the domain $\Omega(t)$, we introduce $\hat{X}(\boldsymbol{\xi}, t)$ defined on $\hat{\Omega}$ by

$$\hat{X}(\boldsymbol{\xi}, t) = X(\boldsymbol{\phi}(\boldsymbol{\xi}, t), t). \quad (2.31)$$

Finally, note that the velocity $\hat{\mathbf{U}}(\boldsymbol{\xi}, t) = \mathbf{U}(\boldsymbol{\phi}(\boldsymbol{\xi}, t), t)$ is the time derivative of the displacement \mathbf{d} ,

$$\hat{\mathbf{U}} = \frac{\partial \mathbf{d}}{\partial t}. \quad (2.32)$$

With this change of coordinates, the system (2.5), (2.6), (2.14) is now defined in the time-independent reference domain $\hat{\Omega}$ and it reads

$$\left\{ \begin{array}{l} \frac{\partial \hat{\rho}}{\partial t} + \frac{\hat{\rho}}{|J|} \nabla_{\boldsymbol{\xi}} \cdot (|J| \mathbf{F}^{-1} \hat{\mathbf{U}}) = 0, \end{array} \right. \quad (2.33)$$

$$\left\{ \begin{array}{l} \hat{\rho} \frac{\partial \hat{\mathbf{U}}}{\partial t} + \mathbf{F}^{-T} \nabla_{\boldsymbol{\xi}} \hat{\rho} = \hat{\rho} \mathbf{g}, \end{array} \right. \quad (2.34)$$

$$\left\{ \begin{array}{l} \frac{\partial \hat{\rho}}{\partial t} + \frac{\hat{\rho} \hat{c}^2}{|J|} \nabla_{\boldsymbol{\xi}} \cdot (|J| \mathbf{F}^{-1} \hat{\mathbf{U}}) = 0. \end{array} \right. \quad (2.35)$$

The boundary conditions become

$$\begin{cases} \hat{\mathbf{U}} \cdot \hat{\mathbf{n}}_b = \hat{u}_b & \text{on } \hat{\Gamma}_b, \\ \hat{p} = p^a & \text{on } \hat{\Gamma}_s, \end{cases}$$

where $\hat{\mathbf{n}}_b$ is a unit vector normal to $\hat{\Gamma}_b$ and pointing towards the exterior of the domain. The variables $\hat{\rho}, \hat{p}, \hat{T}$ satisfy the same equation of state,

$$\hat{p} = f_p(\hat{\rho}, \hat{T}), \quad (2.36)$$

and the speed of sound is a function of the new variables, $\hat{c} = c(\hat{\rho}, \hat{s})$.

2.2.3 Linearization and wave equation

We assume that the source of the tsunami is a displacement of magnitude a at the seafloor occurring in an ocean at rest as described in Section 2.2.1. In particular, for this rest state, there is no mean current and the temperature, pressure and density vary only vertically. The magnitude of the displacement is assumed small compared to the water height H . The ratio of the bottom displacement amplitude to the water height is denoted $\varepsilon = a/H \ll 1$, and the source term can be expressed as

$$\hat{u}_b = \varepsilon \hat{u}_{b,1} + \mathcal{O}(\varepsilon^2). \quad (2.37)$$

The linearization of Equations (2.33)-(2.35) around the rest state corresponds to the following asymptotic expansion:

$$\mathbf{d}(\boldsymbol{\xi}, t) = \varepsilon \mathbf{d}_1(\boldsymbol{\xi}, t) + \mathcal{O}(\varepsilon^2), \quad (2.38)$$

$$\hat{\rho}(\boldsymbol{\xi}, t) = \hat{\rho}_0(\boldsymbol{\xi}) + \varepsilon \hat{\rho}_1(\boldsymbol{\xi}, t) + \mathcal{O}(\varepsilon^2), \quad (2.39)$$

$$\hat{p}(\boldsymbol{\xi}, t) = \hat{p}_0(\boldsymbol{\xi}) + \varepsilon \hat{p}_1(\boldsymbol{\xi}, t) + \mathcal{O}(\varepsilon^2). \quad (2.40)$$

Note that the displacement has no zero order term, because the reference configuration used to define the Lagrangian description is the state given by the initial conditions. It holds then that $\mathbf{d}_0 = 0$, $\hat{\mathbf{U}}_0 = 0$ and $\hat{\Omega} = \Omega(0)$.

Remark: In comparison with the linearization done by Auclair et al. (2021), where the expansion of the density and the pressure is justified with the decomposition into hydrostatic and non-hydrostatic components, the asymptotic expansion (2.39) - (2.40) is obtained in a more straightforward way. Indeed, it only requires the assumption of a small perturbation.

From the expansion, one deduces the following Taylor expansions for the other functions:

$$\hat{\mathbf{U}} = \varepsilon \hat{\mathbf{U}}_1 + \mathcal{O}(\varepsilon^2), \quad (2.41)$$

$$\mathbf{F} = \mathbf{I} + \varepsilon \nabla_{\boldsymbol{\xi}} \mathbf{d}_1 + \mathcal{O}(\varepsilon^2), \quad (2.42)$$

$$\mathbf{F}^{-1} = \mathbf{I} - \varepsilon \nabla_{\boldsymbol{\xi}} \mathbf{d}_1 + \mathcal{O}(\varepsilon^2), \quad (2.43)$$

$$J = 1 + \varepsilon \nabla_{\boldsymbol{\xi}} \cdot \mathbf{d}_1 + \mathcal{O}(\varepsilon^2). \quad (2.44)$$

Injecting these expressions in Equations (2.33)-(2.35) yields the system

$$\begin{cases} \frac{\partial}{\partial t} (\hat{\rho}_0 + \varepsilon \hat{\rho}_1) + \varepsilon \hat{\rho}_0 \nabla_\xi \cdot \hat{\mathbf{U}}_1 = \mathcal{O}(\varepsilon^2), & (2.45) \\ \varepsilon \hat{\rho}_0 \frac{\partial \hat{\mathbf{U}}_1}{\partial t} + (I - \varepsilon \nabla_\xi \mathbf{d}_1)^T \nabla_\xi \hat{\rho}_0 + \varepsilon \nabla_\xi \hat{\rho}_1 = (\hat{\rho}_0 + \varepsilon \hat{\rho}_1) \mathbf{g} + \mathcal{O}(\varepsilon^2), & (2.46) \\ \frac{\partial}{\partial t} (\hat{\rho}_0 + \varepsilon \hat{\rho}_1) + \varepsilon \hat{\rho}_0 c^2(\hat{\rho}_0, \hat{T}_0) \nabla_\xi \cdot \hat{\mathbf{U}}_1 = \mathcal{O}(\varepsilon^2). & (2.47) \end{cases}$$

By separating the powers of ε , we obtain two systems: a limit system when $\varepsilon \rightarrow 0$ and a system for the first-order corrections. Since the limit system corresponds to the initial conditions described in Section 2.2.1, the model reduces to the first-order system.

First-order system: a wave-like equation for the velocity

The system for the correction terms reads in $\hat{\Omega}$,

$$\begin{cases} \hat{\rho}_0 \frac{\partial \hat{\mathbf{U}}_1}{\partial t} + \nabla_\xi \hat{\rho}_1 - (\nabla_\xi \mathbf{d}_1)^T \nabla_\xi \hat{\rho}_0 = \hat{\rho}_1 \mathbf{g}, & (2.48) \\ \frac{\partial \hat{\rho}_1}{\partial t} + \hat{\rho}_0 \nabla_\xi \cdot \hat{\mathbf{U}}_1 = 0, & (2.49) \\ \frac{\partial \hat{\rho}_1}{\partial t} + \hat{\rho}_0 \hat{c}_0^2 \nabla_\xi \cdot \hat{\mathbf{U}}_1 = 0, & (2.50) \end{cases}$$

with the boundary conditions

$$\begin{cases} \hat{\mathbf{U}}_1 \cdot \hat{\mathbf{n}}_b = \hat{u}_{b,1} & \text{on } \hat{\Gamma}_b, & (2.51) \\ \hat{\rho}_1 = 0 & \text{on } \hat{\Gamma}_s. & (2.52) \end{cases}$$

In this system, the speed of sound is evaluated at the limit – or background – pressure and temperature, $\hat{c}_0 = c(\hat{\rho}_0, \hat{T}_0)$. In particular, \hat{c}_0 can be written as a function of depth. With an adapted temperature profile, it is then possible to recover the typical speed of sound profile creating the SOFAR channel.

The pressure $\hat{\rho}_1$ and density $\hat{\rho}_1$ can be eliminated in (2.48) thanks to the other equations: differentiating in time (2.48) and replacing $\hat{\rho}_1$ and $\hat{\rho}_1$ with (2.49), (2.50) we obtain a second-order equation for $\hat{\mathbf{U}}_1$,

$$\hat{\rho}_0 \frac{\partial^2 \hat{\mathbf{U}}_1}{\partial t^2} - \nabla_\xi (\hat{\rho}_0 \hat{c}_0^2 \nabla_\xi \cdot \hat{\mathbf{U}}_1) - (\nabla_\xi \hat{\mathbf{U}}_1)^T \hat{\rho}_0 \mathbf{g} + \hat{\rho}_0 \nabla_\xi \cdot \hat{\mathbf{U}}_1 \mathbf{g} = 0 \text{ in } \hat{\Omega}. \quad (2.53)$$

Using (2.50), the surface boundary condition (2.52) is formulated for $\hat{\mathbf{U}}_1$, hence the two boundary conditions for the wave-like equation (2.53) are

$$\begin{cases} \hat{\mathbf{U}}_1 \cdot \hat{\mathbf{n}}_b = \hat{u}_{b,1} & \text{on } \hat{\Gamma}_b, & (2.54) \\ \nabla_\xi \cdot \hat{\mathbf{U}}_1 = 0 & \text{on } \hat{\Gamma}_s. & (2.55) \end{cases}$$

The wave-like equation (2.53) is completed with vanishing initial condition for $\hat{\mathbf{U}}_1(0)$ and $\partial_t \hat{\mathbf{U}}_1(0)$. The system (2.53) includes both gravity and acoustic terms. This equation, which describes the velocity of a compressible, non-viscous fluid, in Lagrangian description, is called the Galbrun equation. It is used in helioseismology and in aeroacoustics (Legendre, 2003; Maeder et al., 2020; Hagg

and Berggren, 2021). However, to our knowledge, this equation has never been used to describe the propagation of hydro-acoustic waves.

We show now that the system (2.53), (2.54), (2.55) is energy preserving. A model describing a physical system should either preserve or dissipate energy, and this property makes it also possible to write a stable numerical scheme. Here the energy equation is obtained by taking the scalar product of (2.53) with $\partial_t \hat{\mathbf{U}}_1$ and integrating over the domain. After some computations (see Appendix A), we have

$$\frac{d}{dt} \mathcal{E} = \int_{\hat{\Gamma}_b} \hat{\rho}_0 (c_0^2 \nabla_\xi \cdot \hat{\mathbf{U}}_1 - \hat{\rho}_0 g \hat{\mathbf{U}}_1 \cdot \mathbf{e}_3) \frac{\partial \hat{u}_{b,1}}{\partial t} d\sigma, \quad (2.56)$$

with the energy being the quadratic functional given by

$$\begin{aligned} \mathcal{E} = \int_{\hat{\Omega}} \rho_0 \frac{1}{2} \left| \frac{\partial \hat{\mathbf{U}}_1}{\partial t} \right|^2 d\xi + \frac{1}{2} \int_{\hat{\Omega}} \hat{\rho}_0 \left(\hat{c}_0 \nabla_\xi \cdot \hat{\mathbf{U}}_1 - \frac{g}{\hat{c}_0} \hat{\mathbf{U}}_1 \cdot \mathbf{e}_3 \right)^2 d\xi \\ + \frac{1}{2} \int_{\hat{\Omega}} \hat{\rho}_0 N_b (\hat{\mathbf{U}}_1 \cdot \mathbf{e}_3)^2 d\xi + \frac{1}{2} \int_{\hat{\Gamma}_s} \hat{\rho}_0 g (\hat{\mathbf{U}}_1 \cdot \mathbf{e}_3)^2 d\sigma. \end{aligned} \quad (2.57)$$

The scalar N_b is the squared Brunt-Väisälä frequency, defined by

$$N_b(\xi_3) = - \left(\frac{g^2}{\hat{c}_0(\xi_3)^2} + g \frac{\hat{\rho}'_0(\xi_3)}{\hat{\rho}_0(\xi_3)} \right). \quad (2.58)$$

The Brunt-Väisälä frequency, or buoyancy frequency, is closely related to the internal waves that appear in a stratified medium (Gill, 1982, Chap. 6). In the ocean, the usual values of N_b are approximately $10^{-8} \text{ rad}^2 \text{ s}^{-2}$ (King et al., 2012).

The physical interpretation for the different terms in the energy is clearer when one writes the wave-like equation (2.53) in terms of the displacement \mathbf{d}_1 instead of the velocity $\hat{\mathbf{U}}_1$. Using $\partial_t \mathbf{d}_1 = \hat{\mathbf{U}}_1$ and integrating Equation (2.53) once in time with the vanishing initial conditions for the displacement, one obtains

$$\hat{\rho}_0 \frac{\partial^2 \mathbf{d}_1}{\partial t^2} - \nabla_\xi (\hat{\rho}_0 \hat{c}_0^2 \nabla_\xi \cdot \mathbf{d}_1) - (\nabla_\xi \mathbf{d}_1)^T \hat{\rho}_0 \mathbf{g} + \hat{\rho}_0 \nabla_\xi \cdot \mathbf{d}_1 \mathbf{g} = 0 \text{ in } \hat{\Omega}. \quad (2.59)$$

The exact same steps of Appendix A, with \mathbf{d}_1 instead of $\hat{\mathbf{U}}_1$, yield the energy equation

$$\frac{d}{dt} \mathcal{E}_d = \int_{\hat{\Gamma}_b} \hat{\rho}_0 (c_0^2 \nabla_\xi \cdot \mathbf{d}_1 - \hat{\rho}_0 g \mathbf{d}_1 \cdot \mathbf{e}_3) \hat{u}_{b,1} d\sigma, \quad (2.60)$$

with the energy

$$\begin{aligned} \mathcal{E}_d = \int_{\hat{\Omega}} \hat{\rho}_0 \frac{1}{2} |\hat{\mathbf{U}}_1|^2 d\xi + \frac{1}{2} \int_{\hat{\Omega}} \hat{\rho}_0 \left(\hat{c}_0 \nabla_\xi \cdot \mathbf{d}_1 - \frac{g}{\hat{c}_0} \mathbf{d}_1 \cdot \mathbf{e}_3 \right)^2 d\xi \\ + \frac{1}{2} \int_{\hat{\Omega}} \hat{\rho}_0 N_b (\mathbf{d}_1 \cdot \mathbf{e}_3)^2 d\xi + \frac{1}{2} \int_{\hat{\Gamma}_s} \hat{\rho}_0 g (\mathbf{d}_1 \cdot \mathbf{e}_3)^2 d\sigma. \end{aligned} \quad (2.61)$$

The first term in Equation (2.61) is the kinetic energy. We show that the second term of Equation (2.61) corresponds to the acoustic energy. First, using Equation (2.50) with the vanishing initial conditions yields $\hat{\rho}_0 \hat{c}_0^2 \cdot \nabla_\xi \mathbf{d}_1 = -\hat{p}_1$. We define then the acoustic pressure

$$p_a = \hat{p}_1 - \nabla \hat{p}_0 \cdot \mathbf{d}_1. \quad (2.62)$$

Indeed, in Lagrangian coordinates, the pressure perturbation \hat{p}_1 has two contributions: the small variations in acoustic pressure and the background pressure being evaluated at a new position. With the definition of p_a and Equation (2.24), it holds that for the second term of (2.61)

$$\frac{1}{2} \int_{\hat{\Omega}} \hat{\rho}_0 \left(\hat{c}_0 \nabla_{\hat{\xi}} \cdot \mathbf{d}_1 - \frac{g}{\hat{c}_0} \mathbf{d}_1 \cdot \mathbf{e}_3 \right)^2 d\hat{\xi} = \frac{1}{2} \int_{\hat{\Omega}} \frac{p_a^2}{\hat{\rho}_0 \hat{c}_0^2} d\hat{\xi}, \quad (2.63)$$

which is the usual expression for the acoustic energy (Lighthill, 1978). The last term of (2.61) is the potential energy associated with the surface waves. Finally, the third term of (2.61) is the potential energy associated with the internal gravity waves (Lighthill, 1978), under the condition

$$N_b > 0. \quad (2.64)$$

When N_b is positive, it is denoted $N_b = N^2$, where N is the buoyancy frequency. The sign of N_b depends on the choice of the state at equilibrium: $\hat{\rho}'_0 = d\hat{\rho}_0/dz$ has to be negative and satisfy

$$\frac{|\hat{\rho}'_0|}{\hat{\rho}_0} > \frac{g}{\hat{c}_0^2}. \quad (2.65)$$

With the term in g^2/\hat{c}_0^2 , we see that the compressibility tends to take the fluid away from its equilibrium. The stratification of the fluid must be strong enough to counter this effect and keep the system stable (see the discussion in Gill, 1982, Chap. 3). As a consequence, if one wants the model to preserve the energy of the system, the background density should not be assumed homogeneous. In the following, we assume that the fluid has a stable stratification, namely that the function N_b is assumed always positive. We will use the notation N^2 in the rest of this paper.

Remark: According to the equation of state (when the salinity is neglected) $\rho = f_\rho(p, T)$, the background density varies because of the variations in temperature and in pressure. The temperature profile can be chosen homogeneous, but the effect of gravity – see Equation (2.24) – prevents the pressure to be independent of depth. Hence in a model with gravity, the fluid is always stratified with the density increasing with depth.

Remark: One can notice that the condition (2.65) is not explicit in Equation (2.53). We obtain this condition when imposing that the energy \mathcal{E}_d is positive.

2.3 Derivation of simplified models

To compare with existing models, we present several simplifications of our model. We first show that in the barotropic case, the system (2.53) - (2.55) is equivalent to the first-order scalar equation of Longuet-Higgins (1950). Our model also reduces to well-known models in the acoustic and incompressible asymptotic regimes, as demonstrated below. Further numerical implementations of our model will make it possible to quantify the impact of assumptions made in more simple models, in particular in the case of acoustic-gravity wave generation by earthquakes or landslides in the ocean.

2.3.1 The barotropic case

We consider the barotropic case, which is a very common assumption for the study of hydro-acoustic waves (see for example Longuet-Higgins (1950), Stiassnie (2010)). For a barotropic fluid,

the pressure is a function of the density only,

$$f_p(\rho, s) = f_p(\rho) = p.$$

Then, using Equation (2.22) and the definition of the speed of sound,

$$\hat{\rho}'_0 = \hat{\rho}'_0 \frac{df_p}{d\rho}(\hat{\rho}_0) \Rightarrow -\hat{\rho}_0 g = \hat{\rho}'_0 \hat{c}_0^2, \quad (2.66)$$

meaning that the Brunt-Väisälä frequency vanishes, $N^2 = 0$. This corresponds to the case where the density is stratified because of the variation of pressure only. To use this equality, we divide Equation (2.53) by $\hat{\rho}_0$,

$$\frac{\partial^2 \hat{\mathbf{U}}_1}{\partial t^2} - \nabla_\xi (\hat{c}_0^2 \nabla_\xi \cdot \hat{\mathbf{U}}_1) - \left(\frac{\hat{\rho}'_0}{\hat{\rho}_0} \hat{c}_0^2 + g \right) \nabla_\xi \cdot \hat{\mathbf{U}}_1 \mathbf{e}_3 + \nabla_\xi (\hat{\mathbf{U}}_1 \cdot \mathbf{e}_3) g = 0, \quad (2.67)$$

and when Equation (2.66) holds, the equation (2.67) can be simplified and reads

$$\frac{\partial^2 \hat{\mathbf{U}}_1}{\partial t^2} - \nabla_\xi (\hat{c}_0^2 \nabla_\xi \cdot \hat{\mathbf{U}}_1) + \nabla_\xi (\hat{\mathbf{U}}_1 \cdot \mathbf{e}_3) g = 0. \quad (2.68)$$

Taking the curl of Equation (2.68) yields

$$\frac{\partial^2 \nabla_\xi \times \hat{\mathbf{U}}_1}{\partial t^2} = 0 \text{ in } \hat{\Omega}. \quad (2.69)$$

With the vanishing initial conditions, we obtain that the velocity of a barotropic fluid is irrotational. This is a well-known result, since the fluid is also inviscid and subject to a potential force only (Guyon, 2001, Chap. 7). By the Helmholtz decomposition theorem (Girault and Raviart, 1986), the fluid velocity is written as the gradient of a potential ψ defined up to a constant. The expression $\hat{\mathbf{U}}_1 = \nabla_\xi \psi$ is used in Equation (2.68) to obtain

$$\nabla_\xi \left(\frac{\partial^2 \psi}{\partial t^2} - \hat{c}_0^2 \Delta_\xi \psi + g \frac{\partial \psi}{\partial \xi_3} \right) = 0. \quad (2.70)$$

The potential ψ being defined up to a constant, it can always be sought as the solution of

$$\frac{\partial^2 \psi}{\partial t^2} - \hat{c}_0^2 \Delta_\xi \psi + g \frac{\partial \psi}{\partial \xi_3} = 0. \quad (2.71)$$

The equation (2.71) is multiplied by $\hat{\rho}_0 / \hat{c}_0^2$, and we use $g / \hat{c}_0^2 = -\hat{\rho}'_0 / \hat{\rho}_0$,

$$\frac{\hat{\rho}_0}{\hat{c}_0^2} \frac{\partial^2 \psi}{\partial t^2} - \hat{\rho}_0 \Delta_\xi \psi - \hat{\rho}'_0 \frac{\partial \psi}{\partial \xi_3} = 0. \quad (2.72)$$

Additionally, since $\hat{\rho}_0$ depends only on ξ_3 , the two last terms can be rewritten,

$$\frac{\hat{\rho}_0}{\hat{c}_0^2} \frac{\partial^2 \psi}{\partial t^2} - \nabla_\xi \cdot (\hat{\rho}_0 \nabla_\xi \psi) = 0. \quad (2.73)$$

Hence, ψ satisfies a wave equation. The boundary conditions are then deduced from Equations (2.54) and (2.55),

$$\left\{ \begin{array}{l} \nabla_\xi \psi \cdot \hat{\mathbf{n}}_b = \hat{u}_{b,1} \text{ on } \hat{\Gamma}_b, \\ \hat{c}_0^2 \Delta_\xi \psi = \frac{\partial^2 \psi}{\partial t^2} + g \frac{\partial \psi}{\partial \xi_3} = 0 \text{ on } \hat{\Gamma}_s. \end{array} \right. \quad (2.74)$$

$$(2.75)$$

The system (2.71),(2.74),(2.75) is the first-order system obtained by Longuet-Higgins (1950). In Longuet-Higgins (1950), the derivation is quite different since the irrotationality assumption is made independently from the fact that the fluid is barotropic, and the boundary conditions are obtained from a linearized surface condition. The linearization made in Longuet-Higgins (1950) gives exactly the same result as the linearization strategy we have presented.

We show that the system (2.73),(2.74),(2.75) is energy preserving. The equation (2.73) is multiplied by $\partial_t \psi$ and integrated by parts,

$$\int_{\hat{\Omega}} \frac{\hat{\rho}_0}{\hat{c}_0^2} \frac{\partial \psi}{\partial t} \frac{\partial^2 \psi}{\partial t^2} d\xi + \int_{\hat{\Omega}} \hat{\rho}_0 \nabla \left(\frac{\partial \psi}{\partial t} \right) \cdot \nabla \psi d\xi - \int_{\hat{\Gamma}_s} \hat{\rho}_0 \frac{\partial \psi}{\partial t} \nabla \psi \cdot \mathbf{e}_3 d\sigma + \int_{\hat{\Gamma}_b} \hat{\rho}_0 \frac{\partial \psi}{\partial t} \nabla \psi \cdot \mathbf{n}_b d\sigma = 0. \quad (2.76)$$

With the boundary conditions (2.74) - (2.75) and after simplifications it holds

$$\frac{d}{dt} \mathcal{E}_{bar} = - \int_{\Gamma_b} \hat{\rho}_0 \frac{\partial \psi}{\partial t} \hat{u}_{b,1} d\sigma, \quad (2.77)$$

where the energy \mathcal{E}_{bar} is defined by

$$\mathcal{E}_{bar} = \frac{1}{2} \int_{\hat{\Omega}} \frac{\hat{\rho}_0}{\hat{c}_0^2} \left(\frac{\partial \psi}{\partial t} \right)^2 d\xi + \frac{1}{2} \int_{\hat{\Omega}} \hat{\rho}_0 |\nabla \psi|^2 d\xi + \frac{1}{2} \int_{\hat{\Gamma}_s} \frac{\hat{\rho}_0}{g} \left(\frac{\partial \psi}{\partial t} \right)^2 d\xi. \quad (2.78)$$

The first term of Equation (2.78) is the acoustic energy. Indeed, with (2.14) and (2.66) one can show that the acoustic pressure p_a and the potential ψ satisfy the usual relation $p_a = -\hat{\rho}_0 \partial_t \psi$ (Lighthill, 1978, Chap.3). The second term of (2.78) is the kinetic energy. Finally, with (2.75), one sees that the third term of (2.78) is the potential energy of the surface waves. To obtain the energy equation for the barotropic system (2.73), it is necessary to use the background density $\hat{\rho}_0$ even if it does not appear in Equation (2.73). The correct manipulation for writing the energy equation was found by comparison with the general case described by Equation (2.53).

Finally, note that when assuming a homogeneous density in the equation (2.73), the system (2.73)-(2.75) reduce to

$$\begin{cases} \frac{\partial^2 \psi}{\partial t^2} - \hat{c}_0^2 \Delta \psi = 0 \text{ in } \hat{\Omega} & (2.79) \\ \nabla_{\xi} \psi \cdot \hat{\mathbf{n}}_b = \hat{u}_{b,1} \text{ on } \hat{\Gamma}_b, & (2.80) \\ \frac{\partial^2 \psi}{\partial t^2} + g \frac{\partial \psi}{\partial \xi_3} = 0 \text{ on } \hat{\Gamma}_s. & (2.81) \end{cases}$$

and the energy equation (2.78) is not modified by this assumption. However, assuming a homogeneous density is not compatible with the derivation of the system (2.73)-(2.75), which relies on the equality $g/\hat{c}_0^2 = -\hat{\rho}'_0/\hat{\rho}_0$. The model (2.79)-(2.81) can be understood as a barotropic model with the additional assumption that both $-\hat{\rho}'_0/\hat{\rho}_0$ and g/\hat{c}_0^2 are neglected inside the domain.

2.3.2 Two asymptotic regimes of the system

In this section, we write the limit models for two asymptotic regimes of the system (2.53)-(2.55). We consider the incompressible regime, where the acoustic waves are neglected, and the acoustic regime, where the effect of gravity is neglected. The wave equation (2.53) is written in non-dimensional form, and we show that it depends on a small non-dimensional parameter. A simplified

model is then obtained by passing formally to the limit when the small parameter vanishes. By making the appropriate choice for the time scale, we obtain first an incompressible approximation, then an acoustic approximation.

Non-dimensional equation

We introduce the following characteristic scales for the system: a time τ , a horizontal scale L , a vertical scale H , a density $\bar{\rho}$ and a fluid velocity U . Since the speed of sound is not assumed constant, we denote by C its characteristic magnitude. Finally, the surface waves velocity is of the order of \sqrt{gH} (Constantin, 2009). We focus on a non-shallow water formulation, hence we take $L = H$. For a shallow water version of the equation, one would choose $H \ll L$.

Two dimensionless numbers are introduced: the Froude number and the Mach number, respectively defined by

$$\text{Fr} = \frac{U}{\sqrt{gH}}, \quad \text{Ma} = \frac{U}{C}. \quad (2.82)$$

To fix the idea, we choose the following numerical values respectively for the speed of sound, the fluid velocity and the surface waves velocity: $C \sim 1480 \text{ m s}^{-1}$, $U \sim 1 \text{ m s}^{-1}$ and $\sqrt{gH} \sim 100 \text{ m s}^{-1}$. The dimensionless numbers are then

$$\text{Fr} = 0.01, \quad \text{Ma} = 6.10^{-4}. \quad (2.83)$$

The characteristic scale for time will be fixed later, as it will depend on the regime we want to study. The variables are put in non-dimensional form and the dimensionless variables are denoted with a $\tilde{\cdot}$, except for the space and time variable for the sake of conciseness. The adimensionned domain is denoted by $\tilde{\Omega}$ and its surface and bottom boundary are respectively $\tilde{\Gamma}_s$ and $\tilde{\Gamma}_b$. The non-dimensional system reads, after simplification by the factor $\bar{\rho}U$,

$$\frac{\tilde{\rho}_0}{\tau^2} \frac{\partial^2 \tilde{\mathbf{U}}_1}{\partial t^2} - \frac{C^2}{L^2} \nabla_\xi (\tilde{\rho}_0 \tilde{c}_0^2 \nabla_\xi \cdot \tilde{\mathbf{U}}_1) + \frac{g}{L} \tilde{\rho}_0 (\nabla_\xi (\tilde{\mathbf{U}}_1 \cdot \mathbf{e}_3) - \nabla_\xi \cdot \tilde{\mathbf{U}}_1 \mathbf{e}_3) = 0, \quad (2.84)$$

with the boundary conditions

$$\begin{cases} \tilde{\mathbf{U}}_1 \cdot \tilde{\mathbf{n}}_b = \tilde{u}_{b,1} & \text{on } \tilde{\Gamma}_b, \\ \nabla_\xi \cdot \tilde{\mathbf{U}}_1 = 0 & \text{on } \tilde{\Gamma}_s, \end{cases} \quad (2.85)$$

$$(2.86)$$

where $\tilde{u}_{b,1}$ is a dimensionless source term.

Incompressible limit

We show that in the incompressible regime, our model is an extension of the classical free-surface Poisson equation to the case of a variable background density.

To study the incompressible limit, the characteristic time τ is chosen to follow the surface waves, which are much slower than the acoustic waves. We take $L/\tau = \sqrt{gH}$. The equation (2.84) becomes

$$\tilde{\rho}_0 \frac{\partial^2 \tilde{\mathbf{U}}_1}{\partial t^2} - \frac{\text{Fr}^2}{\text{Ma}^2} \nabla_\xi (\tilde{\rho}_0 \tilde{c}_0^2 \nabla_\xi \cdot \tilde{\mathbf{U}}_1) + \tilde{\rho}_0 (\nabla_\xi (\tilde{\mathbf{U}}_1 \cdot \mathbf{e}_3) - \nabla_\xi \cdot \tilde{\mathbf{U}}_1 \mathbf{e}_3) = 0. \quad (2.87)$$

The small parameter $\delta = \text{Ma}/\text{Fr} \sim 6.10^{-2}$ is introduced in the equation,

$$\tilde{\rho}_0 \frac{\partial^2 \tilde{\mathbf{U}}_1}{\partial t^2} - \frac{1}{\delta^2} \nabla_\xi (\tilde{\rho}_0 \tilde{c}_0^2 \nabla_\xi \cdot \tilde{\mathbf{U}}_1) + \tilde{\rho}_0 (\nabla_\xi (\tilde{\mathbf{U}}_1 \cdot \mathbf{e}_3) - \nabla_\xi \cdot \tilde{\mathbf{U}}_1 \mathbf{e}_3) = 0, \quad (2.88)$$

and the goal is now to calculate the limit of equation (2.88) when δ goes to zero. We make the following ansatz for $\tilde{\mathbf{U}}_1$:

$$\tilde{\mathbf{U}}_1 = \tilde{\mathbf{U}}_{1,0} + \delta^2 \tilde{\mathbf{U}}_{1,2} + \mathcal{O}(\delta^3), \quad (2.89)$$

where $\tilde{\mathbf{U}}_{1,0}$, $\tilde{\mathbf{U}}_{1,1}$ and $\tilde{\mathbf{U}}_{1,2}$ are independent of δ . Since Equation (2.88) has only even powers of δ , the term $\tilde{\mathbf{U}}_{1,1}$ is equal to zero. Replacing $\tilde{\mathbf{U}}_1$ by its ansatz in the wave equation (2.88) and separating the powers of δ yields an equation for each term of the asymptotic development of $\tilde{\mathbf{U}}_1$. The equation obtained with the terms in δ^{-2} reads

$$\nabla_\xi (\tilde{\rho}_0 \tilde{c}_0^2 \nabla_\xi \cdot \tilde{\mathbf{U}}_{1,0}) = 0, \quad (2.90)$$

and the equation obtained with the terms in δ^0 reads

$$\tilde{\rho}_0 \frac{\partial^2 \tilde{\mathbf{U}}_{1,0}}{\partial t^2} - \nabla_\xi (\tilde{\rho}_0 \tilde{c}_0^2 \nabla_\xi \cdot \tilde{\mathbf{U}}_{1,2}) + \tilde{\rho}_0 (\nabla_\xi (\tilde{\mathbf{U}}_{1,0} \cdot \mathbf{e}_3) - \nabla_\xi \cdot \tilde{\mathbf{U}}_{1,0} \mathbf{e}_3) = 0. \quad (2.91)$$

With the terms in δ^0 of the boundary conditions, we have

$$\begin{cases} \nabla_\xi \cdot \tilde{\mathbf{U}}_{1,0} = 0 & \text{on } \tilde{\Gamma}_s, \\ \tilde{\mathbf{U}}_{1,0} \cdot \tilde{\mathbf{n}}_b = \tilde{u}_{b,1} & \text{on } \tilde{\Gamma}_b. \end{cases} \quad (2.92)$$

$$(2.93)$$

Additionally, the terms in δ^2 of the boundary conditions read

$$\begin{cases} \nabla_\xi \cdot \tilde{\mathbf{U}}_{1,2} = 0 & \text{on } \tilde{\Gamma}_s, \\ \tilde{\mathbf{U}}_{1,2} \cdot \tilde{\mathbf{n}}_b = 0 & \text{on } \tilde{\Gamma}_b. \end{cases} \quad (2.94)$$

$$(2.95)$$

We show now that the limit model represents an incompressible flow. The Helmholtz decomposition of $\tilde{\mathbf{U}}_{1,0}$ reads

$$\tilde{\mathbf{U}}_{1,0} = \nabla_\xi \varphi_{1,0} + \nabla_\xi \times \boldsymbol{\psi}_{1,0}, \quad (2.96)$$

where $\varphi_{1,0}$ vanishes on $\tilde{\Gamma}_s$ and $\tilde{\Gamma}_b$. Injecting the decomposition of $\tilde{\mathbf{U}}_{1,0}$ in Equation (2.90) yields

$$\nabla_\xi (\tilde{\rho}_0 \tilde{c}_0^2 \Delta_\xi \varphi_{1,0}) = 0, \quad (2.97)$$

hence the term inside the gradient is constant in space. Since the velocity $\tilde{\mathbf{U}}_{1,0}$ is equal to zero at infinity, we obtain that $\Delta_\xi \varphi_{1,0} = 0$ in $\tilde{\Omega}$ (the quantity $\tilde{\rho}_0 \tilde{c}_0$ being always strictly positive). With the vanishing boundary conditions for $\varphi_{1,0}$, we obtain that $\varphi_{1,0}$ is equal to zero everywhere in $\tilde{\Omega}$. Then, taking the divergence of $\tilde{\mathbf{U}}_{1,0}$ yields

$$\nabla_\xi \cdot \tilde{\mathbf{U}}_{1,0} = \nabla_\xi \cdot (\nabla_\xi \times \boldsymbol{\psi}_{1,0}) = 0, \quad (2.98)$$

hence $\tilde{\mathbf{U}}_{1,0}$ is divergence-free.

Now, using the property $\nabla \cdot \tilde{\mathbf{U}}_{1,0}$ in the equation (2.91) and rearranging some terms, we obtain

$$\tilde{\rho}_0 \frac{\partial^2 \tilde{\mathbf{U}}_{1,0}}{\partial t^2} - \nabla_\xi (\tilde{\rho}_0 \tilde{c}_0^2 \nabla_\xi \cdot \tilde{\mathbf{U}}_{1,2}) + \nabla_\xi (\tilde{\rho}_0 \tilde{\mathbf{U}}_{1,0} \cdot \mathbf{e}_3) - \tilde{\rho}'_0 (\tilde{\mathbf{U}}_{1,0} \cdot \mathbf{e}_3) \mathbf{e}_3 = 0. \quad (2.99)$$

Taking the curl of this equation yields

$$\nabla_\xi \times \left(\tilde{\rho}_0 \frac{\partial^2 \tilde{\mathbf{U}}_{1,0}}{\partial t^2} - \tilde{\rho}'_0 (\tilde{\mathbf{U}}_{1,0} \cdot \mathbf{e}_3) \mathbf{e}_3 \right) = 0, \quad (2.100)$$

This means that these terms can be expressed as the gradient of a potential function defined up to a constant and denoted $-\tilde{\varphi}_0$,

$$\tilde{\rho}_0 \frac{\partial^2 \tilde{\mathbf{U}}_{1,0}}{\partial t^2} - \tilde{\rho}'_0 (\tilde{\mathbf{U}}_{1,0} \cdot \mathbf{e}_3) \mathbf{e}_3 = -\nabla_\xi \tilde{\varphi}_0. \quad (2.101)$$

The new function $\tilde{\varphi}_0$ can be understood as the Lagrange multiplier for the incompressibility constraint. However, one must be cautious that $\tilde{\varphi}_0$ is not similar to a pressure in this case, and rather plays the role of a velocity potential, as we will see later in the case of homogeneous density. The function $\tilde{\varphi}_0$ can be expressed differently. By using the definition (2.101) in the equation (2.99), we have

$$\nabla_\xi (-\tilde{\varphi}_0 - \tilde{\rho}_0 \tilde{c}_0^2 \nabla_\xi \cdot \tilde{\mathbf{U}}_{1,2} + \tilde{\rho}_0 \tilde{\mathbf{U}}_{1,0} \cdot \mathbf{e}_3) = 0, \quad (2.102)$$

and since the potential $\tilde{\varphi}_0$ is defined up to a constant, it can be chosen such that, in $\hat{\Omega}$, we have

$$\tilde{\varphi}_0 = -\tilde{\rho}_0 \tilde{c}_0^2 \nabla_\xi \cdot \tilde{\mathbf{U}}_{1,2} + \tilde{\rho}_0 \tilde{\mathbf{U}}_{1,0} \cdot \mathbf{e}_3. \quad (2.103)$$

We deduce from this equality and (2.94) the boundary condition

$$\tilde{\varphi}_0 = \tilde{\rho}_0 \tilde{\mathbf{U}}_{1,0} \cdot \mathbf{e}_3 \quad \text{on } \tilde{\Gamma}_s. \quad (2.104)$$

To recover a dimensional system, the terms are multiplied by their corresponding characteristic scales, and $\hat{\varphi}_0 = \tilde{\rho} U \tilde{\varphi}_0$ is defined. The limit solution $\hat{\mathbf{U}}_{1,0} = U \tilde{\mathbf{U}}_{1,0}$ satisfies

$$\begin{cases} \hat{\rho}_0 \frac{\partial^2 \hat{\mathbf{U}}_{1,0}}{\partial t^2} - g \hat{\rho}'_0 (\hat{\mathbf{U}}_{1,0} \cdot \mathbf{e}_3) \mathbf{e}_3 + g \nabla_\xi \hat{\varphi}_0 = 0 & \text{in } \hat{\Omega}, \\ \nabla_\xi \cdot \hat{\mathbf{U}}_{1,0} = 0 & \text{in } \hat{\Omega}, \end{cases} \quad (2.105)$$

with the boundary conditions

$$\begin{cases} \hat{\mathbf{U}}_{1,0} \cdot \hat{\mathbf{n}}_b = \hat{u}_{b,1} & \text{on } \hat{\Gamma}_b, \\ \nabla_\xi \cdot \hat{\mathbf{U}}_{1,0} = 0 & \text{on } \hat{\Gamma}_s, \\ \hat{\varphi}_0 = \hat{\rho}_0 \hat{\mathbf{U}}_{1,0} \cdot \mathbf{e}_3 & \text{on } \hat{\Gamma}_s, \end{cases} \quad (2.107)$$

$$\quad (2.108)$$

$$\quad (2.109)$$

We show that the model (2.105)-(2.109) preserves an energy. Taking the scalar product of (2.105) with $\partial_t \hat{\mathbf{U}}_{1,0}$ and integrating over $\hat{\Omega}$ yields

$$\frac{1}{2} \frac{d}{dt} \int_{\hat{\Omega}} \hat{\rho}_0 \left| \frac{\partial \hat{\mathbf{U}}_{1,0}}{\partial t} \right|^2 d\xi - \int_{\hat{\Omega}} g \hat{\rho}'_0 (\hat{\mathbf{U}}_{1,0} \cdot \mathbf{e}_3) \mathbf{e}_3 \cdot \frac{\partial \hat{\mathbf{U}}_{1,0}}{\partial t} d\xi + \int_{\hat{\Omega}} g \frac{\partial \hat{\mathbf{U}}_{1,0}}{\partial t} \cdot \nabla_\xi \hat{\varphi}_0 d\xi = 0. \quad (2.110)$$

The last term of Equation (2.110) is integrated by parts. With the vanishing divergence of $\hat{\mathbf{U}}_{1,0}$ and the bottom condition (2.107) it holds that

$$\int_{\hat{\Omega}} g \frac{\partial \hat{\mathbf{U}}_{1,0}}{\partial t} \cdot \nabla_\xi \hat{\varphi}_0 d\xi = \int_{\hat{\Gamma}_s} g \hat{\varphi}_0 \frac{\partial \hat{\mathbf{U}}_{1,0}}{\partial t} \cdot \mathbf{e}_3 d\sigma - \int_{\hat{\Gamma}_b} g \hat{\varphi}_0 \frac{\partial \hat{u}_{b,1}}{\partial t} d\sigma, \quad (2.111)$$

then $\hat{\varphi}_0$ is replaced in the surface integral using Equation (2.109),

$$\begin{aligned} \frac{1}{2} \frac{d}{dt} \int_{\hat{\Omega}} \hat{\rho}_0 \left| \frac{\partial \hat{\mathbf{U}}_{1,0}}{\partial t} \right|^2 d\xi - \int_{\hat{\Omega}} g \hat{\rho}'_0 (\hat{\mathbf{U}}_{1,0} \cdot \mathbf{e}_3) \mathbf{e}_3 \cdot \frac{\partial \hat{\mathbf{U}}_{1,0}}{\partial t} d\xi \\ + \int_{\hat{\Gamma}_s} g \hat{\rho}_0 \hat{\mathbf{U}}_{1,0} \cdot \mathbf{e}_3 \frac{\partial \hat{\mathbf{U}}_{1,0}}{\partial t} \cdot \mathbf{e}_3 d\sigma = \int_{\hat{\Gamma}_b} g \hat{\varphi}_0 \frac{\partial \hat{u}_{b,1}}{\partial t} d\sigma. \end{aligned} \quad (2.112)$$

By defining the energy

$$\mathcal{E}_{incomp} = \frac{1}{2} \int_{\hat{\Omega}} \hat{\rho}_0 \left| \frac{\partial \hat{\mathbf{U}}_{1,0}}{\partial t} \right|^2 d\xi - \frac{1}{2} \int_{\hat{\Omega}} g \hat{\rho}'_0 |\hat{\mathbf{U}}_{1,0} \cdot \mathbf{e}_3|^2 d\xi + \frac{1}{2} \int_{\hat{\Gamma}_s} g \hat{\rho}_0 |\hat{\mathbf{U}}_{1,0} \cdot \mathbf{e}_3|^2 d\sigma, \quad (2.113)$$

the equation (2.110) can be formulated in the following way:

$$\frac{d}{dt} \mathcal{E}_{incomp} = \int_{\hat{\Gamma}_b} g \varphi_0 \frac{\partial \hat{u}_{b,1}}{\partial t}. \quad (2.114)$$

Each term of \mathcal{E}_{incomp} has the same interpretation as in \mathcal{E} . Note that the acoustic term of \mathcal{E} is not present in \mathcal{E}_{incomp} . The potential energy associated with the internal waves is also written differently, as in the formal limit $\hat{c}_0 \rightarrow \infty$, the buoyancy frequency reads $N^2 = -g \hat{\rho}'_0 / \hat{\rho}_0$.

Remark: The condition $|\hat{\rho}'_0| / \hat{\rho}_0 > g / \hat{c}_0^2$ is no longer required because the destabilizing effects in the energy equation (2.56) come from the compressibility, and here it is neglected. This can be seen by formally assuming that the sound speed is infinite, then the squared buoyancy frequency reads $N^2 = -g \hat{\rho}'_0 / \hat{\rho}_0$. Density must still decrease with depth, but can be homogeneous.

The system (2.106)-(2.105) represents an incompressible fluid. However, this system is different from the classical Poisson equation found in the literature (Lighthill, 1978) because of the assumption of a non-homogeneous background density. For the sake of comparison with other models, assume now that the ocean at rest has a homogeneous density, $\hat{\rho}'_0 = 0$. Taking the divergence of Equation (2.105) yields

$$\Delta_{\xi} \hat{\varphi}_0 = 0. \quad (2.115)$$

The boundary conditions are written differently to ease the comparison. The bottom boundary condition is obtained by taking the scalar product of Equation (2.105) with $\hat{\mathbf{n}}_b$, and replacing the first term with Equation (2.107) differentiated twice in time,

$$-\hat{\rho}_0 \frac{\partial^2 \hat{u}_{b,1}}{\partial t^2} - g \hat{\rho}'_0 (\hat{\mathbf{U}}_{1,0} \cdot \mathbf{e}_3) \mathbf{e}_3 \cdot \hat{\mathbf{n}}_b + g \nabla_{\xi} \hat{\varphi}_0 \cdot \hat{\mathbf{n}}_b = 0. \quad (2.116)$$

For the surface condition, the equation (2.109) is differentiated twice in time and the term in $\partial_{tt}^2 \hat{\mathbf{U}}_{1,0}$ is replaced with (2.105),

$$\frac{\partial^2 \hat{\varphi}_0}{\partial t^2} - g \hat{\rho}'_0 (\hat{\mathbf{U}}_{1,0} \cdot \mathbf{e}_3) + g \frac{\partial \hat{\varphi}_0}{\partial \xi_3} = 0 \quad \text{on } \hat{\Gamma}_s. \quad (2.117)$$

With the assumption of a homogeneous density, the boundary conditions (2.116), (2.117) read then

$$\begin{cases} \nabla_{\xi} \hat{\varphi}_0 \cdot \hat{\mathbf{n}}_b = -\hat{\rho}_0 g \hat{u}_{b,1} & \text{on } \hat{\Gamma}_b, \\ \frac{\partial^2 \hat{\varphi}_0}{\partial t^2} + g \frac{\partial \hat{\varphi}_0}{\partial \xi_3} = 0 & \text{on } \hat{\Gamma}_s. \end{cases} \quad (2.118)$$

$$\quad (2.119)$$

The Poisson equation (2.115) with boundary conditions (2.118) - (2.119) is the system satisfied by the velocity flow of an incompressible homogeneous free-surface fluid (Lighthill, 1978, Chap. 3.1). Note that it was required that $\hat{\rho}'_0 \neq 0$ in the system (2.53) to obtain an a priori positive energy. Here this assumption is dropped, however, a rather simple expression for the preserved energy can

be derived: multiplying Equation (2.115) by $\partial_t \hat{\varphi}_0$, integrating by parts and using Equation (2.118)-(2.119), we obtain

$$\int_{\hat{\Omega}} \Delta_{\xi} \hat{\varphi}_0 \frac{\partial \hat{\varphi}_0}{\partial t} d\xi = - \int_{\hat{\Omega}} \nabla_{\xi} \varphi \cdot \nabla_{\xi} \left(\frac{\partial \hat{\varphi}_0}{\partial t} \right) d\xi - \int_{\Gamma_s} \frac{1}{g} \frac{\partial \hat{\varphi}_0}{\partial t} \frac{\partial^2 \hat{\varphi}_0}{\partial t^2} d\sigma + \int_{\Gamma_b} \hat{\rho}_0 g \frac{\partial \hat{\varphi}_0}{\partial t} \hat{u}_{b,1} d\sigma. \quad (2.120)$$

We define the energy

$$\mathcal{E}_{Poisson} = \frac{1}{2} \left(\int_{\hat{\Omega}} |\nabla_{\xi} \hat{\varphi}|^2 d\xi + \int_{\Gamma_s} \frac{1}{g} \left(\frac{\partial \hat{\varphi}_0}{\partial t} \right)^2 d\sigma \right), \quad (2.121)$$

Then it holds that

$$\frac{d}{dt} \mathcal{E}_{Poisson} = - \int_{\Gamma_b} \hat{\rho}_0 g \frac{\partial \hat{\varphi}_0}{\partial t} \hat{u}_{b,1} d\sigma. \quad (2.122)$$

By comparison with the energy of the barotropic system (2.78), we see that the first term of (2.121) is the kinetic energy and the second term of (2.121) is the potential energy associated with the surface waves.

Acoustic limit

Another possible simplification of the system (2.53) - (2.55) is to keep only the acoustic terms. This choice is justified for short time scale, because the propagation speed of the acoustic waves and the gravity waves have different orders of magnitude (Longuet-Higgins, 1950). Here we show that in the acoustic limit, the model reduces to a classical acoustic equation.

With the time scale $L/\tau = C$, corresponding to the acoustic wave, and with the same small parameter $\delta = \text{Ma}/\text{Fr}$ as before, the system (2.84) becomes

$$\tilde{\rho}_0 \frac{\partial^2 \tilde{\mathbf{U}}_1}{\partial t^2} - \nabla_{\xi} (\tilde{\rho}_0 \tilde{c}_0^2 \nabla_{\xi} \cdot \tilde{\mathbf{U}}_1) + \delta^2 \tilde{\rho}_0 (\nabla_{\xi} (\tilde{\mathbf{U}}_1 \cdot \mathbf{e}_3) - \nabla_{\xi} \cdot \tilde{\mathbf{U}}_1 \mathbf{e}_3) = 0 \quad \text{in } \tilde{\Omega}, \quad (2.123)$$

With the boundary conditions

$$\begin{cases} \tilde{\mathbf{U}}_1 \cdot \tilde{\mathbf{n}}_b = \tilde{u}_{b,1} & \text{on } \tilde{\Gamma}_b, \\ \nabla_{\xi} \cdot \tilde{\mathbf{U}}_1 = 0 & \text{on } \tilde{\Gamma}_s. \end{cases} \quad (2.124)$$

$$(2.125)$$

As before, we make the following ansatz for $\tilde{\mathbf{U}}_1$:

$$\tilde{\mathbf{U}}_1 = \tilde{\mathbf{U}}_{1,0} + \delta^2 \tilde{\mathbf{U}}_{1,2} + \mathcal{O}(\delta^3). \quad (2.126)$$

One can see that the limit term $\delta \rightarrow 0$ for the volumic equation (2.123) is

$$\tilde{\rho}_0 \frac{\partial^2 \tilde{\mathbf{U}}_{1,0}}{\partial t^2} - \nabla_{\xi} (\tilde{\rho}_0 \tilde{c}_0^2 \nabla_{\xi} \cdot \tilde{\mathbf{U}}_{1,0}) = 0. \quad (2.127)$$

Taking the curl of this equation yields

$$\frac{\partial^2}{\partial t^2} (\nabla_{\xi} \times (\tilde{\rho}_0 \tilde{\mathbf{U}}_{1,0})) = 0, \quad (2.128)$$

hence the curl of $\tilde{\rho}_0 \tilde{\mathbf{U}}_{1,0}$ is affine in time. Moreover, it is equal to zero due to the vanishing initial conditions. By the Helmholtz decomposition theorem, the term $\tilde{\rho}_0 \tilde{\mathbf{U}}_{1,0}$ can be expressed as the gradient of some function $\tilde{\psi}_0$ defined up to a constant,

$$\tilde{\rho}_0 \tilde{\mathbf{U}}_{1,0} = \nabla_\xi \tilde{\psi}_0. \quad (2.129)$$

By substituting in equation (2.127), we have

$$\nabla_\xi \left(\frac{\partial^2 \tilde{\psi}_0}{\partial t^2} - \tilde{\rho}_0 \tilde{c}_0^2 \nabla_\xi \cdot (\tilde{\rho}_0^{-1} \nabla_\xi \tilde{\psi}_0) \right) = 0, \quad (2.130)$$

then it holds that

$$\frac{\partial^2 \tilde{\psi}_0}{\partial t^2} - \tilde{\rho}_0 \tilde{c}_0^2 \nabla_\xi \cdot (\tilde{\rho}_0^{-1} \nabla_\xi \tilde{\psi}_0) = 0, \quad (2.131)$$

since $\tilde{\psi}_0$ is defined up to a constant. We need the boundary conditions to conclude. Evaluating Equation (2.127) at the surface yields

$$\tilde{\rho}_0 \frac{\partial^2 \tilde{\mathbf{U}}_{1,0}}{\partial t^2} - \frac{\partial}{\partial \xi_3} (\tilde{\rho}_0 \tilde{c}_0^2 \nabla_\xi \cdot \tilde{\mathbf{U}}_{1,0}) \mathbf{e}_3 = 0 \quad \text{on } \tilde{\Gamma}_s. \quad (2.132)$$

Using the surface condition (2.125) in (2.132) yields

$$\tilde{\rho}_0 \frac{\partial^2 \tilde{\mathbf{U}}_{1,0}}{\partial t^2} = 0 \quad \text{on } \tilde{\Gamma}_s. \quad (2.133)$$

With the definition of the potential $\tilde{\psi}_0$, it holds that

$$\frac{\partial^2 \nabla \tilde{\psi}_0}{\partial t^2} = 0 \quad \text{on } \tilde{\Gamma}_s, \quad (2.134)$$

hence one has

$$\frac{\partial^2 \tilde{\psi}_0}{\partial t^2} = C(t) \quad \text{on } \tilde{\Gamma}_s, \quad (2.135)$$

where C does not depend on space. Moreover, since $\tilde{\psi}_0$ vanishes at infinity, the constant C is equal to zero, hence $\partial_{tt}^2 \tilde{\psi}_0 = 0$ on $\tilde{\Gamma}_s$. With the vanishing initial conditions, this implies that $\tilde{\psi}_0 = 0$ on $\tilde{\Gamma}_s$. To recover a dimensional system, the terms are multiplied by their corresponding characteristic scales, and $\hat{\psi}_0 = \bar{\rho} U L \tilde{\psi}_0$ is defined. The system reads then

$$\frac{\partial^2 \hat{\psi}_0}{\partial t^2} - \hat{\rho}_0 \hat{c}_0^2 \nabla_\xi \cdot (\hat{\rho}_0^{-1} \nabla_\xi \hat{\psi}_0) = 0 \quad \text{in } \hat{\Omega}, \quad (2.136)$$

with the boundary conditions

$$\begin{cases} \nabla_\xi \hat{\psi}_0 \cdot \hat{\mathbf{n}}_b = \hat{u}_{b,1} & \text{on } \hat{\Gamma}_b, \\ \hat{\psi}_0 = 0 & \text{on } \hat{\Gamma}_s. \end{cases} \quad (2.137)$$

$$(2.138)$$

The system (2.136)-(2.138) is the classical wave equation for the potential $\hat{\psi}_0$, with a propagation speed \hat{c}_0^2 and a non-homogeneous density.

An energy equation can be obtained by multiplying Equation (2.136) by $\partial_t \hat{\psi}_0 / (\hat{\rho}_0 \hat{c}_0^2)$ and integrating over the domain. The result reads after an integration by parts

$$\frac{d}{dt} \mathcal{E}_{acoustic} = - \int_{\hat{\Gamma}_b} \frac{1}{\hat{\rho}_0} \frac{\partial \hat{\psi}_0}{\partial t} \hat{u}_{b,1} d\sigma, \quad (2.139)$$

where the acoustic energy is

$$\mathcal{E}_{acoustic} = \frac{1}{2} \int_{\hat{\Omega}} \frac{1}{\hat{\rho}_0 \hat{c}_0^2} \left(\frac{\partial \hat{\psi}_0}{\partial t} \right)^2 d\xi + \frac{1}{2} \int_{\hat{\Omega}} \frac{1}{\hat{\rho}_0} |\nabla \hat{\psi}_0|^2 d\xi. \quad (2.140)$$

With the same analysis as in the previous cases, one can show that the first term of (2.140) is the acoustic energy, and the second term is the kinetic energy.

Remark: In Sections 2.3.2 and 2.3.2, the equations (2.115) - (2.119) and (2.136)-(2.138) use the Lagrangian description whereas the equations from the literature use the Eulerian description. In the general case, the use of different coordinate systems would cause two problems. First, when doing the change of coordinates, new terms should appear from the space or time differentiation. Second, the description of the domain is different, and this implies that the boundary conditions are not evaluated at the same location. In the next section, we will show that the first problem does not exist in our case, due to the lack of a background velocity. As for the second problem, the linear Eulerian models are obtained by evaluating the boundary conditions at a fixed water height. In this regard, they use the same boundary as if they were in a Lagrangian description of the domain, so that the comparison remains valid.

The equations with their boundary conditions and the associated energy, for the general model and its different simplifications, are summarized in Table 2.1.

2.4 The model in Eulerian coordinates

The equations we have been working on are defined on the reference domain $\hat{\Omega}$. However, the linear equations for the acoustic-gravity waves are generally written in Eulerian coordinates. To compare our model with those from the literature, the equations must be formulated on the moving domain $\Omega(t)$. In this section, we present a method to write the system in Eulerian coordinate.

2.4.1 General method

The aim is to write the equation on a moving domain $\Omega(t)$, hence a transformation $\phi : \hat{\Omega} \rightarrow \Omega(t)$ is needed. We start by using a first-order approximation of the real transformation ϕ . The transformation ϕ is developed for small displacements,

$$\phi(\xi, t) = \xi + \varepsilon \phi_1(\xi, t) + \mathcal{O}(\varepsilon^2). \quad (2.141)$$

Let $\phi_\varepsilon(\xi, t) = \xi + \varepsilon \phi_1(\xi, t)$ be its first-order approximation. Here, ϕ_ε is used to define the equivalent domain and its boundary,

$$\Omega_\varepsilon(t) = \phi_\varepsilon(\hat{\Omega}), \quad \Gamma_{s,eq} = (\phi_\varepsilon(\hat{\Gamma}_s)), \quad \Gamma_{b,eq} = (\phi_\varepsilon(\hat{\Gamma}_b)). \quad (2.142)$$

The coordinates on the equivalent domain are written $\mathbf{x} = (x, y, z)$. For any generic function $\hat{X}(\xi, t)$ defined in $\hat{\Omega}$, a function $X(\mathbf{x}, t)$ is defined in Ω_ε by the following change of variables:

$$X(\mathbf{x}, t) = \hat{X}(\phi_\varepsilon^{-1}(\mathbf{x}, t), t), \quad (2.143)$$

which is equivalent to

$$\hat{X}(\xi, t) = X(\phi_\varepsilon(\xi, t), t). \quad (2.144)$$

	Equation in $\hat{\Omega}$	Boundary conditions	Energy
General model (Section 2.2.3)	$\hat{\rho}_0 \frac{\partial^2 \hat{\mathbf{U}}_1}{\partial t^2} - \nabla (\hat{\rho}_0 \hat{c}_0^2 \nabla \cdot \hat{\mathbf{U}}_1) - \rho_0 g ((\nabla \cdot \hat{\mathbf{U}}_1 \cdot \mathbf{e}_3) + \nabla \cdot \hat{\mathbf{U}}_1 \mathbf{e}_3) = 0$	$\hat{\mathbf{U}}_1 \cdot \hat{\mathbf{n}}_b = \hat{u}_{b,1}, \quad \hat{\Gamma}_b$ $\nabla \cdot \hat{\mathbf{U}}_1 = 0, \quad \hat{\Gamma}_s$	$\mathcal{E} = \frac{1}{2} \int_{\hat{\Omega}} \hat{\rho}_0 \left(\left \frac{\partial \hat{\mathbf{U}}_1}{\partial t} \right ^2 + \left(\hat{c}_0 \nabla \cdot \hat{\mathbf{U}}_1 - \frac{g}{\hat{c}_0} \nabla \cdot \hat{\mathbf{U}}_1 \cdot \mathbf{e}_3 \right)^2 \right) + \frac{1}{2} \int_{\hat{\Omega}} \hat{\rho} N^2 (\hat{\mathbf{U}}_1 \cdot \mathbf{e}_3)^2 d\boldsymbol{\xi} + \frac{1}{2} \int_{\hat{\Gamma}_s} \hat{\rho}_0 g (\hat{\mathbf{U}}_1 \cdot \mathbf{e}_3)^2 d\sigma$
Barotropic case (Section 2.3.1)	$\frac{\hat{\rho}_0}{\hat{c}_0^2} \frac{\partial^2 \psi}{\partial t^2} - \nabla \cdot (\hat{\rho}_0 \nabla \psi) = 0, = 0,$ $\hat{\mathbf{U}}_1 = \nabla \psi$	$\nabla \psi \cdot \hat{\mathbf{n}}_b = \hat{u}_{b,1}, \quad \hat{\Gamma}_b$ $\frac{\partial^2 \psi}{\partial t^2} + g \frac{\partial \psi}{\partial \xi_3} = 0, \quad \hat{\Gamma}_s$	$\mathcal{E}_{bar} = \frac{1}{2} \int_{\hat{\Omega}} \hat{\rho}_0 \left(\frac{1}{\hat{c}_0^2} \left(\frac{\partial \psi}{\partial t} \right)^2 + \nabla \psi ^2 \right) d\boldsymbol{\xi} + \frac{1}{2} \int_{\hat{\Gamma}_s} \frac{\hat{\rho}_0}{g} \left(\frac{\partial \psi}{\partial t} \right)^2 d\sigma$
Incompressible limit (Section 2.3.2)	$\hat{\rho}_0 \frac{\partial^2 \hat{\mathbf{U}}_{1,0}}{\partial t^2} - g \hat{\rho}'_0 (\hat{\mathbf{U}}_{1,0} \cdot \mathbf{e}_3) \mathbf{e}_3 + g \nabla \hat{\phi}_0 = 0,$ $\nabla \cdot \hat{\mathbf{U}}_{1,0} = 0$	$\hat{\mathbf{U}}_{1,0} \cdot \hat{\mathbf{n}}_b = \hat{u}_{b,1}, \quad \hat{\Gamma}_b$ $\nabla \cdot \hat{\mathbf{U}}_{1,0} = 0, \quad \hat{\Gamma}_s$ $\hat{\phi}_0 = g \hat{\rho}_0 \hat{\mathbf{U}}_{1,0} \cdot \mathbf{e}_3, \quad \hat{\Gamma}_s$	$\mathcal{E}_{incomp} = \frac{1}{2} \int_{\hat{\Omega}} \left(\hat{\rho}_0 \left \frac{\partial \hat{\mathbf{U}}_{1,0}}{\partial t} \right ^2 - g \hat{\rho}'_0 \hat{\mathbf{U}}_{1,0} \cdot \mathbf{e}_3 ^2 \right) d\boldsymbol{\xi} + \frac{1}{2} \int_{\hat{\Gamma}_s} g \hat{\rho}_0 \hat{\mathbf{U}}_{1,0} \cdot \mathbf{e}_3 ^2 d\sigma$
Incompressible limit, homogeneous density (Section 2.3.2)	$\Delta \hat{\phi}_0 = 0,$ $\frac{\partial^2 \hat{\mathbf{U}}_{1,0}}{\partial t^2} = -\frac{g}{\hat{\rho}_0} \nabla \hat{\phi}_0$	$\nabla \hat{\phi}_0 \cdot \hat{\mathbf{n}}_b = -\hat{\rho}_0 g \hat{u}_{b,1}, \quad \hat{\Gamma}_b$ $\frac{\partial^2 \hat{\phi}_0}{\partial t^2} + g \frac{\partial \hat{\phi}_0}{\partial \xi_3} = 0, \quad \hat{\Gamma}_s$	$\mathcal{E}_{Poisson} = \frac{1}{2} \left(\int_{\hat{\Omega}} \nabla \hat{\phi}_0 ^2 d\boldsymbol{\xi} + \int_{\hat{\Gamma}_s} \frac{1}{g} \left(\frac{\partial \hat{\phi}_0}{\partial t} \right)^2 d\sigma \right)$
Acoustic limit (Section 2.3.2)	$\frac{\partial^2 \hat{\psi}_0}{\partial t^2} - \hat{\rho}_0 \hat{c}_0^2 \nabla \cdot (\hat{\rho}_0^{-1} \nabla \hat{\psi}_0) = 0,$ $\hat{\mathbf{U}}_1 = \nabla \hat{\psi}_0$	$\nabla \hat{\psi}_0 \cdot \hat{\mathbf{n}}_b = \hat{u}_{b,1}, \quad \hat{\Gamma}_b$ $\hat{\psi}_0 = 0, \quad \hat{\Gamma}_s$	$\mathcal{E}_{acoustic} = \frac{1}{2} \int_{\hat{\Omega}} \frac{1}{\hat{\rho}_0} \left(\frac{\partial \hat{\psi}_0}{\partial t} \right)^2 + \nabla \hat{\psi}_0 ^2 d\boldsymbol{\xi}$

Table 2.1: Summary of the equations, boundary conditions and energy for the general model and its simplifications. For conciseness the operator $\nabla_{\boldsymbol{\xi}}$ and $\Delta_{\boldsymbol{\xi}}$ are denoted respectively ∇ and Δ .

as long as $\boldsymbol{\phi}_\varepsilon$ is invertible. Then, if the function \hat{X} has a first-order approximation $\hat{X} = \hat{X}_0 + \varepsilon\hat{X}_1 + \mathcal{O}(\varepsilon^2)$, then the function X also has a first-order approximation $X = X_0 + \varepsilon X_1 + \mathcal{O}(\varepsilon^2)$ and it holds that (see Appendix B)

$$\begin{cases} \nabla_\xi \hat{X}_0 = \nabla X_0, & (2.145) \\ \frac{\partial \hat{X}_0}{\partial t} = \frac{\partial X_0}{\partial t}, & (2.146) \\ \nabla_\xi \hat{X}_1 = (\nabla_\xi \mathbf{d}_1)^T \nabla X_0 + \nabla X_1, & (2.147) \\ \frac{\partial \hat{X}_1}{\partial t} = \frac{\partial X_1}{\partial t} + \mathbf{U}_1 \cdot \nabla X_0. & (2.148) \end{cases}$$

In the following, when writing the equations satisfied by the free surface of Ω_ε , we will also use

$$\frac{\partial \boldsymbol{\phi}_\varepsilon}{\partial t} = \varepsilon \hat{\mathbf{U}}_1. \quad (2.149)$$

2.4.2 The model in Eulerian coordinates

Using the change of variable (2.144) in the system (2.48)–(2.50) and with the equalities (2.145)–(2.148), we obtain the following system for $\mathbf{U}_1, \rho_1, \rho_1$, defined in Ω_ε :

$$\begin{cases} \rho_0 \frac{\partial \mathbf{U}_1}{\partial t} + \nabla \rho_1 = \rho_1 \mathbf{g}, & (2.150) \\ \frac{\partial \rho_1}{\partial t} + \nabla \cdot (\rho_0 \mathbf{U}_1) = 0, & (2.151) \\ \frac{\partial \rho_1}{\partial t} + \nabla \rho_0 \cdot \mathbf{U}_1 + \rho_0 c_0^2 \nabla \cdot \mathbf{U}_1 = 0. & (2.152) \end{cases}$$

And ρ_0, ρ_0 satisfy the limit equations

$$\begin{cases} \frac{\partial \rho_0}{\partial t} = 0, & (2.153) \\ \nabla \rho_0 = \rho_0 \mathbf{g}. & (2.154) \end{cases}$$

To close the system (2.150)–(2.154), boundary conditions should be prescribed. To get a linear problem, one wants to prescribe this condition on the fixed domain $\hat{\Omega}$. To do so we assume in the following that the equations (2.150)–(2.154) are defined in $\hat{\Omega}$. It would be true if $\hat{\Omega} \subset \Omega_\varepsilon$, but the inclusion is in general not verified. Because of this approximation, errors of order $\mathcal{O}(\varepsilon)$ may be introduced. For this reason, the system in Lagrangian coordinates should be preferred, at least for future extension of this work.

Boundary conditions and free surface description

Following the approach of Nougier et al. (2015), we show that a description for the free surface can be obtained. In the following, the components of the fluid velocity are denoted $\mathbf{U}_1 = (U_1^1, U_1^2, U_1^3)^T$. The surface is defined by $\Gamma_{s,eq} = \boldsymbol{\phi}_\varepsilon(\hat{\Gamma}_s)$, and we assume that at each time t , it can be parametrized as the graph η_ε . The elevation η_ε is a function of x, y and t and can be decomposed in the following way:

$$\eta_\varepsilon(x, y, t) = H + \varepsilon \eta_1(x, y, t). \quad (2.155)$$

From the correspondence between the free surface and the particle displacement, it holds that

$$\boldsymbol{\phi}_\varepsilon^3(\xi_1, \xi_2, H, t) = \eta_\varepsilon(x(\xi_1, \xi_2, H, t), y(\xi_1, \xi_2, H, t), t). \quad (2.156)$$

Differentiating (2.156) in time and using the equation (2.149) yields

$$\varepsilon \hat{U}_1^3(\xi_1, \xi_2, H, t) = \frac{\partial \eta_\varepsilon}{\partial t} + \varepsilon \hat{U}_1^1(\xi_1, \xi_2, H, t) \frac{\partial \eta_\varepsilon}{\partial x} + \varepsilon \hat{U}_1^2(\xi_1, \xi_2, H, t) \frac{\partial \eta_\varepsilon}{\partial y}. \quad (2.157)$$

We use the change of variables $\phi_\varepsilon(\boldsymbol{\xi}, t) = \boldsymbol{\xi} + \varepsilon \boldsymbol{\phi}_1(\boldsymbol{\xi}, t)$,

$$\begin{aligned} \varepsilon U_1^3(\phi_\varepsilon(\xi_1, \xi_2, H, t), t) &= \frac{\partial \eta_\varepsilon}{\partial t} + \varepsilon U_1^1(\phi_\varepsilon(\xi_1, \xi_2, H, t), t) \frac{\partial \eta_\varepsilon}{\partial x} \\ &\quad + \varepsilon U_1^2(\phi_\varepsilon(\xi_1, \xi_2, H, t), t) \frac{\partial \eta_\varepsilon}{\partial y}. \end{aligned} \quad (2.158)$$

After a Taylor development and keeping only the terms in ε , it holds that

$$U_1^3(x, y, H, t) = \frac{\partial \eta_1}{\partial t}, \quad (2.159)$$

which is the linearized equation for the free surface. Then the dynamic boundary conditions are linearized. With the change of variables, the boundary conditions (2.24), (2.51) and (2.52) become

$$\begin{cases} \mathbf{U}_1 \cdot \mathbf{n}_b = u_{b,1} & \text{on } \Gamma_{b,eq}, \\ p_0 = p^a & \text{on } \Gamma_{s,eq}, \\ p_1 = 0 & \text{on } \Gamma_{s,eq}. \end{cases} \quad (2.160)$$

$$p_0 = p^a \quad \text{on } \Gamma_{s,eq}, \quad (2.161)$$

$$p_1 = 0 \quad \text{on } \Gamma_{s,eq}. \quad (2.162)$$

If we linearize (2.162) only, we would miss the first-order term coming from (2.161). From (2.161) and (2.162), we deduce the boundary condition for the pressure

$$p_0 + \varepsilon p_1 = p^a \quad \text{on } \Gamma_{s,eq}. \quad (2.163)$$

A Taylor development of p_0 and p_1 around $z = H$ on $\Gamma_{s,eq}$ yields

$$p_0(H) + \varepsilon(p_1(x, y, H, t) + p_0'(H)\eta_1) + \mathcal{O}(\varepsilon^2) = p^a. \quad (2.164)$$

After an identification of the powers of ε , it holds that

$$p_0(H) = p^a, \quad p_1(x, y, H, t) = \rho_0(x, y, H, t)g\eta_1(x, y, t). \quad (2.165)$$

In a similar way, the linearization of Equation (2.160) reads

$$U_1^3(x, y, z_b) - U_1^1(x, y, z_b) \partial_x z_b - U_1^2(x, y, z_b) \partial_y z_b = u_{b,1}(x, y, t). \quad (2.166)$$

Hence the equations for $\mathbf{U}_1, \rho_1, p_1$ can be fully defined on the domain $\hat{\Omega}$, with an error in $\mathcal{O}(\varepsilon^2)$. Finally, note that the system (2.150)-(2.152) with the boundary conditions (2.165),(2.166) and the kinematic condition (2.159) is shown to be energy preserving, locally as well as over a whole water column (Lighthill, 1978; Lotto and Dunham, 2015).

In this section, we have derived the linear equation in Eulerian coordinates, even though an approximation on the domain in which the equations are defined was necessary. The computations of Section 2.4.1 also justify that in the absence of mean flow and with the evaluation of the boundary conditions at a fixed height, the linear system in Eulerian coordinates is similar to that in Lagrangian coordinate, up to terms in $\mathcal{O}(\varepsilon^2)$. At the same time, the linearization in the Lagrangian coordinates is better defined. For this reason, the system in Lagrangian coordinates is preferred for the rest of this work. We conclude this paper with the study of the dispersion relation obtained from Equation (2.53).

2.5 Dispersion relation

A key aspect of wave models is the related dispersion relation, which we derive here from Equation (2.53) and solve numerically. First note that if one defines the equivalent pressure p_ε , the equivalent density ρ_ε and the equivalent velocity \mathbf{U}_ε by

$$p_\varepsilon = p_0 + \varepsilon p_1, \quad \rho_\varepsilon = \rho_0 + \varepsilon \rho_1, \quad \mathbf{U}_\varepsilon = \varepsilon \mathbf{U}_1, \quad (2.167)$$

then a combination of the equations (2.150)–(2.154) yields the following system for p_ε , ρ_ε and \mathbf{U}_ε :

$$\begin{cases} \rho_0 \frac{\partial \mathbf{U}_\varepsilon}{\partial t} + \nabla p_\varepsilon = \rho_\varepsilon \mathbf{g} + \mathcal{O}(\varepsilon^2), & (2.168) \\ \frac{\partial \rho_\varepsilon}{\partial t} + \nabla \cdot (\rho_0 \mathbf{U}_\varepsilon) = \mathcal{O}(\varepsilon^2), & (2.169) \\ \frac{\partial p_\varepsilon}{\partial t} + \nabla p_0 \cdot \mathbf{U}_\varepsilon + \rho_0 c_0^2 \nabla \cdot \mathbf{U}_\varepsilon = \mathcal{O}(\varepsilon^2). & (2.170) \end{cases}$$

This system is comparable – up to the terms in $\mathcal{O}(\varepsilon^2)$ – to the system studied in the paper by Auclair et al. (2021). Auclair et al. (2021) thoroughly analyze the dispersion relation for the model of a stratified compressible fluid with a constant sound speed.

To make the computations clearer, the problem is restricted to a 2-dimensional configuration in ξ_1 and ξ_3 . We also assume that the bottom is flat. Following the approach of Auclair et al. (2021), the angular frequency ω and the horizontal wavenumber frequency k_x are defined, and we seek a solution of the form

$$\hat{\rho}_0 \hat{\mathbf{U}}_1(\xi_1, \xi_3, t) = \begin{pmatrix} \tilde{U}^1(\xi_3) \\ \tilde{U}^3(\xi_3) \end{pmatrix} e^{i(k_x \xi_1 - \omega t)}. \quad (2.171)$$

First, Equation (2.53) is written differently to make the unknown $\hat{\rho}_0 \hat{\mathbf{U}}_1$ appear,

$$\frac{\partial^2 \hat{\rho}_0 \hat{\mathbf{U}}_1}{\partial t^2} - \nabla_\xi (\hat{c}_0^2 \nabla_\xi \cdot (\hat{\rho}_0 \hat{\mathbf{U}}_1)) - \nabla_\xi \left(\frac{\hat{c}_0^2 N_0^2}{g} \rho_0 \hat{\mathbf{U}}_1 \cdot \mathbf{e}_3 \right) - g \nabla_\xi \cdot (\hat{\rho}_0 \hat{\mathbf{U}}_1) \mathbf{e}_3 = 0 \quad (2.172)$$

Using the ansatz (2.171) in Equation (2.172) yields

$$\omega^2 \tilde{U}^1 + ik_x \left(\hat{c}_0^2 (ik_x \tilde{U}^1 + (\tilde{U}^3)') + \frac{\hat{c}_0^2 N^2}{g} \tilde{U}^3 \right) = 0, \quad (2.173)$$

$$\omega^2 \tilde{U}^3 + \partial_3 \left(\hat{c}_0^2 (ik_x \tilde{U}^1 + (\tilde{U}^3)') \right) + \partial_3 \left(\frac{\hat{c}_0^2 N^2}{g} \tilde{U}^3 \right) + g (ik_x \tilde{U}^1 + (\tilde{U}^3)') = 0. \quad (2.174)$$

Using the equation (2.173), the horizontal component \tilde{U}^1 is expressed as a function of the vertical component,

$$\tilde{U}^1 = -ik_x \frac{\hat{c}_0^2 D (\tilde{U}^3)' + (\hat{c}_0^2 - gD) \tilde{U}^3}{D(\omega^2 - \hat{c}_0^2 k_x^2)}, \quad (2.175)$$

where D is a depth scale, defined by

$$\frac{1}{D} = \frac{N^2}{g} + \frac{g}{\hat{c}_0^2} = \frac{\hat{\rho}'_0}{\hat{\rho}_0}. \quad (2.176)$$

We also define the quantity

$$S = 2 \frac{\hat{c}'_0}{\hat{c}_0}. \quad (2.177)$$

Replacing \tilde{U}^1 in the equation (2.174) yields, after some computations,

$$(\tilde{U}^3)'' + \left(\frac{1}{D} + \omega^2 S^2 \right) (\tilde{U}^3)' + \left(\frac{\omega^2}{\hat{c}_0^2} + k_x^2 \frac{N^2 - \omega^2}{\omega^2} - \frac{D'}{D^2} + S \left(\frac{g}{\hat{c}_0^2} + \frac{N^2}{g} \frac{\omega^2}{\omega^2 - \hat{c}_0^2 k_x^2} \right) \right) \tilde{U}^3 = 0. \quad (2.178)$$

To write an harmonic equation, the following change of variable is made:

$$\tilde{U}^3(z) = \tilde{U}^3(H) F(z) \exp \left(\int_z^H \frac{\alpha}{2} dz' \right), \quad \alpha = \frac{1}{D} + \omega^2 S. \quad (2.179)$$

Then $F(0) = 0$, $F(H) = 1$ and F satisfies the equation

$$F'' + k_z^2 F = 0 \quad (2.180)$$

where the vertical wavenumber k_z is defined by

$$k_z^2 + k_x^2 \frac{N^2 - \omega^2}{\omega^2} + \frac{\omega^2}{\hat{c}_0^2} - \frac{1 + 2D'}{4D^2} - \frac{1}{2} \omega^2 S' + S \left(\frac{g}{\hat{c}_0^2} + \frac{N^2}{g} \frac{\omega^2}{\omega^2 - \hat{c}_0^2 k_x^2} - \frac{\omega^2}{2D} - \frac{1}{4} \omega^4 S \right) = 0, \quad (2.181)$$

The equation (2.181) is the dispersion relation for the two wavenumbers k_x , k_z and the frequency ω . It is a generalization of the inner dispersion relation by Auclair et al. (2021) to the case of a non-constant sound speed. Indeed, with a constant sound speed one has $S = 0$ and (2.181) is exactly the inner dispersion relation in Auclair et al. (2021).

Remark. In the most general case, the scalars N , D and S depend on the depth z , hence k_z also depends on z . It is then not clear whether the solution to Equation (2.180) and the profile \tilde{U}^3 can be written explicitly. When k_z does not depend on z , as in the study by Auclair et al. (2021), the expression of the profile \tilde{U}^3 is used with the boundary conditions to obtain a boundary dispersion relation. In our case, k_z is not a constant, and the boundary dispersion relation is not easily deduced.

Numerical approximation of the dispersion relation

An evaluation of the equation (2.181) is possible once the limit state for the pressure and the density is computed. The differential equation for the pressure (2.22) is numerically solved for the temperature profile shown in figure 2.3a.

Then the density and the speed of sound are computed from the tabulations given by IAPWS-SR7 (2009). Figure 2.3b, 2.3c show the obtained density and speed of sound. With these profiles, the dispersion relation (2.181) is computed. Figure 2.4 shows the contours of the vertical wavenumber as a function of the horizontal wavenumber and the angular frequency, at different depths. For the sake of comparison, the plotted variables are the adimensionned variables $\delta_x = k_x H$, $\delta_z = k_z H$ and $\log_{10}(\delta_\omega)$, where $\delta_\omega = \omega \sqrt{H/g}$.

Although Figure 2.4 is close to the one in the paper by Auclair et al. (2021), one can notice the influence of the ocean depth on the contours. This first result suggests that the variation of the parameters \hat{c}_0 , N , D with depth plays a non-negligible role in the waves dispersion.

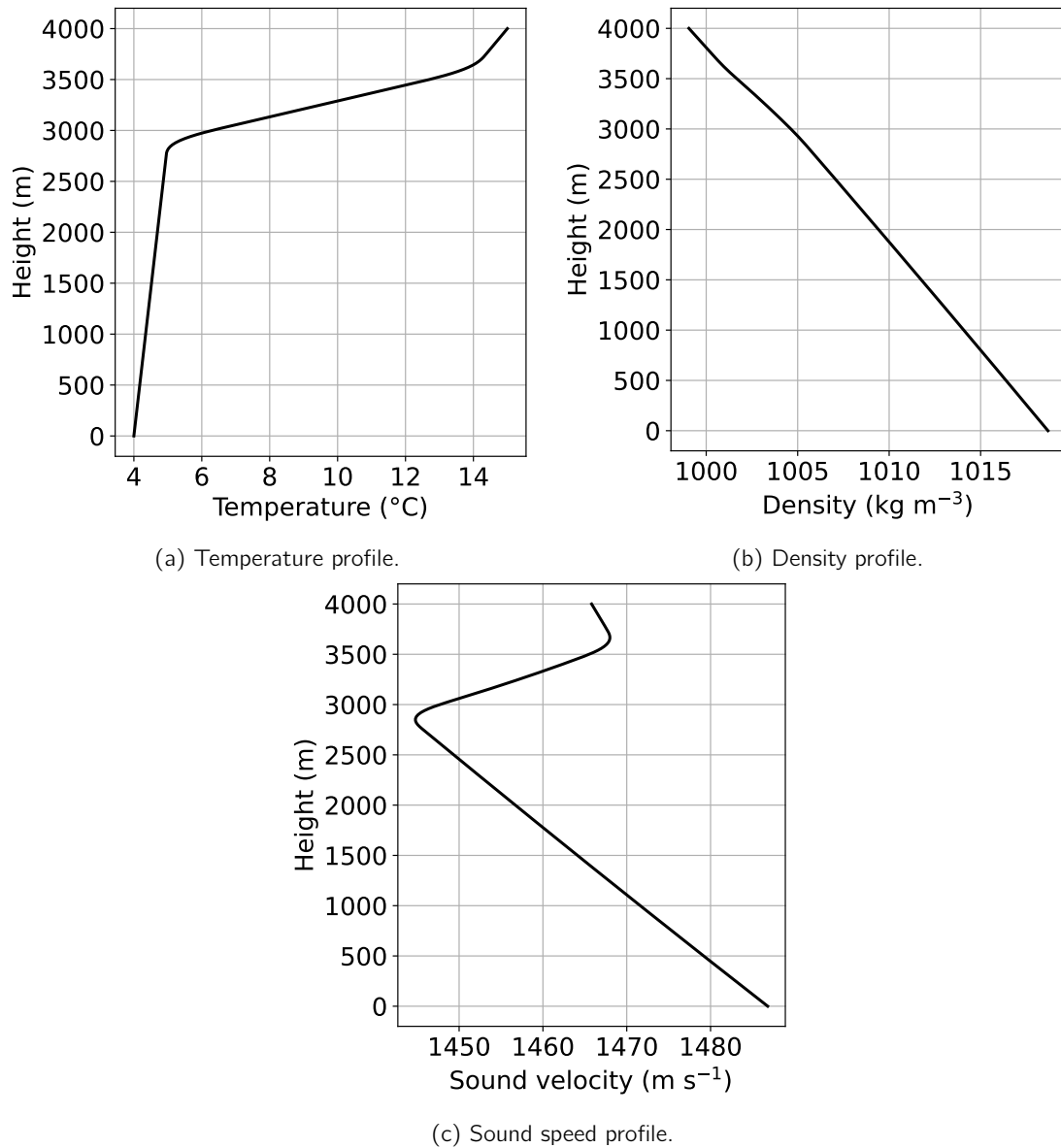


Figure 2.3: Temperature, density and sound speed profiles used for the computation of the dispersion relation where $\xi_3 = 0$ is the seafloor and $\xi_3 = 4000$ m is the ocean surface: [2.3a](#) temperature profile ; [2.3b](#) density profile and [2.3c](#) sound speed profile.

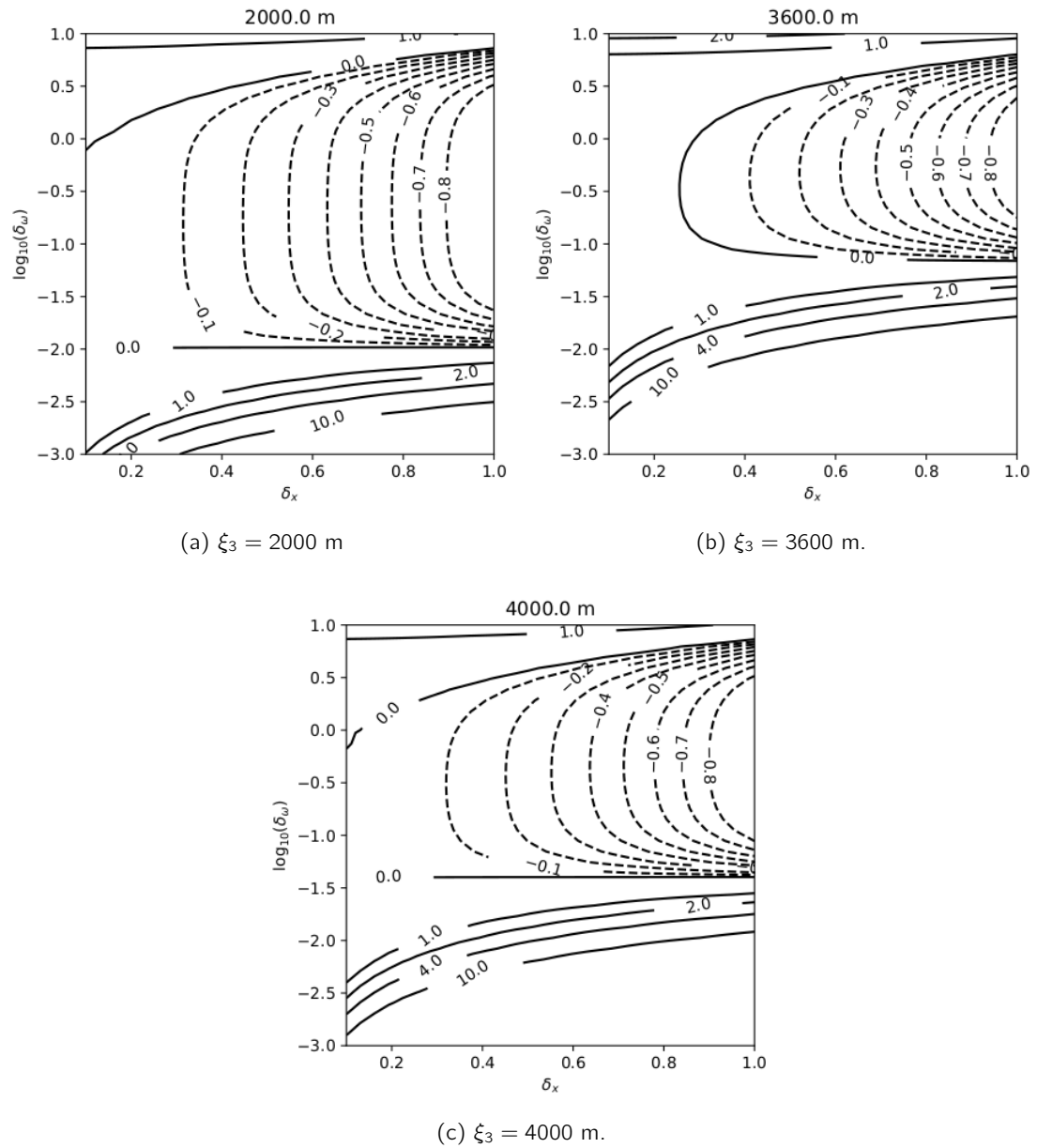


Figure 2.4: Contour of the vertical wavenumber as a function of the horizontal wavenumber δ_x and the angular frequency δ_ω , at different depths ξ_3 : 2.4a $\xi_3 = 2000$ m; 2.4b $\xi_3 = 3600$ m; 2.4c $\xi_3 = 4000$ m.

2.6 Conclusion and future work

In this work, we have presented a system describing the propagation of acoustic-gravity waves in a free-surface fluid over an varying bed (bathymetry) and with a variable sound speed, applicable to describe in particular hydro-acoustic and tsunami waves generated by earthquakes or landslides in the ocean. Through a rigorous linearization of the compressible Euler equation, we have obtained a model able to represent many physical phenomena, such as the SOFAR channel or the propagation of internal waves. The variety of these phenomena is well represented in the dispersion relation.

In the derivation, only a few assumptions are made and some common simplifying hypotheses were avoided. In particular, the fluid is not necessarily assumed barotropic and its flow is not assumed irrotational. Thanks to this approach, many terms representing different physical phenomena are kept in the wave-like equation. With a numerical approximation, one could then compute their respective magnitude, and justify which terms can be neglected. Note also that in the present work the source term is a displacement of the seabed, but this is not restrictive and other source terms could be used (a change in the surface pressure for example).

With additional assumptions compatible with the derivation of the system, such as considering a barotropic fluid, or restricting the model to the incompressible regime or to the acoustic regime, we are able to recover simpler models widely studied in the literature. The mathematical study of the more complete model can help gain insight on the other ones. For example, we could clearly identify the assumptions made in the hydro-acoustic waves model used by Stiasnie (2010); Sammarco et al. (2013) and others. Namely, in those models, the fluid is assumed barotropic, and the effects of stratification and gravity are neglected inside the domain. The study of the more complete model also helped to write the conservation of energy in each simplified case. The linear model in Lagrangian coordinates can also be used to recover the linearized Euler equations in Eulerian coordinates. This brings a clear understanding of the usual – nevertheless non-satisfactory – assumption that is used to derive the aforementioned models in Eulerian coordinates.

The wave-like formulation of the model makes it a good candidate for a numerical approximation by the finite element method. The fact that it preserves an energy suggests that the problem is well posed, which motivates a more thorough study of the mathematical problem. Numerical implementation of this model will make it possible to simulate acoustic-gravity waves generated by earthquakes and landslide sources accounting for the complex bathymetry, thus contributing to improve early-warning systems. It will also help to quantify the errors made in more simple models, such as the hypothesis of an irrotational flow. These two aspects will be investigated in a future work.

Appendix

A Derivation of the energy equation

In this section, an energy equation for the system (2.53) is obtained. Recall that the system (2.53) reads in $\hat{\Omega}$,

$$\hat{\rho}_0 \frac{\partial^2 \hat{\mathbf{U}}_1}{\partial t^2} - \nabla_{\xi} (\hat{\rho}_0 \hat{c}_0^2 \nabla_{\xi} \cdot \hat{\mathbf{U}}_1) - (\nabla_{\xi} \hat{\mathbf{U}}_1)^T \hat{\rho}_0 \mathbf{g} + \hat{\rho}_0 \nabla_{\xi} \cdot \hat{\mathbf{U}}_1 \mathbf{g} = 0, \quad (182)$$

with the boundary conditions

$$\begin{cases} \hat{\mathbf{U}}_1 \cdot \mathbf{n}_b = \hat{u}_{b,1} & \text{on } \hat{\Gamma}_b, \\ \nabla_{\xi} \cdot \hat{\mathbf{U}}_1 = 0 & \text{on } \hat{\Gamma}_s. \end{cases} \quad (183)$$

$$(184)$$

By taking the scalar product of (2.53) with $\partial_t \hat{\mathbf{U}}_1$ and integrating over the domain we have

$$\begin{aligned} \int_{\Omega} \frac{\partial \hat{\mathbf{U}}_1}{\partial t} \cdot \left(\hat{\rho}_0 \frac{\partial^2 \hat{\mathbf{U}}_1}{\partial t^2} \right) d\xi - \int_{\Omega} \frac{\partial \hat{\mathbf{U}}_1}{\partial t} \cdot (\nabla_{\xi} (\hat{\rho}_0 \hat{c}_0^2 \nabla_{\xi} \cdot \hat{\mathbf{U}}_1)) d\xi \\ + \int_{\Omega} \frac{\partial \hat{\mathbf{U}}_1}{\partial t} \cdot (\nabla_{\xi} (\hat{\mathbf{U}}_1 \cdot \mathbf{e}_3) \hat{\rho}_0 g) d\xi - \int_{\Omega} \frac{\partial \hat{\mathbf{U}}_1}{\partial t} \cdot (\hat{\rho}_0 \nabla_{\xi} \cdot \hat{\mathbf{U}}_1 g \mathbf{e}_3) d\xi = 0. \end{aligned} \quad (185)$$

For the first integral of (185), it holds that

$$\int_{\Omega} \frac{\partial \hat{\mathbf{U}}_1}{\partial t} \cdot \left(\hat{\rho}_0 \frac{\partial^2 \hat{\mathbf{U}}_1}{\partial t^2} \right) d\xi = \frac{d}{dt} \int_{\Omega} \frac{\hat{\rho}_0}{2} \left| \frac{\partial \hat{\mathbf{U}}_1}{\partial t} \right|^2 d\xi. \quad (186)$$

The second term of (185) is integrated by parts, using $\nabla_{\xi} \cdot \hat{\mathbf{U}}_1 = 0$ on the surface and $\hat{\mathbf{U}}_1 \cdot \hat{\mathbf{n}}_b = \hat{u}_{b,1}$ at the bottom (hence $\partial_t (\hat{\mathbf{U}}_1 \cdot \hat{\mathbf{n}}_b) = \partial_t \hat{u}_{b,1}$),

$$\begin{aligned} - \int_{\Omega} \frac{\partial \hat{\mathbf{U}}_1}{\partial t} \cdot \nabla_{\xi} (\hat{\rho}_0 \hat{c}_0^2 \nabla_{\xi} \cdot \hat{\mathbf{U}}_1) d\xi = \frac{1}{2} \frac{d}{dt} \int_{\Omega} \hat{\rho}_0 \hat{c}_0^2 |\nabla_{\xi} \cdot \hat{\mathbf{U}}_1|^2 d\xi \\ - \int_{\hat{\Gamma}_b} \hat{\rho}_0 \hat{c}_0^2 \nabla_{\xi} \cdot \hat{\mathbf{U}}_1 \frac{\partial \hat{u}_{b,1}}{\partial t} d\sigma. \end{aligned} \quad (187)$$

For the computation of the two last integral of (185), we define

$$(I) = \int_{\Omega} \frac{\partial \hat{\mathbf{U}}_1}{\partial t} \cdot (\nabla_{\xi} (\hat{\mathbf{U}}_1 \cdot \mathbf{e}_3) \hat{\rho}_0 g) d\xi - \int_{\Omega} \frac{\partial \hat{\mathbf{U}}_1}{\partial t} \cdot (\hat{\rho}_0 \nabla_{\xi} \cdot \hat{\mathbf{U}}_1 g \mathbf{e}_3) d\xi, \quad (188)$$

an we denote by $\hat{\mathbf{n}}_b$ the vector normal to the boundary $\partial\Omega$. Here, (I) is integrated by parts and reads

$$\begin{aligned} (I) = \int_{\partial\Omega} \hat{\rho}_0 g \hat{\mathbf{U}}_1 \cdot \mathbf{e}_3 \frac{\partial \hat{\mathbf{U}}_1}{\partial t} \cdot \hat{\mathbf{n}}_b d\sigma - \int_{\Omega} g \hat{\mathbf{U}}_1 \cdot \mathbf{e}_3 \nabla_{\xi} \cdot (\hat{\rho}_0 \frac{\partial \hat{\mathbf{U}}_1}{\partial t}) d\xi \\ - \int_{\Omega} \hat{\rho}_0 g \frac{\partial \hat{\mathbf{U}}_1}{\partial t} \cdot \mathbf{e}_3 \nabla_{\xi} \cdot \hat{\mathbf{U}}_1 d\xi. \end{aligned} \quad (189)$$

The boundary term is simplified using $\partial_t (\hat{\mathbf{U}}_1 \cdot \hat{\mathbf{n}}_b) = \partial_t \hat{u}_{b,1}$ at the bottom. On the boundary $\hat{\Gamma}_s$, the surface is horizontal, hence the normal vector is the unit vector \mathbf{e}_3 , so it holds that

$$\begin{aligned} (I) = \int_{\hat{\Gamma}_b} \hat{\rho}_0 g \hat{\mathbf{U}}_1 \cdot \mathbf{e}_3 \frac{\partial \hat{u}_{b,1}}{\partial t} d\sigma + \int_{\hat{\Gamma}_s} \hat{\rho}_0 g \hat{\mathbf{U}}_1 \cdot \mathbf{e}_3 \frac{\partial \hat{\mathbf{U}}_1}{\partial t} \cdot \mathbf{e}_3 d\sigma \\ - \int_{\Omega} g \hat{\mathbf{U}}_1 \cdot \mathbf{e}_3 \nabla_{\xi} \cdot (\hat{\rho}_0 \frac{\partial \hat{\mathbf{U}}_1}{\partial t}) d\xi - \int_{\Omega} \hat{\rho}_0 g \frac{\partial \hat{\mathbf{U}}_1}{\partial t} \cdot \mathbf{e}_3 \nabla_{\xi} \cdot \hat{\mathbf{U}}_1 d\xi. \end{aligned} \quad (190)$$

Next we develop the gradient in the third integral of Equation (190). Note that $\hat{\rho}_0$ depends only on the vertical coordinate, then we have

$$- \int_{\Omega} g \hat{\mathbf{U}}_1 \cdot \mathbf{e}_3 \frac{\partial \hat{\mathbf{U}}_1}{\partial t} \cdot \nabla_{\xi} \hat{\rho}_0 = - \int_{\Omega} g \hat{\mathbf{U}}_1 \cdot \mathbf{e}_3 \frac{\partial \hat{\mathbf{U}}_1}{\partial t} \cdot \mathbf{e}_3 \frac{d\hat{\rho}_0}{d\xi_3} = - \frac{1}{2} \frac{d}{dt} \int_{\Omega} \hat{\rho}'_0 g |\hat{\mathbf{U}}_1 \cdot \mathbf{e}_3|^2, \quad (191)$$

hence we obtain

$$\begin{aligned}
(I) = & \int_{\hat{\Gamma}_b} \hat{\rho}_0 g \hat{\mathbf{U}}_1 \cdot \mathbf{e}_3 \frac{\partial \hat{u}_{b,1}}{\partial t} d\sigma + \frac{1}{2} \frac{d}{dt} \int_{\hat{\Gamma}_s} \hat{\rho}_0 g |\hat{\mathbf{U}}_1 \cdot \mathbf{e}_3|^2 d\sigma \\
& - \frac{1}{2} \frac{d}{dt} \int_{\Omega} g \hat{\rho}'_0 |\hat{\mathbf{U}}_1 \cdot \mathbf{e}_3|^2 d\xi - \int_{\Omega} \hat{\rho}_0 g \hat{\mathbf{U}}_1 \cdot \mathbf{e}_3 \frac{\partial}{\partial t} (\nabla_{\xi} \cdot \hat{\mathbf{U}}_1) d\xi \\
& - \int_{\Omega} \hat{\rho}_0 g \frac{\partial \hat{\mathbf{U}}_1}{\partial t} \cdot \mathbf{e}_3 \nabla_{\xi} \cdot \hat{\mathbf{U}}_1 d\xi. \quad (192)
\end{aligned}$$

The two last terms of (192) are put together,

$$\begin{aligned}
(I) = & \int_{\hat{\Gamma}_b} \hat{\rho}_0 g \hat{\mathbf{U}}_1 \cdot \mathbf{e}_3 \frac{\partial \hat{u}_{b,1}}{\partial t} d\sigma + \frac{1}{2} \frac{d}{dt} \int_{\hat{\Gamma}_s} \hat{\rho}_0 g |\hat{\mathbf{U}}_1 \cdot \mathbf{e}_3|^2 d\sigma \\
& - \frac{1}{2} \frac{d}{dt} \int_{\Omega} g \hat{\rho}'_0 |\hat{\mathbf{U}}_1 \cdot \mathbf{e}_3|^2 d\xi - \frac{d}{dt} \int_{\Omega} \hat{\rho}_0 g \hat{\mathbf{U}}_1 \cdot \mathbf{e}_3 \nabla_{\xi} \cdot \hat{\mathbf{U}}_1 d\xi. \quad (193)
\end{aligned}$$

Summing the terms (186), (187) and (193) yields

$$\begin{aligned}
& \frac{d}{dt} \int_{\Omega} \rho_0 \frac{1}{2} \left| \frac{\partial \hat{\mathbf{U}}_1}{\partial t} \right|^2 d\xi + \frac{1}{2} \frac{d}{dt} \int_{\Omega} \hat{\rho}_0 \left(\hat{c}_0 \nabla_{\xi} \cdot \hat{\mathbf{U}}_1 - \frac{g}{\hat{c}_0} \hat{\mathbf{U}}_1 \cdot \mathbf{e}_3 \right)^2 d\xi \\
& - \frac{1}{2} \frac{d}{dt} \int_{\Omega} \hat{\rho}_0 (\hat{\mathbf{U}}_1 \cdot \mathbf{e}_3)^2 \left(\frac{g^2}{\hat{c}_0^2} + \frac{g \hat{\rho}'_0}{\hat{\rho}_0} \right) d\xi + \frac{1}{2} \frac{d}{dt} \int_{\hat{\Gamma}_s} \hat{\rho}_0 g (\hat{\mathbf{U}}_1 \cdot \mathbf{e}_3)^2 d\sigma \\
& = \int_{\hat{\Gamma}_b} \rho_0 \left(\hat{c}_0^2 \nabla_{\xi} \cdot \hat{\mathbf{U}}_1 - \hat{\rho}_0 g \hat{\mathbf{U}}_1 \cdot \mathbf{e}_3 \right) \frac{\partial \hat{u}_{b,1}}{\partial t} d\sigma, \quad (194)
\end{aligned}$$

and by defining

$$N_b = - \left(\frac{g^2}{\hat{c}_0^2} + \frac{g \hat{\rho}'_0}{\hat{\rho}_0} \right), \quad (195)$$

we obtain the energy equation (2.56).

B From the Lagrangian to the Eulerian coordinates

In this section, we derive the relations between the zero- and first-order approximation in Eulerian and in Lagrangian coordinates, when differentiating with respect to time or space. First note that ϕ_0 and ϕ_1 can be expressed in terms of the displacement \mathbf{d} . From the assumption of small displacements, it holds that $\mathbf{d} = \varepsilon \mathbf{d}_1 + \mathcal{O}(\varepsilon^2)$, then identifying the powers of ε and summing yields

$$\boldsymbol{\phi}_{\varepsilon}(\boldsymbol{\xi}, t) = \boldsymbol{\xi} + \varepsilon \mathbf{d}_1(\boldsymbol{\xi}, t).$$

From the change of coordinate we have

$$\nabla_{\xi} \hat{X} = (\nabla_{\xi} \phi_{\varepsilon})^T \nabla X = (Id + \varepsilon \nabla_{\xi} \mathbf{d}_1)^T \nabla X,$$

and using this identity for $\hat{X} = \hat{X}_0 + \varepsilon \hat{X}_1$ yields

$$\nabla_{\xi} (\hat{X}_0 + \varepsilon \hat{X}_1) = \nabla X_0 + \varepsilon ((\nabla_{\xi} \mathbf{d}_1)^T \nabla X_0 + \nabla X_1) + \mathcal{O}(\varepsilon^2).$$

By identifying the powers of ε , it holds that

$$\nabla_{\xi} \hat{X}_0 = \nabla X_0, \quad \nabla_{\xi} \hat{X}_1 = (\nabla_{\xi} \mathbf{d}_1)^T \nabla X_0 + \nabla X_1.$$

The same method is used for the time derivative. Starting with

$$\frac{\partial \hat{X}}{\partial t}(\boldsymbol{\xi}, t) = \frac{\partial X}{\partial t}(\boldsymbol{\phi}_\varepsilon(\boldsymbol{\xi}), t) + \frac{\partial \boldsymbol{\phi}_\varepsilon}{\partial t}(\boldsymbol{\xi}) \cdot \nabla X(\boldsymbol{\phi}_\varepsilon(\boldsymbol{\xi}), t),$$

we obtain after replacing X and \hat{X} by their first-order approximation,

$$\frac{\partial \hat{X}_0}{\partial t} + \varepsilon \frac{\partial \hat{X}_1}{\partial t} = \frac{\partial X_0}{\partial t} + \varepsilon \left(\frac{\partial X_1}{\partial t} + \frac{\partial \mathbf{d}_1}{\partial t} \cdot \nabla X_0 \right) + \mathcal{O}(\varepsilon^2).$$

With $\partial_t \mathbf{d}_1(\boldsymbol{\xi}, t) = \hat{\mathbf{U}}_1(\boldsymbol{\xi}, t) = \mathbf{U}_1(\mathbf{x}, t)$, it holds that

$$\frac{\partial X_0}{\partial t} + \varepsilon \left(\frac{\partial X_1}{\partial t} + \mathbf{U}_1 \cdot \nabla X_0 \right) + \mathcal{O}(\varepsilon^2).$$

We identify the powers of ε ,

$$\frac{\partial \hat{X}_0}{\partial t} = \frac{\partial X_0}{\partial t}, \quad \frac{\partial \hat{X}_1}{\partial t} = \frac{\partial X_1}{\partial t} + \mathbf{U}_1 \cdot \nabla X_0.$$

Mathematical analysis and numerical approximation of the model

Contents

3.1	Introduction	62
3.2	Preliminary definitions	65
3.3	Analysis of the potential-based formulation	69
3.3.1	Variational formulation	69
3.3.2	Existence and uniqueness results	70
3.3.3	Energy identity	71
3.4	Analysis of the velocity-based formulation	72
3.4.1	Variational formulation and uniqueness result	72
3.4.2	Existence results	74
3.5	Equivalence of the velocity and the potential formulations	78
3.5.1	Equivalence for the relaxed problem	78
3.5.2	The equivalence for the non-relaxed formulations	81
3.6	Numerical illustration	82
3.6.1	Discretization	83
3.6.2	Numerical example: tsunami and hydro-acoustic waves generation	86
3.7	Conclusion and future work	89

The content of this chapter will be submitted as a paper under the title "Well-posedness and potential-based formulation for the propagation of acoustic and tsunami waves".

Abstract: In this chapter, we study the model presented in Chapter 2, describing the propagation of acoustic and surface gravity waves. We introduce first the suitable mathematical framework for the analysis. An alternative formulation, based on a new variable, is then introduced. The new variable can be understood as a "generalized potential", in the sense that the new variable corresponds to the fluid potential in the particular case of an irrotational flow. The new formulation presents several advantages, both for the analysis and the numerical resolution. We prove then the well-posedness of both formulations, and show that they are equivalent. Finally, the formulations are discretized with a spectral element method in space and a finite difference method in time, and

we illustrate numerically the equivalence.

3.1 Introduction

Context and motivation. There is a growing interest for models coupling acoustic waves and surface gravity waves, since they could greatly improve tsunami early-warning systems. A linear model describing the propagation of acoustic and gravity waves was presented by Dubois et al. (2023). This model can be seen as a particular case of the Galbrun equation, with a vanishing mean flow and a non-homogeneous boundary condition of Dirichlet type. There is a wide literature concerning the Galbrun equation, however the functional framework for its well-posedness is still subject to debate (Maeder et al., 2020). Moreover, most of the studies on the Galbrun equation focus on the harmonic case (see the review made by Maeder et al., 2020, and the references therein). The literature on the analysis of the evolution problem is scarcer. We refer to the work by Bonnet-Bendhia et al. (2006), and the paper by Hägg and Berggren (2021). Bonnet-Bendhia et al. (2006) study the Galbrun equation with a uniform mean flow by using a regularization method. In their work, Hägg and Berggren (2021) show that the solution to the Galbrun equation can be deduced from the solution to the linearized Euler equation.

For the case of a vanishing mean flow with homogeneous Dirichlet conditions, it was already noted by Berriri (2006) that the problem is well-posed in $H_0(\text{div}, \Omega)$, the space of functions defined on Ω , with a squared integrable divergence, and whose normal trace vanishes at the boundary of the domain. However, the model presented by Dubois et al. (2023) does not fall under this category because of the presence of a boundary term, and as we will show, the lifting of the boundary term is not as trivial as one could expect. The frame proposed by Hägg and Berggren (2021) is adapted to the model, but it requires to solve first the so-called linearized Euler equations.

In this work, we propose a method for showing existence and uniqueness in the case of a vanishing mean flow and for non-homogeneous boundary conditions. Moreover, we propose an equivalent dual problem whose mathematical study and discretisation are more straightforward than the original formulation. Finally, we present some numerical simulation validating the model by comparison with the literature, and illustrating the equivalence between both formulations.

The system of partial differential equations. In what follows, the equations are written in Lagrangian coordinates, and denote by Ω the reference domain representing an ocean at rest. The coordinates of Ω are written (\mathbf{x}, z) , with the horizontal coordinate $\mathbf{x} \in \mathbb{R}^{d-1}$, $d = 2$ or $d = 3$. The domain is unbounded in the horizontal direction and bounded in the vertical direction, with a fixed surface at $z = H$ and a time-independant topography $z_b(\mathbf{x})$ at the bottom, see Fig. 3.1. The domain is written

$$\Omega = \{(\mathbf{x}, z) \mid \mathbf{x} \in \mathbb{R}^{d-1}, z_b(\mathbf{x}) \leq z \leq H\},$$

and its boundary is denoted $\Gamma = \partial\Omega$. The topography is assumed to satisfy the following conditions,

$$z_b \in W^{1,\infty}(\mathbb{R}^{d-1}) \quad \text{and} \quad \exists H_- > 0 \text{ such that } 0 \leq z_b(\mathbf{x}) \leq H_- < H.$$

These properties ensure that the domain Ω does not degenerate and is Lipschitz. The surface and bottom boundaries are respectively

$$\Gamma_s = \{(\mathbf{x}, H) \mid \mathbf{x} \in \mathbb{R}^{d-1}\} \quad \text{and} \quad \Gamma_b = \{(\mathbf{x}, z) \mid \mathbf{x} \in \mathbb{R}^{d-1}, z = z_b(\mathbf{x})\}.$$

The considered set of partial differential equation has been introduced by Dubois et al. (2023), it consists in a linear system of equations for the fluid velocity $\mathbf{U}(\mathbf{x}, z, t)$ and reads

$$\rho_0 \frac{\partial^2 \mathbf{U}}{\partial t^2} - \nabla (\rho_0 c_0^2 \nabla \cdot \mathbf{U} - \rho_0 g \mathbf{U} \cdot \mathbf{e}_z) - \nabla \cdot (\rho_0 g \mathbf{U}) \mathbf{e}_z = 0, \quad \text{in } \Omega \times [0, T]. \quad (3.1)$$

Equation (3.1) represents the propagation of the acoustic, internal gravity and surface gravity waves in a stably stratified fluid. The vector $\mathbf{e}_z = (0 \ 0 \ 1)^t$ is the unit vector along the z -axis. The constant scalar $g > 0$ is the acceleration of gravity. The parameters ρ_0 and c_0 are respectively the fluid background density and the sound speed. They depend on z only, and we make the following assumptions,

$$\rho_0 \in C^1([0, H]) \quad \text{and} \quad c_0 \in C^0([0, H]). \quad (3.2)$$

The velocity and the density must satisfy some positivity properties, one of which being non-standard: there exist $\beta_1 > 0$ and $\beta_2 > 0$ such that, for all $z \in [0, H]$,

$$\rho_0(z) > \beta_1, \quad c_0(z) > \beta_2 \quad \text{and} \quad N^2(z) = -\frac{g}{\rho_0(z)} \frac{d\rho_0(z)}{dz} - \frac{g^2}{c_0^2(z)} \geq 0.$$

The scalar N^2 is called the Brunt-Väisälä frequency, or buoyancy frequency. It corresponds to the frequency of the internal gravity waves (Gill, 1982). The case $N^2 < 0$ corresponds to a fluid that is denser above and lighter below, hence it is an unstable equilibrium. Since the linearization is done around a stable equilibrium we assume in the following $N^2 \geq 0$. The case $N^2 = 0$ corresponds to the case of a constant temperature, in which case the fluid is called barotropic.

Equation (3.1) is completed with boundary conditions. On the bottom Γ_b , the condition represents a localized displacement of amplitude u_b of the seabed, caused for example by an earthquake or a landslide. On the surface Γ_s , the condition represents a stress-free boundary condition. Here the stress is a pressure, and is proportional to the divergence of the velocity field. The boundary conditions read then

$$\mathbf{U} \cdot \mathbf{n}_b = u_b \quad \text{on } \Gamma_b \times [0, T], \quad \nabla \cdot \mathbf{U} = 0 \quad \text{on } \Gamma_s \times [0, T], \quad (3.3)$$

where, as usual, \mathbf{n} is the outward unitary normal of the domain Ω . The regularity of the displacement u_b will be stated later. Finally, in our context it is relevant to choose vanishing initial conditions, which also simplifies the forthcoming analysis,

$$\mathbf{U}(\mathbf{x}, z, 0) = 0, \quad \frac{\partial \mathbf{U}}{\partial t}(\mathbf{x}, z, 0) = 0 \quad \text{on } \Omega. \quad (3.4)$$

The dual problem. It is shown later that the problem (3.1)-(3.3) can be written as an abstract wave equation using an unbounded linear operator G ,

$$\frac{d^2 \mathbf{U}}{dt^2} + G^* \tilde{G} \mathbf{U} = 0, \quad (3.5)$$

where G^* is the adjoint of G and \tilde{G} is an extension of G . The introduction of this non-symmetric formulation using the extension \tilde{G} is motivated by the presence of a non-homogeneous essential condition in the boundary conditions (3.3). The expression (3.5) will be obtained rigorously in what follows. One originality of this work is to construct and analyse a “dual” wave-like problem for a new unknown Φ , satisfying

$$\frac{d^2 \Phi}{dt^2} + \tilde{G} G^* \Phi = 0. \quad (3.6)$$

Such problem is shown to be equivalent – in a sense given rigorously later – to the problem (3.5). Moreover, it presents several advantages from mathematical and numerical perspectives. The new unknown Φ has three scalar components, $\Phi = (\varphi, \psi, \gamma)^t$, where φ and ψ are scalar fields and $\gamma = \varphi|_{\Gamma_s}$. In the computations below, we show that Φ is related to the velocity \mathbf{U} by the formula

$$\mathbf{U} = -\nabla\varphi + N\left(\psi + \frac{N}{g}\varphi\right)\mathbf{e}_z, \quad (3.7)$$

hence it can be seen as a generalized potential. We also show that φ and ψ satisfy a second set of partial differential equations describing the same physical system as (3.1)-(3.3), more precisely

$$\begin{cases} \frac{\partial^2\varphi}{\partial t^2} + c_0^2\nabla \cdot \left(-\nabla\varphi + N\left(\psi + \frac{N}{g}\varphi\right)\mathbf{e}_z\right) + g\frac{\partial\varphi}{\partial z} - gN\left(\psi + \frac{N}{g}\varphi\right) = 0, & \text{in } \Omega \times [0, T], \\ \frac{\partial^2\psi}{\partial t^2} - N\frac{\partial\varphi}{\partial z} + N^2\left(\psi + \frac{N}{g}\varphi\right) = 0, & \text{in } \Omega \times [0, T]. \end{cases} \quad (3.8)$$

The system is completed with the same bottom boundary condition,

$$\mathbf{U} \cdot \mathbf{n} = -\nabla\varphi \cdot \mathbf{n} + N\left(\psi + \frac{N}{g}\varphi\right)(\mathbf{e}_z \cdot \mathbf{n}) = u_b, \quad \text{on } \Gamma_b \times [0, T]. \quad (3.10)$$

This condition is – mathematically speaking – a natural condition for the potentials (φ, ψ) . It is easier to consider than condition (3.3), for both the analysis and the discretisation. Finally, the surface boundary condition involves a second-order time derivative that accounts for gravity waves,

$$\frac{\partial^2\varphi}{\partial t^2} - g\mathbf{U} \cdot \mathbf{n} = 0, \quad \text{on } \Gamma_s \times [0, T]. \quad (3.11)$$

The initial conditions are deduced from (3.4), they read

$$\varphi(\mathbf{x}, z, 0) = \frac{\partial\varphi}{\partial t}(\mathbf{x}, z, 0) = 0, \quad \psi(\mathbf{x}, z, 0) = \frac{\partial\psi}{\partial t}(\mathbf{x}, z, 0) = 0 \quad \text{on } \Omega. \quad (3.12)$$

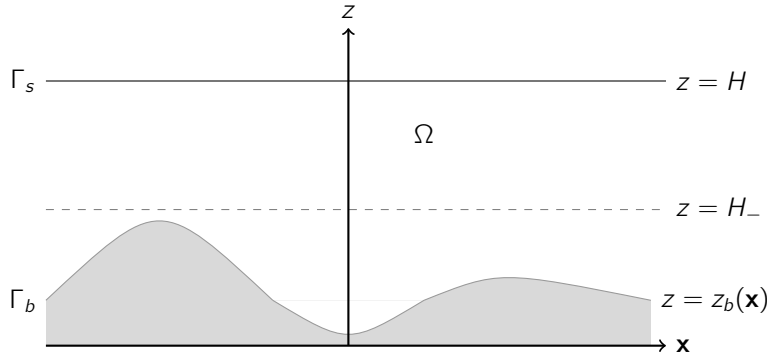
When $d = 3$, the system (3.8) - (3.12) involves only two scalar fields (φ and ψ), compared to three for the velocity based formulation (3.1). Moreover, this system is a generalisation to the one commonly introduced in hydrodynamics (Gill, 1982). Indeed, when considering the barotropic case, we have $N = 0$ and the system of partial differential equations (3.8)-(3.9) reduces to

$$\begin{cases} \frac{\partial^2\varphi}{\partial t^2} - c_0^2\Delta\varphi + g\frac{\partial\varphi}{\partial z} = 0, & \text{in } \Omega \times [0, T], \\ \frac{\partial^2\psi}{\partial t^2} = 0, & \text{in } \Omega \times [0, T]. \end{cases} \quad (3.13)$$

Because of the vanishing initial conditions, we have that $\psi = 0$. The system is then described by the function φ only. The boundary conditions are also simplified,

$$\frac{\partial^2\varphi}{\partial t^2} + g\nabla\varphi \cdot \mathbf{n} = 0, \quad \text{on } \Gamma_s \times [0, T] \quad \text{and} \quad \nabla\varphi \cdot \mathbf{n} = u_b, \quad \text{on } \Gamma_b \times [0, T]. \quad (3.15)$$

This simplified system corresponds to the system of equations that was already introduced in the literature (Dubois et al., 2023; Longuet-Higgins, 1950).

Figure 3.1: The domain Ω

Organisation of the work. We start by presenting in Section 3.2 the functional spaces and the operators used for studying the problems (3.1)-(3.4) and (3.8)-(3.12). In Section 3.3, we study first **the potential-based formulation** (3.8)-(3.12). Even though this formulation is rather uncommon we start with this one because the analysis is much more direct than the analysis of **the velocity-based formulation** (3.1)-(3.4). The velocity formulation is then studied in Section 3.4. The main difficulty of this section lies in finding a lifting operator for the boundary source term. The equivalence of the two formulations is proved in Section 3.5. In Section 3.6 we present a discretisation procedure of the two formulation using spectral finite elements (Cohen, 2001; Komatitsch and Tromp, 1999) and show some numerical illustrations for the equivalence between these two formulations.

3.2 Preliminary definitions

Hilbert spaces and trace operators. We start by introducing the space of H^1 -functions,

$$H^1(\Omega) = \{\varphi \in L^2(\Omega) \mid \nabla \varphi \in L^2(\Omega)^d\},$$

as well as the usual surjective trace operator

$$\gamma_0 : H^1(\Omega) \rightarrow H^{1/2}(\Gamma),$$

that is the extension to function in $H^1(\Omega)$ of the trace operator $\varphi \mapsto \varphi|_{\Gamma}$, defined for smooth functions. The forthcoming analysis requires the use of the standard space of square integrable functions with square integrable divergence,

$$H(\text{div}, \Omega) = \{\mathbf{U} \in L^2(\Omega)^d \mid \nabla \cdot \mathbf{U} \in L^2(\Omega)\}.$$

The space $H(\text{div}, \Omega)$ is equipped with the usual scalar product

$$\forall (\mathbf{U}, \tilde{\mathbf{U}}) \in H(\text{div}, \Omega) \times H(\text{div}, \Omega), \quad (\mathbf{U}, \tilde{\mathbf{U}})_{H(\text{div}, \Omega)} = (\mathbf{U}, \tilde{\mathbf{U}})_{L^2(\Omega)^d} + (\nabla \cdot \mathbf{U}, \nabla \cdot \tilde{\mathbf{U}})_{L^2(\Omega)},$$

In the following we use trace operators acting either on Γ_s or on Γ_b only. We introduce the trace operator acting on the surface

$$\gamma_{0,s} : H^1(\Omega) \rightarrow H^{1/2}(\Gamma_s), \quad \gamma_{0,s}(\varphi) = \gamma_0(\varphi)|_{\Gamma_s},$$

and the trace operator acting on the bottom

$$\gamma_{0,b} : H^1(\Omega) \rightarrow H^{1/2}(\Gamma_b), \quad \gamma_{0,s}(\varphi) = \gamma_0(\varphi)|_{\Gamma_b}.$$

Since Γ_s and Γ_b are “well-separated” – namely the distance between the two boundary is at least $H - H_-$ that is strictly positive – one can also define a surjective normal trace operators acting either on Γ_s or on Γ_b only. We introduce the normal trace operator

$$\gamma_{1,s} : H(\text{div}, \Omega) \rightarrow H^{-1/2}(\Gamma_s).$$

When applied to smooth functions, it corresponds to the operator $\gamma_{1,s}(\mathbf{U}) = (\mathbf{U} \cdot \mathbf{n})|_{\Gamma_s}$. For functions in $H(\text{div}, \Omega)$ the operator $\gamma_{1,s}$ is defined as follows. We introduce a function χ depending on z only, and satisfying

$$\chi \in C^1([0, H]), \quad \chi(H) = 1, \quad \text{and} \quad \chi(z) = 0 \text{ for } z < H_-.$$

The normal trace operator on the surface is then defined by

$$\forall (\mathbf{U}, \varphi) \in H(\text{div}, \Omega) \times H^1(\Omega), \quad \langle \gamma_{1,s}(\mathbf{U}), \gamma_{0,s}(\varphi) \rangle_{\Gamma_s} = (\nabla \cdot (\chi \mathbf{U}), \varphi)_{L^2(\Omega)} + (\chi \mathbf{U}, \nabla \varphi)_{L^2(\Omega)^d},$$

where the duality product between $H^{-1/2}(\Gamma_s)$ and $H^{1/2}(\Gamma_s)$ is denoted $\langle \cdot, \cdot \rangle_{\Gamma_s}$. In a similar way we introduce $\gamma_{1,b}$, the normal trace operator acting on Γ_b only. We denote by $\langle \cdot, \cdot \rangle_{\Gamma_b}$ the duality product between $H^{-1/2}(\Gamma_b)$ and $H^{1/2}(\Gamma_b)$ and define the normal trace for functions in $H(\text{div}, \Omega)$ by

$$\forall (\mathbf{U}, \varphi) \in H(\text{div}, \Omega) \times H^1(\Omega),$$

$$\langle \gamma_{1,b}(\mathbf{U}), \gamma_{0,b}(\varphi) \rangle_{\Gamma_b} = (\nabla \cdot ((1 - \chi) \mathbf{U}), \varphi)_{L^2(\Omega)} + ((1 - \chi) \mathbf{U}, \nabla \varphi)_{L^2(\Omega)^d}.$$

Finally, for any function $\mathbf{U} \in H(\text{div}, \Omega)$, when stating that $\gamma_{1,s}(\mathbf{U}) \in L^2(\Gamma_s)$ we mean that $\gamma_{1,s}(\mathbf{U})$ is a function in $H^{-1/2}(\Gamma_s)$ which can be identified with a function in $L^2(\Gamma_s)$, and that the duality product reduces to the scalar product in $L^2(\Gamma_s)$. This can be written as follows,

$$\forall \mathbf{U} \in H(\text{div}, \Omega), \quad \gamma_{1,s}(\mathbf{U}) \in L^2(\Gamma_s) \Rightarrow \exists f \in L^2(\Gamma_s) / \langle \gamma_{1,b}(\mathbf{U}), \gamma_{0,b}(\varphi) \rangle_{\Gamma_b} = \int_{\Gamma_s} f \gamma_{0,b}(\varphi) \, ds.$$

When \mathbf{U} is smooth, the function f is given by $f = (\mathbf{U} \cdot \mathbf{n})|_{\Gamma_s}$.

The operator G and its extension \tilde{G} . To introduce the operator associated to the evolution problem (3.1) and the abstract wave equation (3.5), we introduce the Hilbert space $\mathcal{H} = L^2(\Omega)^d$ equipped with the following weighted scalar product,

$$(\mathbf{U}, \tilde{\mathbf{U}})_{\mathcal{H}} = \int_{\Omega} \rho_0 \mathbf{U} \cdot \tilde{\mathbf{U}} \, dx. \quad (3.16)$$

we also define the space \mathcal{G} ,

$$\mathcal{G} = L^2(\Omega) \times L^2(\Omega) \times L^2(\Gamma_s), \quad (3.17)$$

equipped with the weighted scalar product

$$\forall \Phi = \begin{pmatrix} \varphi \\ \psi \\ \gamma \end{pmatrix} \in \mathcal{G}, \quad \forall \tilde{\Phi} = \begin{pmatrix} \tilde{\varphi} \\ \tilde{\psi} \\ \tilde{\gamma} \end{pmatrix} \in \mathcal{G}, \quad (\Phi, \tilde{\Phi})_{\mathcal{G}} = \int_{\Omega} \frac{\rho_0}{c_0^2} \varphi \tilde{\varphi} \, dx + \int_{\Omega} \rho_0 \psi \tilde{\psi} \, dx + \int_{\Gamma_s} \frac{\rho_0}{g} \gamma \tilde{\gamma} \, ds. \quad (3.18)$$

We first define the operator \tilde{G} used in Equation (3.5). The domain of \tilde{G} is denoted $\mathcal{D}(\tilde{G}) \subset \mathcal{H}$ and is defined by

$$\mathcal{D}(\tilde{G}) = \{\mathbf{U} \in H(\text{div}, \Omega) \mid \gamma_{1,s}(\mathbf{U}) \in L^2(\Gamma_s)\}. \quad (3.19)$$

The operator $\tilde{G} : \mathcal{D}(\tilde{G}) \subset \mathcal{H} \rightarrow \mathcal{G}$ is then defined by

$$\forall \mathbf{U} \in \mathcal{D}(\tilde{G}), \quad \tilde{G}\mathbf{U} = \begin{pmatrix} c_0^2 \left(\nabla \cdot \mathbf{U} - \frac{g}{c_0^2} \mathbf{U} \cdot \mathbf{e}_z \right) \\ N\mathbf{U} \cdot \mathbf{e}_z \\ -g\gamma_{1,s}(\mathbf{U}) \end{pmatrix}. \quad (3.20)$$

It can be shown that the operator \tilde{G} is closed and densely defined. As already mentioned, it is useful to see the operator \tilde{G} as an extension of an operator G , defined on the domain $\mathcal{D}(G) \subset \mathcal{H}$, given by

$$\mathcal{D}(G) = \{\mathbf{U} \in H(\text{div}, \Omega) \mid \gamma_{1,s}(\mathbf{U}) \in L^2(\Gamma_s), \gamma_{1,b}(\mathbf{U}) = 0\}. \quad (3.21)$$

We have $\mathcal{D}(G) \subset \mathcal{D}(\tilde{G})$ and defined G so as to satisfy, for all $\mathbf{U} \in \mathcal{D}(G)$, $G\mathbf{U} = \tilde{G}\mathbf{U}$, therefore

$$\forall \mathbf{U} \in \mathcal{D}(G), \quad G\mathbf{U} = \begin{pmatrix} c_0^2 \left(\nabla \cdot \mathbf{U} - \frac{g}{c_0^2} \mathbf{U} \cdot \mathbf{e}_z \right) \\ N\mathbf{U} \cdot \mathbf{e}_z \\ -g\gamma_{1,s}(\mathbf{U}) \end{pmatrix}. \quad (3.22)$$

The operator G is also densely defined and closed.

The adjoint operators G^* and \tilde{G}^* and a Green's formula. Since G and \tilde{G} are densely defined and closed, their adjoint – denoted respectively G^* and \tilde{G}^* – exist and are also densely defined and closed. We give their expression in this section. In the following, the space of smooth functions with compact support in Ω is denoted $\mathcal{D}(\Omega)$.

Theorem 3.1. *The operator $G^* : \mathcal{D}(G^*) \subset \mathcal{G} \rightarrow \mathcal{H}$ is defined by*

$$\mathcal{D}(G^*) = \{\Phi = (\varphi, \psi, \gamma)^t \in \mathcal{G} \mid \varphi \in H^1(\Omega), \gamma = \gamma_{0,s}(\varphi)\},$$

and, for all $\Phi = (\varphi, \psi, \gamma)^t \in \mathcal{D}(G^*)$,

$$G^*\Phi = -\nabla\varphi + N \left(\psi + \frac{N}{g}\varphi \right) \mathbf{e}_z. \quad (3.23)$$

Proof. Let \mathbf{U} be a function in $\mathcal{D}(\Omega)^d$, and let $\Phi = (\varphi \ \psi \ \gamma)^T$ belong to $\mathcal{D}(G^*)$. It holds, by definition of the adjoint,

$$(G\mathbf{U}, \Phi)_{\mathcal{G}} = (\mathbf{U}, G^*\Phi)_{\mathcal{H}} = (\mathbf{U}, \tilde{\mathbf{U}})_{\mathcal{H}},$$

for some $\tilde{\mathbf{U}} \in \mathcal{H}$. The equality above is developed using the definition of G ,

$$(G\mathbf{U}, \Phi)_{\mathcal{G}} = -\langle \nabla(\rho_0\varphi), \mathbf{U} \rangle_{\Omega} + \int_{\Omega} \rho_0 \left(N\psi - \frac{g}{c_0^2}\varphi \right) \mathbf{U} \cdot \mathbf{e}_z \, dx = (\mathbf{U}, \tilde{\mathbf{U}})_{\mathcal{H}}, \quad (3.24)$$

where $\langle \cdot, \cdot \rangle_{\Omega}$ correspond to the duality product in $\mathcal{D}(\Omega)^d$. The equality (3.24) shows that $\nabla(\rho_0\varphi)$ belongs to $L^2(\Omega)^3$, hence, since ρ_0 is smooth, $\varphi \in H^1(\Omega)$. Equation (3.24) also shows that

$$G^*\Phi = \tilde{\mathbf{U}} = -\rho_0^{-1}\nabla(\rho_0\varphi) + \left(N\psi - \frac{g}{c_0^2}\varphi \right) \mathbf{e}_z.$$

The simpler expression (3.23) is obtained by distributing the gradient and using the definition of the scalar N . \square

The following Green formula holds

Lemma 3.1. For all $\mathbf{U} \in D(\tilde{G})$ and $\Phi = (\varphi, \psi, \gamma)^t \in D(G^*)$, it holds

$$(\tilde{G}\mathbf{U}, \Phi)_{\mathcal{G}} + (\mathbf{U}, G^*\Phi)_{\mathcal{H}} = \langle \gamma_{1,b}(\mathbf{U}), \gamma_{0,b}(\varphi) \rangle_{\Gamma_b}. \quad (3.25)$$

Proof. For $\mathbf{U} \in D(\overline{\Omega})^d$ and $\Phi = (\varphi, \psi, \varphi|_{\Gamma_s})^t$ with φ and ψ in $\mathcal{D}(\overline{\Omega})$, we have

$$(\tilde{G}\mathbf{U}, \Phi)_{\mathcal{G}} + (\mathbf{U}, G^*\Phi)_{\mathcal{H}} = \int_{\Gamma_b} \varphi|_{\Gamma_b} (\mathbf{U} \cdot \mathbf{n}_b)|_{\Gamma_b} ds = \langle \gamma_{1,b}(\mathbf{U}), \gamma_{0,b}(\varphi) \rangle_{\Gamma_b}.$$

We conclude by using the density of $\mathcal{D}(\overline{\Omega})^d$ in $H(\text{div}, \Omega)$ and the density of $\mathcal{D}(\overline{\Omega})$ in $H^1(\Omega)$ and in $L^2(\Omega)$ (see Girault and Raviart, 1986). \square

Thanks to the Lemma 3.1 we deduce the expression of \tilde{G}^* .

Corollary 3.1. The operator $\tilde{G}^* : \mathcal{D}(\tilde{G}^*) \subset \mathcal{G} \rightarrow \mathcal{H}$ is defined by $\mathcal{D}(\tilde{G}^*) \subset \mathcal{D}(G^*)$ and for all $\Phi \in \mathcal{D}(\tilde{G}^*)$, $\tilde{G}^*\Phi = G^*\Phi$, moreover,

$$\mathcal{D}(\tilde{G}^*) = \{\Phi = (\varphi, \psi, \gamma)^t \in \mathcal{G} \mid \varphi \in H^1(\Omega), \gamma_{0,s}(\varphi) = \gamma, \gamma_{0,b}(\varphi) = 0\}. \quad (3.26)$$

Proof. Since $\mathcal{D}(G) \subset \mathcal{D}(\tilde{G})$, we have the inclusion $\mathcal{D}(\tilde{G}^*) \subset \mathcal{D}(G^*)$ and G^* is an extension of \tilde{G}^* . Therefore Lemma 3.1 can be used as follows: for all $\mathbf{U} \in D(\tilde{G})$ and $\Phi = (\varphi, \psi, \gamma)^t \in \mathcal{D}(\tilde{G}^*)$, it holds

$$(\tilde{G}\mathbf{U}, \Phi)_{\mathcal{G}} - (\mathbf{U}, \tilde{G}^*\Phi)_{\mathcal{H}} = \langle \gamma_{1,b}(\mathbf{U}), \gamma_{0,b}(\varphi) \rangle_{\Gamma_b}, \quad (3.27)$$

which shows that $\langle \gamma_{1,b}(\mathbf{U}), \gamma_{0,b}(\varphi) \rangle_{\Gamma_b} = 0$. Using the surjectivity of the normal trace operator $\gamma_{1,b}$, we deduce that $\gamma_{0,b}(\varphi) = 0$. \square

The space $\mathcal{D}(G^*)$ is equipped with the graph norm,

$$\|\Phi\|_{\mathcal{D}(G^*)}^2 = \|\Phi\|_{\mathcal{G}}^2 + \|G^*\Phi\|_{\mathcal{H}}^2.$$

And we have the following result,

Proposition 3.1. There exists a constant $C_c > 0$ such that

$$\forall \Phi = \begin{pmatrix} \varphi \\ \psi \\ \gamma \end{pmatrix} \in \mathcal{D}(G^*), \quad \|\Phi\|_{\mathcal{D}(G^*)} \geq C_c \|\varphi\|_{H^1(\Omega)}.$$

Proof. In the proof, we use the symbol \lesssim for inequalities that hold up to a constant independent of Φ . For $\Phi \in \mathcal{D}(G^*)$, we have

$$\|\varphi\|_{L^2(\Omega)^3}^2 \lesssim \int_{\Omega} \frac{\rho_0}{c_0^2} \varphi dx \leq \|\Phi\|_{\mathcal{G}}^2 \quad \text{and} \quad \|\nabla\varphi\|_{L^2(\Omega)^d}^2 \lesssim \|\nabla\varphi\|_{\mathcal{H}}^2.$$

It holds, by the triangular inequality,

$$\|\nabla\varphi\|_{\mathcal{H}}^2 \lesssim \left\| -\nabla\varphi + N(\psi + \frac{N}{g}\varphi)\mathbf{e}_z \right\|_{\mathcal{H}}^2 + \left\| N(\psi + \frac{N}{g}\varphi)\mathbf{e}_z \right\|_{\mathcal{H}}^2,$$

hence the norm of the gradient is bounded by $\|G^*\Phi\|_{\mathcal{H}}^2 + \|\Phi\|_{\mathcal{G}}^2$, which concludes the proof. \square

In this section, we have introduced all the necessary operators for the study of the potential-based problem (3.8)-(3.12) and the velocity-based problem (3.1)-(3.4). The next section is dedicated to the study of the problem (3.8)-(3.12). We show that the problem is well-posed and that its solution satisfies an energy equality.

3.3 Analysis of the potential-based formulation

We recall the system of PDE satisfied by the potentials φ and ψ ,

$$\begin{cases} \frac{\partial^2 \varphi}{\partial t^2} + c_0^2 \nabla \cdot \left(-\nabla \varphi + N \left(\psi + \frac{N}{g} \varphi \right) \mathbf{e}_z \right) + g \frac{\partial \varphi}{\partial z} - g N \left(\psi + \frac{N}{g} \varphi \right) = 0, & \text{in } \Omega \times [0, T], \\ \frac{\partial^2 \psi}{\partial t^2} - N \frac{\partial \varphi}{\partial z} + N^2 \left(\psi + \frac{N}{g} \varphi \right) = 0, & \text{in } \Omega \times [0, T], \end{cases} \quad (3.28)$$

$$(3.29)$$

with the bottom boundary condition

$$-\nabla \varphi \cdot \mathbf{n} + N \left(\psi + \frac{N}{g} \varphi \right) (\mathbf{e}_z \cdot \mathbf{n}) = u_b, \quad \text{on } \Gamma_b \times [0, T], \quad (3.30)$$

and the surface boundary condition

$$\frac{\partial^2 \varphi}{\partial t^2} - g \left(-\nabla \varphi \cdot \mathbf{n} + N \left(\psi + \frac{N}{g} \varphi \right) (\mathbf{e}_z \cdot \mathbf{n}) \right) \cdot \mathbf{n} = 0, \quad \text{on } \Gamma_s \times [0, T]. \quad (3.31)$$

The system (3.28)-(3.31) is completed with vanishing initial conditions.

3.3.1 Variational formulation

The natural idea for writing the variational formulation associated to (3.28)-(3.29) consists in testing (3.28)-(3.29) against a function $(\tilde{\varphi}, \tilde{\psi}) \in H^1(\Omega) \times L^2(\Omega)$. After integrating by parts and using the boundary conditions (3.30)-(3.31), we obtain the problem: given u_b regular enough, find

$$\begin{pmatrix} \varphi \\ \psi \end{pmatrix} \in L^2(0, T; H^1(\Omega) \times L^2(\Omega)), \quad \frac{d}{dt} \begin{pmatrix} \varphi \\ \psi \end{pmatrix} \in L^2(0, T; L^2(\Omega)^2), \quad (3.32)$$

solution to

$$\begin{aligned} & \frac{d^2}{dt^2} \int_{\Omega} \frac{\rho_0}{c_0^2} \varphi \tilde{\varphi} \, dx + \frac{d^2}{dt^2} \int_{\Omega} \rho_0 \psi \tilde{\psi} \, dx \\ & + \int_{\Omega} \rho_0 \left(-\nabla \varphi + N \left(\psi + \frac{N}{g} \varphi \right) \mathbf{e}_z \right) \cdot \left(-\nabla \tilde{\varphi} + N \left(\tilde{\psi} + \frac{N}{g} \tilde{\varphi} \right) \mathbf{e}_z \right) \, dx \\ & + \frac{d^2}{dt^2} \int_{\Gamma_s} \frac{\rho_0}{g} \varphi \tilde{\varphi} \, ds + \int_{\Gamma_b} \rho_0 u_b \tilde{\varphi} \, ds = 0, \quad \forall \begin{pmatrix} \tilde{\varphi} \\ \tilde{\psi} \end{pmatrix} \in H^1(\Omega) \times L^2(\Omega). \end{aligned} \quad (3.33)$$

The formulation (3.33) will be useful for the numerical approximation. Indeed, the natural spaces for the discretization are classical: $H^1(\Omega)$ for φ and $L^2(\Omega)$ for ψ . Moreover, for $d = 3$, the velocity formulation has three scalar unknowns whereas the potential formulation requires only two scalars unknowns. Finally, the boundary source term appears naturally as a Neumann condition in this formulation.

However, the existence of a solution to (3.28)-(3.29) cannot be directly proved by standard methods (see Lions and Magenes, 1972), because of the surface condition (3.31) involving the second-order time derivative of φ .

3.3.2 Existence and uniqueness results

We introduce a new unknown to the problem, denoted $\gamma \in L^2(\Gamma_s)$, and we define the vector of unknowns

$$\Phi(t) = \begin{pmatrix} \varphi(t) \\ \psi(t) \\ \gamma(t) \end{pmatrix} \in \mathcal{G}. \quad (3.34)$$

From the variational formulation (3.33) we deduce that the problem (3.28) - (3.31) reduces to the following abstract formulation: assume $u_b \in H^1(0, T; H^{-1/2}(\Gamma_b))$ given, find

$$\Phi \in L^2(0, T; \mathcal{D}(G^*)), \quad \frac{d}{dt}\Phi \in L^2(0, T; \mathcal{G}),$$

solution to

$$\begin{cases} \frac{d^2}{dt^2}(\Phi(t), \tilde{\Phi})_{\mathcal{G}} + (G^*\Phi(t), G^*\tilde{\Phi})_{\mathcal{H}} = \ell_b(t, \tilde{\Phi}), & \forall \tilde{\Phi} \in \mathcal{D}(G^*), \quad \text{in } \mathcal{D}'(0, T), \\ \Phi(0) = \frac{d}{dt}\Phi(0) = 0, & \text{in } \Omega, \end{cases} \quad (3.35)$$

$$\Phi(0) = \frac{d}{dt}\Phi(0) = 0, \quad \text{in } \Omega, \quad (3.36)$$

where $\ell_b : (0, T) \times \mathcal{D}(G^*) \rightarrow \mathbb{R}$ is the linear form

$$\ell_b(t, \Phi) = \langle u_b(t), \gamma_{0,b}(\varphi) \rangle_{\Gamma_b}. \quad (3.37)$$

Note that if $\Phi \in \mathcal{D}(G^*)$, then γ is the surface trace of φ , and the equation (3.35) is exactly the equation (3.33). For the formulation (3.35)-(3.36) we have the following result,

Proposition 3.2. *Assume that $u_b \in H^1(0, T; H^{-1/2}(\Gamma_b))$. Then the problem (3.35)-(3.36) has a unique solution and, up to a modification on zero measure sets,*

$$\Phi \in C^0([0, T]; \mathcal{D}(G^*)) \cap C^1([0, T]; \mathcal{G})$$

Proof. If the data ℓ_b has sufficient regularity, the existence and uniqueness of solution to the problem (3.35)-(3.36) follows directly from standard results, see e.g. Lions and Magenes (1972) and Joly et al. (2008). More precisely, we need to show that

$$\ell_b \in H^1(0, T; \mathcal{D}(G^*)').$$

First we show that, for almost all $t \in (0, T)$, the form $\ell_b(t)$ is a bounded linear functional on $\mathcal{D}(G^*)$. Let $\Phi = (\varphi, \psi, \gamma_{0,s}(\varphi))^t \in \mathcal{D}(G^*)$. From the continuity of the trace operator, there exists a scalar $C_H > 0$ depending only on H , such that

$$|\langle \ell_b(t), \Phi \rangle| = |\langle u_b(t), \gamma_{0,b}(\varphi) \rangle_{\Gamma_b}| \leq C_H \|u_b(t)\|_{H^{-1/2}(\Gamma_b)} \|\varphi\|_{H^1(\Omega)},$$

and from Proposition 3.1 we obtain

$$|\langle \ell_b(t), \Phi \rangle| \leq C_H C_c^{-1} \|u_b(t)\|_{H^{-1/2}(\Gamma_b)} \|\Phi\|_{\mathcal{D}(G^*)},$$

hence $\ell_b(t)$ is bounded. From the continuity in time of u_b , we have $\ell_b \in H^1(0, T; \mathcal{D}(G^*)')$. \square

3.3.3 Energy identity

An energy identity for the system (3.35)-(3.36) is obtained following the usual approach (Lions and Magenes, 1972). We define the energy

$$\mathcal{E}(t) = \frac{1}{2} (\|\partial_t \Phi\|_{\mathcal{G}}^2 + \|G^* \Phi\|_{\mathcal{H}}^2).$$

Taking formally $\tilde{\Phi} = \partial_t \Phi$ in the weak formulation (3.35) yields

$$(\partial_{tt}^2 \Phi, \partial_t \Phi)_{\mathcal{G}} + (G^* \Phi, G^* \partial_t \Phi)_{\mathcal{H}} = \langle u_b, \gamma_{0,b}(\partial_t \varphi) \rangle_b,$$

which is equivalent to

$$\frac{d\mathcal{E}}{dt} = \frac{d}{dt} \langle u_b, \gamma_{0,b}(\varphi) \rangle_b - \langle \partial_t u_b, \gamma_{0,b}(\varphi) \rangle_b. \quad (3.38)$$

Integrating the above equation from 0 to t and using the vanishing initial conditions yields

$$\mathcal{E}(t) = \langle u_b(t), \gamma_{0,b}(\varphi(t)) \rangle_b - \int_0^t \langle \partial_t u_b(t'), \gamma_{0,b}(\varphi(t')) \rangle_b dt'. \quad (3.39)$$

One can show that the identity (3.39) holds for the solutions given by Proposition 3.2 (Joly et al., 2008). Such inequality is the starting point to derive an estimation of the solution. We give below such estimate as well as its proof.

Proposition 3.3. *There exists $C > 0$ such that for any solution Φ to (3.35)-(3.36),*

$$\sup_{t' \in [0, t]} \mathcal{E}(t') \leq C(t^2 + 1)B^2(t), \quad (3.40)$$

Where B is given by

$$B(t) = \sup_{t' \in [0, t]} \|u_b(t')\|_{H^{-1/2}(\Gamma_b)} + \int_0^t \|\partial_t u_b(t')\|_{H^{-1/2}(\Gamma_b)} dt'. \quad (3.41)$$

Proof. Starting with the equation (3.39), we have for the right-hand side

$$\mathcal{E}(t) = \langle u_b(t), \gamma_{0,b}(\varphi(t)) \rangle_b - \int_0^t \langle \partial_t u_b(t'), \gamma_{0,b}(\varphi(t')) \rangle_b dt' \leq B(t) \sup_{t' \in [0, t]} \|\gamma_{0,b}(\varphi)(t')\|_{H^{1/2}(\Gamma_b)}. \quad (3.42)$$

To estimate the norm on $H^{1/2}(\Gamma_b)$, we use the continuity of the trace and Proposition 3.1,

$$\sup_{t' \in [0, t]} \|\gamma_{0,b}(\varphi)(t')\|_{H^{1/2}(\Gamma_b)} \lesssim \sup_{t' \in [0, t]} \|\Phi(t')\|_{\mathcal{D}(G^*)}, \quad (3.43)$$

where we use the symbol \lesssim for inequalities that hold up to a constant independent of Φ and t . We show now that the graph norm in the right-hand side of (3.43) can be bounded by the energy \mathcal{E} . From the definition of the scalar product in $\mathcal{D}(G^*)$ and the energy, we have

$$\|\Phi(t')\|_{\mathcal{D}(G^*)}^2 = \|\Phi(t')\|_{\mathcal{G}}^2 + \|G^* \Phi(t')\|_{\mathcal{H}}^2 \leq \|\Phi(t')\|_{\mathcal{G}}^2 + 2\mathcal{E}(t'). \quad (3.44)$$

Since the initial conditions vanish, it holds

$$\Phi(t) = \int_0^t \partial_t \Phi(t') dt' \Rightarrow \|\Phi(t)\|_{\mathcal{G}} \leq \int_0^t \|\partial_t \Phi(t')\|_{\mathcal{G}} dt' \leq \int_0^t \sqrt{2\mathcal{E}(t')} dt'.$$

Using this inequality to simplify (3.44) yields

$$\|\Phi(t')\|_{\mathcal{D}(G^*)}^2 \leq \left(\int_0^s \sqrt{2\mathcal{E}(r)} \, dr \right)^2 + 2\mathcal{E}(t') \leq \left(t' \sup_{r \in [0, t']} \sqrt{2\mathcal{E}(r)} \right)^2 + 2\mathcal{E}(t').$$

This shows that the graph norm of $\Phi(t')$ is bounded by the energy, more precisely,

$$\sup_{t' \in [0, t]} \|\Phi(t')\|_{\mathcal{D}(G^*)}^2 \leq 2(t^2 + 1) \sup_{t' \in [0, t]} \mathcal{E}(t').$$

Hence we have

$$\mathcal{E}(t) \lesssim \sqrt{(t^2 + 1)B} \sup_{t' \in [0, t]} \sqrt{\mathcal{E}(t')}, \quad (3.45)$$

which allows to deduce (3.40) using the Young inequality. \square

The well-posedness of the potential-based formulation (3.35) was obtained by standard tools (Lions and Magenes, 1972) and the only thing to show was that the data ℓ_b has enough regularity. The study of the velocity-based formulation is more involved, and is the subject of the next section.

3.4 Analysis of the velocity-based formulation

The system of partial differential equations for the velocity-based formulation reads: let \mathbf{U} be solution to

$$\rho_0 \frac{\partial^2 \mathbf{U}}{\partial t^2} - \nabla (\rho_0 c_0^2 \nabla \cdot \mathbf{U} - \rho_0 g \mathbf{U} \cdot \mathbf{e}_z) - \nabla \cdot (\rho_0 g \mathbf{U}) \mathbf{e}_z = 0, \quad \text{in } \Omega \times [0, T], \quad (3.46)$$

with the boundary conditions

$$\mathbf{U} \cdot \mathbf{n} = u_b \quad \text{on } \Gamma_b \times [0, T], \quad \nabla \cdot \mathbf{U} = 0 \quad \text{on } \Gamma_s \times [0, T], \quad (3.47)$$

and with vanishing initial conditions.

3.4.1 Variational formulation and uniqueness result

The variational formulation associated to the evolution problem (3.46)-(3.47) is obtained by testing the system (3.46) against a function $\tilde{\mathbf{U}}$ and integrating over Ω . The test function $\tilde{\mathbf{U}}$ is chosen such that its normal trace on Γ_b vanishes. Using the boundary conditions (3.47) we obtain:

$$\begin{aligned} \frac{d^2}{dt^2} \int_{\Omega} \rho_0 \mathbf{U}(t) \tilde{\mathbf{U}} \, dx + \int_{\Omega} \rho_0 c_0^2 \left(\nabla \cdot \mathbf{U}(t) - \frac{g}{c_0^2} \mathbf{U}(t) \cdot \mathbf{e}_z \right) \left(\nabla \cdot \tilde{\mathbf{U}} - \frac{g}{c_0^2} \tilde{\mathbf{U}} \cdot \mathbf{e}_z \right) \, dx \\ + \int_{\Omega} \rho_0 N^2 \mathbf{U}(t) \cdot \mathbf{e}_z \tilde{\mathbf{U}} \cdot \mathbf{e}_z \, dx + \int_{\Gamma_s} \rho_0 g \mathbf{U}(t) \cdot \mathbf{n} \tilde{\mathbf{U}} \cdot \mathbf{n} \, ds = 0. \end{aligned} \quad (3.48)$$

The formulation above is completed with the non-homogeneous boundary condition $\mathbf{U} \cdot \mathbf{n} = u_b$ on Γ_b . These formal computations show that the adequate variational formulation to study is the following: assume $u_b \in H^2(0, T; H^{-1/2}(\Gamma_b))$ given, and find

$$\mathbf{U} \in L^2(0, T; \mathcal{D}(\tilde{\mathcal{G}})), \quad \frac{d}{dt} \mathbf{U} \in L^2(0, T; \mathcal{H}),$$

solution to

$$\left\{ \begin{array}{l} \frac{d^2}{dt^2}(\mathbf{U}, \tilde{\mathbf{U}})_{\mathcal{H}} + (\tilde{G}\mathbf{U}, G\tilde{\mathbf{U}})_G = 0, \quad \forall \tilde{\mathbf{U}} \in \mathcal{D}(G), \quad \text{in } \mathcal{D}'(0, T), \\ \gamma_{1,b}(\mathbf{U}) = u_b, \quad \text{in } (0, T), \end{array} \right. \quad (3.49)$$

$$\left. \begin{array}{l} \\ \\ \mathbf{U}(0) = \frac{d}{dt}\mathbf{U}(0) = 0 \quad \text{in } \Omega. \end{array} \right\} \quad (3.50)$$

$$\left. \begin{array}{l} \\ \\ \mathbf{U}(0) = \frac{d}{dt}\mathbf{U}(0) = 0 \quad \text{in } \Omega. \end{array} \right\} \quad (3.51)$$

Note that compared to Section 3.3.2 we have assumed slightly more regularity in time for the source term u_b . This is another drawback of the velocity-field formulation and is due to the nature of the condition: here the inhomogeneous boundary condition in (3.47) is of essential type (similar to an inhomogeneous Dirichlet boundary condition). Of course one could weaken this regularity assumption, however, from our current analysis this would also weaken the regularity of the solution. It is rather direct – using Lions-Magenes theory (Lions and Magenes, 1972) – to prove the following result.

Theorem 3.2. *The solution to (3.49)-(3.51) is unique.*

Proof. The problem (3.49)-(3.51) with $u_b \equiv 0$ amounts to find $\mathbf{U}(t) \in \mathcal{D}(G)$ solution to

$$\frac{d^2}{dt^2}(\mathbf{U}, \tilde{\mathbf{U}})_{\mathcal{H}} + (G\mathbf{U}, G\tilde{\mathbf{U}})_G = 0, \quad \forall \tilde{\mathbf{U}} \in \mathcal{D}(G), \quad \text{in } \mathcal{D}'(0, T), \quad (3.52)$$

with vanishing initial data. It follows from Lions and Magenes (1972) that this problem has a unique solution and it is zero. \square

Existence and stability results with respect to the data u_b are more difficult to obtain because of the essential inhomogeneous boundary condition. The common approach consists in decomposing the solution to the non-homogeneous problem \mathbf{U} as $\mathbf{U} = \mathbf{U}_0 + L(u_b)$, where the function $\mathbf{U}_0 \in \mathcal{D}(G)$ is solution to a homogeneous problem, and the operator L is a lifting operator. We aim to define a lifting operator in a way that preserves the symmetry between the potential-based and the velocity-based problems. Hence the lifting should be defined as $L(u_b) = -G^*\Phi_b$, where $\Phi_b \in \mathcal{D}(G_\alpha^*)$ is solution to the elliptic problem

$$\forall \tilde{\Phi} = \begin{pmatrix} \tilde{\Phi} \\ \tilde{\mathbf{V}} \end{pmatrix} \in \mathcal{D}(G^*) \text{ with } \tilde{\Phi} = \begin{pmatrix} \tilde{\varphi} \\ \tilde{\psi} \\ \tilde{\gamma} \end{pmatrix}, \quad (G^*\Phi_b, G^*\tilde{\Phi})_{\mathcal{H}} = \langle u_b, \gamma_{0,b}(\tilde{\varphi}) \rangle_{\Gamma_b}. \quad (3.53)$$

However, in our case, defining such a lifting is not trivial because of the following result.

Theorem 3.3. *The range of the operators G and G^* are not closed.*

Proof. We consider only the case $d = 2$, and show that there is no scalar $C > 0$ such that, for all function $\mathbf{U}(t) \in \mathcal{D}(G) \cap \text{Ker}(G)^\perp$, it holds

$$\|G\mathbf{U}\|_G^2 \geq C\|\mathbf{U}\|_{\mathcal{H}}^2. \quad (3.54)$$

This property implies that the range of G is not closed hence the range of G^* also is not closed. First note that $\text{Ker}(G) = \{0\}$. Indeed, the kernel of G is defined by

$$\text{Ker}(G) = \{\mathbf{U} \in \mathcal{D}(G) \mid U_z = 0, \partial_x U_x = 0, \gamma_{1,s}(\mathbf{U}) = 0\},$$

Hence, for every $\mathbf{U} = (U_x, U_z) \in \text{Ker}(G)$, it holds $U_z = 0$ and U_x is constant in the x direction. Since the domain is infinite in the x direction, U_x is also equal to zero. Hence $\mathcal{D}(G^*) \cap \text{Ker}(G)^\perp = \mathcal{D}(G^*)$.

Now, let $u \in \mathcal{D}(\Omega)$ be a function with compact support in $\mathbb{R} \times (H_-, H)$, and for each integer $n > 1$ let the function $u_n \in \mathcal{D}(\Omega)$ be defined by $u_n(\mathbf{x}) = u(x, n(z - z_0))$, with $z_0 = (H - H_-)/2$. We have

$$\|\partial_x u_n\|_{L^2(\Omega)} = \frac{1}{n} \|\partial_x u\|_{L^2(\Omega)}, \quad \|\partial_z u_n\|_{L^2(\Omega)} = \|\partial_z u\|_{L^2(\Omega)}.$$

Then let $\mathbf{U}_n \in \mathcal{D}(G)$ be defined by

$$\mathbf{U}_n(x, z) = \begin{pmatrix} \partial_z u_n(x, z) \\ -\partial_x u_n(x, z) \end{pmatrix} = \begin{pmatrix} n(\partial_z u)(x, n(z - z_0)) \\ -(\partial_x u)(x, n(z - z_0)) \end{pmatrix}.$$

We have $G\mathbf{U}_n = (-g\partial_x u_n, N\partial_x u_n, 0)^t$ and

$$\|G\mathbf{U}_n\|_{\mathcal{G}}^2 = \frac{1}{n} \|\sqrt{g^2 + N^2} \partial_x u\|_{L^2(\Omega)}^2, \quad \|\mathbf{U}_n\|_{\mathcal{H}}^2 = \frac{1}{n} \|\partial_x u\|_{L^2(\Omega)}^2 + \|\partial_z u\|_{L^2(\Omega)}^2. \quad (3.55)$$

For n going to infinity we have $\|G\mathbf{U}_n\|_{\mathcal{G}}^2$ goes to zero and $\|\mathbf{U}_n\|_{\mathcal{H}}^2$ converges to $\|\partial_z u\|_{L^2(\Omega)}^2$, hence (3.54) can not hold. \square

Since the range of G is not closed, the bilinear form of the problem (3.53) is not coercive and the existence of solution is not guaranteed. As a result, we cannot define in a straightforward way a lifting operator. Instead, we consider in the next section a relaxed version of the problem (3.49)-(3.51). Thanks to the relaxation we are able to show the existence of the lifting operator.

3.4.2 Existence results

A relaxed formulation

Instead of studying the existence of a solution for problem (3.49)-(3.51), we introduce a relaxed problem for a new unknown satisfying – assuming that the solution $\mathbf{U}(t)$ to (3.49)-(3.51) exists – for $\alpha > 0$

$$\mathbf{U}_\alpha(t) = e^{-\alpha t} \mathbf{U}(t), \quad \text{in } \mathcal{D}'(0, T).$$

The variational formulation for this new unknown is then given by: Assume $u_b \in H^2(0, T; H^{-1/2}(\Gamma_b))$ given, find

$$\mathbf{U}_\alpha \in L^2(0, T; \mathcal{D}(\tilde{G})), \quad \frac{d}{dt} \mathbf{U}_\alpha \in L^2(0, T; \mathcal{H}), \quad (3.56)$$

solution to

$$\left\{ \begin{array}{l} \frac{d^2}{dt^2} (\mathbf{U}_\alpha, \tilde{\mathbf{U}})_{\mathcal{H}} + 2\alpha \frac{d}{dt} (\mathbf{U}_\alpha, \tilde{\mathbf{U}})_{\mathcal{H}} \\ \quad + \alpha^2 (\mathbf{U}_\alpha, \tilde{\mathbf{U}})_{\mathcal{H}} + (\tilde{G}\mathbf{U}_\alpha, G\tilde{\mathbf{U}})_{\mathcal{G}} = 0, \quad \forall \tilde{\mathbf{U}} \in \mathcal{D}(G), \quad \text{in } \mathcal{D}'(0, T), \quad (3.57) \\ \gamma_{1,b}(\mathbf{U}_\alpha) = e^{-\alpha t} u_b, \quad \text{in } (0, T), \quad (3.58) \\ \mathbf{U}(0) = \frac{d}{dt} \mathbf{U}(0) = 0, \quad \text{in } \Omega. \quad (3.59) \end{array} \right.$$

Lemma 3.2. *Let \mathbf{U}_α be a solution to (3.57)-(3.59). Then $e^{\alpha t} \mathbf{U}_\alpha$ is the unique solution to (3.49)-(3.51).*

As an immediate consequence of the lemma above, we have that problem (3.57)-(3.59) has a unique solution. The relaxed formulation can be written in a more compact form by introducing the space

$$\mathcal{G} = \mathcal{G} \times \mathcal{H}, \quad (\cdot, \cdot)_{\mathcal{G}} = (\cdot, \cdot)_{\mathcal{G}} + (\cdot, \cdot)_{\mathcal{H}},$$

and the operators $G_\alpha : \mathcal{D}(G_\alpha) = \mathcal{D}(G) \subset \mathcal{H} \rightarrow \mathcal{G}$, defined by

$$\forall \mathbf{U} \in \mathcal{D}(G), \quad G_\alpha \mathbf{U} = \begin{pmatrix} G\mathbf{U} \\ \alpha \mathbf{U} \end{pmatrix}.$$

The operator $\tilde{G}_\alpha : \mathcal{D}(\tilde{G}) \subset \mathcal{H} \rightarrow \mathcal{G}$ is defined similarly. The variational formulation (3.57)-(3.59) is then equivalent to: find \mathbf{U}_α with the regularity (3.56) and solution to

$$\left\{ \begin{array}{l} \frac{d^2}{dt^2}(\mathbf{U}_\alpha, \tilde{\mathbf{U}})_{\mathcal{H}} + 2\alpha \frac{d}{dt}(\mathbf{U}_\alpha, \tilde{\mathbf{U}})_{\mathcal{H}} + (\tilde{G}_\alpha \mathbf{U}_\alpha, G_\alpha \tilde{\mathbf{U}})_{\mathcal{G}} = 0, \quad \forall \tilde{\mathbf{U}} \in \mathcal{D}(G_\alpha), \quad \text{in } \mathcal{D}'(0, T), \quad (3.60) \\ \gamma_{1,b}(\mathbf{U}_\alpha) = e^{-\alpha t} u_b, \quad \text{in } (0, T), \quad (3.61) \\ \mathbf{U}_\alpha(0) = \frac{d}{dt} \mathbf{U}_\alpha(0) = 0 \quad \text{in } \Omega. \quad (3.62) \end{array} \right.$$

Lifting operator for the relaxed problem

The operators G_α and \tilde{G}_α are densely defined and closed, so are their adjoints G_α^* and \tilde{G}_α^* . We have, in particular,

$$\mathcal{D}(G_\alpha^*) = \mathcal{D}(G^*) \times \mathcal{H}, \quad \text{and} \quad \forall (\Phi, \mathbf{V}) \in \mathcal{D}(G_\alpha^*), \quad G_\alpha^* \begin{pmatrix} \Phi \\ \mathbf{V} \end{pmatrix} = G^* \Phi + \alpha \mathbf{V} \in \mathcal{H}. \quad (3.63)$$

Theorem 3.4. *The range of the operators G_α and G_α^* are closed.*

Proof. Since $G_\alpha = \begin{pmatrix} G \\ \alpha I \end{pmatrix}$, we have $\text{Ker } G_\alpha = \emptyset$. Then, for $\mathbf{U} \in \mathcal{D}(G_\alpha) \cap \text{Ker}(G_\alpha)^\perp = \mathcal{D}(G_\alpha)$, it holds

$$\|G_\alpha \mathbf{U}\|_{\mathcal{G}}^2 = \|G\mathbf{U}\|_{\mathcal{G}}^2 + \|\alpha \mathbf{U}\|_{\mathcal{H}}^2 \geq \alpha^2 \|\mathbf{U}\|_{\mathcal{H}}^2,$$

which concludes the proof. \square

This result is key for constructing a lifting operator. We recall that the kernel of the operator G_α^* is a closed subspace of \mathcal{G} and we introduce $Q_\alpha \in \mathcal{L}(\mathcal{G})$, the orthogonal projection on $\text{Ker}(G_\alpha^*)$. Then $Q_\alpha^2 = Q_\alpha$ and Q_α is self-adjoint.

Theorem 3.5. *For $\alpha \leq 1$ we have*

$$\forall \Phi \in \mathcal{D}(G_\alpha^*), \quad \|Q_\alpha \Phi\|_{\mathcal{G}}^2 + \|G_\alpha^* \Phi\|_{\mathcal{H}}^2 \geq \alpha^2 \|\Phi\|_{\mathcal{G}}^2.$$

Proof. Let $\Phi \in \mathcal{D}(G_\alpha^*)$. We have $\|Q_\alpha \Phi\|_{\mathcal{G}}^2 + \|(1 - Q_\alpha) \Phi\|_{\mathcal{G}}^2 = \|\Phi\|_{\mathcal{G}}^2$, and therefore

$$\|G_\alpha^* \Phi\|_{\mathcal{H}}^2 = \|G_\alpha^* (1 - Q_\alpha) \Phi\|_{\mathcal{H}}^2 \geq \alpha^2 \|(1 - Q_\alpha) \Phi\|_{\mathcal{G}}^2.$$

Hence we have

$$\|Q_\alpha \Phi\|_{\mathcal{G}}^2 + \|G_\alpha^* \Phi\|_{\mathcal{H}}^2 \geq \|Q_\alpha \Phi\|_{\mathcal{G}}^2 + \alpha^2 \|(1 - Q_\alpha) \Phi\|_{\mathcal{G}}^2 \geq \alpha^2 \|\Phi\|_{\mathcal{G}}^2.$$

\square

The exact expression of Q_α is of no practical interest in what follows. It has to be noted however that it is non trivial, in particular, this is due to the fact that $\text{Ker } G^*$ is an infinite dimensional space. Thanks to Proposition 3.1, we also have directly the following bound for the $H^1(\Omega)$ -norm,

Lemma 3.3. *There exists a scalar $C > 0$ such that*

$$\forall \Phi = \begin{pmatrix} \Phi \\ \mathbf{V} \end{pmatrix} \in \mathcal{D}(G_\alpha^*) \text{ with } \Phi = \begin{pmatrix} \varphi \\ \psi \\ \gamma \end{pmatrix}, \quad \|\Phi\|_G^2 + \|G_\alpha^* \Phi\|_{\mathcal{H}}^2 \geq C \|\varphi\|_{H^1(\Omega)}^2.$$

Aiming at defining the aforementioned lifting operator of a data $u_b \in H^{-1/2}(\Gamma_b)$, we introduce the following problem: find $\Phi_b \in \mathcal{D}(G_\alpha^*)$ solution to

$$\forall \tilde{\Phi} = \begin{pmatrix} \tilde{\Phi} \\ \tilde{\mathbf{V}} \end{pmatrix} \in \mathcal{D}(G_\alpha^*) \text{ with } \tilde{\Phi} = \begin{pmatrix} \tilde{\varphi} \\ \tilde{\psi} \\ \tilde{\gamma} \end{pmatrix}, \quad (Q_\alpha \Phi_b, \tilde{\Phi})_G + (G_\alpha^* \Phi_b, G_\alpha^* \tilde{\Phi})_{\mathcal{H}} = \langle u_b, \gamma_{0,b}(\tilde{\varphi}) \rangle_{\Gamma_b}. \quad (3.64)$$

Thanks to Theorem 3.5 and Lemma 3.3, it is classical to show that Equation (3.64) admits a unique solution $\Phi_b \in \mathcal{D}(G_\alpha^*)$ that depends continuously on u_b (it is a standard application of Lax-Milgram Lemma). We then construct the lifting operator $L_\alpha \in \mathcal{L}(L^2(\Gamma_b), \mathcal{H})$ by setting

$$\forall u_b \in L^2(\Gamma_b), \quad L_\alpha(u_b) = -G_\alpha^* \Phi_b.$$

Proposition 3.4. *The function $L_\alpha(u_b) \in \mathcal{H}$ has the following properties:*

$$L_\alpha(u_b) \in \mathcal{D}(\tilde{G}_\alpha), \quad \tilde{G}_\alpha L_\alpha(u_b) = Q_\alpha \Phi_b \in \text{Ker}(G_\alpha^*), \quad \text{and} \quad \gamma_{1,b}(L_\alpha(u_b)) = u_b.$$

Proof. In the equation (3.64) we choose as test function $\tilde{\Phi}$ in $\mathcal{D}(\tilde{G}_\alpha^*)$. Since $\gamma_{0,b}(\tilde{\varphi}) = 0$, we obtain

$$(G_\alpha^* \Phi_b, \tilde{G}_\alpha^* \tilde{\Phi})_{\mathcal{H}} = -(Q_\alpha \Phi_b, \tilde{\Phi})_G, \quad \forall \tilde{\Phi} \in \mathcal{D}(\tilde{G}_\alpha^*). \quad (3.65)$$

This implies

$$G_\alpha^* \Phi_b \in \mathcal{D}(\tilde{G}_\alpha^{**}) = \mathcal{D}(\tilde{G}_\alpha) \quad \text{and} \quad \tilde{G}_\alpha^{**} G_\alpha^* \Phi_b = \tilde{G}_\alpha G_\alpha^* \Phi_b = -Q_\alpha \Phi_b = -\tilde{G}_\alpha L_\alpha(u_b), \quad (3.66)$$

where we have used that $\tilde{G}_\alpha^{**} = \tilde{G}_\alpha$ since \tilde{G}_α is closed and densely defined. To prove the last property, we use the abstract Green's formula of Lemma 3.1,

$$\begin{aligned} (G_\alpha^* \Phi_b, G_\alpha^* \tilde{\Phi})_{\mathcal{H}} &= (G_\alpha^* \Phi_b, G^* \tilde{\Phi})_{\mathcal{H}} + (G_\alpha^* \Phi_b, \alpha \tilde{\mathbf{V}})_{\mathcal{H}} \\ &= (\tilde{G}(G_\alpha^* \Phi_b), \tilde{\Phi})_{\mathcal{H}} - \langle \gamma_{1,b}(G_\alpha^* \Phi_b), \gamma_{0,b}(\tilde{\varphi}) \rangle_{\Gamma_b} + (G_\alpha^* \Phi_b, \alpha \tilde{\mathbf{V}})_{\mathcal{H}}. \end{aligned}$$

Hence we have

$$(G_\alpha^* \Phi_b, G_\alpha^* \tilde{\Phi})_{\mathcal{H}} = (\tilde{G}_\alpha(G_\alpha^* \Phi_b), \tilde{\Phi})_G - \langle \gamma_{1,b}(G_\alpha^* \Phi_b), \gamma_{0,b}(\tilde{\varphi}) \rangle_{\Gamma_b},$$

and with the equations (3.64) and (3.66) we obtain

$$(G_\alpha^* \Phi_b, G_\alpha^* \tilde{\Phi})_{\mathcal{H}} = -(Q_\alpha \Phi_b, \tilde{\Phi})_G - \langle \gamma_{1,b}(G_\alpha^* \Phi_b), \gamma_{0,b}(\tilde{\varphi}) \rangle_{\Gamma_b} \quad (3.67)$$

$$= -(Q_\alpha \Phi_b, \tilde{\Phi})_G + \langle u_b, \gamma_{0,b}(\tilde{\varphi}) \rangle_{\Gamma_b}, \quad (3.68)$$

from which we deduce that $\gamma_{1,b}(L_\alpha(u_b)) = -\gamma_{1,b}(G_\alpha^* \Phi_b) = u_b$. □

Remark 3.1. Assume now that $u_b \in L^2(0, T; H^{-1/2}(\Gamma_b))$. The operator L_α being continuous from $H^{-1/2}(\Gamma_b)$ to \mathcal{H} , one can deduce that

$$L_\alpha(u_b) \in L^2(0, T; \mathcal{H}).$$

Proposition 3.4 can be extended: we have, for almost all $t \in (0, T)$,

$$L_\alpha(u_b(t)) \in \mathcal{D}(\tilde{G}_\alpha), \quad \tilde{G}_\alpha L_\alpha(u_b(t)) \in \text{Ker } G_\alpha^*, \quad \text{and} \quad \gamma_{1,s}(L_\alpha(u_b(t))) = u_b(t).$$

Moreover, the regularity in time of $L(u_b)$ depends straightforwardly on the regularity in time of u_b . In particular,

$$u_b \in H^k(0, T; H^{-1/2}(\Gamma_b)) \Rightarrow L_\alpha(u_b) \in H^k(0, T; \mathcal{D}(\tilde{G}_\alpha)). \quad (3.69)$$

Existence result

We show now the existence of the solution to the relaxed problem.

Proposition 3.5. If $u_b \in H^2(0, T; H^{-1/2}(\Gamma_b))$, the problem (3.60)-(3.62) admits a unique solution. It satisfies, up to modifications on zero measure sets,

$$\mathbf{U}_\alpha \in C^1([0, T]; \mathcal{H}) \cap C^0([0, T]; \mathcal{D}(\tilde{G}_\alpha)). \quad (3.70)$$

Proof. Using the lifting operator, we look first for $\mathbf{U}_{\alpha,0}(t) \in \mathcal{D}(G_\alpha)$ such that, for all $\tilde{\mathbf{U}} \in \mathcal{D}(G_\alpha)$,

$$\left\{ \begin{array}{l} \frac{d^2}{dt^2}(\mathbf{U}_{\alpha,0}, \tilde{\mathbf{U}})_{\mathcal{H}} + 2\alpha \frac{d}{dt}(\mathbf{U}_{\alpha,0}, \tilde{\mathbf{U}})_{\mathcal{H}} + (G_\alpha \mathbf{U}_{\alpha,0}, G_\alpha \tilde{\mathbf{U}})_{\mathcal{G}} \\ \quad = \left(\frac{d^2}{dt^2}(e^{-\alpha t} L_\alpha(u_b)) + 2\alpha \frac{d}{dt}(e^{-\alpha t} L_\alpha(u_b)), \tilde{\mathbf{U}} \right)_{\mathcal{H}} \\ \quad = e^{-\alpha t} \left(\frac{d^2}{dt^2} L_\alpha(u_b) - \alpha^2 L_\alpha(u_b), \tilde{\mathbf{U}} \right)_{\mathcal{H}} \quad \text{in } \mathcal{D}'(0, T), \\ \mathbf{U}_{\alpha,0}(0) = \frac{d}{dt} \mathbf{U}_{\alpha,0}(0) = 0, \quad \text{in } \Omega. \end{array} \right. \quad (3.71)$$

$$(3.72)$$

From the remark above, the data is in $L^2(0, T; \mathcal{D}(\tilde{G}_\alpha))$. The existence and uniqueness of $\mathbf{U}_{\alpha,0}$ is a standard result (see Dautray and Lions, 2000), and $\mathbf{U}_{\alpha,0}$ has the following regularity,

$$\mathbf{U}_{\alpha,0} \in C^1([0, T]; \mathcal{H}) \cap C^0([0, T]; \mathcal{D}(G_\alpha)). \quad (3.73)$$

Let $\mathbf{U}_\alpha = \mathbf{U}_{\alpha,0} + L_\alpha(e^{-\alpha t} u_b)$. Up to a modification on zero-measure sets, $H^2(0, T; \mathcal{H}) \subset C^1([0, T]; \mathcal{H})$ (see Evans, 2004), hence from the regularity of both functions we have

$$\mathbf{U}_\alpha \in C^1([0, T]; \mathcal{H}) \cap C^0([0, T]; \mathcal{D}(G_\alpha)). \quad (3.74)$$

Finally we compute that \mathbf{U}_α is solution to (3.60). The main part of this computation is classical, but we give some details for the following term,

$$(\tilde{G}_\alpha \mathbf{U}_\alpha, G_\alpha \tilde{\mathbf{U}})_{\mathcal{G}} = (\tilde{G}_\alpha \mathbf{U}_{\alpha,0}, G_\alpha \tilde{\mathbf{U}})_{\mathcal{G}} - (\tilde{G}_\alpha L_\alpha(e^{-\alpha t}), G_\alpha \tilde{\mathbf{U}})_{\mathcal{G}} \quad (3.75)$$

Since $\mathbf{U}_{\alpha,0} \in \mathcal{D}(G_\alpha)$ it holds $\tilde{G}_\alpha \mathbf{U}_{\alpha,0} = G_\alpha \mathbf{U}_{\alpha,0}$, hence the first term of (3.75) is replaced using (3.71). For the second term of (3.75), from the properties of the lifting operator given in Proposition 3.4, it holds

$$(\tilde{G}_\alpha L_\alpha(e^{-\alpha t} u_b), G_\alpha \tilde{\mathbf{U}})_{\mathcal{G}} = (G_\alpha^*(\tilde{G}_\alpha L_\alpha(e^{-\alpha t} u_b)), \tilde{\mathbf{U}})_{\mathcal{H}} = 0. \quad (3.76)$$

□

The existence and uniqueness of the solution to the problems (3.78)-(3.79) and (3.80)-(3.81) are a direct application of well-known results, given e.g. in Dautray and Lions (2000). There exists a unique solution \mathbf{U}_α to (3.78)-(3.79), and a unique solution Φ_α to (3.80)-(3.81), and they satisfy

$$\mathbf{U}_\alpha \in C^1([0, T]; \mathcal{H}) \cap C^0([0, T]; \mathcal{D}(G_\alpha)), \quad \Phi_\alpha \in C^1([0, T]; \mathbf{G}) \cap C^0([0, T]; \mathcal{D}(G_\alpha^*)).$$

We state now the equivalence between the problems (3.78)-(3.79) and (3.80)-(3.81),

Theorem 3.8. *Let $\Phi_\alpha \in \mathcal{D}(G_\alpha^*)$ be the solution to the problem (3.80)-(3.81). If $F_\Phi \in L^2(0, T; \mathcal{D}(G_\alpha^*))$, then $\mathbf{U}_\alpha = G_\alpha^* \Phi_\alpha$ is the unique solution to the problem (3.78)-(3.79), with source term defined by $F_U = G_\alpha^* F_\Phi$.*

Proof. We introduce the function Ψ_α defined by

$$\Psi_\alpha(t) = \int_0^t \Phi_\alpha(t') dt'.$$

Integrating in time (3.80) yields an equation for Ψ_α , for all $\tilde{\Phi} \in \mathcal{D}(G_\alpha^*)$,

$$\frac{d^2}{dt^2}(\Psi_\alpha, \tilde{\Phi})_{\mathbf{G}} + 2\alpha \frac{d}{dt}(\Psi_\alpha, \tilde{\Phi})_{\mathbf{G}} + (G_\alpha^* \Psi_\alpha, G_\alpha^* \tilde{\Phi})_{\mathcal{H}} = \left(\int_0^t F_\Phi(t') dt', \tilde{\Phi} \right)_{\mathbf{G}}, \quad (3.82)$$

and since we have by construction $\Psi_\alpha \in C^2([0, T]; \mathbf{G}) \cap C^1([0, T]; \mathcal{D}(G_\alpha^*))$, we deduce from (3.82) that

$$\Psi_\alpha \in C^0([0, T]; \mathcal{D}(G_\alpha G_\alpha^*)). \quad (3.83)$$

Now, for all $\tilde{\mathbf{U}} \in D(G_\alpha^* G_\alpha)$ we set $\tilde{\Phi} = G_\alpha \tilde{\mathbf{U}}$ in (3.82). We obtain, using the definition of the adjoint of G_α , Equation (3.83) and the assumption that $F_\Phi \in L^2(0, T; \mathcal{D}(G_\alpha^*))$,

$$\frac{d^2}{dt^2}(G_\alpha^* \Psi_\alpha, \tilde{\mathbf{U}})_{\mathcal{H}} + 2\alpha \frac{d}{dt}(G_\alpha^* \Psi_\alpha, \tilde{\mathbf{U}})_{\mathcal{H}} + (G_\alpha G_\alpha^* \Psi_\alpha, G_\alpha \tilde{\mathbf{U}})_{\mathbf{G}} = \left(\int_0^t G_\alpha^* F_\Phi(t') dt', \tilde{\mathbf{U}} \right)_{\mathcal{H}}. \quad (3.84)$$

Therefore, setting $\mathbf{V}_\alpha = G_\alpha^* \Psi_\alpha$, we have that

$$\mathbf{V}_\alpha \in C^1([0, T]; \mathcal{H}) \cap C^0([0, T]; \mathcal{D}(G_\alpha))$$

is solution to: for all $\tilde{\mathbf{U}} \in D(G_\alpha^* G_\alpha)$

$$\frac{d^2}{dt^2}(\mathbf{V}_\alpha, \tilde{\mathbf{U}})_{\mathcal{H}} + 2\alpha \frac{d}{dt}(\mathbf{V}_\alpha, \tilde{\mathbf{U}})_{\mathcal{H}} + (G_\alpha \mathbf{V}_\alpha, G_\alpha \tilde{\mathbf{U}})_{\mathbf{G}} = \left(\int_0^t G_\alpha^* F_\Phi(t') dt', \tilde{\mathbf{U}} \right)_{\mathcal{H}}. \quad (3.85)$$

Since G_α is a closed densely defined operator, $\mathcal{D}(G_\alpha^* G_\alpha)$ is dense in $\mathcal{D}(G_\alpha)$ by the Von Neumann theorem, hence (3.85) can be extended to functions in $\tilde{\mathbf{U}} \in \mathcal{D}(G_\alpha)$. At this point we have shown that

$$\mathbf{V}_\alpha = \int_0^t G_\alpha^* \Phi_\alpha(t') dt',$$

is solution to (3.78)-(3.79), with source term given by

$$F_U = \int_0^t G_\alpha^* F_\Phi(t') dt'.$$

Since F_U is differentiable in time, by construction one can deduce that the time derivative of \mathbf{V}_α is solution to (3.78) – (3.79) with source term $G_\alpha^* F_\Phi(t')$, which allows us to conclude. \square

We consider now the case of a source term located at the bottom, namely the relaxed problem (3.60)-(3.61) and its dual formulation: find

$$\Phi_\alpha \in L^2(0, T; \mathcal{D}(G_\alpha^*)), \quad \frac{d}{dt}\Phi_\alpha \in L^2(0, T; \mathcal{G})$$

solution to

$$\left\{ \begin{array}{l} \frac{d^2}{dt^2}(\Phi_\alpha, \tilde{\Phi})_{\mathcal{G}} + 2\alpha \frac{d}{dt}(\Phi_\alpha, \tilde{\Phi})_{\mathcal{G}} \\ \quad + (G_\alpha^* \Phi_\alpha, G_\alpha^* \tilde{\Phi})_{\mathcal{H}} = \langle e^{-\alpha t} u_b, \tilde{\varphi} \rangle_{\Gamma_b} \quad \forall \tilde{\Phi} \in \mathcal{D}(G_\alpha^*), \quad \text{in } \mathcal{D}'(0, T), \quad (3.86) \\ \Phi_\alpha(0) = \partial_t \Phi_\alpha(0) = 0 \quad \text{in } \Omega. \quad (3.87) \end{array} \right.$$

Since the right-hand side of (3.86) is a bounded linear functional on $\mathcal{D}(G_\alpha^*)$ (see the proof of Proposition 3.2), the solution to (3.86)-(3.87) exists and is unique. The equivalence is deduced from the case with volumic sources, namely we have the following result,

Proposition 3.6. *Let $u_b \in H^2(0, T; H^{-1/2}(\Gamma_b))$, and let Φ_α be the solution to the problem (3.86)-(3.87). Then $\mathbf{U}_\alpha = G_\alpha^* \Phi_\alpha$ is the unique solution to the problem (3.60)-(3.62).*

Proof. Let Φ_b be the solution to (3.64) associated to the data u_b . The equation (3.86) can be written

$$\frac{d^2}{dt^2}(\Phi_\alpha, \tilde{\Phi})_{\mathcal{G}} + 2\alpha \frac{d}{dt}(\Phi_\alpha, \tilde{\Phi})_{\mathcal{G}} + (G_\alpha^* \Phi_\alpha, G_\alpha^* \tilde{\Phi})_{\mathcal{H}} = e^{-\alpha t} (Q_\alpha \Phi_b, \tilde{\Phi})_{\mathcal{G}} + e^{-\alpha t} (G_\alpha^* \Phi_b, G_\alpha^* \tilde{\Phi})_{\mathcal{H}}. \quad (3.88)$$

Let $\Phi_0 = \Phi_\alpha - e^{-\alpha t} \Phi_b$. We define

$$\begin{aligned} F_\Phi &= -\frac{d^2}{dt^2}(e^{-\alpha t} \Phi_b) - 2\alpha \frac{d}{dt}(e^{-\alpha t} \Phi_b) + e^{-\alpha t} Q_\alpha \Phi_b \\ &= e^{-\alpha t} (\alpha^2 \Phi_b - \frac{d^2}{dt^2} \Phi_b + Q_\alpha \Phi_b) \in L^2(0, T; \mathcal{D}(G_\alpha^*)), \end{aligned}$$

then Φ_0 is solution to

$$\frac{d^2}{dt^2}(\Phi_0, \tilde{\Phi})_{\mathcal{G}} + 2\alpha \frac{d}{dt}(\Phi_0, \tilde{\Phi})_{\mathcal{G}} + (G_\alpha^* \Phi_0, G_\alpha^* \tilde{\Phi})_{\mathcal{H}} = (F_\Phi, \tilde{\Phi})_{\mathcal{G}}.$$

Using Theorem 3.8, the function $\mathbf{U}_{\alpha,0}$ defined by $\mathbf{U}_{\alpha,0} = G_\alpha^* \Phi_0 \in \mathcal{D}(G_\alpha)$ is solution to

$$\frac{d^2}{dt^2}(\mathbf{U}_{\alpha,0}, \tilde{\mathbf{U}})_{\mathcal{H}} + 2\alpha \frac{d}{dt}(\mathbf{U}_{\alpha,0}, \tilde{\mathbf{U}})_{\mathcal{H}} + (G_\alpha \mathbf{U}_{\alpha,0}, G_\alpha \tilde{\mathbf{U}})_{\mathcal{G}} = (G_\alpha^* F_\Phi, \tilde{\mathbf{U}})_{\mathcal{G}},$$

where, by construction,

$$G_\alpha^* F_\Phi = e^{-\alpha t} \left(\frac{d^2}{dt^2} L_\alpha(u_b) - \alpha^2 L_\alpha(u_b) \right).$$

This shows that $\mathbf{U}_{\alpha,0} = G_\alpha^* \Phi_0$ is indeed the solution of (3.71). It remains only to define, as in the proof of Theorem 3.5, the function $\mathbf{U}_\alpha = \mathbf{U}_{\alpha,0} + e^{-\alpha t} L_\alpha(u_b) = \mathbf{U}_{\alpha,0} - e^{-\alpha t} G_\alpha^* \Phi_b$ and observe that it is solution to (3.60) with the required regularity. \square

We have shown that for the relaxed problems, the solution \mathbf{U}_α to the velocity-based problem (3.60)-(3.62) is obtained from the solution Φ to the potential-based problem (3.86)-(3.87), thanks to the relation $\mathbf{U}_\alpha = G_\alpha^* \Phi$. We aim now to prove a similar relation for the original, non-relaxed problems (3.49) and (3.35). It should be noted that the dual formulation of the relaxed velocity-based problem is not a relaxed version of the potential-based problem (3.35)-(3.36). More precisely, one does not have – unlike the velocity problem – a relation of the form $\Phi(t) = e^{\alpha t} \Phi(t)$, where Φ is the solution to (3.35)-(3.36) and Φ is the solution to (3.86)-(3.87). Deducing Φ from Φ requires a limit process where $\alpha \rightarrow 0$.

3.5.2 The equivalence for the non-relaxed formulations

At this point we have shown that \mathbf{U} , the solution to (3.49)-(3.51), can be expressed as

$$\mathbf{U} = e^{\alpha t} \mathbf{U}_\alpha = e^{\alpha t} G_\alpha^* \Phi_\alpha.$$

The main idea is now to pass to the limit when α goes to zero in the equality above, to conclude that $\mathbf{U} = G^* \Phi$, where Φ is solution to (3.35)-(3.36). Note that the weak convergence

$$G_\alpha^* \Phi_\alpha \rightharpoonup_{L^2(0,T;\mathcal{H})} G^* \Phi$$

would implies that $\mathbf{U} = G^* \Phi$. It is then sufficient to prove that the weak convergence holds and that the limit Φ is solution to (3.35)-(3.36).

Following the same proof as Proposition 3.3, the following estimation can be proved,

$$\frac{1}{2} \left\| \frac{d}{dt} \Phi_\alpha(t) \right\|_{\mathcal{G}}^2 + 2\alpha \int_0^t \|\Phi_\alpha(t')\|_{\mathcal{G}}^2 dt' + \frac{1}{2} \|G_\alpha^* \Phi_\alpha(t)\|_{\mathcal{H}}^2 \lesssim B_\alpha^2(t), \quad (3.89)$$

where the inequality above holds up to a constant independent of Φ_α or the source term u_b , and with

$$B_\alpha(t) = \sup_{s \in [0,t]} \|e^{-\alpha s} u_b(s)\|_{H^{-1/2}(\Gamma_b)} + \int_0^t \|\partial_t(e^{-\alpha s} u_b(t'))\|_{H^{-1/2}(\Gamma_b)} dt'.$$

For $\alpha \leq 1$, it holds $B_\alpha(t) \leq B(t)$, where $B(t)$ is defined in (3.41). When $\alpha = 1$ we have $B_\alpha = B$. Therefore, the right-hand side of the estimation (3.89) can be replaced by a positive function independent of α . For $\alpha \leq 1$, we have

$$\left\| \frac{d}{dt} \Phi_\alpha(t) \right\|_{\mathcal{G}} + \|G_\alpha^* \Phi_\alpha(t)\|_{\mathcal{H}} \lesssim B(t). \quad (3.90)$$

From (3.86), we also deduce an estimate of the second order time derivative in the Hilbert space $\mathcal{D}(G_\alpha^*)'$,

$$\left\| \frac{d^2}{dt^2} \Phi_\alpha(t) \right\|_{\mathcal{D}(G_\alpha^*)'} \lesssim B(t). \quad (3.91)$$

Those preliminary observations allow us to state the following result.

Lemma 3.4. *The functions $G_\alpha^* \Phi_\alpha$ for $\alpha \in \mathbb{R}^+$ converges weakly in $L^2(0, T; \mathcal{H})$ to $G^* \Phi$ when $\alpha \rightarrow 0$ with Φ solution to (3.35)-(3.36).*

Proof. Using the estimates (3.90)-(3.91) and the fact that Φ_α vanishes at the initial time, we have that Φ_α , when considered as a sequence in α , is bounded in the Hilbert space

$$H^2(0, T; \mathcal{D}(G_\alpha^*)') \cap H^1(0, T; \mathcal{G}) \cap L^2(0, T; \mathcal{D}(G_\alpha^*)),$$

hence it converges weakly – up to a subsequence – to a function Φ in this space. Recall that the domain of the operator G_α^* is independent of α , from the definition $\mathcal{D}(G_\alpha^*) = \mathcal{D}(G^*) \times \mathcal{H}$. Decomposing $\Phi = (\Phi \mathbf{V})^t$ and passing to the limit in the formulation (3.86), we obtain

$$\frac{d^2}{dt^2}(\Phi, \tilde{\Phi})_{\mathcal{G}} + (G^* \Phi, G^* \tilde{\Phi})_{\mathcal{H}} = \langle u_b, \tilde{\varphi} \rangle_{\Gamma_b} \quad \forall \tilde{\Phi} = (\Phi \ 0)^t \in \mathcal{D}(G^*) \times \mathcal{H}, \quad \text{in } \mathcal{D}'(0, T), \quad (3.92)$$

and

$$\frac{d^2}{dt^2}(\mathbf{V}, \tilde{\mathbf{V}})_{\mathcal{H}} = 0 \quad \forall \tilde{\mathbf{V}} = (0 \ \tilde{\mathbf{V}})^t \in \mathcal{D}(G^*) \times \mathcal{H}, \quad \text{in } \mathcal{D}'(0, T). \quad (3.93)$$

Hence Φ is solution to (3.35). Equation (3.93) and the vanishing initial conditions give $\mathbf{V} \equiv 0$.

This almost concludes the proof. Indeed, only initial condition must be investigated to conclude. From the energy estimate (3.90) we also have the weak convergence in $H^1(0, T; \mathbf{G})$, therefore, for all $\tilde{\Phi} \in \mathbf{G}$,

$$(\Phi_\alpha(0), \tilde{\Phi})_{\mathbf{G}} = \frac{1}{T} \int_0^T \frac{d}{dt}((t-T)(\Phi_\alpha, \tilde{\Phi})_{\mathbf{G}}) dt \xrightarrow{\alpha \rightarrow 0} \frac{1}{T} \int_0^T \frac{d}{dt}((t-T)(\Phi, \tilde{\Phi})_{\mathbf{G}}) dt = (\Phi(0), \tilde{\Phi})_{\mathbf{G}},$$

hence $\Phi(0) = \Phi_\alpha(0) = 0$. Similarly, thanks to the weak convergence in $H^2(0, T; (\mathcal{D}(G^*) \times \mathcal{H})')$ we conclude that

$$\frac{d}{dt} \Phi(0) = \frac{d}{dt} \Phi_\alpha(0) = 0.$$

□

We have shown that Φ converges weakly to Φ , that the limit Φ is solution to (3.35)-(3.36), and that $G_\alpha^* \Phi_\alpha$ converges weakly to $G^* \Phi$. Then $\mathbf{U} = G^* \Phi$ is solution to (3.49)-(3.51), which proves Theorem 3.6.

3.6 Numerical illustration

To illustrate the equivalence between the two formulations, we solve numerically both problems for the same test case in a 2D domain. The problems are solved with a spectral element method. We first describe the choice of initial conditions, then we present the discretization. Finally we describe the test case and give some illustrations.

Initial conditions. As stated in the introduction, the background functions ρ_0, c_0 must satisfy the following positivity property,

$$-\frac{g}{\rho_0} \frac{d\rho_0}{dz} - \frac{g^2}{c_0^2} = N^2 \geq 0. \quad (3.94)$$

For the simulation presented here, we choose a simplified case, namely N^2 and c_0^2 are chosen constant. This gives an ordinary differential equation satisfied by ρ_0 ,

$$\frac{d\rho_0}{dz} + \rho_0 \left(\frac{N^2}{g} + \frac{g}{c_0^2} \right) = 0, \quad (3.95)$$

hence the density profile has the form

$$\rho_0(z) = \rho_0(0) \exp(-n^2 z), \quad n^2 = \frac{N^2}{g} + \frac{g}{c_0^2} > 0. \quad (3.96)$$

3.6.1 Discretization

For each problem, we present the variational formulation to be discretized and introduce the notations for the finite element approximation. The space discretization is done with a high-order spectral element method (Komatitsch and Vilotte, 1998; Cohen, 2001), and we give the fully-discrete scheme based on a second-order discretization in time.

Velocity-based formulation

For the continuous problem (3.49)-(3.51), the velocity is sought in a subspace of $H(\text{div}, \Omega)$. The discretization of $H(\text{div}, \Omega)$ can be done using e.g. Raviart-Thomas elements (Brezzi and Fortin, 1991). However, the problem is discretized in $H^1(\Omega)^d$ for the simplicity of implementation. Such a strategy is certainly not adequate for harmonic problems (Bonnet-Ben Dhia et al., 2007), or for transient problems with a mean flow (Bonnet-Bendhia et al., 2006). However, for the current problem we have not observed poor behaviour of the solution with this choice. The following variational formulation is discretized: find

$$\mathbf{U} \in C^1([0, T]; \mathcal{H}) \cap C^0([0, T]; H^1(\Omega)) \quad (3.97)$$

solution to

$$\begin{cases} \frac{d^2}{dt^2}(\mathbf{U}(t), \tilde{\mathbf{U}})_{\mathcal{H}} + (\tilde{G}\mathbf{U}(t), G\tilde{\mathbf{U}})_{\mathcal{G}} = 0, & \forall \tilde{\mathbf{U}} \in H^1(\Omega), \quad \forall t \in [0, T], \\ \mathbf{U}(t) \cdot \mathbf{n}_b = u_b, & \text{a. e. on } \Gamma_b, \quad \forall t \in [0, T]. \end{cases} \quad (3.98)$$

$$\mathbf{U}(t) \cdot \mathbf{n}_b = u_b, \quad \text{a. e. on } \Gamma_b, \quad \forall t \in [0, T]. \quad (3.99)$$

We denote by $\mathcal{V}_h \subset H^1(\Omega)$ the finite-dimensional space obtained by the discretisation of $H^1(\Omega)$. The scalar product in \mathcal{H} is approximated using a quadrature formula, and its approximation is denoted $(\cdot, \cdot)_{\mathcal{H}_h}$. Similarly, let $(\cdot, \cdot)_{\mathcal{G}_h}$ be the approximation of the scalar product on \mathcal{G} . We define the bilinear form $a_h : \mathcal{V}_h \times \mathcal{V}_{0,h} \rightarrow \mathbb{R}$ by

$$a_h(\mathbf{U}_h, \tilde{\mathbf{U}}_h) = (\tilde{G}\mathbf{U}_h, G\tilde{\mathbf{U}}_h)_{\mathcal{G}_h}, \quad \forall \mathbf{U}_h \in \mathcal{V}_h, \quad \forall \tilde{\mathbf{U}}_h \in \mathcal{V}_h. \quad (3.100)$$

The finite-element approximation of (3.98)-(3.99) reads: find

$$\mathbf{U}_h \in C^1([0, T]; \mathcal{H}_h) \cap C^0([0, T]; \mathcal{V}_h) \quad (3.101)$$

solution to

$$\begin{cases} \frac{d^2}{dt^2}(\mathbf{U}_h, \tilde{\mathbf{U}}_h)_{\mathcal{H}_h} + a_h(\mathbf{U}_h, \tilde{\mathbf{U}}_h) = 0, & \forall \tilde{\mathbf{U}}_h \in \mathcal{V}_h, \quad \forall t \in [0, T], \\ \mathbf{U}_h \cdot \mathbf{n}_b = u_{b,h}, & \text{a. e. on } \Gamma_b, \quad \forall t \in [0, T], \end{cases} \quad (3.102)$$

$$\mathbf{U}_h \cdot \mathbf{n}_b = u_{b,h}, \quad \text{a. e. on } \Gamma_b, \quad \forall t \in [0, T], \quad (3.103)$$

where $u_{b,h}$ is some discretization of the source term. The boundary condition (3.103) is either explicitly imposed for a flat bottom, or enforced with a Lagrange multiplier. In this work, we focus on the case of a flat bottom ($z_b \equiv 0$).

Potential-based formulation

As presented in Section 3.3, we use the variational formulation (3.33). The problem is written as a coupled system for the variables $(\varphi(t), \psi(t)) \in H^1(\Omega) \times L^2(\Omega)$ for all time $t \in [0, T]$. By taking

test function $\tilde{\psi} = 0$ in (3.33), the variational formulation reads

$$\begin{aligned} \frac{d^2}{dt^2} \left(\int_{\Omega} \frac{\rho_0}{c_0^2} \varphi \tilde{\varphi} \, dx + \int_{\Gamma_s} \frac{\rho_0}{g} \varphi \tilde{\varphi} \right) + \int_{\Omega} \rho_0 \left(\nabla \varphi - \frac{N^2}{g} \varphi \mathbf{e}_z \right) \cdot \left(\nabla \tilde{\varphi} - \frac{N^2}{g} \tilde{\varphi} \mathbf{e}_z \right) \, dx \\ - \int_{\Omega} \rho_0 N \psi \mathbf{e}_z \cdot \left(\nabla \tilde{\varphi} - \frac{N^2}{g} \tilde{\varphi} \mathbf{e}_z \right) \, dx = - \int_{\Gamma_b} \frac{\rho_0}{g} u_b \tilde{\varphi}, \end{aligned} \quad (3.104)$$

and by taking test function $\tilde{\varphi} = 0$ in (3.33), the variational formulation reads

$$\frac{d^2}{dt^2} \int_{\Omega} \rho_0 \psi \tilde{\psi} \, dx - \int_{\Omega} \rho_0 \left(\nabla \varphi - \frac{N^2}{g} \varphi \mathbf{e}_z \right) \cdot (N \tilde{\psi} \mathbf{e}_z) \, dx + \int_{\Omega} \rho_0 N^2 \psi \tilde{\psi} \, dx = 0. \quad (3.105)$$

We introduce the discretisation of $L^2(\Omega)$, denoted $\mathcal{L}_h(\Omega)$. The scalar product on $L^2(\Omega)$ is approximated with a quadrature formula, and its approximation is denoted $(\cdot, \cdot)_{\mathcal{L}_h(\Omega)}$. Similarly, the approximation of the scalar product on $L^2(\Gamma_s)$ is denoted $(\cdot, \cdot)_{\mathcal{L}_h(\Gamma_s)}$. The following bilinear forms are defined for $\varphi_h, \tilde{\varphi}_h \in \mathcal{V}_h$ and $\psi_h, \tilde{\psi}_h \in \mathcal{L}_h(\Omega)$,

$$m_{\varphi,h}(\varphi_h, \tilde{\varphi}_h) = \left(\frac{\rho_0}{c_0^2} \varphi_h, \tilde{\varphi}_h \right)_{\mathcal{L}_h(\Omega)} + \left(\frac{\rho_0}{g} \varphi_h, \tilde{\varphi}_h \right)_{\mathcal{L}_h(\Gamma_s)}, \quad m_{\psi,h}(\psi, \tilde{\psi}) = (\rho_0 \psi, \tilde{\psi})_{\mathcal{L}_h(\Omega)}, \quad (3.106)$$

$$a_{\varphi,h}(\varphi, \varphi) = (\nabla \varphi - N^2 \varphi \mathbf{e}_z, \nabla \varphi - N^2 \varphi \mathbf{e}_z)_{\mathcal{H}_h}, \quad a_{\psi,h}(\psi, \tilde{\psi}) = (\rho_0 N^2 \psi, \tilde{\psi})_{\mathcal{L}_h(\Omega)}, \quad (3.107)$$

$$c_h(\psi, \tilde{\varphi}) = (-\rho_0 N \psi \mathbf{e}_z, \nabla \tilde{\varphi} - N \tilde{\varphi} \mathbf{e}_z)_{\mathcal{H}_h}. \quad (3.108)$$

For the source term u_b , we introduce the discretisation of the space $L^2(\Gamma_b)$, denoted $\mathcal{L}_h(\Gamma_b)$. The approximation of the scalar product on $L^2(\Gamma_b)$ is denoted $(\cdot, \cdot)_{\mathcal{L}_h(\Gamma_b)}$. The semi-discrete variational formulation reads then: find

$$(\varphi_h, \psi_h) \in C^0([0, T]; \mathcal{V}_h \times \mathcal{L}_h(\Omega)), \quad \frac{d}{dt}(\varphi_h, \psi_h) \in C^0([0, T]; \mathcal{L}_h(\Omega) \times \mathcal{L}_h(\Omega)) \quad (3.109)$$

solution

$$\begin{cases} \frac{d^2}{dt^2} m_{\varphi,h}(\varphi_h, \tilde{\varphi}_h) + a_{\varphi,h}(\varphi_h, \tilde{\varphi}_h) + c_h(\psi_h, \tilde{\varphi}_h) = \ell_h(\tilde{\varphi}_h), & \forall \tilde{\varphi}_h \in \mathcal{V}_h, \quad \forall t \in [0, T], \\ \frac{d^2}{dt^2} m_{\psi,h}(\psi_h, \tilde{\psi}_h) + a_{\psi,h}(\psi_h, \tilde{\psi}_h) + c_h(\tilde{\psi}_h, \varphi_h) = 0, & \forall \tilde{\psi}_h \in \mathcal{L}_h(\Omega), \quad \forall t \in [0, T], \end{cases} \quad (3.110)$$

with $\ell_h(\varphi_h) = -(\rho_0/g u_{b,h}, \tilde{\varphi}_h)_{\mathcal{L}_h(\Gamma_b)}$. The velocity \mathbf{U} is computed from the variables (φ, ψ) , using the relation $\mathbf{U} = G^* \Phi$. The finite-element approximation used for computing \mathbf{U}_h reads then:

$$(\mathbf{U}_h, \tilde{\mathbf{U}}_h)_{\mathcal{H}_h} = b_{\varphi,h}(\varphi_h, \tilde{\mathbf{U}}_h) + b_{\psi,h}(\psi_h, \tilde{\mathbf{U}}_h), \quad \forall \tilde{\mathbf{U}}_h \in \mathcal{V}_{0,h}, \quad (3.112)$$

where $b_{\varphi,h} : \mathcal{V}_h \times \mathcal{V}_{0,h} \rightarrow \mathbb{R}$ and $b_{\psi,h} : \mathcal{L}_h \times \mathcal{V}_{0,h} \rightarrow \mathbb{R}$ are the following bilinear forms,

$$b_{\varphi,h}(\varphi_h, \tilde{\mathbf{U}}_h) = -(\nabla \varphi_h - \frac{N^2}{g} \mathbf{e}_z \varphi_h, \tilde{\mathbf{U}}_h)_{\mathcal{H}_h}, \quad b_{\psi,h}(\psi_h, \tilde{\mathbf{U}}_h) = (N \psi_h \mathbf{e}_z, \tilde{\mathbf{U}}_h)_{\mathcal{H}_h}. \quad (3.113)$$

Spectral element method

For the approximation of the functional spaces and the various bilinear forms involved in both formulations, we use the spectral element method. The discretization is presented here for 2D

problems, but the method would be the same for 3D problems. The domain is discretized into quadrilaterals denoted $\{K_i\}_{i \in \{1, \dots, N\}}$. The obtained discrete domain is denoted Ω_h with a discrete bottom boundary $\Gamma_{b,h}$. The bottom boundary consists in vertices denoted $V_i, i \in \{1, \dots, N_b\}$. We denote by \hat{K} the unit square and $\mathbf{F}_i, i \in \{1, \dots, N\}$ the invertible transformation from \hat{K} to the quadrilateral K_i . Let also \hat{V} be the unit line, and the invertible transformation from \hat{V} to V_i is $F_{i|\hat{V}}$. We have then for the discrete domain

$$\Omega_h = \bigcup_{i=1}^N K_i, \quad K_i \cap K_j = \emptyset, \quad \mathbf{F}_i(\hat{K}) = K_i, \quad (3.114)$$

and for the discrete bottom boundary

$$\Gamma_{b,h} = \bigcup_{i=1}^{N_b} V_i, \quad V_i \cap V_j = \emptyset, \quad \mathbf{F}_{i|\hat{V}}(\hat{V}) = V_i. \quad (3.115)$$

We now introduce the approximation of the functional spaces. Let $\mathcal{Q}_{r,q}$ be the set of polynomials with degree r in the x coordinate and degree q in the z coordinate, and let \mathcal{Q}_r be the set of polynomials with degree r in the x coordinate. Then $\mathcal{L}_h(\Omega)$ and \mathcal{V}_h are defined as follows,

$$\mathcal{V}_h = \{\phi \in C^0(\Omega_h) \mid \phi|_{K_i} \circ \mathbf{F}_i \in \mathcal{Q}_{q,r}(\hat{K})\}, \quad \mathcal{L}_h(\Omega) = \{\phi \in L^2(\Omega_h) \mid \phi|_{K_i} \circ \mathbf{F}_i \in \mathcal{Q}_{q,r}(\hat{K})\}, \quad (3.116)$$

and the space $\mathcal{L}_h(\Gamma_b)$ is defined as follows,

$$\mathcal{L}_h(\Gamma_b) = \{\phi \in L^2(\Gamma_b) \mid \phi|_{V_i} \circ F_{i|\hat{V}} \in \mathcal{Q}_r(\hat{V})\}. \quad (3.117)$$

Each variable is decomposed on the basis of its functional space. For the velocity-based formulation, we obtain the global vector \mathbf{U}_h with two components for each degree of freedom, the mass matrix \mathbb{M}_U and the stiffness matrix \mathbb{K}_U . The semi-discrete scheme corresponding to the finite-element approximation (3.102) reads

$$\frac{d^2}{dt^2} \mathbb{M}_U \mathbf{U}_h + \mathbb{K}_U \mathbf{U}_h = 0, \quad (3.118)$$

For the potential-based formulation the decomposition on each basis yields the global vectors φ_h , ψ_h and $u_{b,h}$, as well as the mass matrices \mathbb{M}_φ , \mathbb{M}_ψ and \mathbb{M}_b , the stiffness matrices \mathbb{K}_φ , \mathbb{K}_ψ , and the interaction matrix $\mathbb{C}_{\psi,\varphi}$. We also obtain the matrices \mathbb{B}_φ , \mathbb{B}_ψ used to deduce the velocity from the potential, see Equation (3.112). The semi-discrete system corresponding to the finite-element approximation (3.110)-(3.112) reads

$$\begin{cases} \frac{d^2}{dt^2} \mathbb{M}_\varphi \varphi_h + \mathbb{K}_\varphi \varphi_h + \mathbb{C}_{\psi\varphi} \psi_h = -\mathbb{M}_b u_{b,h}, & (3.119) \end{cases}$$

$$\begin{cases} \frac{d^2}{dt^2} \mathbb{M}_\psi \psi_h + \mathbb{K}_\psi \psi_h + \mathbb{C}_{\psi\varphi}^T \varphi_h = 0, & (3.120) \end{cases}$$

$$\begin{cases} \mathbb{M}_U \mathbf{U}_h = \mathbb{B}_\varphi \varphi_h + \mathbb{B}_\psi \psi_h. & (3.121) \end{cases}$$

By using the Gauss-Lobatto quadrature rule for the integral approximations, we obtain mass lumping, meaning that the mass matrices \mathbb{M}_U , \mathbb{M}_φ , \mathbb{M}_ψ and \mathbb{M}_b are diagonal.

Time discretisation

The time interval $[0, T]$ is partitionned into M equal intervals of length $\Delta t = T/M$. The finite-element approximations (3.118) and (3.119)-(3.120) are discretized in time with a leapfrog scheme. We consider the sequence $\{\mathbf{U}_h^n \in \mathcal{V}_{0,h}\}_{n \in \{1, \dots, M\}}$ solution to

$$\mathbb{M}_U \frac{\mathbf{U}_h^{n+1} - 2\mathbf{U}_h^n + \mathbf{U}_h^{n-1}}{\Delta t^2} + \mathbb{K}_U \mathbf{U}_h^n = 0. \quad (3.122)$$

For the potential-based formulation, we consider the sequences $\{\phi^n \in \mathcal{V}_h\}_{n \in \{1, \dots, M\}}$ and $\{\psi^n \in \mathcal{L}_h\}_{n \in \{1, \dots, M\}}$ solution to

$$\left\{ \begin{array}{l} \mathbb{M}_\phi \frac{\phi^{n+1} - 2\phi^n + \phi^{n-1}}{\Delta t^2} + \mathbb{K}_\phi \phi^n + \mathbb{C}_{\phi\psi} \psi^n = \mathbb{M}_\phi f_\phi, \end{array} \right. \quad (3.123)$$

$$\left\{ \begin{array}{l} \mathbb{M}_\psi \frac{\psi^{n+1} - 2\psi^n + \psi^{n-1}}{\Delta t^2} + \mathbb{K}_\psi \phi^n + \mathbb{C}_{\phi\psi}^t \phi^n = 0, \end{array} \right. \quad (3.124)$$

and the velocity is then computed with

$$\mathbb{M}_U \mathbf{U}_h^n = \mathbb{B}_\phi \phi_h^n + \mathbb{B}_\psi \psi_h^n. \quad (3.125)$$

3.6.2 Numerical example: tsunami and hydro-acoustic waves generation

In order to validate and compare the formulations (3.122) and (3.123)-(3.125), we reproduce the test case presented by Sammarco et al. (2013). A tsunami is generated by an elevation of the seabed, in a 2D domain with no topography. Sammarco et al. (2013) consider a model in which the flow is assumed irrotational, with velocity potential ϕ . The vertical distance between the seabed and the mean water level is denoted $h(x, y, t)$. The background data are all assumed constant and the model, solved with a finite elements method, reads

$$\frac{\partial^2 \phi}{\partial t^2} - c^2 \Delta \phi = 0,$$

with boundary conditions

$$\frac{\partial^2 \phi}{\partial t^2} + g \frac{\partial \phi}{\partial z} = 0, \text{ at } z = h(x, y, t), \quad \nabla \phi \cdot \mathbf{n} = \frac{\partial h}{\partial t}, \text{ at } z = 0.$$

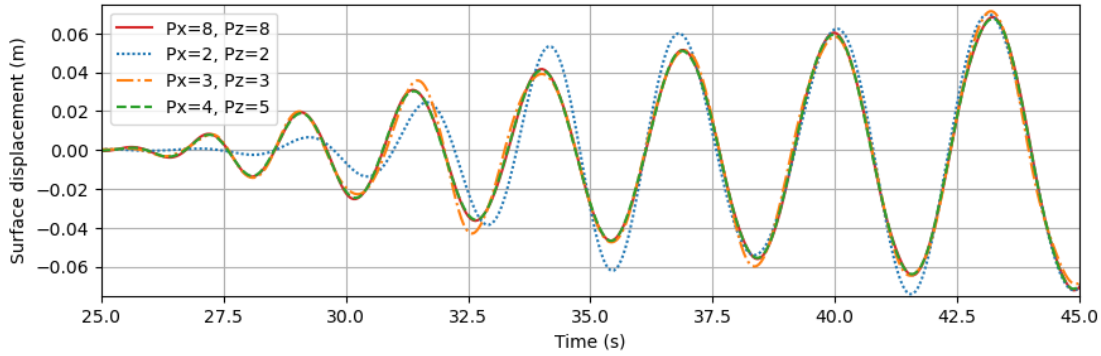
We give now the characteristics of the source term. A 20 km-wide area rises at one meter per second during one second. The source term takes the form $\partial_t h(x, t) = u_b(x, t) = f(x)g(t)$, where f and g are smoothed rectangular functions.

The tsunami propagates over 50 km. Since we impose no conditions on the lateral boundaries, the computational domain is much wider to avoid reflections inside the domain of interest.

Convergence analysis. For each formulation, several mesh refinements and elements orders are tested. The aim is to show that the simulations converge, and to select parameters that are precise enough and not too costly. We denote by P_x, P_z the finite elements orders respectively in the x and in the z coordinates, and by N_x, N_z the number of mesh subdivision respectively in the x and in the z coordinates. Several combinations of P_x and P_z are tested while keeping N_x and N_z fixed. To show the convergence, we plot the time evolution of the surface displacement at a point 50 km away

Px	Pz	Nx	Nz	DoFs
2	2	101	10	8 526
3	3	101	10	18 848
4	5	101	10	41 310
8	8	101	10	131 058

Table 3.1: Tested cases for the velocity formulation.

Figure 3.2: Vertical displacement at $x = 50$ km for the velocity formulation at different elements orders.

from the source center. The tsunami is simulated for 50 s, and the computational domain is 101 km long. For the velocity-based scheme, the results are shown in Figure 3.2 and the convergence is reached for $P_x = 4$, $P_z = 5$. For the potential-based scheme, the results are shown in Figure 3.3, and we also plot in Figure 3.4 the vertical displacement of the seabed at the source center. In Figure 3.3, all tested orders with $P_x > 3$ converge, but we see in Figure 3.4 that for $P_x \leq 4$ the vertical velocity exhibits small oscillations. The convergence is reached for $P_x = 3$, $P_z = 5$.

The total number of degrees of freedom (DoFs) for each case is given in Table 3.1 for the velocity formulation, and in Table 3.2 for the dual formulation. We see that for the same mesh refinement and the same elements orders, the potential formulation has more degrees of freedoms than the velocity formulation. This is due to the discretization of the discontinuous space L^2 .

Snapshots and free-surface elevation. From the comparison made in the previous paragraph, we use $P_x=4$, $P_z=5$ for the velocity-based formulation and $P_x=3$, $P_z=5$ for the potential-based

Px	Pz	Nx	Nz	DoFs
2	2	101	10	13 353
3	3	101	10	25 584
3	5	101	10	39 744
8	8	101	10	147 339

Table 3.2: Tested cases for the potential formulation.

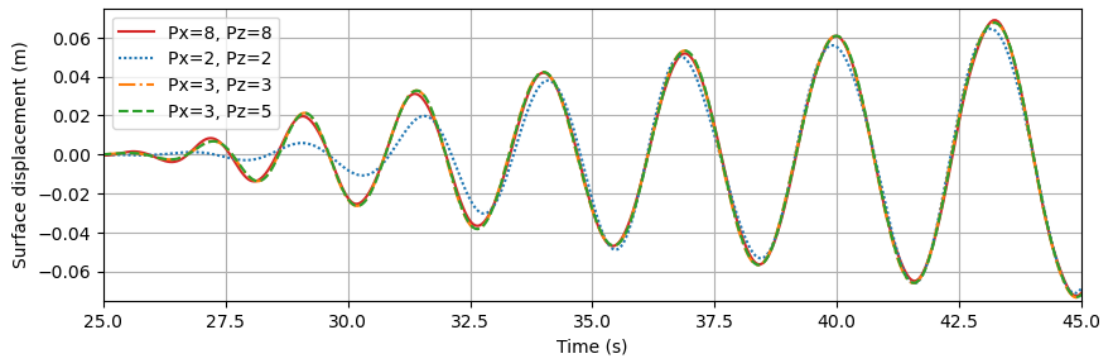


Figure 3.3: Vertical displacement at $x = 50\text{km}$ for the potential formulation at different elements orders.

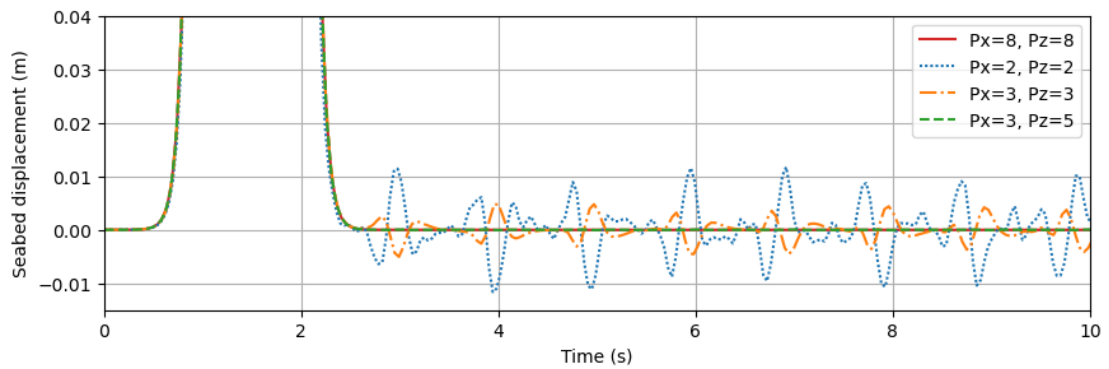


Figure 3.4: Vertical displacement at $x = 50\text{ km}$ for the potential formulation at different elements orders.

formulation. The tsunami is simulated for 1000 s, and the computational domain is 1051 km long. The velocity-based formulation has then 428 910 DoFs and the potential-based formulation has 413 094 DoFs. The computational time for the velocity-based formulation was 771 seconds, and for the potential-based formulation it was 1197 seconds. Here, the potential-based formulation requires more computational time than the velocity-based formulation. This is because we study the displacement, which is obtained by integrating in time the velocity. Hence, to compute the displacement as precisely as possible, the velocity is computed at each time step. The system (3.125) is then solved at each time step, leading to an additional computational cost. The code could be faster by using an efficient time integration rule which would not require to compute the velocity at each time step, or by studying the potential associated to the displacement.

Figure 3.5 shows the time evolution of the surface displacement for a point with abscissa 50 km away from the source center. The orange curve is the displacement d_ϕ computed from the potential formulation, and the blue curve is the displacement d_U computed from the velocity formulation. The curves are almost superimposed, which illustrates the fact that both formulations are equivalent. For comparison, the surface elevation obtained by Sammarco et al. (2013) is shown on Figure 3.6. The result is very similar to Figure 3.5. In particular, the tsunami arrival times are in good agreement.

Figure 3.7 shows the error $|d_\phi - d_U|$ between the potential-based and the velocity-based formulations. The error has a magnitude of less than 5 percents, and it oscillates with a period of approximately 4 second. The error averaged over a period is plotted in the same figure. We see that the averaged error slowly increases, which could be caused by the time integration: small errors add up and become non-negligible for large times.

Figure 3.8 shows snapshots of the Eulerian domain near the earthquake at several times. The Eulerian domain is obtained by deforming the domain at rest with the displacement vector field. The colors correspond to the magnitude of the vertical velocity. On each snapshot, we see the permanent deformation of the seabed over $[-10 ; 10]$ km caused by the earthquake. The surface deformation is due to the acoustic waves propagating for early times ($t=49s$), then in the next two snapshots ($t=147s$ and $t=343s$), we see the tsunami propagating in both directions. In the last snapshot ($t=833s$), the tsunami is away from the considered domain and it remains only acoustic waves.

3.7 Conclusion and future work

In this work, we have presented two different formulations for a model describing the propagation of acoustic-gravity waves in a stratified ocean (Dubois et al., 2023). We have first shown the well-posedness of both formulations. For the velocity-based formulation, the study is complicated by the presence of an essential boundary condition of Dirichlet type. To show the existence of solution, we have introduced an equivalent relaxed problem. We have then proved the equivalence between both formulation by using energy estimates. For both formulations, a discretization using the spectral element method is presented, and the schemes are validated on a two-dimensional numerical test case. The test case also illustrates the equivalence between both formulation. The numerical illustration suggests that the potential-based formulation is better suited to numerical approximations, in particular for 3D problems. This formulation is also easier to handle from a mathematical point of view since it requires no essential boundary condition.

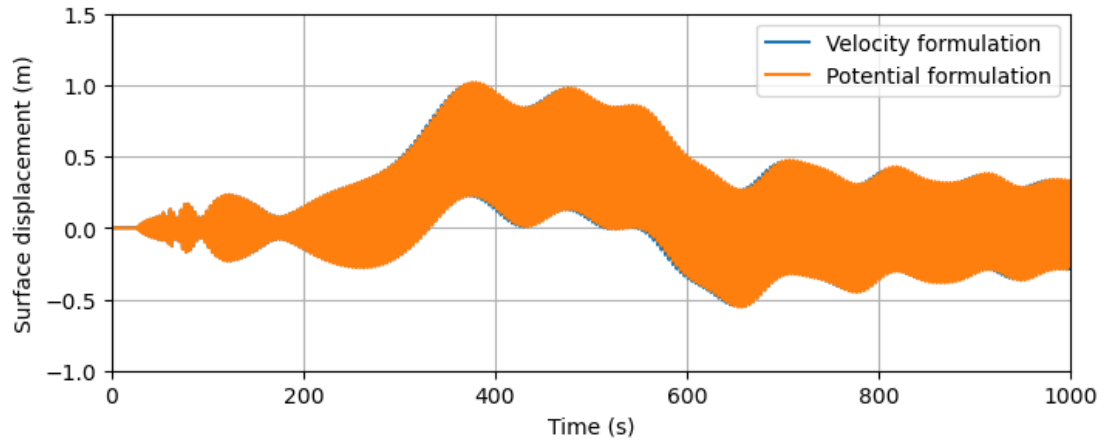


Figure 3.5: Vertical displacement at $x = 50$ km, computed from the velocity-based (blue) and the potential-based (orange) formulations.

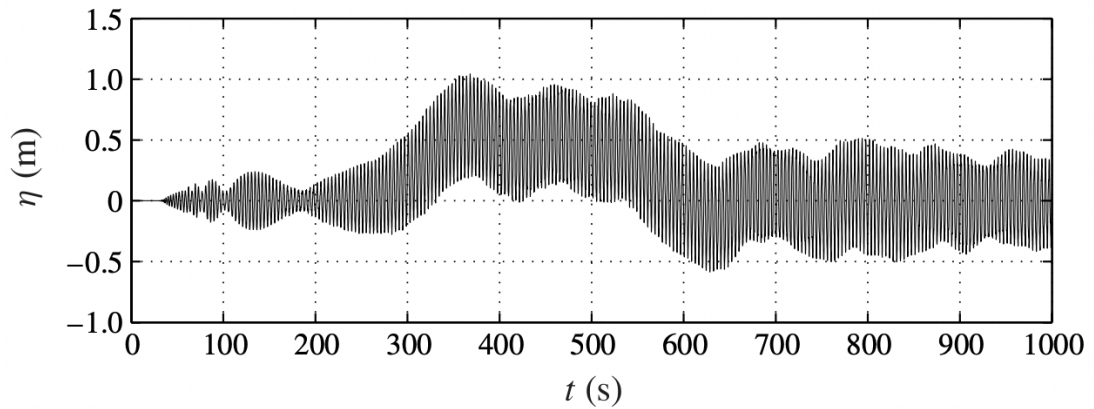


Figure 3.6: Vertical displacement at $x = 50$ km, by Sammarco et al. (2013).

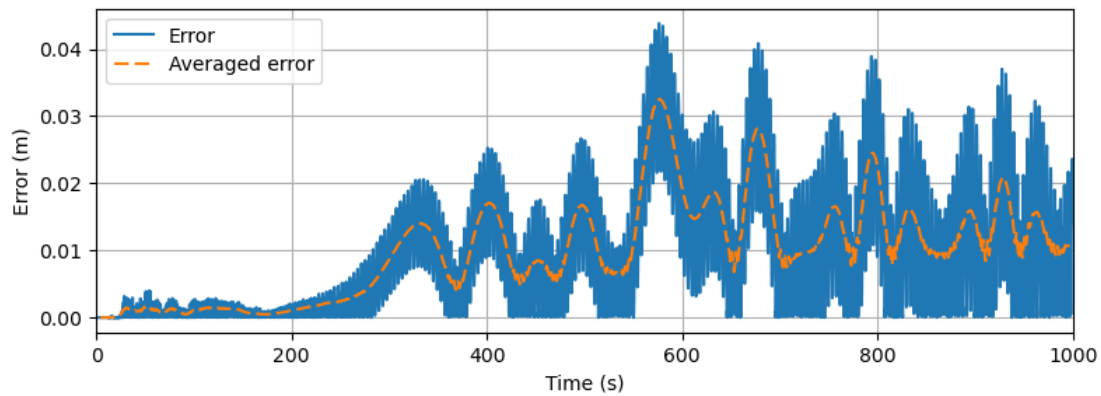


Figure 3.7: Vertical displacement at $x = 50$ km from the velocity-based and the potential-based formulations, and absolute error.

As mentioned in the introduction, the velocity-based problem can be seen as the Galbrun equation with no mean flow. For the Galbrun equation with a mean flow, the choice of the correct functional framework for the analysis is still an open question. It could be interesting to investigate whether a potential-based formulation could be obtained for the Galbrun equation with a mean flow. Moreover, from a numerical point of view, both the transient problem with a mean flow and the harmonic problems – even without mean flow – are known to present spurious modes when discretized in a simple way (Bonnet-Ben Dhia et al., 2007; Bonnet-Bendhia et al., 2006). One could also study the discretisation of the potential-based formulation in the harmonic regime and check whether spurious modes are present.

Finally, it should be noted that the equation (3.7) relating the velocity to the potential yields a natural splitting between the irrotational and the rotational components of the velocity. The potential-based formulation could be used to study the contribution of the rotational component in cases where it is usually neglected.

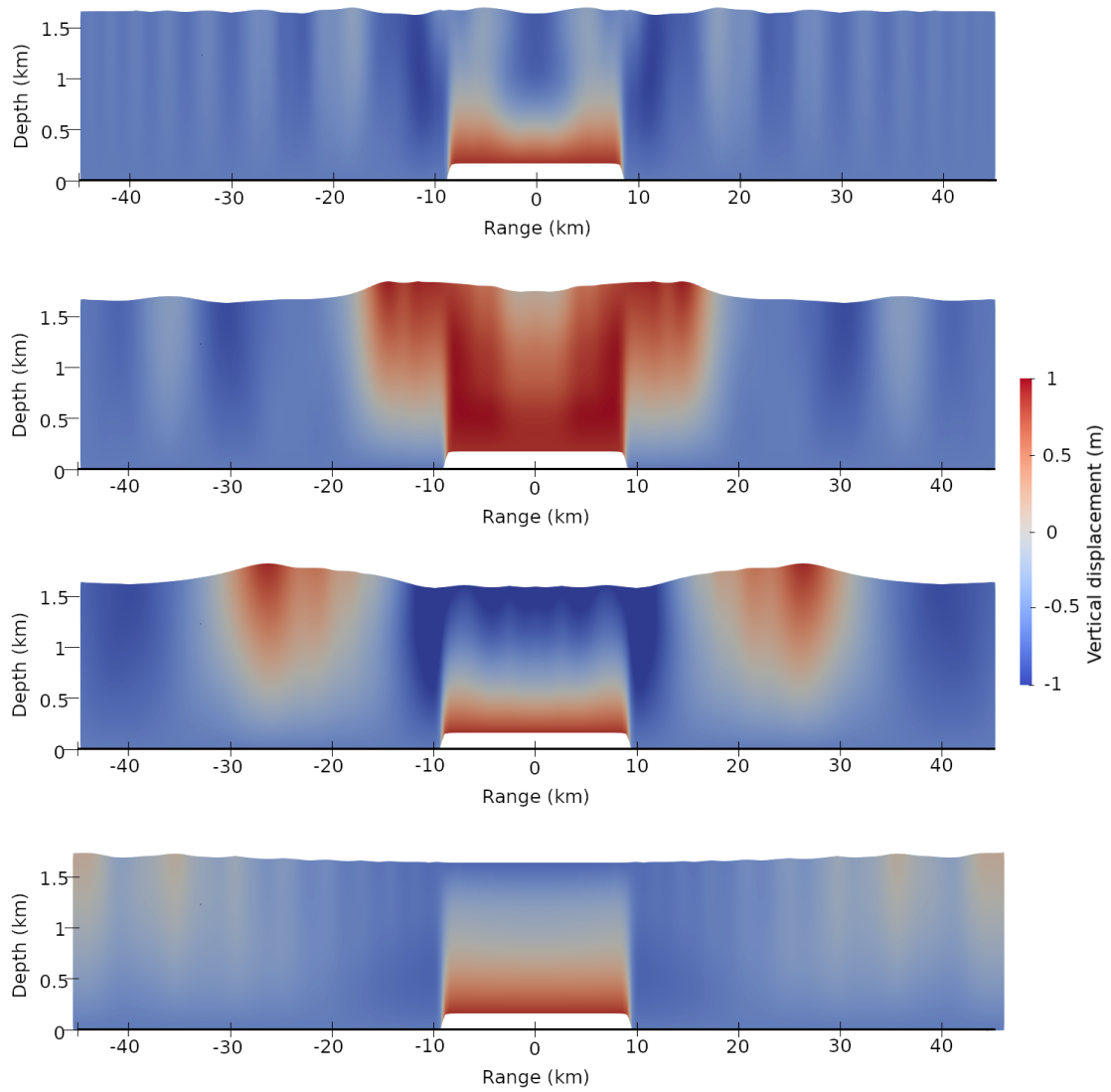


Figure 3.8: Snapshots of the displacement obtained with the potential formulation, for the times $t = 49.0$ s, $t = 147.1$ s, $t = 343.3$ s, $t = 833.8$ s.

Coupling with the earth: the gravito-elastic equations

Contents

4.1 Introduction	94
4.2 The equations for linear elasticity with a prestress	95
4.2.1 The equations in Eulerian coordinates	95
4.2.2 The equations in Lagrangian coordinates	96
4.2.3 Linearization around the equilibrium state	98
4.2.4 The linear equations for the fluid-solid system	99
4.3 Mathematical analysis	100
4.3.1 A first variational formulation	101
4.3.2 The modified variational formulation	102
4.3.3 Mathematical analysis of the modified formulation	107
4.3.4 Energy estimates	110
4.4 Numerical illustration	112
4.5 Conclusion and future work	115
Appendix	115
A The bilinear form in the fluid domain	115
B An expression for the extended density	116

Abstract: This chapter presents an ongoing work. We extend the model presented in Chapter 2, so as to take the interaction with the seabed into account. Instead of assuming a rigid seabed, we consider an elastic domain below the fluid layer. The fluid-solid system is modeled as one elastic domain, with different parameters for the fluid and solid sub-domains. One novelty of this work is that the domain is subject to a prestress, accounting for the effect of gravity and initial stress in the Earth. We first derive a linear system describing the coupled motion of the fluid and the solid in a prestressed state. We study then the mathematical properties of the model. A first variational formulation is deduced, however, one cannot show the well-posedness of this formulation. We propose then a second variational formulation, relying on continuous extensions of the background parameters. We show the well-posedness of the second variational formulation and give energy estimates. Finally, we present a numerical approximation obtained with a spectral element method.

4.1 Introduction

The model presented in Chapter 2 uses the assumption of a rigid earth, thanks to the boundary condition $\mathbf{U} \cdot \mathbf{n} = u_b$ on Γ_b . This assumption is commonly made in hydro-acoustic models for tsunami early-warning systems (Longuet-Higgins, 1950; Yamamoto, 1982; Stiasnie, 2010; Kadri and Stiasnie, 2013).

Several studies have shown the limitations of this assumption for the propagation of hydro-acoustic waves and tsunamis. Nosov and Kolesov (2007) show that some spectral characteristics of the bottom pressure are not well reproduced by the classical model for hydro-acoustic waves. They suggest that taking into account the interaction of the acoustic waves with the earth is crucial for a correct estimation of the bottom pressure. Other studies, such as the work by Abdolali et al. (2019), show that the prediction for the tsunami arrival could be slightly improved by assuming an elastic earth (see also the references cited by Richard et al., 2023). In their work, Abdolali et al. (2019) study the influence of several parameters on the propagation of tsunamis. They use a system of three scalar wave equations: one for the tsunami, one for the compressional waves (or P-waves) and one for the shear waves (or S-waves) for the earth. The tested parameters are the effect of gravity on the water density, the seafloor elasticity and the compressibility of water. By studying the dispersion relation, the authors show that each parameter can change by a few percent the phase speed of the tsunami.

A correct modeling of the interaction between the earth and the ocean is also necessary for a better understanding of the generation of tsunami and hydro-acoustic waves from a seabed displacement. The generation phase is a complex process where the seismic waves, the acoustic waves and the tsunami are superimposed (Krenz et al., 2021; Abrahams et al., 2023). One of the early work on the acoustic-elastic coupling for tsunami generation is done by Maeda and Furumura (2013). In this work, the authors propose a fully-coupled model for the hydro-acoustic waves, the tsunami and the seismic waves. The fluid layer is represented by an elastic medium where no shear wave can propagate ($\mu = 0$). The free-surface displacement and the equilibrium with gravity at rest are explicitly added in the equations by introducing a quasi-static pressure. Numerical example are then obtained in 2D and 3D with a finite-difference method. Another fully-coupled model is proposed by Lotto and Dunham (2015). The author extend the classical acoustic-elastic equations (see for example Komatitsch and Tromp, 1999) to the tsunami generation by adding the surface equation for free-surface flows with gravity. This model is then extended by Krenz et al. (2021) to a 3D formulation; an implementation in the software SeiSol is also presented. The 3D model is used as reference in the study by Abrahams et al. (2023), where four different models for the generation and propagation of tsunami, hydroacoustic and seismic waves are compared. Richard et al. (2023) proposes a model combining a weakly compressible Boussinesq model for the ocean is coupled with visco-elastic equations for the earth. The authors show that the obtained model is hyperbolic and that it preserves energy.

To our knowledge, no well-posedness result and no mathematical framework for the analysis of the above models have been proposed – except from the model proposed by Richard et al. (2023), which relies on a different equation for the fluid. Moreover, most models neglect the effect of gravity in the earth while retaining it in the ocean, which may be problematic for the transmission conditions. We mention the work by Valette (1986) and de Hoop et al. (2017) for the mathematical analysis of the earth oscillation with fluid and solid layers. Their model consider the whole earth with an arbitrary number of fluid and solid layers. They show the well-posedness of the system and give stability estimates. Their analysis could be adapted to the case of a system with one ocean layer and one seabed layer, however the method used is rather difficult to read.

In this chapter, we propose a model coupling the tsunami, the hydroacoustic waves and the seismic waves for a layer of compressible, stratified ocean above a layer of elastic earth. In Section 4.2, we derive the equations for linear elasticity in a pre-stressed medium by using the same linearization method as in Chapter 2. The fluid and the solid are considered as two layers of the elastic medium, with different parameters (in particular $\mu = 0$ in the fluid). We present in Section 4.3 the mathematical analysis. For numerical purposes, a first variational formulation is introduced, but it is not well-posed. We present then a second variational formulation, obtained by introducing a fictitious pressure in the neighbourhood of the fluid-solid interface. For this second formulation, we prove existence and uniqueness of solution, and give some stability estimates. In Section 4.4, the first variational formulation is discretized with a spectral element method, and we show a simple test case.

4.2 The equations for linear elasticity with a prestress

In this section, we show how to derive the gravito-elastic equations for the Earth. The obtained system is a simplified version of the global Earth model (see e.g. Dahlen and Tromp, 1998) to the case of a constant gravity acceleration vector, without the Coriolis effect, and considering only a portion of the Earth.

We start by deriving the equation of linear elasticity for an elastic domain subject to a pre-stress, caused by the effect of gravity. We recall the nonlinear equation in Eulerian coordinates, then write them in Lagrangian coordinates, and give the constitutive equations for elasticity with a pre-stress. The equations are then linearized. Finally, the fluid-solid case is deduced, by considering the fluid as an elastic solid with a vanishing shear wave velocity.

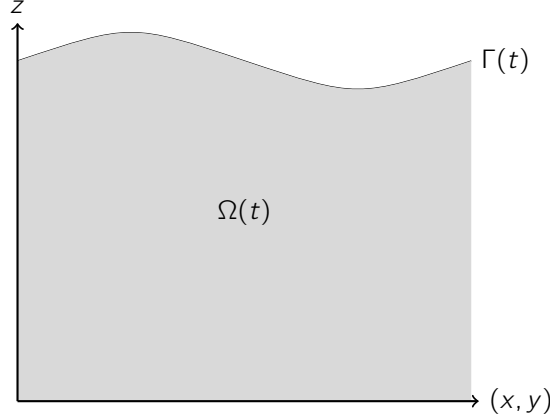
4.2.1 The equations in Eulerian coordinates

We consider a time-dependant domain $\Omega(t)$, representing a portion of Earth. On the contrary to the models presented by Valette (1986) and de Hoop et al. (2017), only a small portion of the Earth is considered. This allows us to neglect the curvature of the Earth and to assume that the gravitational acceleration is a constant vector. Moreover, since our aim is to focus on the interaction between the ocean and a portion of earth below it, we only consider the upper layer of Earth as assimilate it to an infinite half-space, see Figure 4.1. The boundary of Ω is the free surface, and is denoted Γ .

The domain is written with the Cartesian coordinates (x, y, z) . The variables of the problem are the density ρ , the velocity \mathbf{U} , and the Cauchy stress tensor $\underline{\underline{T}}$. The equations for the conservation of mass and momentum read in $\Omega(t)$

$$\begin{cases} \frac{\partial \rho}{\partial t} + \nabla \cdot (\rho \mathbf{U}) = 0, & (4.1) \\ \frac{\partial}{\partial t}(\rho \mathbf{U}) + \nabla \cdot (\rho \mathbf{U} \otimes \mathbf{U}) - \nabla \cdot \underline{\underline{T}} = -\rho g \mathbf{e}_z + \mathbf{S}, & (4.2) \end{cases}$$

The vector $-g \mathbf{e}_z$ is the gravitational acceleration and \mathbf{S} is a external force representing the source of the tsunami, for example a fault slip in the solid layer (Lotto and Dunham, 2015). The external force is assumed to vanish at initial time, $\mathbf{S}(x, y, z, t = 0) = 0$. The constitutive law relating the stress tensor to the displacement will be given in Lagrangian coordinates in the next section.

Figure 4.1: The domain $\Omega(t)$

Boundary conditions. We define the boundary and the transmission conditions. Since the domain Ω is semi-infinite, there is only the surface condition. The surface is assumed to be stress-free. We denote by \mathbf{n} the unit vector normal to surface pointing outwards, and the condition reads

$$\underline{\underline{T}} \cdot \mathbf{n} = 0, \quad \text{on } \Gamma. \quad (4.3)$$

Initial state. We assume that the initial state is a state at rest, namely $\mathbf{U}(x, y, z, 0) = 0$. The domain at initial time is denoted $\Omega(0)$. We also assume that the source term vanishes for $t = 0$. Then the initial state is at equilibrium if the initial stress, denoted by $\underline{\underline{T}}_0$, satisfies

$$\nabla \cdot \underline{\underline{T}}_0 = -\rho_0 g \mathbf{e}_z, \quad \text{in } \Omega(0). \quad (4.4)$$

4.2.2 The equations in Lagrangian coordinates

Following the classical approach (Ciarlet, 1988; Dahlen and Tromp, 1998), the system is studied in Lagrangian coordinates. This offers two advantages: the linearization process is rigorously justified, and the resulting model remains valid for a large initial stress (Dahlen and Tromp, 1998).

Notations. We choose a reference domain $\hat{\Omega}$ with coordinates $\boldsymbol{\xi} = (\xi_1, \xi_2, \xi_3)$. We denote by $\nabla_{\boldsymbol{\xi}}$ the differentiation with respect to the Lagrangian coordinates. The equations (4.1) and (4.2) are written in the reference domain by using the following change of coordinates: For all time t , we define the transformation $\boldsymbol{\phi}_t : \hat{\Omega} \rightarrow \Omega(t)$, and for any variable X defined on $\Omega(t)$, we define the variable \hat{X} on $\hat{\Omega}$ by

$$\hat{X}(\boldsymbol{\xi}, t) = X(\mathbf{x}, t), \quad \mathbf{x} = \boldsymbol{\phi}_t(\boldsymbol{\xi}).$$

We also define $\boldsymbol{\phi} : (\boldsymbol{\xi}, t) \mapsto \boldsymbol{\phi}_t(\boldsymbol{\xi})$. The gradient of $\boldsymbol{\phi}$ is denoted $\underline{\underline{F}}$, its Jacobian is denoted J , and we define the displacement \mathbf{d} ,

$$\mathbf{d}(\boldsymbol{\xi}, t) = \boldsymbol{\phi}(\boldsymbol{\xi}, t) - \boldsymbol{\xi}, \quad \underline{\underline{F}} = \nabla_{\boldsymbol{\xi}} \boldsymbol{\phi}, \quad J = \det(\underline{\underline{F}}).$$

The spatial derivative are transformed by the change of coordinates. For a tensor $\underline{\underline{X}}$ it holds

$$\nabla \cdot \underline{\underline{X}} = \nabla_{\boldsymbol{\xi}} \cdot (J \hat{\underline{\underline{X}}} \underline{\underline{F}}^{-T}). \quad (4.5)$$

In view of the equation (4.5), we define the first Piola-Kirchhoff stress tensor, denoted $\underline{\underline{\hat{P}}}$, by

$$\underline{\underline{\hat{P}}} = J \underline{\underline{\hat{T}}} \underline{\underline{F}}^{-T}. \quad (4.6)$$

We also define the second Piola-Kirchhoff stress tensor, denoted $\underline{\underline{\hat{\Sigma}}}$, by

$$\underline{\underline{\hat{\Sigma}}} = \underline{\underline{F}}^{-1} \underline{\underline{\hat{P}}}. \quad (4.7)$$

The tensors $\underline{\underline{\hat{T}}}$ and $\underline{\underline{\hat{\Sigma}}}$ are symmetric, and $\underline{\underline{\hat{P}}}$ is in general not symmetric.

Conservation equations in Lagrangian coordinates. The mass conservation reads in Lagrangian coordinates $\partial_t(J\hat{\rho}) = 0$, hence if we denote by $\hat{\rho}_0$ the density at initial time, it holds

$$J\hat{\rho} = \hat{\rho}_0.$$

The momentum equation (4.2) is written in Lagrangian coordinates thanks to Equation (4.5),

$$\hat{\rho} \frac{\partial \hat{\mathbf{U}}}{\partial t} - J^{-1} \nabla_{\xi} \cdot \underline{\underline{\hat{P}}} = -\hat{\rho} g \mathbf{e}_3 + \hat{\mathbf{S}}, \quad (4.8)$$

where \mathbf{e}_3 is the unit vector in the vertical direction oriented upwards. Multiplying Equation (4.8) by J and using the property $J\hat{\rho} = \hat{\rho}_0$ yields

$$\hat{\rho}_0 \frac{\partial \hat{\mathbf{U}}}{\partial t} - \nabla_{\xi} \cdot (\underline{\underline{F}} \underline{\underline{\hat{\Sigma}}}) = -\hat{\rho}_0 g \mathbf{e}_3 + J \hat{\mathbf{S}}. \quad (4.9)$$

Constitutive equations. The domain is assumed to be an elastic medium. One can then show (see Dahlen and Tromp, 1998) that the second Piola-Kirchhoff stress tensor is a function only of the strain,

$$\underline{\underline{\hat{\Sigma}}} = \underline{\underline{\hat{\Sigma}}}(\underline{\underline{F}}^t \underline{\underline{F}} - \underline{\underline{I}}). \quad (4.10)$$

System of equations for the nonlinear elasticity. As a summary, the equations read in the reference domain $\hat{\Omega}$

$$\left\{ \begin{array}{l} \hat{\rho}_0 \frac{\partial \hat{\mathbf{U}}}{\partial t} - \nabla_{\xi} \cdot \underline{\underline{\hat{P}}} = -\hat{\rho}_0 g \mathbf{e}_3 + J \hat{\mathbf{S}}, \\ \hat{\rho} J = \hat{\rho}_0, \end{array} \right. \quad (4.11)$$

$$\left\{ \begin{array}{l} \underline{\underline{\hat{P}}} = \underline{\underline{F}} \underline{\underline{\hat{\Sigma}}}, \\ \underline{\underline{\hat{\Sigma}}} = \underline{\underline{\hat{\Sigma}}} \left(\frac{1}{2} (\underline{\underline{F}}^t \underline{\underline{F}} - \underline{\underline{I}}) \right), \end{array} \right. \quad (4.12)$$

$$\left\{ \begin{array}{l} \underline{\underline{\hat{\Sigma}}} = \underline{\underline{\hat{\Sigma}}} \left(\frac{1}{2} (\underline{\underline{F}}^t \underline{\underline{F}} - \underline{\underline{I}}) \right), \end{array} \right. \quad (4.13)$$

with the boundary condition

$$J^{-1} (\underline{\underline{\hat{P}}} \underline{\underline{F}}^T) \cdot \mathbf{n} = 0 \quad \text{on } \hat{\Gamma}. \quad (4.14)$$

The initial conditions for the Lagrangian velocity and the first Piola-Kirchhoff stress tensor are the same as in Eulerian coordinates, namely

$$\hat{\mathbf{U}}(0) = 0, \quad \nabla_{\xi} \cdot \underline{\underline{\hat{P}}}(0) = -\hat{\rho}_0 g \mathbf{e}_3.$$

Notations. In the remaining of this chapter, the equations will always be given in Lagrangian coordinates. For simplicity, the notation \hat{X} and the index ξ in the operator ∇_{ξ} are dropped and the coordinates are denoted $\mathbf{x} = (x, y, z)$.

4.2.3 Linearization around the equilibrium state

The linearization is done around the initial state, which is assumed to be at equilibrium. We also choose this initial state to be the reference state, then it holds $\phi(\mathbf{x}, 0) = \mathbf{I}$.

The equilibrium state. In the equilibrium state, it holds $\phi(\mathbf{x}, 0) = \mathbf{I}$, hence there is no displacement and no deformation. The domain is assumed to be prestressed. The prestress, denoted $\underline{\underline{\Sigma}}_0$ is defined by $\underline{\underline{\Sigma}}_0 = \underline{\underline{\Sigma}}(0)$ the prestress. The momentum equation for the equilibrium state with no source term \mathbf{S} yields the following equation satisfied by the prestress,

$$\nabla \cdot \underline{\underline{\Sigma}}_0 = -\rho_0 g \mathbf{e}_z. \quad (4.16)$$

The boundary condition yields

$$\underline{\underline{\Sigma}}_0 \cdot \mathbf{n} = 0. \quad (4.17)$$

Since there is no deformation, the two Piola-Kirchhoff stress tensors coincide: $\underline{\underline{\Sigma}}_0 = \underline{\underline{P}}_0$, hence $\underline{\underline{P}}_0$ is symmetric. In the following, we assume that the stress tensor $\underline{\underline{\Sigma}}$ derives from a potential $\underline{W}(\underline{F}, \underline{\underline{\Sigma}}_0)$, depending on the deformation \underline{F} and on the prestress $\underline{\underline{\Sigma}}_0$. This assumption differs from the classical linear elasticity, where no prestress is generally assumed.

Linearization. The linearization corresponds to the following asymptotic expansion,

$$\mathbf{d} = \delta \mathbf{d}_1 + \mathcal{O}(\delta^2), \quad \rho = \rho_0 + \delta \rho_1 + \mathcal{O}(\delta^2), \quad (4.18)$$

$$\underline{\underline{\Sigma}} = \underline{\underline{\Sigma}}_0 + \delta \underline{\underline{\Sigma}}_1 + \mathcal{O}(\delta^2), \quad \underline{\underline{P}} = \underline{\underline{P}}_0 + \delta \underline{\underline{P}}_1 + \mathcal{O}(\delta^2). \quad (4.19)$$

From those expansions one deduces the following expansions for the other variables,

$$\mathbf{U} = \delta \mathbf{U}_1 + \mathcal{O}(\delta^2), \quad F = \mathbf{I} + \delta \nabla \mathbf{d}_1 + \mathcal{O}(\delta^2), \quad J = 1 + \delta \nabla \cdot \mathbf{d}_1 + \mathcal{O}(\delta^2). \quad (4.20)$$

The linearization of the relation (4.7) yields a relation between the two Piola-Kirchhoff stress tensors,

$$\underline{\underline{P}}_1 = \underline{\underline{\Sigma}}_1 + \nabla \mathbf{d}_1 \underline{\underline{\Sigma}}_0. \quad (4.21)$$

The stress tensor linearization is more complex and makes appear a fourth-order tensor (Dahlen and Tromp, 1998). Using the assumption that $\underline{\underline{\Sigma}}$ derives from a potential $\underline{W}(\underline{F}, \underline{\underline{P}}_0)$, the linearization of the stress tensor reads

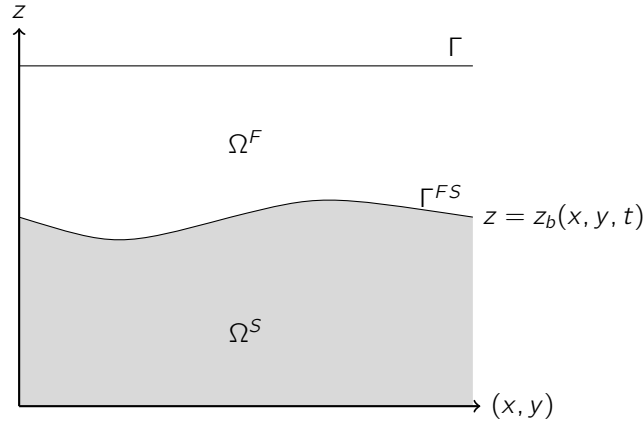
$$\underline{\underline{\Sigma}} = \underline{\underline{\Sigma}}_0 + \delta \underline{\underline{\mathbf{A}}} : \underline{\underline{\varepsilon}}(\mathbf{d}_1) + \mathcal{O}(\delta^2),$$

where $\underline{\underline{\varepsilon}}(\mathbf{d}_1) = \frac{1}{2}(\nabla \mathbf{d}_1 + (\nabla \mathbf{d}_1)^\dagger)$ is the linearized strain tensor, and $\underline{\underline{\mathbf{A}}}$ is a fourth-order tensor acting on $\underline{\underline{\varepsilon}}$. Using the relation (4.21) we have

$$\underline{\underline{\Sigma}}_1 = \underline{\underline{\mathbf{A}}} : \underline{\underline{\varepsilon}}, \quad \underline{\underline{P}}_1 = \underline{\underline{\mathbf{A}}} : \underline{\underline{\varepsilon}} + \nabla \mathbf{d}_1 \underline{\underline{P}}_0. \quad (4.22)$$

The linear elasticity assumption. The expression of the fourth-order tensor $\underline{\underline{\mathbf{A}}}$ depends on the choice of the dependency $\underline{W}(F, \underline{\underline{P}}_0)$, see e.g. Shams et al. (2011). We follow here the choices made by Dahlen and Tromp (1998). The Earth is assumed to be an elastic medium with a pre-stress, and the first-order stress $\underline{\underline{\Sigma}}_1$ is taken as the superposition of an initial stress $\underline{\underline{\Sigma}}_0$ and an elastic response represented by an elastic stress tensor $\underline{\underline{\Gamma}}$,

$$(\underline{\underline{\mathbf{A}}} : \underline{\underline{\varepsilon}})_{ij} = \underline{\underline{\Gamma}}_{ij} + \frac{1}{2} \sum_{k,l} (P_{ij} \delta_{kl} + P_{kl} \delta_{ij} - P_{ik} \delta_{jl} - P_{jk} \delta_{il} - P_{il} \delta_{jk} - P_{jl} \delta_{ik}) \varepsilon_{kl}, \quad (4.23)$$

Figure 4.2: The domain Ω with a fluid layer Ω^F and a solid layer Ω^S .

where P_{ij} is the (i, j) -th component of $\underline{\underline{P}}_0$, and the fourth-order elastic stress tensor $\underline{\underline{\Gamma}}$ has the classical expression

$$\underline{\underline{\Gamma}} : \underline{\underline{\varepsilon}} = \lambda(\text{tr}\underline{\underline{\varepsilon}})\underline{\underline{I}} + 2\mu\underline{\underline{\varepsilon}}. \quad (4.24)$$

Using the fact that $\underline{\underline{P}}_0$ and $\underline{\underline{\varepsilon}}$ are symmetric, after computations it holds

$$\underline{\underline{\mathbf{A}}} : \underline{\underline{\varepsilon}} = \lambda(\text{tr}\underline{\underline{\varepsilon}})\underline{\underline{I}} + 2\mu\underline{\underline{\varepsilon}} + \frac{1}{2}(\text{tr}(\underline{\underline{\varepsilon}})\underline{\underline{P}}_0 + (\underline{\underline{P}}_0 : \underline{\underline{\varepsilon}})\underline{\underline{I}}) - (\underline{\underline{P}}_0\underline{\underline{\varepsilon}} + \underline{\underline{\varepsilon}}\underline{\underline{P}}_0) \quad (4.25)$$

The first-order system of equations. Replacing all the variables by their ansatz and collecting the terms in δ^1 yields the system for the first-order corrections in Ω ,

$$\begin{cases} \rho_0 \frac{\partial \mathbf{U}_1}{\partial t} - \nabla \cdot \underline{\underline{P}}_1 = \mathbf{S}, & (4.26) \\ \underline{\underline{P}}_1 = \underline{\underline{\mathbf{A}}} : \underline{\underline{\varepsilon}} + \nabla \mathbf{d}_1 \underline{\underline{P}}_0, & (4.27) \end{cases}$$

with the boundary conditions on Γ

$$\underline{\underline{P}}_1 \cdot \mathbf{n} = 0, \quad \text{on } \Gamma. \quad (4.28)$$

and the initial conditions

$$\mathbf{U}_1(0) = 0, \quad \underline{\underline{P}}_1(0) = 0, \quad \text{in } \Omega. \quad (4.29)$$

4.2.4 The linear equations for the fluid-solid system

The system (4.26)-(4.29) is adapted to the case where the domain is composed of a fluid layer and a solid layer. We consider a domain Ω composed of a fluid layer Ω^F and a semi-infinite solid layer Ω^S , see Figure 4.2. The surface of the fluid domain is denoted Γ and the interface between the fluid and solid domains is denoted Γ^{FS} . In the following, for every quantity X defined on Ω , its restriction to Ω^F respectively Ω^S will be denoted X^F respectively X^S . Finally, we denote the indicator functions of the fluid domain and the solid domain respectively by χ_S and χ_F .

We aim to an earth-ocean model only in the area near the ocean bottom. For this reason, the solid is assumed to be of homogeneous density. In the water, we have $\mu = 0$, $\lambda = \rho_0 c_0^2$, and the

static stress tensor has the form $\underline{\underline{P}}_0^F = -\rho_0 \underline{\underline{I}}$. From Equation (4.25), the fourth order stress tensor reads then in Ω^F :

$$\underline{\underline{A}} : \underline{\underline{\varepsilon}} = \rho_0 c_0^2 \nabla \cdot \underline{\underline{\mathbf{d}}_1} - \rho_0 (\nabla \cdot \underline{\underline{\mathbf{d}}_1} - 2\underline{\underline{\varepsilon}}), \quad (4.30)$$

hence $\underline{\underline{P}}_1$ reads in Ω^F :

$$\underline{\underline{P}}_1 = \rho_0 c_0^2 \nabla \cdot \underline{\underline{\mathbf{d}}_1} - \rho_0 (\nabla \cdot \underline{\underline{\mathbf{d}}_1} - \nabla \underline{\underline{\mathbf{d}}_1}^t). \quad (4.31)$$

The system (4.26)-(4.27), formulated with the velocity $\underline{\underline{\mathbf{U}}}_1$ and $\partial_t \underline{\underline{P}}_1$, reads

$$\begin{cases} \frac{\partial \underline{\underline{\mathbf{U}}}_1}{\partial t} - \rho_0^{-1} \nabla \cdot \underline{\underline{P}}_1 = \rho_0^{-1} \underline{\underline{\mathbf{S}}} & \text{in } \Omega, \quad (4.32) \\ \partial_t \underline{\underline{P}}_1 = (\rho_0 c_0^2 \nabla \cdot \underline{\underline{\mathbf{U}}}_1 - \rho_0 (\nabla \cdot \underline{\underline{\mathbf{U}}}_1 - \nabla \underline{\underline{\mathbf{U}}}_1^t)) \chi_F + (\underline{\underline{A}} : \underline{\underline{\varepsilon}}(\underline{\underline{\mathbf{U}}}_1) + \nabla \underline{\underline{\mathbf{U}}}_1 \underline{\underline{P}}_0) \chi_S & \text{in } \Omega, \quad (4.33) \end{cases}$$

Differentiating once (4.32) yields the following second-order equation,

$$\frac{\partial^2 \underline{\underline{\mathbf{U}}}_1}{\partial t^2} - \rho_0^{-1} \nabla \cdot (\partial_t \underline{\underline{P}}_1) = \rho_0^{-1} \partial_t \underline{\underline{\mathbf{S}}}. \quad (4.34)$$

We recall the boundary condition

$$\partial_t \underline{\underline{P}}_1 \cdot \underline{\underline{\mathbf{n}}} = 0 \quad \text{on } \Gamma, \quad (4.35)$$

and the initial condition

$$\underline{\underline{\mathbf{U}}}_1(0) = 0, \quad \text{in } \Omega. \quad (4.36)$$

For conciseness, we keep the expression $\partial_t \underline{\underline{P}}_1$ but it should be noted that $\partial_t \underline{\underline{P}}_1$ can be replaced by an expression in $\underline{\underline{\mathbf{U}}}_1$ using Equation (4.33). To simplify the notations, we define

$$\underline{\underline{\mathbf{f}}} = \rho_0^{-1} \partial_t \underline{\underline{\mathbf{S}}}. \quad (4.37)$$

The system (4.34) with the boundary and initial conditions (4.35), (4.36) is a fully-coupled model for the propagation for tsunami, hydro-acoustic waves and seismic waves.

Remark 4.1. *Transmissions conditions between the fluid and the solid are derived from the above equations, even if they will not be used in the remaining of this chapter. We denote by $\underline{\underline{\mathbf{n}}}^{FS}$ the unit vector normal to the fluid-solid interface. From Equation (4.34), only the divergence of $\underline{\underline{P}}_1$ should be well-defined, hence the continuity of the traction $\underline{\underline{P}}_1 \cdot \underline{\underline{\mathbf{n}}}$ is expected.*

For the velocity $\underline{\underline{\mathbf{U}}}_1$, the minimal regularity in space is less clear, we cannot deduce the transmission condition yet. In the case of two solid layers, the transmission condition would be the continuity of all components of $\underline{\underline{\mathbf{U}}}$. Usually, for fluids, only the divergence of $\underline{\underline{\mathbf{U}}}$ is well defined. Then the continuity would be imposed on the normal velocity $\underline{\underline{\mathbf{U}}} \cdot \underline{\underline{\mathbf{n}}}$ only. In our case, the required regularity for the velocity will be given later.

4.3 Mathematical analysis

In this section, we focus on the mathematical analysis of the model. A first variational formulation for the problem (4.44) is obtained. This first formulation, written with a bilinear form \tilde{a} , will be used for the numerical approximation, but we show that it is not suited for the mathematical analysis. We show then that the bilinear form \tilde{a} is equal – for smooth functions – to a second bilinear form denoted a , and that a is coercive in a larger functional space.

Functional spaces. We start by introducing the necessary functional spaces. We introduce the space of H^1 -functions,

$$H^1(\Omega) = \{\varphi \in L^2(\Omega) \mid \nabla \varphi \in L^2(\Omega)\}. \quad (4.38)$$

By abuse of notation we say that a vector function \mathbf{U} or a tensor \underline{T} are in $H^1(\Omega)$ if all their components are in $H^1(\Omega)$. We also define the space of vector field whose divergence is squared integrable,

$$H(\text{div}, \Omega) = \{\mathbf{U} \in L^2(\Omega)^3 \mid \nabla \cdot \mathbf{U} \in L^2(\Omega)\}, \quad (4.39)$$

and the space of tensor fields whose divergence is squared integrable,

$$H(\mathbf{div}, \Omega) = \{\underline{T} \in L^2(\Omega)^{3 \times 3} \mid \nabla \cdot \underline{T} \in L^2(\Omega)^3\}. \quad (4.40)$$

The spaces $H^1(\Omega)$, $H(\text{div}, \Omega)$ and $H(\mathbf{div}, \Omega)$ are equipped with their usual scalar products. The usual normal trace operators are defined on $H(\text{div}, \Omega)$ and $H(\mathbf{div}, \Omega)$; for the sake of conciseness, the normal trace of a function \mathbf{U} is denoted by $\mathbf{U} \cdot \mathbf{n}$ and the duality brackets are written as boundary integrals. We denote by \mathcal{H} the Hilbert space $\mathcal{H} = L^2(\Omega)^3$, equipped with the following weighted scalar product,

$$(\mathbf{U}, \tilde{\mathbf{U}})_{\mathcal{H}} = \int_{\Omega} \rho_0 \mathbf{U} \cdot \tilde{\mathbf{U}} \, dx. \quad (4.41)$$

4.3.1 A first variational formulation

We assume that \mathbf{U}_1 , \underline{P}_1 are smooth functions in time, and we make the following regularity assumption:

$$\mathbf{U}_1 : [0, T] \rightarrow H^1(\Omega), \quad \text{and} \quad \underline{P}_1 : [0, T] \rightarrow H(\mathbf{div}, \Omega),$$

This implies in particular that the normal trace of \underline{P}_1 is well-defined, so that the boundary condition (4.35) has a meaning. As we will show later, the assumption $\mathbf{U}(t) \in H^1(\Omega)$ is too strong, but we keep it for now to obtain the first variational formulation. The equation (4.34) is multiplied by a test function $\tilde{\mathbf{U}}$ regular enough,

$$\frac{d^2}{dt^2}(\mathbf{U}_1, \tilde{\mathbf{U}})_{\mathcal{H}} - \int_{\Omega} [\nabla \cdot (\partial_t \underline{P}_1)] \cdot \tilde{\mathbf{U}} \, dx = (\mathbf{f}, \tilde{\mathbf{U}})_{\mathcal{H}}. \quad (4.42)$$

The second integral on the left-hand side is integrated by parts,

$$\frac{d^2}{dt^2}(\mathbf{U}_1, \tilde{\mathbf{U}})_{\mathcal{H}} + \int_{\Omega} (\partial_t \underline{P}_1) : \nabla \tilde{\mathbf{U}} \, dx - \int_{\Gamma} (\partial_t \underline{P}_1 \cdot \mathbf{n}) \cdot \tilde{\mathbf{U}} \, ds = (\mathbf{f}, \tilde{\mathbf{U}})_{\mathcal{H}}. \quad (4.43)$$

With the stress-free condition (4.35) at the surface, the boundary term vanish. Then $\partial_t \underline{P}_1$ is replaced by its expression (4.33), and we obtain the variational formulation: Find $\mathbf{U}_1(t) \in \tilde{H}^1(\Omega)$ such that

$$\frac{d^2}{dt^2}(\mathbf{U}_1, \tilde{\mathbf{U}})_{\mathcal{H}} + \tilde{a}(\mathbf{U}_1, \tilde{\mathbf{U}}) = (\mathbf{f}, \tilde{\mathbf{U}})_{\mathcal{H}} \quad \forall \tilde{\mathbf{U}} \in H^1(\Omega), \quad (4.44)$$

where \tilde{a} is the bilinear form defined by $\tilde{a} : H^1(\Omega) \times H^1(\Omega) \rightarrow \mathbb{R}$ and

$$\begin{aligned} \tilde{a}(\mathbf{U}, \tilde{\mathbf{U}}) = & \int_{\Omega^F} (\rho_0 c_0^2 - p_0) \nabla \cdot \mathbf{U} \nabla \cdot \tilde{\mathbf{U}} \, dx + \int_{\Omega^F} p_0 \nabla \mathbf{U}^t : \nabla \tilde{\mathbf{U}} \, dx \\ & + \int_{\Omega^S} (\underline{\mathbf{A}} : \underline{\underline{\varepsilon}}(\mathbf{U}) + \nabla \mathbf{U} \underline{P}_0) : \nabla \tilde{\mathbf{U}} \, dx. \end{aligned} \quad (4.45)$$

In the next section, we show the technical difficulties related to the analysis of the formulation (4.44). We derive then a formally equivalent second variational formulation, written with a second bilinear form a , and we prove that this second formulation is well-posed in an adequate functional space. By formally equivalent, we mean that $a(\mathbf{U}, \tilde{\mathbf{U}}) = \tilde{a}(\mathbf{U}, \tilde{\mathbf{U}})$ for functions in $H^1(\Omega)$, where the equality is obtained by algebraic computations and integrations by parts. Since the formulation (4.44) has a simpler expression, it will be used for the numerical approximation in Section 4.4.

Limitation of the first variational formulation. In the expression (4.45), the first integral over the fluid domain is written with $\nabla \cdot \mathbf{U} \nabla \cdot \tilde{\mathbf{U}}$, which is coercive in $H(\mathbf{div}, \Omega) \times H(\mathbf{div}, \Omega)$. However, the second integral is written with an unusual term for linear elasticity problems, namely $\rho_0 \nabla \mathbf{U}^t : \nabla \tilde{\mathbf{U}}$. This term can be written differently to make more classical operators appear,

$$\nabla \mathbf{U}^t : \nabla \tilde{\mathbf{U}} = 2 \underline{\underline{\varepsilon}}(\mathbf{U}_1) : \underline{\underline{\varepsilon}}(\tilde{\mathbf{U}}) - \nabla \mathbf{U} : \nabla \tilde{\mathbf{U}}. \quad (4.46)$$

From the Korn inequality (see e.g. Duvaut and Lions, 1976), it holds for some scalar C_K independent of \mathbf{U}

$$\|\underline{\underline{\varepsilon}}(\mathbf{U})\|_{L^2(\Omega)}^2 + \|\mathbf{U}\|_{L^2(\Omega)}^2 \geq C_K \|\mathbf{U}\|_{H^1(\Omega)}. \quad (4.47)$$

Without more informations on C_K , we cannot conclude on the existence of a lower bound of the form

$$\nabla \mathbf{U}^t : \nabla \mathbf{U} + \lambda \|\mathbf{U}\|_{\mathcal{H}}^2 \geq C \|\mathbf{U}\|_{H^1(\Omega)}, \quad (4.48)$$

which is needed to prove the existence and uniqueness of solution to (4.44). To our knowledge, even the sign of $\nabla \mathbf{U}^t : \nabla \mathbf{U}$ is not clear. Moreover, the form $\nabla \mathbf{U}^t : \nabla \tilde{\mathbf{U}}$ is continuous in $H^1 \times H^1$, but not in a larger space.

4.3.2 The modified variational formulation

In this section, we aim to write a second variational formulation, which will allow us to show the well-posedness of the problem. We recall first the strong formulation (4.34),

$$\frac{\partial^2 \mathbf{U}_1}{\partial t^2} - \rho_0^{-1} \nabla \cdot (\partial_t \underline{\underline{P}}_1) = \mathbf{f}. \quad (4.49)$$

Testing against a function $\tilde{\mathbf{U}}$ with enough regularity yields

$$\frac{d^2}{dt^2} (\mathbf{U}_1, \tilde{\mathbf{U}})_{\mathcal{H}} + \int_{\Omega} -[\nabla \cdot (\partial_t \underline{\underline{P}}_1)] \cdot \tilde{\mathbf{U}} \, dx = (\mathbf{f}, \tilde{\mathbf{U}})_{\mathcal{H}}. \quad (4.50)$$

As presented in Section 4.3.1, the term $\rho_0 \nabla \mathbf{U}^t : \nabla \mathbf{U}$ is continuous in $H^1(\Omega) \times H^1(\Omega)$, which is not consistent for the fluid domain, and it has an undefined sign. To avoid this term, the idea is to compute differently some terms in the fluid domain. We present first the idea for a domain with only a fluid layer, and show then how the method is extended to the case of a fluid-solid domain.

In a fluid layer only

Assume for now that the domain is composed of a fluid layer only. The layer spans is an infinite half-plane with surface Γ . In Equation (4.50), we have then for the term in $\partial_t \underline{\underline{P}}_1$:

$$\int_{\Omega} -[\nabla \cdot (\partial_t \underline{\underline{P}}_1)] \cdot \tilde{\mathbf{U}} \, dx = \int_{\Omega} -[\nabla \cdot (\rho_0 c_0^2 \nabla \cdot \mathbf{U}_1 \underline{\underline{I}} - \rho_0 (\nabla \cdot \mathbf{U}_1 \underline{\underline{I}} - \nabla \mathbf{U}_1^t))] \cdot \tilde{\mathbf{U}} \, dx. \quad (4.51)$$

If we distribute the divergence only in the second part of the right-hand side, and use the property

$$\nabla \cdot (\nabla \cdot \underline{\mathbf{X}}_1 - \nabla \mathbf{X}_1^t) = 0, \quad (4.52)$$

we obtain

$$\int_{\Omega} -[\nabla \cdot (\partial_t \underline{P}_1)] \cdot \tilde{\mathbf{U}} \, dx = \int_{\Omega} -[\nabla \cdot (\rho_0 c_0^2 \nabla \cdot \mathbf{U}_1)] \cdot \tilde{\mathbf{U}} \, dx + \int_{\Omega} [(\nabla \cdot \mathbf{U}_1 - \nabla \mathbf{U}_1^t) \nabla \rho_0] \cdot \tilde{\mathbf{U}} \, dx. \quad (4.53)$$

After some computations (see Appendix A), we obtain the following expression,

$$\begin{aligned} \int_{\Omega} -[\nabla \cdot (\partial_t \underline{P}_1)] \cdot \tilde{\mathbf{U}} \, dx &= \int_{\Omega} \rho_0 \left(c_0 \nabla \cdot \mathbf{U}_1 - \frac{g}{c_0} \mathbf{U}_1 \cdot \mathbf{e}_z \right) \left(c_0 \nabla \cdot \tilde{\mathbf{U}} - \frac{g}{c_0} \tilde{\mathbf{U}} \cdot \mathbf{e}_z \right) \, dx \\ &- \int_{\Omega} \rho_0 \left(\frac{\rho'_0}{\rho_0} + \frac{g^2}{c_0^2} \right) \mathbf{U}_1 \cdot \mathbf{e}_z \tilde{\mathbf{U}} \cdot \mathbf{e}_z \, dx + \int_{\Gamma} \rho_0 g \mathbf{U}_1 \cdot \mathbf{e}_z \tilde{\mathbf{U}} \cdot \mathbf{e}_z \, ds - \int_{\Gamma} \rho_0 c_0^2 \nabla \cdot \mathbf{U}_1 \tilde{\mathbf{U}} \cdot \mathbf{e}_z \, ds. \end{aligned} \quad (4.54)$$

The surface condition (4.35) with the condition $\rho_0 = 0$ on Γ imply that $\nabla \cdot \mathbf{U}_1 = 0$ on Γ , hence the last boundary term vanish. It is then possible to rewrite (4.50) as

$$\frac{d^2}{dt^2} (\mathbf{U}_1, \tilde{\mathbf{U}})_{\mathcal{H}} + a_F(\mathbf{U}_1, \tilde{\mathbf{U}}) = (\mathbf{f}, \tilde{\mathbf{U}})_{\mathcal{H}}, \quad (4.55)$$

where a_F is the following bilinear form,

$$\begin{aligned} a_F(\mathbf{U}, \tilde{\mathbf{U}}) &= \int_{\Omega} \rho_0 \left(c_0 \nabla \cdot \mathbf{U} - \frac{g}{c_0} \mathbf{U} \cdot \mathbf{e}_z \right) \left(c_0 \nabla \cdot \tilde{\mathbf{U}} - \frac{g}{c_0} \tilde{\mathbf{U}} \cdot \mathbf{e}_z \right) \, dx + \int_{\Omega} \rho_0 N^2 \mathbf{U} \cdot \mathbf{e}_z \tilde{\mathbf{U}} \cdot \mathbf{e}_z \, dx \\ &+ \int_{\Gamma} \rho_0 g \mathbf{U} \cdot \mathbf{e}_z \tilde{\mathbf{U}} \cdot \mathbf{e}_z \, dx, \end{aligned} \quad (4.56)$$

with $N^2 = -(g\rho'_0/\rho_0 + g^2/c_0^2)$. The scalar N^2 is assumed positive (see the discussion in Chapters 2 and 3). We recognize the weak formulation of the model developed in Chapter 2.

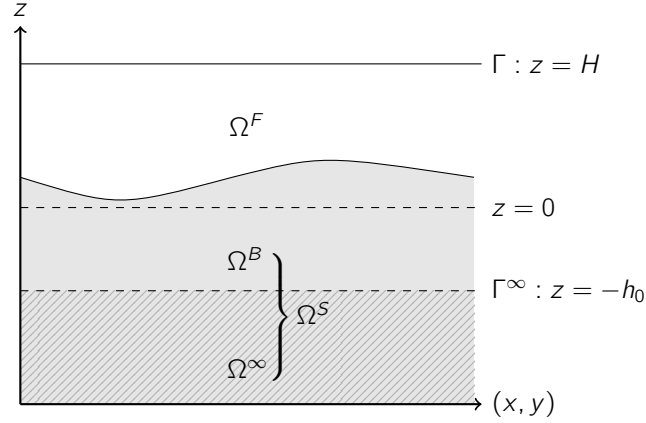
Now, if the domain is composed of a fluid and a solid region, the constitutive law is discontinuous. Applying the divergence in the first step of the computations would then yield boundary terms, whose symmetry and positivity are not clear. To extend the integral over Ω^F to an integral over Ω , we introduce continuous extensions of the background density and pressure.

A continuous extension of the background density and pressure.

To use the method described above in the case of a fluid-solid domain, we introduce an extension of the pressure. The extension is denoted $\tilde{\rho}_0$; it should be continuous, and we choose it so as to vanish for $z \rightarrow -\infty$. We also introduce an extension of the fluid density, denoted $\tilde{\rho}_0$, so that both extensions satisfy $\nabla \tilde{\rho}_0 = -\tilde{\rho}_0 g \mathbf{e}_z$, as in the fluid domain.

The solid domain Ω^S is decomposed into a vertically bounded region Ω^B and an unbounded region Ω^∞ . The boundary between Ω^B and Ω^∞ , denoted Γ^∞ , corresponds to $z = -h_0$ for some $h_0 > 0$. The decomposition is shown in Figure 4.3. The extensions $\tilde{\rho}_0, \tilde{\rho}_0$ are constructed such that

- $\tilde{\rho}_0$ and $\tilde{\rho}_0$ are continuous in Ω ,
- $\nabla \tilde{\rho}_0 = -\tilde{\rho}_0 g \mathbf{e}_z$ in Ω ,
- $\tilde{\rho}_0 = 0$ and $\tilde{\rho}_0 = 0$ in Ω^∞ ,

Figure 4.3: The decomposition of the domain Ω .

- $\tilde{\rho}_0 = 0, \tilde{p}_0 = 0$ on Γ^∞ .

To satisfy the last condition, the extended pressure is defined by

$$\tilde{p}_0(z) = \int_z^h \tilde{\rho}_0(z') g dz'. \quad (4.57)$$

It remains to define $\tilde{\rho}_0$. Since the fluid density at rest is assumed to depend only on depth, and the topography is defined by a function $z_b \geq 0$, we can see ρ_0^F as a function defined on $[0, H]$. We choose the extension to be affine by parts in Ω^B . In order to satisfy both conditions: $\tilde{\rho}_0 = 0$ and $\tilde{\rho}_0 = 0$ on Γ^∞ , we define $\tilde{\rho}_0$ in four parts:

$$\tilde{\rho}_0 = \begin{cases} \rho_0^F(z), & 0 < z < H, \\ a_1 z + b_1, & -h_0/2 < z < 0, \\ a_2 z + b_2, & -h_0 < z < -h_0/2, \\ 0, & z < -h_0. \end{cases} \quad (4.58)$$

The scalars a_1, a_2, b_1, b_2 depend on h_0 and on ρ_0^F , they are computed in Appendix B. Hence, $\tilde{\rho}_0$ and \tilde{p}_0 are continuous on Ω , and it holds $\nabla \tilde{p}_0 = -\tilde{\rho}_0 g \mathbf{e}_z$ on Ω . Finally, it should be noted that by construction, we have $\tilde{p}_0 \geq 0$. The extension $\tilde{\rho}_0$ and \tilde{p}_0 are shown in Figure 4.4.

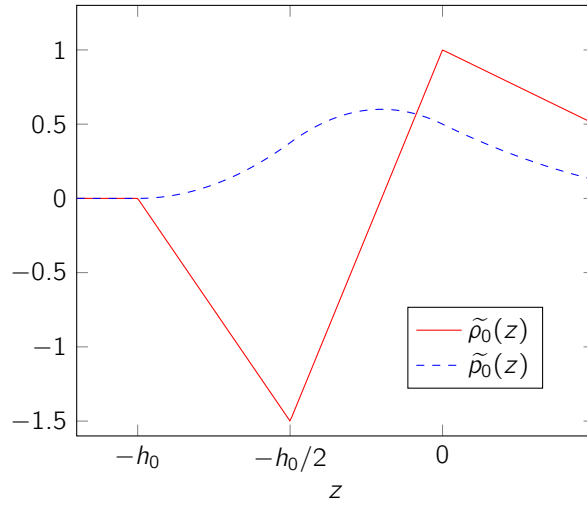
A new expression for the stress tensor

The extended pressure \tilde{p}_0 is used to rewrite the stress tensor \underline{P}_1 . The stress tensor is written

$$\partial_t \underline{P}_1 = \partial_t \underline{P}_1 - \tilde{p}_0 (\nabla \cdot \mathbf{U}_1 \underline{I} - \nabla \mathbf{U}_1^t) \chi_B + \tilde{p}_0 (\nabla \cdot \mathbf{U}_1 \underline{I} - \nabla \mathbf{U}_1^t) \chi_B, \quad (4.59)$$

and using the expression (4.33), it reads

$$\begin{aligned} \partial_t \underline{P}_1 = & (\rho_0 c_0^2 \nabla \cdot \mathbf{U}_1 \underline{I} - \tilde{p}_0 (\nabla \cdot \mathbf{U}_1 \underline{I} - \nabla \mathbf{U}_1^t)) \chi_F + \partial_t \underline{P}_1^S \chi_S \\ & - \tilde{p}_0 (\nabla \cdot \mathbf{U}_1 \underline{I} - \nabla \mathbf{U}_1^t) \chi_B + \tilde{p}_0 (\nabla \cdot \mathbf{U}_1 \underline{I} - \nabla \mathbf{U}_1^t) \chi_B. \end{aligned} \quad (4.60)$$

Figure 4.4: The functions $\tilde{\rho}_0$ and $\tilde{\rho}_0$.

The terms $\tilde{\rho}_0(\nabla \mathbf{U}_1^t - \nabla \cdot \mathbf{U}_1 \underline{l})$ coincide in Ω^F and Ω^B . Using $\tilde{\rho}_0 = 0$ in Ω^∞ , we have

$$\partial_t \underline{P}_1 = (\rho_0 c_0^2 \nabla \cdot \mathbf{U}_1 \underline{l}) \chi_F - \tilde{\rho}_0 (\nabla \cdot \mathbf{U}_1 \underline{l} - \nabla \mathbf{U}_1^t) + (\partial_t \underline{P}_1^S + \tilde{\rho}_0 (\nabla \cdot \mathbf{U}_1 \underline{l} - \nabla \mathbf{U}_1^t)) \chi_S. \quad (4.61)$$

To reproduce the situation of a fluid-only domain, the stress tensor \underline{P}_1^S is decomposed as follows,

$$\underline{P}_1^S = \tilde{\underline{P}}_1^S + \tilde{\rho}_0 \tilde{c}_0^2 \text{tr}(\underline{\underline{\varepsilon}}(\mathbf{U}_1)) \underline{l}, \quad (4.62)$$

where \tilde{c}_0 is some extension to Ω of the sound speed c_0 . The extension can be discontinuous, but it should remain strictly positive. It holds then

$$\partial_t \underline{P}_1 = \tilde{\rho}_0 \tilde{c}_0^2 \nabla \cdot \mathbf{U}_1 \underline{l} - \tilde{\rho}_0 (\nabla \cdot \mathbf{U}_1 \underline{l} - \nabla \mathbf{U}_1^t) + \left(\partial_t \tilde{\underline{P}}_1^S + \tilde{\rho}_0 (\nabla \cdot \mathbf{U}_1 \underline{l} - \nabla \mathbf{U}_1^t) \right) \chi_S. \quad (4.63)$$

In this new expression for the stress tensor, the two first terms are defined on the whole domain, and we can reproduce the computations (4.51)-(4.54) described above. However, there is now the additional term $\tilde{\rho}_0 \nabla \mathbf{U}^t$ in Ω^S ; it seems that the difficulty is merely shifted from the fluid to the solid region. Here the important thing to note is that, contrarily to Ω^F , the constitutive law in Ω^S will make it possible to control the additional pressure.

The modified variational formulation.

With the new expression (4.63) for the stress tensor, we derive a variational formulation for the system (4.49). To write the second variational formulation, we introduce the following bilinear form a ,

$$a(\mathbf{U}, \tilde{\mathbf{U}}) = a_\Omega(\mathbf{U}, \tilde{\mathbf{U}}) + a_S(\mathbf{U}, \tilde{\mathbf{U}}), \quad (4.64)$$

where a_Ω is defined by

$$a_\Omega(\mathbf{U}, \tilde{\mathbf{U}}) = \int_\Omega \tilde{\rho}_0 \left(\tilde{c}_0 \nabla \cdot \mathbf{U} - \frac{g}{c_0} \mathbf{U} \cdot \mathbf{e}_z \right) \left(\tilde{c}_0 \nabla \cdot \tilde{\mathbf{U}} - \frac{g}{c_0} \tilde{\mathbf{U}} \cdot \mathbf{e}_z \right) dx + \int_\Omega \tilde{\rho}_0 \tilde{N}_b \mathbf{U} \cdot \mathbf{e}_z \tilde{\mathbf{U}} \cdot \mathbf{e}_z dx + \int_\Gamma \tilde{\rho}_0 g \mathbf{U} \cdot \mathbf{e}_z \tilde{\mathbf{U}} \cdot \mathbf{e}_z dx, \quad (4.65)$$

with $\tilde{N}_b = -(g\tilde{\rho}_0'/\tilde{\rho}_0 + g^2/\tilde{c}_0^2)$, and where a_S is defined by

$$a_S(\mathbf{U}, \tilde{\mathbf{U}}) = \int_{\Omega^S} \left(\tilde{\underline{\mathbf{A}}} : \underline{\underline{\varepsilon}}(\mathbf{U}_1) + \nabla \mathbf{U} \underline{\underline{P}}_0 - \tilde{\rho}_0(\nabla \mathbf{U}^t - \nabla \cdot \mathbf{U} \underline{\underline{I}}) \right) : \nabla \tilde{\mathbf{U}} \, dx. \quad (4.66)$$

The following equality holds,

Theorem 4.1. *For functions $\mathbf{U}, \tilde{\mathbf{U}} \in H^1(\Omega)$, it holds*

$$\tilde{a}(\mathbf{U}, \tilde{\mathbf{U}}) = a(\mathbf{U}, \tilde{\mathbf{U}}). \quad (4.67)$$

Proof. First note that when replacing in Equation (4.63) the tensors $\underline{\underline{P}}_1$ and $\tilde{\underline{\underline{P}}}_1^S$ with the expression (4.33), the equality (4.63) can be understood as an equality for functions $\mathbf{U} \in H^1(\Omega)$:

$$\begin{aligned} & (\rho_0 c_0^2 \nabla \cdot \mathbf{U} - \rho_0(\nabla \cdot \mathbf{U} \underline{\underline{I}} - \nabla \mathbf{U}^t)) \chi_F + (\underline{\underline{\mathbf{A}}} : \underline{\underline{\varepsilon}}(\mathbf{U}) + \nabla \mathbf{U} \underline{\underline{P}}_0) \chi_S \\ &= \tilde{\rho}_0 \tilde{c}_0^2 \nabla \cdot \mathbf{U} \underline{\underline{I}} - \tilde{\rho}_0(\nabla \cdot \mathbf{U} \underline{\underline{I}} - \nabla \mathbf{U}^t) + \left(\tilde{\underline{\underline{\mathbf{A}}}} : \underline{\underline{\varepsilon}}(\mathbf{U}) + \nabla \mathbf{U}_1 \underline{\underline{P}}_0 + \tilde{\rho}_0(\nabla \cdot \mathbf{U} \underline{\underline{I}} - \nabla \mathbf{U}^t) \right) \chi_S, \end{aligned} \quad (4.68)$$

with $\tilde{\underline{\underline{\mathbf{A}}}} = \underline{\underline{\mathbf{A}}} - \tilde{\rho}_0 \tilde{c}_0^2 \operatorname{tr} \underline{\underline{I}}$.

To show the equality, we start with Equation (4.45). For functions $\mathbf{U}, \tilde{\mathbf{U}}$ in $C^\infty(\Omega)$ with compact support in Ω , integration by parts yields

$$\begin{aligned} \tilde{a}(\mathbf{U}, \tilde{\mathbf{U}}) &= - \int_{\Omega} \left[\nabla \cdot ((\rho_0 c_0^2 \nabla \cdot \mathbf{U} \underline{\underline{I}} + \rho_0(\nabla \mathbf{U}^t - \nabla \cdot \mathbf{U} \underline{\underline{I}})) \chi_F + (\underline{\underline{\mathbf{A}}} : \underline{\underline{\varepsilon}}(\mathbf{U}) + \nabla \mathbf{U} \underline{\underline{P}}_0) \chi_S) \right] \cdot \tilde{\mathbf{U}} \, dx \\ &\quad + \int_{\Gamma} [(\rho_0 c_0^2 \nabla \cdot \mathbf{U} \underline{\underline{I}} + \rho_0(\nabla \mathbf{U}^t - \nabla \cdot \mathbf{U} \underline{\underline{I}}) \cdot \mathbf{n}) \cdot \tilde{\mathbf{U}}] \, ds. \end{aligned} \quad (4.69)$$

We use the fact that $\rho_0 = 0$ on Γ , and the equality (4.68). It holds then

$$\begin{aligned} \tilde{a}(\mathbf{U}, \tilde{\mathbf{U}}) &= \underbrace{\int_{\Omega} \left[\nabla \cdot (\tilde{\rho}_0 \tilde{c}_0^2 \nabla \cdot \mathbf{U} \underline{\underline{I}} - \tilde{\rho}_0(\nabla \cdot \mathbf{U} \underline{\underline{I}} - \nabla \mathbf{U}^t)) \right] \cdot \tilde{\mathbf{U}} \, ds}_{(I_1)} + \int_{\Gamma} \rho_0 c_0^2 \nabla \cdot \mathbf{U} \mathbf{n} \cdot \tilde{\mathbf{U}} \, ds \\ &\quad + \underbrace{\int_{\Omega} \left[\nabla \cdot \left((\tilde{\underline{\underline{\mathbf{A}}}} : \underline{\underline{\varepsilon}}(\mathbf{U}) + \nabla \mathbf{U} \underline{\underline{P}}_0 + \tilde{\rho}_0(\nabla \cdot \mathbf{U} \underline{\underline{I}} - \nabla \mathbf{U}^t)) \chi_S \right) \right] \cdot \tilde{\mathbf{U}} \, dx}_{(I_2)}. \end{aligned} \quad (4.70)$$

The first integral is computed as in Equations (4.51)-(4.54), and we have

$$\begin{aligned} (I_1) &= \int_{\Omega} \tilde{\rho}_0 \left(\tilde{c}_0 \nabla \cdot \mathbf{U} - \frac{g}{\tilde{c}_0} \mathbf{U} \cdot \mathbf{e}_z \right) \left(\tilde{c}_0 \nabla \cdot \tilde{\mathbf{U}} - \frac{g}{\tilde{c}_0} \tilde{\mathbf{U}} \cdot \mathbf{e}_z \right) \, dx \\ &\quad - \int_{\Omega} \tilde{\rho}_0 \left(\frac{\tilde{\rho}_0'}{\tilde{\rho}_0} + \frac{g^2}{\tilde{c}_0^2} \right) \mathbf{U} \cdot \mathbf{e}_z \tilde{\mathbf{U}} \cdot \mathbf{e}_z \, dx + \int_{\Gamma} \tilde{\rho}_0 g \mathbf{U} \cdot \mathbf{e}_z \tilde{\mathbf{U}} \cdot \mathbf{e}_z \, ds - \int_{\Gamma} \tilde{\rho}_0 \tilde{c}_0^2 \nabla \cdot \mathbf{U} \tilde{\mathbf{U}} \cdot \mathbf{e}_z \, ds. \end{aligned} \quad (4.71)$$

The second integral is integrated by parts. Because of the indicator function χ_S , the boundary term vanishes, yielding

$$(I_2) = - \int_{\Omega^S} \left(\tilde{\underline{\underline{\mathbf{A}}}} : \underline{\underline{\varepsilon}}(\mathbf{U}) + \nabla \mathbf{U}_1 \underline{\underline{P}}_0 + \tilde{\rho}_0(\nabla \cdot \mathbf{U} \underline{\underline{I}} - \nabla \mathbf{U}^t) \right) : \nabla \cdot \tilde{\mathbf{U}} \, dx. \quad (4.72)$$

On the surface Γ , we have $\tilde{\rho}_0 = \rho_0$ and $\tilde{c}_0 = c_0$, hence some boundary terms cancel out. Gathering all the terms yields then

$$\begin{aligned} \tilde{a}(\mathbf{U}, \tilde{\mathbf{U}}) &= \int_{\Omega} \tilde{\rho}_0 \left(\tilde{c}_0 \nabla \cdot \mathbf{U} - \frac{g}{c_0} \mathbf{U} \cdot \mathbf{e}_z \right) \left(\tilde{c}_0 \nabla \cdot \tilde{\mathbf{U}} - \frac{g}{c_0} \tilde{\mathbf{U}} \cdot \mathbf{e}_z \right) dx \\ &\quad - \int_{\Omega} \tilde{\rho}_0 \left(\frac{\tilde{\rho}_0'}{\tilde{\rho}_0} + \frac{g^2}{\tilde{c}_0^2} \right) \mathbf{U} \cdot \mathbf{e}_z \tilde{\mathbf{U}} \cdot \mathbf{e}_z dx + \int_{\Gamma} \tilde{\rho}_0 g \mathbf{U} \cdot \mathbf{e}_z \tilde{\mathbf{U}} \cdot \mathbf{e}_z ds \\ &\quad - \int_{\Omega^S} \left(\tilde{\mathbf{A}} : \underline{\underline{\varepsilon}}(\mathbf{U}) + \nabla \mathbf{U}_1 \underline{\underline{P}}_0 + \tilde{\rho}_0 (\nabla \cdot \mathbf{U} \underline{\underline{I}} - \nabla \mathbf{U}^t) \right) : \nabla \tilde{\mathbf{U}} dx, \end{aligned} \quad (4.73)$$

and concludes the proof by density. \square

We define now the functional space for the variational formulation. Let $\mathcal{V} \subset \mathcal{H}$ be defined by

$$\mathcal{V} = \{ \mathbf{U} \in H(\operatorname{div}, \Omega), \mid \mathbf{U}|_{\Omega^S} \in H^1(\Omega^S), \mathbf{U} \cdot \mathbf{n} \in L^2(\Gamma) \}. \quad (4.74)$$

We define the following scalar product on \mathcal{V} ,

$$\begin{aligned} (\mathbf{U}, \tilde{\mathbf{U}})_{\mathcal{V}} &= \int_{\Omega^F} \rho_0 \frac{g^2}{c_0^2} \mathbf{U} \cdot \tilde{\mathbf{U}} dx + \int_{\Omega^S} \rho_0^2 \frac{g^2}{\lambda} \mathbf{U} \cdot \tilde{\mathbf{U}} dx + \int_{\Omega^S} \tilde{\rho}_0 \nabla \mathbf{U} : \nabla \tilde{\mathbf{U}} dx \\ &\quad + \int_{\Omega^S} \rho_0 c_0^2 \nabla \cdot \mathbf{U} \nabla \cdot \tilde{\mathbf{U}} dx + \int_{\Omega^F} \lambda \nabla \cdot \mathbf{U} \nabla \cdot \tilde{\mathbf{U}} dx + \int_{\Gamma} \rho_0 g \mathbf{U} \cdot \mathbf{n} \tilde{\mathbf{U}} \cdot \mathbf{n}, \end{aligned} \quad (4.75)$$

The bilinear form (4.64) is well-defined if $\mathbf{U} \in \mathcal{V}$. The variational formulation reads then: Find \mathbf{U}_1 satisfying

$$\mathbf{U}_1 \in C^1([0, T]; \mathcal{H}), \quad \frac{d}{dt} \mathbf{U}_1 \in C^0([0, T]; \mathcal{V}) \quad (4.76)$$

and solution to

$$\frac{d^2}{dt^2} (\mathbf{U}_1, \tilde{\mathbf{U}})_{\mathcal{H}} + a(\mathbf{U}_1, \tilde{\mathbf{U}}) = (\mathbf{f}, \tilde{\mathbf{U}})_{\mathcal{H}}, \quad \forall \tilde{\mathbf{U}} \in \mathcal{V}, \quad \text{in } \mathcal{D}'(0, T), \quad (4.77)$$

with vanishing initial conditions.

Remark 4.2. We can now conclude the remark 4.1: since $\mathbf{U} \in H(\operatorname{div}, \Omega)$, the transmission condition for the velocity is the continuity of the normal velocity $\mathbf{U} \cdot \mathbf{n}^{FS}$.

4.3.3 Mathematical analysis of the modified formulation

The aim of this section is to study the properties of the bilinear form $a : \mathcal{V} \times \mathcal{V} \rightarrow \mathbb{R}$ defined by (4.64)-(4.66). More precisely we will show that, for some $\alpha > 0$, it holds

$$a(\mathbf{U}, \mathbf{U}) + \alpha \|\mathbf{U}\|_{\mathcal{H}}^2 \geq \|\mathbf{U}\|_{\mathcal{V}}^2. \quad (4.78)$$

We start with the following property of a .

Proposition 4.1. The bilinear form $a : \mathcal{V} \times \mathcal{V} \rightarrow \mathbb{R}$ is symmetric.

Proof. The form a_Ω is symmetric, we focus on a_S . With $\nabla \mathbf{U}^t = 2\underline{\underline{\underline{\varepsilon}}}(\mathbf{U}) - \nabla \mathbf{U}$, it holds

$$\begin{aligned} \int_{\Omega^s} \left(\underline{\underline{\underline{\mathbf{A}}}} : \underline{\underline{\underline{\varepsilon}}}(\mathbf{U}) + \nabla \mathbf{U} \underline{\underline{\underline{P}}}_0 - \tilde{\rho}_0 (\nabla \mathbf{U}^t - \nabla \cdot \underline{\underline{\underline{U}}}) \right) : \nabla \tilde{\mathbf{U}} \, dx \\ = \int_{\Omega^s} \left((\underline{\underline{\underline{\mathbf{A}}}} - 2\tilde{\rho}_0 \underline{\underline{\underline{I}}}) : \underline{\underline{\underline{\varepsilon}}}(\mathbf{U}) + \nabla \mathbf{U}_1 (\underline{\underline{\underline{P}}}_0 + \tilde{\rho}_0 \underline{\underline{\underline{I}}}) + \tilde{\rho}_0 \nabla \cdot \underline{\underline{\underline{U}}}) \right) : \nabla \tilde{\mathbf{U}} \, dx. \end{aligned} \quad (4.79)$$

From the expression (4.25) of $\underline{\underline{\underline{\mathbf{A}}}}$, and usual identities for symmetric tensors, we obtain

$$\begin{aligned} (\underline{\underline{\underline{\mathbf{A}}}} : \underline{\underline{\underline{\varepsilon}}}(\mathbf{U})) : \nabla \tilde{\mathbf{U}} &= (\lambda - \tilde{\rho}_0 \tilde{c}_0^2) \nabla \cdot \mathbf{U} \nabla \cdot \tilde{\mathbf{U}} + 2\mu \underline{\underline{\underline{\varepsilon}}}(\mathbf{U}) : \underline{\underline{\underline{\varepsilon}}}(\tilde{\mathbf{U}}) \\ &+ \frac{1}{2} \nabla \cdot \mathbf{U} \underline{\underline{\underline{P}}}_0 : \underline{\underline{\underline{\varepsilon}}}(\tilde{\mathbf{U}}) + \frac{1}{2} \nabla \cdot \tilde{\mathbf{U}} \underline{\underline{\underline{P}}}_0 : \underline{\underline{\underline{\varepsilon}}}(\mathbf{U}) - (\underline{\underline{\underline{P}}}_0 \underline{\underline{\underline{\varepsilon}}}(\mathbf{U}) + \underline{\underline{\underline{\varepsilon}}}(\mathbf{U}) \underline{\underline{\underline{P}}}_0) : \underline{\underline{\underline{\varepsilon}}}(\tilde{\mathbf{U}}). \end{aligned} \quad (4.80)$$

Since $\underline{\underline{\underline{P}}}_0$ is a symmetric tensor, all terms in (4.80) are symmetric. \square

We show now that a is coercive, under some conditions on the parameters.

Proposition 4.2. *For $\|\underline{\underline{\underline{P}}}_0\|_{L^2(\Omega)^{3 \times 3}} / \min(\lambda, \mu)$ sufficiently small, for $\lambda > 0$, and for $\mu > \tilde{\rho}_0$, there exists a scalar α independant of \mathbf{U} such that*

$$a(\mathbf{U}, \mathbf{U}) + \alpha^2 \|\mathbf{U}\|_{\mathcal{H}}^2 \geq \|\mathbf{U}\|_{\mathcal{V}}^2. \quad (4.81)$$

Proof. For $\mathbf{U} \in \mathcal{V}$, the term a_Ω reads

$$\begin{aligned} a_\Omega(\mathbf{U}, \mathbf{U}) &= \int_{\Omega} \tilde{\rho}_0 \left(\tilde{c}_0 \nabla \cdot \mathbf{U} - \frac{g}{\tilde{c}_0} \mathbf{U} \cdot \mathbf{e}_z \right)^2 \, dx + \int_{\Omega} \tilde{\rho}_0 \tilde{N}_b (\mathbf{U} \cdot \mathbf{e}_z)^2 \, dx + \int_{\Gamma} \tilde{\rho}_0 g (\mathbf{U} \cdot \mathbf{e}_z)^2 \, dx \\ &= \int_{\Omega} \tilde{\rho}_0 \tilde{c}_0^2 (\nabla \cdot \mathbf{U})^2 \, dx - 2 \int_{\Omega} \tilde{\rho}_0 g \nabla \cdot \mathbf{U} \mathbf{U} \cdot \mathbf{e}_z \, dx - \int_{\Omega} \tilde{\rho}_0' g (\mathbf{U} \cdot \mathbf{e}_z)^2 \, dx \\ &\quad + \int_{\Gamma} \tilde{\rho}_0 g (\mathbf{U} \cdot \mathbf{e}_z)^2 \, dx. \end{aligned} \quad (4.82)$$

The third term of the right-hand side is a zero-order term that will be controlled by $\alpha^2 \|\mathbf{U}\|_{\mathcal{H}}^2$. For the first two terms, the integrals are decomposed as one part in the fluid domain, and one part in the solid domain.

$$\begin{aligned} \int_{\Omega} \tilde{\rho}_0 \tilde{c}_0^2 (\nabla \cdot \mathbf{U})^2 \, dx - 2 \int_{\Omega} \tilde{\rho}_0 g \nabla \cdot \mathbf{U} \mathbf{U} \cdot \mathbf{e}_z \, dx \\ = \int_{\Omega^F} \rho_0 c_0^2 (\nabla \cdot \mathbf{U})^2 \, dx - 2 \int_{\Omega^F} \rho_0 g \nabla \cdot \mathbf{U} \mathbf{U} \cdot \mathbf{e}_z \, dx \\ \quad + \int_{\Omega^s} \tilde{\rho}_0 \tilde{c}_0^2 (\nabla \cdot \mathbf{U})^2 \, dx - 2 \int_{\Omega^s} \tilde{\rho}_0 g \nabla \cdot \mathbf{U} \mathbf{U} \cdot \mathbf{e}_z \, dx. \end{aligned} \quad (4.83)$$

By the Young inequality, for $\varepsilon > 0$, we have

$$-2 \int_{\Omega^F} \rho_0 g \nabla \cdot \mathbf{U} \mathbf{U} \cdot \mathbf{e}_z \, dx \geq -2 \int_{\Omega^F} \varepsilon \rho_0 c_0^2 |\nabla \cdot \mathbf{U}|^2 \, dx - 2 \int_{\Omega^F} \rho_0 \frac{g^2}{\varepsilon c_0^2} |\mathbf{U} \cdot \mathbf{e}_z|^2 \, dx, \quad (4.84)$$

hence we have, for some $\alpha > 0$,

$$\begin{aligned} a_\Omega(\mathbf{U}, \mathbf{U}) + \alpha \|\mathbf{U}\|_{\mathcal{H}}^2 &\geq \int_{\Omega^F} (\rho_0 c_0^2 - 2\varepsilon \rho_0 c_0^2) (\nabla \cdot \mathbf{U})^2 \, dx + \int_{\Omega^F} \rho_0 \frac{g^2}{c_0^2} \mathbf{U} \cdot \tilde{\mathbf{U}} \, dx + \int_{\Omega^s} \frac{\rho_0^2 g^2}{\lambda} \mathbf{U} \cdot \tilde{\mathbf{U}} \, dx \\ &\quad + \int_{\Gamma} \rho_0 g (\mathbf{U} \cdot \mathbf{e}_z)^2 \, dx + \int_{\Omega^s} \tilde{\rho}_0 \tilde{c}_0^2 (\nabla \cdot \mathbf{U})^2 \, dx - 2 \int_{\Omega^s} \tilde{\rho}_0 g \nabla \cdot \mathbf{U} \mathbf{U} \cdot \mathbf{e}_z \, dx. \end{aligned} \quad (4.85)$$

Note that, by construction, $\tilde{\rho}_0$ is negative in some subdomain of Ω^S .

We recall now the expression (4.66) of a_S .

$$a_S(\mathbf{U}, \mathbf{U}) = \int_{\Omega^S} \left(\tilde{\mathbf{A}} : \underline{\underline{\boldsymbol{\varepsilon}}}(\mathbf{U}) + \nabla \mathbf{U} \underline{\underline{P}}_0 - \tilde{\rho}_0 (\nabla \mathbf{U}^t - \nabla \cdot \mathbf{U} \underline{\underline{I}}) \right) : \nabla \mathbf{U} \, dx. \quad (4.86)$$

Here, $\tilde{\mathbf{A}}$ is replaced by its expression. We also use $\nabla \mathbf{U}^t = 2\underline{\underline{\boldsymbol{\varepsilon}}}(\mathbf{U}) - \nabla \mathbf{U}$. We have then

$$\begin{aligned} a_S(\mathbf{U}, \mathbf{U}) &= \int_{\Omega^S} \left(\lambda \operatorname{tr} \underline{\underline{\boldsymbol{\varepsilon}}} \underline{\underline{I}} + 2\mu \underline{\underline{\boldsymbol{\varepsilon}}} + \frac{1}{2} (\operatorname{tr}(\underline{\underline{\boldsymbol{\varepsilon}}}) \underline{\underline{P}}_0 + (\underline{\underline{P}}_0 : \underline{\underline{\boldsymbol{\varepsilon}}}) \underline{\underline{I}}) - (\underline{\underline{P}}_0 \underline{\underline{\boldsymbol{\varepsilon}}} + \underline{\underline{\boldsymbol{\varepsilon}}} \underline{\underline{P}}_0) \right) : \nabla \mathbf{U} \, dx \\ &\quad - \int_{\Omega^S} \tilde{\rho}_0 \tilde{c}_0^{-2} (\nabla \cdot \mathbf{U})^2 \, dx + \int_{\Omega^S} (\nabla \mathbf{U} \underline{\underline{P}}_0 - \tilde{\rho}_0 (2\underline{\underline{\boldsymbol{\varepsilon}}}(\mathbf{U}) - \nabla \mathbf{U} - \nabla \cdot \mathbf{U} \underline{\underline{I}})) : \nabla \mathbf{U} \, dx. \end{aligned} \quad (4.87)$$

After simplifications, it holds

$$\begin{aligned} a_S(\mathbf{U}, \mathbf{U}) &= \int_{\Omega^S} (\lambda - \tilde{\rho}_0 \tilde{c}_0^{-2} + \tilde{\rho}_0) (\nabla \cdot \mathbf{U})^2 \, dx + \int_{\Omega^S} 2(\mu - \tilde{\rho}_0) \underline{\underline{\boldsymbol{\varepsilon}}}(\mathbf{U}) : \underline{\underline{\boldsymbol{\varepsilon}}}(\mathbf{U}) \, dx \\ &\quad + \int_{\Omega^S} \left(\frac{1}{2} (\operatorname{tr}(\underline{\underline{\boldsymbol{\varepsilon}}}) \underline{\underline{P}}_0 + (\underline{\underline{P}}_0 : \underline{\underline{\boldsymbol{\varepsilon}}}) \underline{\underline{I}}) - (\underline{\underline{P}}_0 \underline{\underline{\boldsymbol{\varepsilon}}} + \underline{\underline{\boldsymbol{\varepsilon}}} \underline{\underline{P}}_0) + \nabla \mathbf{U} \underline{\underline{P}}_0 \right) : \nabla \mathbf{U} \, dx \\ &\quad + \int_{\Omega^S} \tilde{\rho}_0 \nabla \mathbf{U} : \nabla \mathbf{U} \, dx. \end{aligned} \quad (4.88)$$

Recall that by construction, $\tilde{\rho}_0 \geq 0$. Using the above expression and the inequality (4.85), we have then for the bilinear form a

$$\begin{aligned} a(\mathbf{U}, \mathbf{U}) + \alpha \|\mathbf{U}\|_{\mathcal{H}}^2 &\geq \int_{\Omega^F} (\rho_0 c_0^2 - \varepsilon \rho_0 c_0^2) (\nabla \cdot \mathbf{U})^2 \, dx + \int_{\Omega^F} \rho_0 \frac{g^2}{c_0^2} \mathbf{U} \cdot \tilde{\mathbf{U}} \, dx + \int_{\Omega^S} \frac{\rho_0^2 g^2}{\lambda} \mathbf{U} \cdot \tilde{\mathbf{U}} \, dx \\ &\quad + \int_{\Gamma} \rho_0 g (\mathbf{U} \cdot \mathbf{e}_z)^2 \, dx - 2 \int_{\Omega^S} \tilde{\rho}_0 g \nabla \cdot \mathbf{U} \mathbf{U} \cdot \mathbf{e}_z \, dx + \int_{\Omega^S} (\lambda + \tilde{\rho}_0) (\nabla \cdot \mathbf{U})^2 \, dx + \int_{\Omega^S} 2(\mu - \tilde{\rho}_0) \underline{\underline{\boldsymbol{\varepsilon}}}(\mathbf{U}) : \underline{\underline{\boldsymbol{\varepsilon}}}(\mathbf{U}) \, dx \\ &\quad + \int_{\Omega^S} \left(\frac{1}{2} (\operatorname{tr}(\underline{\underline{\boldsymbol{\varepsilon}}}) \underline{\underline{P}}_0 + (\underline{\underline{P}}_0 : \underline{\underline{\boldsymbol{\varepsilon}}}) \underline{\underline{I}}) - (\underline{\underline{P}}_0 \underline{\underline{\boldsymbol{\varepsilon}}} + \underline{\underline{\boldsymbol{\varepsilon}}} \underline{\underline{P}}_0) + \nabla \mathbf{U} \underline{\underline{P}}_0 \right) : \nabla \mathbf{U} \, dx \\ &\quad + \int_{\Omega^S} \tilde{\rho}_0 \nabla \mathbf{U} : \nabla \mathbf{U} \, dx. \end{aligned} \quad (4.89)$$

Using again the Young inequality for the term in $\nabla \cdot \mathbf{U} \mathbf{U} \cdot \mathbf{e}_z$, we have

$$\begin{aligned} a(\mathbf{U}, \mathbf{U}) + \alpha \|\mathbf{U}\|_{\mathcal{H}}^2 &\geq \int_{\Omega^F} (\rho_0 c_0^2 - \varepsilon \rho_0 c_0^2) (\nabla \cdot \mathbf{U})^2 \, dx + \int_{\Omega^F} \rho_0 \frac{g^2}{c_0^2} \mathbf{U} \cdot \tilde{\mathbf{U}} \, dx + \int_{\Omega^S} \frac{\rho_0^2 g^2}{\lambda} \mathbf{U} \cdot \tilde{\mathbf{U}} \, dx \\ &\quad + \int_{\Gamma} \rho_0 g (\mathbf{U} \cdot \mathbf{e}_z)^2 \, dx + \int_{\Omega^S} (\lambda + \tilde{\rho}_0 - \varepsilon \lambda) (\nabla \cdot \mathbf{U})^2 \, dx + \int_{\Omega^S} 2(\mu - \tilde{\rho}_0) \underline{\underline{\boldsymbol{\varepsilon}}}(\mathbf{U}) : \underline{\underline{\boldsymbol{\varepsilon}}}(\mathbf{U}) \, dx \\ &\quad + \int_{\Omega^S} \left(\frac{1}{2} (\operatorname{tr}(\underline{\underline{\boldsymbol{\varepsilon}}}) \underline{\underline{P}}_0 + (\underline{\underline{P}}_0 : \underline{\underline{\boldsymbol{\varepsilon}}}) \underline{\underline{I}}) - (\underline{\underline{P}}_0 \underline{\underline{\boldsymbol{\varepsilon}}} + \underline{\underline{\boldsymbol{\varepsilon}}} \underline{\underline{P}}_0) + \nabla \mathbf{U} \underline{\underline{P}}_0 \right) : \nabla \mathbf{U} \, dx \\ &\quad + \int_{\Omega^S} \tilde{\rho}_0 \nabla \mathbf{U} : \nabla \mathbf{U} \, dx. \end{aligned} \quad (4.90)$$

From the Korn inequality, we have

$$\begin{aligned}
a(\mathbf{U}, \mathbf{U}) + \alpha \|\mathbf{U}\|_{\mathcal{H}}^2 &\geq \int_{\Omega^F} (\rho_0 c_0^2 - \varepsilon \rho_0 c_0^2) (\nabla \cdot \mathbf{U})^2 \, dx + \int_{\Omega^F} \rho_0 \frac{g^2}{c_0^2} \mathbf{U} \cdot \tilde{\mathbf{U}} \, dx + \int_{\Omega^S} \frac{\rho_0^2 g^2}{\lambda} \mathbf{U} \cdot \tilde{\mathbf{U}} \, dx \\
&+ \int_{\Gamma} \rho_0 g (\mathbf{U} \cdot \mathbf{e}_z)^2 \, dx + \int_{\Omega^S} (\lambda + \tilde{\rho}_0 - \varepsilon \lambda) (\nabla \cdot \mathbf{U})^2 \, dx + 2C_K \|\mathbf{U}\|_{H^1(\Omega^S)}^2 + \int_{\Omega^S} \tilde{\rho}_0 \nabla \mathbf{U} : \nabla \mathbf{U} \, dx \\
&+ \int_{\Omega^S} \left(\frac{1}{2} (\text{tr}(\underline{\underline{\varepsilon}}) \underline{\underline{P}}_0 + (\underline{\underline{P}}_0 : \underline{\underline{\varepsilon}}) \underline{\underline{I}}) - (\underline{\underline{P}}_0 \underline{\underline{\varepsilon}} + \underline{\underline{\varepsilon}} \underline{\underline{P}}_0) + \nabla \mathbf{U} \underline{\underline{P}}_0 \right) : \nabla \mathbf{U} \, dx. \quad (4.91)
\end{aligned}$$

For $\|\underline{\underline{P}}_0\|_{L^2(\Omega^S)^{3 \times 3}}$ small enough, the terms in the last integral are controlled by the other terms, which proves the coercivity. \square

We can now show the well-posedness of the modified variational formulation,

Theorem 4.2. *For $\mathbf{f} \in L^1_{loc}(0, T; L^2(\Omega))$, and under the conditions of Proposition 4.2, the problem (4.77) admits a unique solution with the regularity (4.76). Moreover, it holds*

$$\frac{d^2}{dt^2} \mathbf{U}_1 \in L^2(0, T; \mathcal{V}'). \quad (4.92)$$

Proof. Since the bilinear form a is symmetric and satisfies $a(\mathbf{U}, \mathbf{U}) + \alpha^2 \|\mathbf{U}\|_{\mathcal{H}} \geq C \|\mathbf{U}\|_{\mathcal{V}}$ for all $\mathbf{U} \in \mathcal{V}$, the theorem is an application of classical results, see for example Dautray and Lions (2000); Joly et al. (2008). \square

4.3.4 Energy estimates.

In the following, we use an energy equality to show that the solution \mathbf{U}_1 depends continuously on the data f . In the case $a(\mathbf{U}, \mathbf{U}) \geq 0$ this result is standard, however in our case we have the weaker inequality $a(\mathbf{U}, \mathbf{U}) + \alpha^2 \|\mathbf{U}\|_{\mathcal{H}}^2 \geq 0$. We show how the usual proof can be adapted to this case. Let the energy \mathcal{E} be defined by

$$\mathcal{E}(t) = \frac{1}{2} (a(\mathbf{U}_1(t), \mathbf{U}_1(t)) + \|\partial_t \mathbf{U}_1(t)\|_{\mathcal{H}}^2 + \alpha^2 \|\mathbf{U}_1(t)\|_{\mathcal{H}}^2).$$

Differentiation in time yields

$$\frac{d\mathcal{E}}{dt} = a(\mathbf{U}, \partial_t \mathbf{U}_1) + (\partial_{tt}^2 \mathbf{U}_1, \partial_t \mathbf{U}_1)_{\mathcal{H}} + \frac{d}{dt} \left(\frac{\alpha^2}{2} \|\mathbf{U}_1\|_{\mathcal{H}}^2 \right).$$

From Theorem 4.1, and integration by parts, we have $a(\mathbf{U}_1, \partial_t \mathbf{U}_1) = (-\rho_0^{-1} \nabla \cdot (\partial_t \underline{\underline{P}}_1), \partial_t \mathbf{U}_1)_{\mathcal{H}}$, hence the above equation reads

$$\frac{d\mathcal{E}}{dt} = (-\rho_0^{-1} \nabla \cdot (\partial_t \underline{\underline{P}}_1), \partial_t \mathbf{U}_1)_{\mathcal{H}} + (\partial_{tt}^2 \mathbf{U}_1, \partial_t \mathbf{U}_1)_{\mathcal{H}} + \frac{d}{dt} \left(\frac{\alpha^2}{2} \|\mathbf{U}_1\|_{\mathcal{H}}^2 \right).$$

Using then (4.49) yields the following equation for the energy,

$$\frac{d\mathcal{E}}{dt} = (\mathbf{f}, \partial_t \mathbf{U}_1)_{\mathcal{H}} + \frac{d}{dt} \left(\frac{\alpha^2}{2} \|\mathbf{U}_1\|_{\mathcal{H}}^2 \right). \quad (4.93)$$

The energy equation (4.93) is used to obtain estimates on the solution.

Proposition 4.3. *For all time t , we have the estimates*

$$\|\partial_t \mathbf{U}_1(t)\|_{\mathcal{H}}^2 \leq 2C(\alpha, T) \sup_{s \in [0, T]} \|\mathbf{f}(s)\|_{\mathcal{H}}^2, \quad \|\mathbf{U}_1(t)\|_{\mathcal{H}}^2 \leq TC(\alpha, T) \sup_{s \in [0, T]} \|\mathbf{f}(s)\|_{\mathcal{H}}^2, \quad (4.94)$$

where

$$C(\alpha, T) = \frac{1}{2\alpha} e^{\alpha T(1+2\alpha T)}.$$

Proof. Integration from 0 to t of the equation (4.93) yields

$$\mathcal{E}(t) - \mathcal{E}(0) = \int_0^t (\mathbf{f}, \partial_t \mathbf{U}_1)_{\mathcal{H}} dt' + \frac{\alpha^2}{2} \|\mathbf{U}_1(t)\|_{\mathcal{H}}^2 - \frac{\alpha^2}{2} \|\mathbf{U}_1(0)\|_{\mathcal{H}}^2.$$

And we have with vanishing initial conditions and with the Cauchy-Schwarz inequality

$$\mathcal{E}(t) \leq \int_0^t \|\mathbf{f}\|_{\mathcal{H}} \|\partial_t \mathbf{U}_1\|_{\mathcal{H}} dt' + \alpha^2 \|\mathbf{U}_1\|_{\mathcal{H}}^2. \quad (4.95)$$

The term $\alpha^2 \|\mathbf{U}_1\|_{\mathcal{H}}^2$ is bounded by the norm of $\partial_t \mathbf{U}_1$. Indeed, from the vanishing initial conditions it holds

$$\mathbf{U}_1(t) = \int_0^t \partial_t \mathbf{U}_1(t') dt' \rightarrow \|\mathbf{U}_1(t)\|_{\mathcal{H}} \leq \int_0^t \|\partial_t \mathbf{U}_1(t')\|_{\mathcal{H}} dt'. \quad (4.96)$$

Moreover, if we use the Cauchy-Schwarz inequality in the space $L^2(0, t; \mathcal{H})$ with $\|\partial_t \mathbf{U}_1\|_{\mathcal{H}}$ and the constant unit function, we obtain

$$\|\mathbf{U}_1(t)\|_{\mathcal{H}} \leq \int_0^t \|\partial_t \mathbf{U}_1\|_{\mathcal{H}} dt' \leq \sqrt{t} \sqrt{\int_0^t \|\partial_t \mathbf{U}_1\|_{\mathcal{H}}^2 dt'}. \quad (4.97)$$

Replacing in (4.95) the second term by (4.97), and using a Young inequality for the first term yields then, for $S(t) = \int_0^t \|\mathbf{f}(t')\|_{\mathcal{H}}^2 dt'$,

$$\mathcal{E}(t) \leq \frac{1}{2\alpha} S(t) + \left(\frac{\alpha}{2} + \alpha^2 t\right) \int_0^t \|\partial_t \mathbf{U}_1\|_{\mathcal{H}}^2 dt'. \quad (4.98)$$

Using then $\|\partial_t \mathbf{U}_1\|_{\mathcal{H}}^2 \leq 2\mathcal{E}$, we have

$$\mathcal{E}(t) \leq \frac{1}{2\alpha} S(t) + \alpha(1 + 2\alpha T) \int_0^t \mathcal{E}(t') dt'. \quad (4.99)$$

From the Gronwall inequality we have then

$$\mathcal{E}(t) \leq \frac{1}{2\alpha} S(t) + \left(\frac{1}{2} + \alpha T\right) \int_0^t S(t') e^{\alpha(1+2\alpha T)(t-t')} dt'. \quad (4.100)$$

Integrating by parts the second term yields

$$\left(\frac{1}{2} + \alpha T\right) \int_0^t S(t') e^{\alpha(1+2\alpha T)(t-t')} dt' = -\frac{1}{2\alpha} S(t) + \frac{1}{2\alpha} \int_0^t \|\mathbf{f}(t')\|_{\mathcal{H}}^2 e^{\alpha(1+2\alpha T)(t-t')} dt', \quad (4.101)$$

hence it holds

$$\mathcal{E}(t) \leq \frac{1}{2\alpha} e^{\alpha T(1+2\alpha T)} \sup_{t' \in [0, T]} \|\mathbf{f}(t')\|_{\mathcal{H}}^2. \quad (4.102)$$

The inequality for $\|\partial_t \mathbf{U}_1\|_{\mathcal{H}}$ follows directly. For $\|\mathbf{U}_1\|_{\mathcal{H}}$ we use again the inequality (4.96), and obtain

$$\|\mathbf{U}_1(t)\|_{\mathcal{H}}^2$$

□

4.4 Numerical illustration

We give a simple illustration in 2D of the model derived in this chapter. We simulate a tsunami generated by an earthquake, represented by a double couple inside the earth.

A damping term is added to avoid reflections with the bottom boundary of the domain, hence the system to be solved is

$$\frac{\partial^2 \mathbf{U}_1}{\partial t^2} + d(z) \frac{\partial \mathbf{U}_1}{\partial t} - \rho_0^{-1} \nabla \cdot (\partial_t \underline{\underline{P}}_1) = \partial_t \mathbf{F}_1, \quad (4.103)$$

where $d(z)$ is a smooth damping function. For the numerical approximation, we consider the formulation (4.44) with the additional damping term,

$$\begin{aligned} \frac{d^2}{dt^2} (\mathbf{U}_1, \tilde{\mathbf{U}})_{\mathcal{H}} + \frac{d}{dt} (d \mathbf{U}_1, \tilde{\mathbf{U}})_{\mathcal{H}} + \int_{\Omega^F} ((\rho_0 c_0^2 - \rho_0) \nabla \cdot \mathbf{U}_1 \underline{\underline{I}} + \rho_0 \nabla \mathbf{U}_1^t) : \nabla \tilde{\mathbf{U}} \, dx \\ + \int_{\Omega^S} (\underline{\underline{A}} : \underline{\underline{\varepsilon}}(\mathbf{U}_1) + \nabla \mathbf{U}_1 \underline{\underline{P}}_0) : \nabla \tilde{\mathbf{U}} \, dx = (\mathbf{f}, \tilde{\mathbf{U}})_{\mathcal{H}}. \end{aligned} \quad (4.104)$$

Discretization. The formulation (4.104) is discretized with a spectral element method (Komatitsch and Vilotte, 1998), as presented in Chap. 3. In the following, we present the 2D discretization, since the simulation presented later is in two dimensions (x, z) . Let \mathcal{V}_h be the finite-dimensional space obtained by the approximation of $H^1(\Omega)$, and \mathcal{H}_h be the finite-dimensional approximation of \mathcal{H} . They are defined as follows. Let Ω_h be the discrete domain obtained by meshing the domain Ω with quadrilaterals $(K_i)_{i \in \{1 \dots N\}}$. The reference square is denoted \hat{K} , and the transformation from a deformed quadrilateral K_j to the reference square is denoted F_j . We have then

$$\Omega_h = \bigcup_{i=1}^N K_i, \quad K_i \cap K_j = \emptyset, \quad \mathbf{F}_i(\hat{K}) = K_i, \quad (4.105)$$

The approximations of the functional space are then defined by

$$\mathcal{V}_h = \{\phi \in C^0(\Omega) \mid \phi|_{K_i} \circ F_i \in \mathcal{Q}_{q,r}(\hat{K})\}, \quad \mathcal{H}_h = \{\phi \in L^2(\Omega) \mid \phi|_{K_i} \circ F_i \in \mathcal{Q}_{q,r}(\hat{K})\}, \quad (4.106)$$

where $\mathcal{Q}_{q,r}$ is the set of polynomials with degree r in the x coordinate and degree q in the z coordinate. The scalar product in \mathcal{H} is approximated using a quadrature formula, and its approximation is denoted $(\cdot, \cdot)_{\mathcal{H}_h}$. We also define the following bilinear forms defined on $\mathcal{V}_h \times \mathcal{V}_h$,

$$a_{F,h}(\mathbf{U}, \tilde{\mathbf{U}}) = \int_{\Omega^F} ((\rho_0 c_0^2 - \rho_0) \nabla \cdot \mathbf{U}_1 \underline{\underline{I}} + \rho_0 \nabla \mathbf{U}_1^t) : \nabla \tilde{\mathbf{U}} \, dx, \quad (4.107)$$

$$a_{S,h}(\mathbf{U}, \tilde{\mathbf{U}}) = \int_{\Omega^S} \lambda \nabla \cdot \mathbf{U} \nabla \cdot \tilde{\mathbf{U}} + 2\mu \underline{\underline{\varepsilon}}(\mathbf{U}_1) : \underline{\underline{\varepsilon}}(\tilde{\mathbf{U}}) \, dx, \quad (4.108)$$

$$b_h(\mathbf{U}, \tilde{\mathbf{U}}) = \int_{\Omega} \rho_0 d \mathbf{U} \cdot \tilde{\mathbf{U}} \, dx, \quad (4.109)$$

where the integrals are approximated by quadrature formulae. The space discretization of the formulation (4.104) reads then: find $\mathbf{U}_h \in \mathcal{V}_h$ solution to

$$\frac{d^2}{dt^2} (\mathbf{U}_h, \tilde{\mathbf{U}}_h)_{\mathcal{H}_h} + \frac{d}{dt} b_h(\mathbf{U}_h, \tilde{\mathbf{U}}_h) + a_{F,h}(\mathbf{U}_h, \tilde{\mathbf{U}}_h) + a_{S,h}(\mathbf{U}_h, \tilde{\mathbf{U}}_h) = (\mathbf{f}_h, \tilde{\mathbf{U}}_h)_{\mathcal{H}_h}, \quad \forall \tilde{\mathbf{U}}_h \in \mathcal{V}_h, \quad (4.110)$$

where \mathbf{f}_h is some discretization of the source term. The functions $\mathbf{U}, \tilde{\mathbf{U}}$ are decomposed on a basis for the space \mathcal{V}_h , which yields the global solution vector \mathbf{U}_h , the mass matrix \mathbb{M} , the mass matrix \mathbb{M}_d corresponding to the bilinear form b_h , and the stiffness matrices $\mathbb{K}_F, \mathbb{K}_S$ corresponding respectively to the bilinear forms $a_{F,h}$ and $a_{S,h}$. Using a Gauss-Lobatto quadrature rule yields diagonal mass matrices \mathbb{M} and \mathbb{M}_d .

For the time discretization, the time interval $[0, T]$ is partitioned into M equal intervals of length $\Delta t = T/M$. The semi-discrete formulation (4.110) is discretized in time using a leapfrog scheme. We consider the sequence $\{\mathbf{U}_h^n \in \mathcal{V}_{0,h}\}_{n \in \{1, \dots, M\}}$ solution to

$$\mathbb{M} \frac{\mathbf{U}_h^{k-1} - 2\mathbf{U}_h^k + \mathbf{U}_h^{k+1}}{\Delta t^2} + \mathbb{M}_d \frac{\mathbf{U}_h^k - \mathbf{U}_h^{k-1}}{\Delta t} + \mathbb{K}_F \mathbf{U}_h^k + \mathbb{K}_S \mathbf{U}_h^k = \mathbb{M} \mathbf{F}, \quad (4.111)$$

Numerical values and source term. We assume that the static stress vanishes in the solid domain, $\underline{\underline{P}}_0^S = 0$, and we take the following numerical values,

$$\begin{aligned} \rho_{ocean} &= 1000 \text{ kg m}^{-3}, & \rho_{earth} &= 2670 \text{ kg m}^{-3}, \\ c &= 1500 \text{ ms}^{-1}, & \lambda &= 1.1 \cdot 10^{11} \text{ kg m}^{-1} \text{s}^{-2}, & \mu &= 5.6 \cdot 10^{10} \text{ kg m}^{-1} \text{s}^{-2}. \end{aligned}$$

The computational domain is 900 km long and 18 km deep. The ocean layer and the earth layer are respectively 3.6 km and 10.8 km thick. The damping function $d(z)$ varies smoothly from 0 to d_{max} in a 3.6 km thick damping layer.

Models for the rupture process of an earthquake are available, see for example the models used by Lotto and Dunham (2015) and Krenz et al. (2021). Here, for simplicity, we choose a simpler model based on a double couple line source as in Maeda and Furumura (2013), Balanche (2010). This source term consists in a stress tensor of the form

$$\underline{\underline{P}}_1(\mathbf{x}, t) = g(t) \begin{pmatrix} 0 & 1 \\ 1 & 0 \end{pmatrix},$$

where $g(t)$ is a function depending on time only. For $g(t)$ we use the single cycle Küpper wavelet as in Maeda and Furumura (2013),

$$g(t) = \frac{9\pi M_0}{16T_0} \left(\sin \frac{\pi t}{T_0} - \frac{1}{3} \sin \frac{3\pi t}{T_0} \right), \quad 0 \leq t \leq T_0. \quad (4.112)$$

Snapshots and bottom pressure recordings. Figure 4.5 illustrates snapshots of the horizontal and vertical displacement fields at times $t = 10$ s, $t = 50$ s, $t = 80$ s. At time $t = 10$ s (Figure 4.5-1), the pressure waves and shear waves propagate in the earth, and the acoustic waves propagate in the ocean. In the vertical displacement (Figure 4.5-1.b), the influence of the seismic waves on the acoustic waves is clearly seen: head waves are created in the ocean because of the presence of the faster seismic waves. At time $t = 50$ s (Figure 4.5-2), the pressure waves in the earth have propagated further than the domain. The shear waves in the earth and the acoustic waves are still visible. In the horizontal displacement figure, we see the tsunami starting to propagate above the earthquake. At time $t = 80$ s (Figure 4.5-3), the seismic waves and the acoustic waves are almost not visible anymore since they have propagated further than the domain. It remains a permanent displacement in the earth, and the propagating tsunami. Those simulations are in good agreement to the ones presented by Maeda and Furumura (2013).

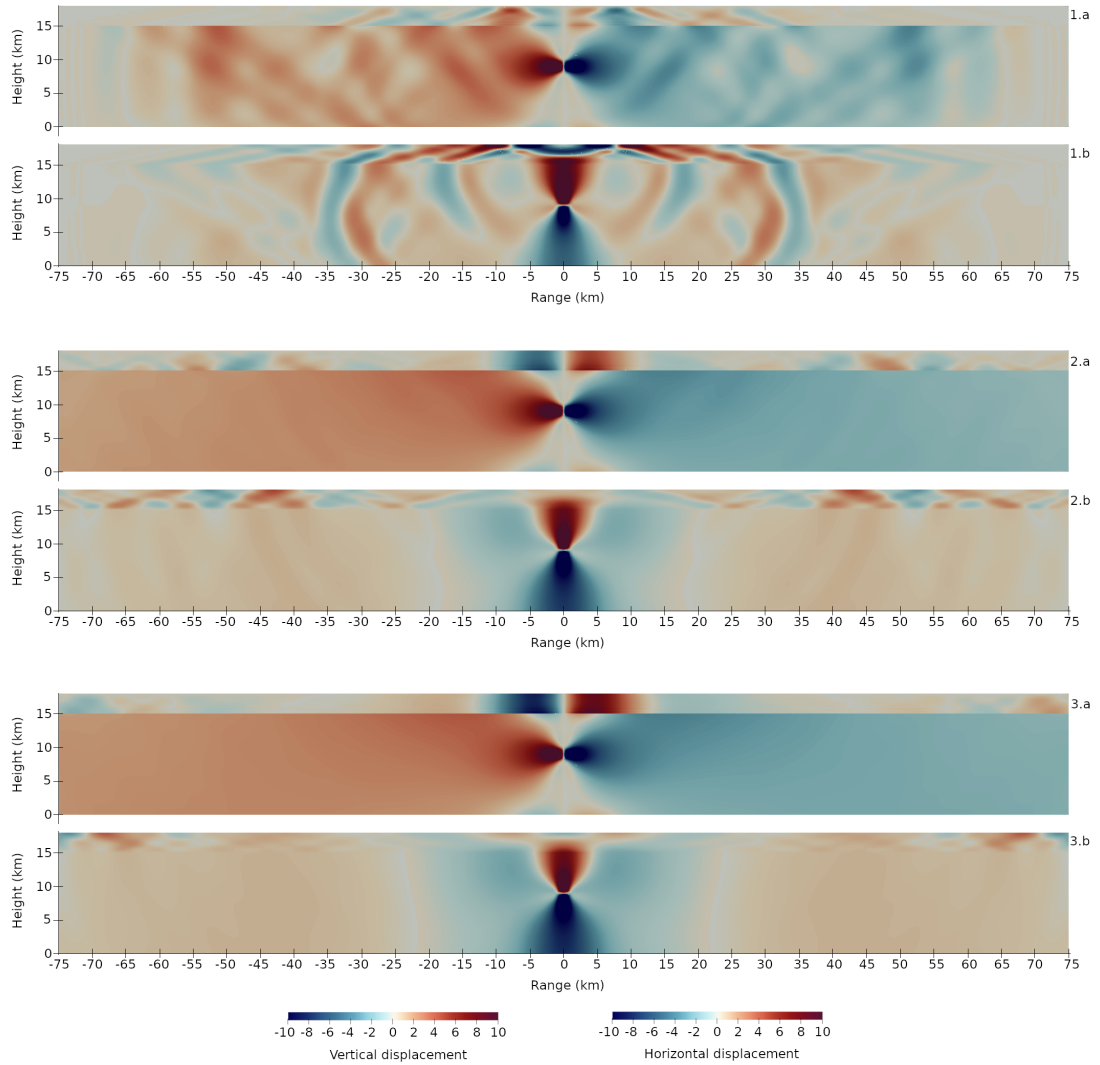


Figure 4.5: Snapshots of the horizontal (figures a) and vertical displacement (figures b) field. Figures 1a, 1b: $t = 10$ s, Figures 2a, 2b: $t = 50$ s, Figures 3a, 3b: $t = 80$ s.

4.5 Conclusion and future work

In this work, we have presented a fully-coupled model for the propagation of tsunamis, hydro-acoustic and seismic waves. One novelty of the model is that it includes a static stress in the earth and in the ocean. The second contribution of this work is to prove that the fully-coupled model is well-posed, under some conditions for the static stress. The model is written as a variational formulation (4.44), which can be discretized in a rather straightforward way, in particular the transmission condition between the earth and the ocean does not need special treatment. However, this first formulation is not adapted for the mathematical analysis. We have then proved that the model can be written with a second variational formulation, which is well-posed. The numerical illustration show good agreement with other models from the litterature (Maeda and Furumura, 2013). This work will be completed with further numerical simulations to test the influence of the pre-stress on the waves in the fluid and in the solid. Moreover, transparent conditions could be used at the boundaries to reduce more effectively the non-physical reflections.

The presence of the pre-stress in the ocean is one of the main difficulties for the mathematical analysis of the model. This difficulty was raised by using an extension of the background pressure. This approach could be applied on the model with the whole earth, as studied by Valette (1986) and de Hoop et al. (2017).

Appendix

A The bilinear form in the fluid domain

We show how the bilinear form for a fully fluid domain can be written as a symmetric expression. The computations are very similar to those made in Section A, however, in Section A they are done for a particular choice of test function, and for an additional boundary condition on the seabed. For completeness, we derive the computation in the present case. We start with Equation (4.53), that we recall here,

$$(I) = \int_{\Omega} -[\nabla \cdot (\partial_t \underline{P}_1)] \cdot \tilde{\mathbf{U}} \, dx = \underbrace{\int_{\Omega} -[\nabla \cdot (\rho_0 c_0^2 \nabla \cdot \mathbf{U}_{1\underline{I}})] \cdot \tilde{\mathbf{U}} \, dx}_{(I_1)} + \underbrace{\int_{\Omega} [(\nabla \cdot \mathbf{U}_{1\underline{I}} - \nabla \mathbf{U}_1^t) \nabla \rho_0] \cdot \tilde{\mathbf{U}} \, dx}_{(I_2)}. \quad (113)$$

The first integral of the right-hand side is integrated by parts,

$$(I_1) = - \int_{\Gamma} \rho_0 c_0^2 \nabla \cdot \mathbf{U}_1 \mathbf{n} \cdot \tilde{\mathbf{U}} \, ds + \int_{\Omega} (\rho_0 c_0^2 \nabla \cdot \mathbf{U}_{1\underline{I}}) : \nabla \tilde{\mathbf{U}} \, dx. \quad (114)$$

For the second integral of the right-hand side, we use the equilibrium equation (4.36) yielding $\nabla \rho_0 = -\rho_0 g \mathbf{e}_z$,

$$(I_2) = - \int_{\Omega} \rho_0 g \nabla \cdot \mathbf{U}_1 \mathbf{e}_z \cdot \tilde{\mathbf{U}} \, dx + \int_{\Omega} \rho_0 g \nabla (\mathbf{U}_1 \cdot \mathbf{e}_z) \cdot \tilde{\mathbf{U}} \, dx. \quad (115)$$

The second term of (115) is integrated by parts,

$$\int_{\Omega} \rho_0 g \nabla (\mathbf{U}_1 \cdot \mathbf{e}_z) \cdot \tilde{\mathbf{U}} \, dx = - \int_{\Omega} g \mathbf{U}_1 \cdot \mathbf{e}_z \nabla \cdot (\rho_0 \tilde{\mathbf{U}}) \, dx + \int_{\Gamma} \rho_0 g \mathbf{U}_1 \cdot \mathbf{e}_z \tilde{\mathbf{U}} \cdot \mathbf{n} \, ds \quad (116)$$

$$= - \int_{\Omega} \rho_0 g \mathbf{U}_1 \cdot \mathbf{e}_z \nabla \cdot \tilde{\mathbf{U}} \, dx - \int_{\Omega} g \mathbf{U}_1 \cdot \mathbf{e}_z \tilde{\mathbf{U}} \cdot \mathbf{e}_z \rho_0' \, dx + \int_{\Gamma} \rho_0 g \mathbf{U}_1 \cdot \mathbf{e}_z \tilde{\mathbf{U}} \cdot \mathbf{n} \, ds. \quad (117)$$

We have used the fact that the density is vertically stratified: $\rho_0 = \rho_0(\xi^3)$, hence $\nabla \rho_0 = \rho'_0(\xi^3) \mathbf{e}_z$. The integral (I_2) reads then

$$(I_2) = - \int_{\Omega} \rho_0 g \nabla \cdot \mathbf{U}_1 \mathbf{e}_z \cdot \tilde{\mathbf{U}} \, dx - \int_{\Omega} \rho_0 g \mathbf{U}_1 \cdot \mathbf{e}_z \nabla \cdot \tilde{\mathbf{U}} \, dx - \int_{\Omega} g \mathbf{U}_1 \cdot \mathbf{e}_z \tilde{\mathbf{U}} \cdot \mathbf{e}_z \rho'_0 \, dx + \int_{\Gamma} \rho_0 g \mathbf{U}_1 \cdot \mathbf{e}_z \tilde{\mathbf{U}} \cdot \mathbf{e}_z \, ds, \quad (118)$$

Since $\mathbf{n} = \mathbf{e}_z$ on Γ . Summing the two integrals (I_1) and (I_2) yields

$$(I) = \int_{\Omega} \rho_0 c_0^2 \nabla \cdot \mathbf{U}_1 \nabla \cdot \tilde{\mathbf{U}} \, dx - \int_{\Gamma} \rho_0 c_0^2 \nabla \cdot \mathbf{U}_1 \mathbf{n} \cdot \tilde{\mathbf{U}} \, ds - \int_{\Omega} \rho_0 g \nabla \cdot \mathbf{U}_1 \mathbf{e}_z \cdot \tilde{\mathbf{U}} \, dx - \int_{\Omega} \rho_0 g \mathbf{U}_1 \cdot \mathbf{e}_z \nabla \cdot \tilde{\mathbf{U}} \, dx - \int_{\Omega} g \mathbf{U}_1 \cdot \mathbf{e}_z \tilde{\mathbf{U}} \cdot \mathbf{e}_z \rho'_0 \, dx + \int_{\Gamma} \rho_0 g \mathbf{U}_1 \cdot \mathbf{e}_z \tilde{\mathbf{U}} \cdot \mathbf{e}_z \, ds. \quad (119)$$

This expression can be reformulated as follows,

$$(I) = \int_{\Omega} \rho_0 \left(c_0 \nabla \cdot \mathbf{U}_1 - \frac{g}{c_0} \mathbf{U}_1 \cdot \mathbf{e}_z \right) \left(c_0 \nabla \cdot \tilde{\mathbf{U}} - \frac{g}{c_0} \tilde{\mathbf{U}} \cdot \mathbf{e}_z \right) \, dx - \int_{\Omega} \rho_0 \left(\frac{\rho'_0}{\rho_0} + \frac{g^2}{c_0^2} \right) \mathbf{U}_1 \cdot \mathbf{e}_z \tilde{\mathbf{U}} \cdot \mathbf{e}_z \, dx + \int_{\Gamma} \rho_0 g \mathbf{U}_1 \cdot \mathbf{e}_z \tilde{\mathbf{U}} \cdot \mathbf{e}_z \, ds - \int_{\Gamma} \rho_0 c_0^2 \nabla \cdot \mathbf{U}_1 \tilde{\mathbf{U}} \cdot \mathbf{e}_z \, ds. \quad (120)$$

B An expression for the extended density

The extensions $\tilde{\rho}_0, \tilde{\rho}_0$ are constructed such that $\tilde{\rho}_0$ and $\tilde{\rho}_0$ are continuous in Ω , $\tilde{\rho}_0 = 0$ and $\tilde{\rho}_0 = 0$ on Γ_{∞} , and $\nabla \tilde{\rho}_0 = -\tilde{\rho}_0 g \mathbf{e}_z$ in Ω^{FB} . We look for an extension of the density of the form (see Figure 4.4)

$$\tilde{\rho}_0 = \begin{cases} \rho_0^F(z), & 0 < z < h, \\ a_1 z + b_1, & -h_0/2 < z < 0, \\ a_2 z + b_2, & -h_0 < z < -h_0/2, \\ 0, & z < -h_0. \end{cases}$$

and the extended pressure is defined by

$$\tilde{p}_0(z) = \int_z^h \tilde{\rho}_0(z') g \, dz'.$$

The continuity of $\tilde{\rho}_0$ imposes that

$$\tilde{\rho}_0(-h_0) = 0, \quad \tilde{\rho}_0(0^-) = \tilde{\rho}_0(0^+), \quad \tilde{\rho}_0(-h_0/2^-) = \tilde{\rho}_0(-h_0/2^+),$$

hence we have

$$b_1 = a_1 h_0, \quad b_2 = \rho_0^F(0), \quad a_1 = -a_2 + \frac{2\rho_0^F(0)}{h_0}.$$

By construction, $\tilde{\rho}_0$ is continuous on Ω^{FB} . The constant a_2 is determined by the condition $\tilde{\rho}_0(-h_0) = 0$.

$$\int_{-h_0}^h \tilde{\rho}_0(z') g \, dz' = g \int_{-h_0}^{-h_0/2} (a_1 z + b_1) \, dz' + g \int_{-h_0/2}^0 (a_2 z + b_2) \, dz' + g \int_0^h \tilde{\rho}_0(z') \, dz'.$$

We denote by $\overline{\rho_0^F}$ the mean of the density in the fluid domain,

$$\overline{\rho_0^F} = 1/h_0 \int_0^h \rho_0.$$

The constant a_2 is then given by

$$a_2 = \frac{1}{h_0} \left(3\rho_0^F(0) + 4\overline{\rho_0^F} \right),$$

and a_1 is given by

$$a_1 = -\frac{1}{h_0} \cdot \left(\rho_0^F(0) + 4\overline{\rho_0^F} \right).$$

Preliminary results for geophysical applications

Contents

5.1 Simulation of acoustic waves generated by landslides	119
5.1.1 Detecting an underwater landslide from interference patterns: the Lloyd mirror	120
5.1.2 Reproducing the Lloyd mirror with static emitters	122
5.1.3 Perspectives	123
5.2 Wave trapping in the SOFAR channel	123
5.2.1 Simulation of trapped waves	127
5.2.2 T-wave propagation from a beam located near the seabed	129
5.2.3 Perspectives	130
5.3 Conclusion and future work	130

Abstract: In this chapter, we present some preliminary simulations for geophysical applications. The simulations are obtained with the model developed in the thesis, and numerically solved with a high-order spectral element method. The first application is the Lloyd mirror, an interference pattern which could help the characterization of underwater landslides. The second application is the wave trapping in the SOFAR channel for waves generated by underwater earthquakes.

5.1 Simulation of acoustic waves generated by landslides

The model developed in Chapter 2 is used to simulate the generation of acoustic waves by an underwater landslide. Detection and characterization of underwater landslides are usually done using seismic waves (Moretti et al., 2012; Yamada et al., 2018; Hibert et al., 2011; Brodsky et al., 2003; Allstadt et al., 2018). On the other hand, there is a growing interest for the use of hydro-acoustic waves to characterize geophysical events.

Many studies have been conducted on the generation of hydro-acoustic waves by underwater earthquakes (Gomez and Kadri, 2021; Auclair et al., 2021; Cecioni et al., 2014); however, fewer studies are dedicated to the waves generated by underwater landslides. We mention the work by

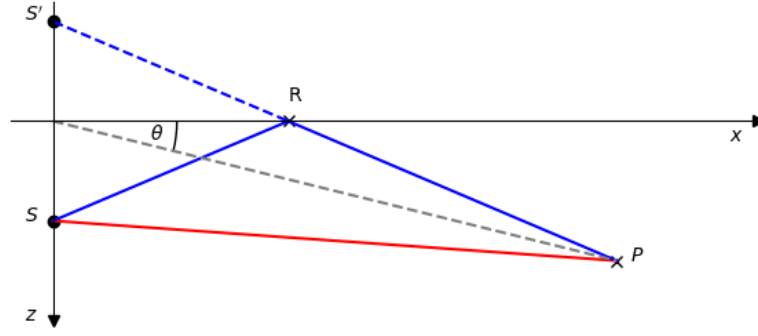


Figure 5.1: The direct path (in red) and the reflected path (in blue) connecting the source S to a point P . The location of the reflection (point R) is deduced from the image source S' . The declination angle θ is also indicated.

Caplan-Auerbach et Al. (Caplan-Auerbach et al., 2001, 2014), which combines in-field measurements and modeling of acoustic rays. Caplan-Auerbach et al. (2014) suggest that the hydro-acoustic signals generated by underwater landslides have a characteristic interference pattern. This pattern could be then used to detect and characterize landslides. In this preliminary work, we partially reproduce a similar interference pattern using a numerical model.

5.1.1 Detecting an underwater landslide from interference patterns: the Lloyd mirror

When considering the propagation of acoustic waves in a bounded medium, the reflection on the boundary can lead to interference patterns called the Lloyd mirror effect (Jensen et al., 2011). To explain this effect, we consider a simplified case, where the ocean is represented by a 2D domain. The domain, with coordinates (x, z) , is bounded above by a free surface, and the interactions with the seabed are neglected. The fluid pressure satisfies then the acoustic equation

$$\frac{\partial^2 p}{\partial t^2} - c^2 \Delta p = 0, \quad p = 0 \text{ on } z = H. \quad (5.1)$$

An acoustic point source located at $(0, z_s)$ emits a wave of the form

$$p(0, z_s, t) = p_0 \exp(-i\omega t), \quad (5.2)$$

where p_0 is the pressure magnitude and ω is the frequency. If we consider the point source as a source emitting rays in all directions, and neglect the reflection with the bottom, every point of the domain is connected to the source by two rays: the direct ray, and the ray reflected by the surface (see Figure 5.1). The solution $p(x, z, t)$ to Equation (5.1) is then a superposition of both paths,

$$p(x, z, t) = A e^{-i\omega t} \left(\frac{e^{ikR_1}}{R_1} - \frac{e^{ikR_2}}{R_2} \right), \quad R_1 = \sqrt{x^2 + (z - z_s)^2}, \quad R_2 = \sqrt{x^2 + (z + z_s)^2}, \quad (5.3)$$

with the source strength A and the wavenumber $k = \omega/c$. To fix the ideas, the pressure field p given by Equation (5.3) is plotted in Figure 5.2, for $k = 66.7 \text{ m}^{-1}$, $A = 1 \text{ Pa.m}$, and for a fixed time t . The figure shows the interference pattern generated by the superposition of the direct ray and the reflected ray at each point.

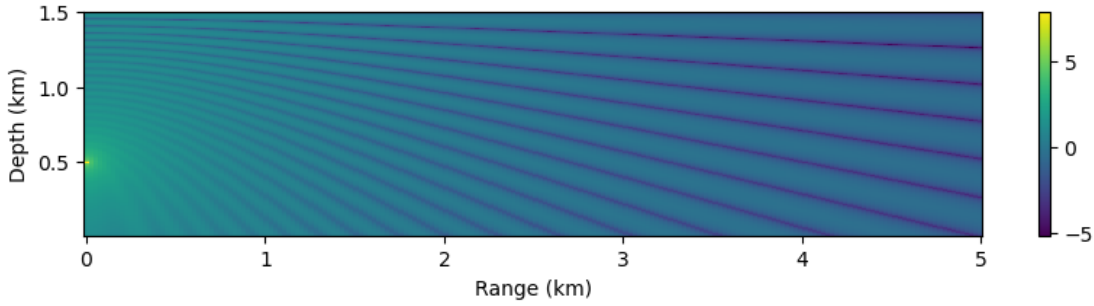


Figure 5.2: Interference pattern obtained from Equation (5.3) for $k = 66.7 \text{ m}^{-1}$, $z_s = 0.5 \text{ km}$. The modulus $|\rho(x, z)|$ is plotted in log scale.

An approximation of the expression (5.3) for the pressure field p can be obtained when considering points far away from the source. More precisely, for points with coordinates (R, z) such that $R \gg z_s$, the expression (5.3) is approximated by

$$p(R, z, t) \sim -A \frac{2i}{R} \sin(kz_s \sin \theta) e^{ikR} e^{-i\omega t}, \quad (5.4)$$

where θ is the declination angle (see Figure 5.1) and depends on the coordinates (x, z) . The expression (5.4) can be used to determine maxima and the minima of the pressure field. The pressure maxima are $|\rho_{\max}| = 2/R$, and they are such that the angle θ , the wavenumber k and the emitter depth z_s satisfy the following relation

$$\sin \theta = (2m - 1) \frac{\pi}{2kz_s}, \quad \text{with } m \in \mathbb{N}^*. \quad (5.5)$$

Similarly, the pressure minima are $|\rho_{\max}| = 0$, and they are reached for

$$\sin \theta = (m - 1) \frac{\pi}{kz_s}, \quad \text{with } m \in \mathbb{N}^*. \quad (5.6)$$

The relations (5.5) and (5.6) yield an interference pattern in the space domain (Figure 5.2). They also yield an interference pattern in the frequency domain, by fixing the angle θ and computing the pressure field for a range of frequencies. In particular, we can associate to each point in space a frequency bandwidth, namely the width between two frequencies corresponding to a minimum pressure. For a given source depth z_s and declination angle θ , the bandwidth Δf is given by

$$\Delta f = \frac{c}{2z_s \sin \theta}. \quad (5.7)$$

Consequently, when recording the pressure at a fixed point and for a moving source (e.g. a landslide), the bandwidth Δf should vary with time. Caplan-Auerbach et al. (2014) present a spectrogram computed from a fixed hydrophone. The spectrogram shows an interference pattern as presented above, with a bandwidth evolving with time. These results suggest that the Lloyd mirror effect could be used to detect underwater landslides.

Remark: Neglecting the interaction with the seabed is a valid assumption when the sound is trapped in the SOFAR channel, or when the seabed is very dissipative. Analytic expressions are also available when taking the interaction with the seabed into account (see Brekhovskikh and Lysanov, 2003).

Name	x (km)	z (km)	Theoretical Δf (Hz)
Emitter (E)	0	0	/
Receiver 1 (R1)	5	0.3	2
Receiver 2 (R2)	8	0.3	3
Receiver 3 (R3)	5	1.35	16
Receiver 4 (R4)	8	1.35	26

Table 5.1: Coordinate of the emitter and the receivers, and the theoretical Δf obtained with Equation (5.7)

5.1.2 Reproducing the Lloyd mirror with static emitters

We reproduce here the interference pattern for a static emitter. We consider the 2D case with coordinates x and z . To illustrate the dependency of the interference bandwidth with the emitter-receiver distance, we fix the emitter location and record the pressure at two different locations.

For the modeling of hydro-acoustic waves, we use the velocity formulation described in Chapter 3: find $\mathbf{U}(t) \in H^1(\Omega)$ solution to

$$\begin{aligned} \frac{d^2}{dt^2} \int_{\Omega} \rho_0 \mathbf{U}(t) \tilde{\mathbf{U}} \, dx + \int_{\Omega} \rho_0 c_0^2 \left(\nabla \cdot \mathbf{U}(t) - \frac{g}{c_0^2} \mathbf{U}(t) \cdot \mathbf{e}_z \right) \left(\nabla \cdot \tilde{\mathbf{U}} - \frac{g}{c_0^2} \tilde{\mathbf{U}} \cdot \mathbf{e}_z \right) \, dx \\ + \int_{\Omega} \rho_0 N^2 \mathbf{U}(t) \cdot \mathbf{e}_z \tilde{\mathbf{U}} \cdot \mathbf{e}_z \, dx + \int_{\Gamma_s} \rho_0 g \mathbf{U}(t) \cdot \mathbf{n} \tilde{\mathbf{U}} \cdot \mathbf{n} \, ds = 0, \quad \forall \tilde{\mathbf{U}} \in H^1(\Omega), \end{aligned} \quad (5.8)$$

satisfying the boundary condition

$$\mathbf{U} \cdot \mathbf{n}_b = u_b, \quad \text{a. e. on } \Gamma_b, \quad \forall t \in [0, T], \quad (5.9)$$

and with vanishing initial conditions. The discretization of the formulation (5.8) is presented in Chapter 3. Note that the z -axis is inverted compared to the previous section: in Section 5.1.1, the z -axis is oriented downwards and the origin $z = 0$ is located on the surface, whereas in the formulation (5.8) the z -axis is oriented upwards with the origin $z = 0$ on the flat seabed. The source term has the form $u_b(x, t) = f(x)g(t)$, where f is a Gaussian function,

$$f(x) = A \exp(-s_x^2 |\mathbf{x} - \mathbf{x}_0|^2), \quad (5.10)$$

and $g(t)$ is a white noise with frequencies ranging from 0 to 20 Hz. The function $g(t)$ is plotted in Figure 5.3. The domain is 2D with coordinates (x, z) ; it is 150 km long and 1.5 km deep. We use the values $A = 1 \text{ m s}^{-1}$, $s_x = 10 \text{ m}^{-1}$ and $\mathbf{x}_0 = (75, 0) \text{ km}$. The coordinates of the receivers are given in Table 5.1.

The spectrograms of the recorded pressure for each receiver are shown in Figure 5.4. For comparison, the spectrogram of the source term is shown in both figures. In the four spectrograms, we see that the frequency ranges from 0 to 20 Hz, which is consistent with the emitter spectrogram. We also see interference figures. For the receivers R1 and R2, the measured bandwidth is approximately 2 Hz. For the receivers R3 and R4, the measured bandwidth is approximately 5 Hz. For the receivers near the surface (R3 and R4), the measured bandwidths do not correspond to the theoretical bandwidths presented in Table 5.1. One reason for this difference could be that the theoretical bandwidth is computed by assuming that the reflection with the seabed are negligible.

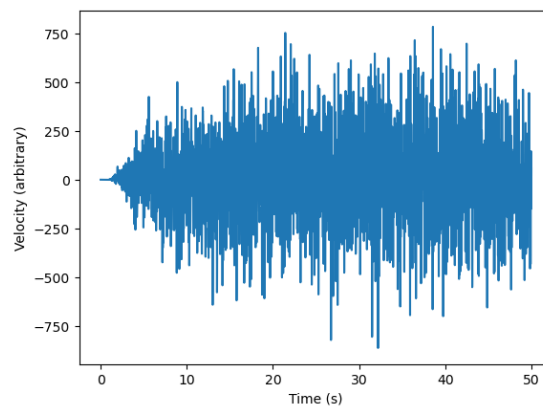


Figure 5.3: The source term

Even though the numerical values do not correspond, we note that the measured bandwidth shares some qualitative properties of the theoretical bandwidth. In particular, the measured bandwidth is larger for the receivers closer to the surface.

5.1.3 Perspectives

With this first experiment, we have shown that the Lloyd mirror can be reproduced in a simple setting. However, the simulation does not show a complete agreement with the theory described by Jensen et al. (2011). One possible explanation could be that different boundary conditions are used for the seabed. It could be useful to investigate whether a theory for other types boundary conditions and non-harmonic sources exists, and compare it with the simulation.

To continue the comparison with the field data presented in the study by Caplan-Auerbach et al. (2014), the same model could be used to simulate a landslide. This will be the subject of a future work.

Finally, the numerical model used to run the simulations can include topography and depth-dependent sound speed. The model could be used to investigate the effects of a topography and a more realistic sound speed profile on the pressure spectrum.

5.2 Wave trapping in the SOFAR channel

In this section, we use the model developed in the thesis to simulate the trapping of acoustic waves in the SOFAR channel.

The SOFAR channel is an open waveguide forming for specific sound speed profiles in the ocean. Sound speed profiles are usually depth-dependent due to the variations of background temperature and pressure in an ocean. For typical temperature profiles, the sound speed presents a minimum around 1 km below the sea surface. Even though the variations are relatively small (around a few percents), this is enough to influence the sound propagation: because of the continuously changing sound speed, rays are refracted and trapped in a channel. This effect is stronger near the sound speed minimum (Jensen et al., 2011; Brekhovskikh and Lysanov, 2003). Rays trapped in this channel interact neither with the surface nor with the seabed. As a result, the energy is much less dissipated, which allows for a propagation over hundreds of kilometers with little energy loss.

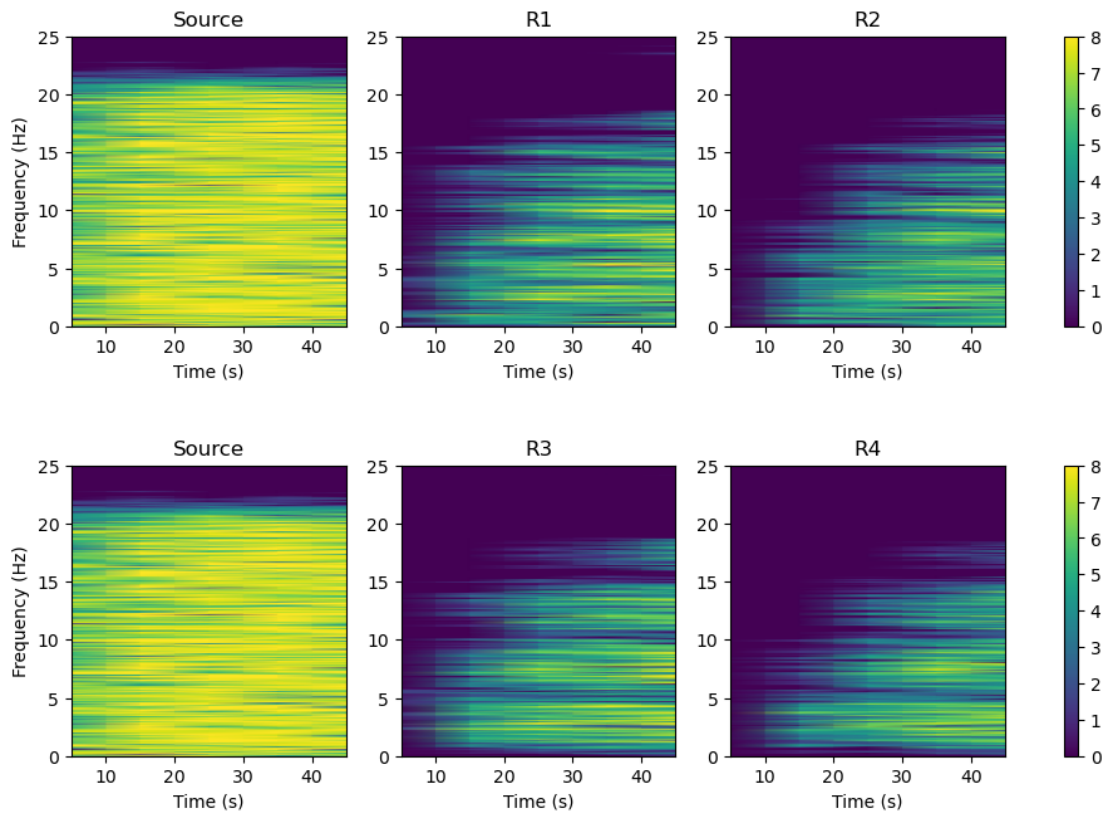


Figure 5.4: Spectrograms for the emitter and for each receiver. The coordinates for each receiver are, in km: $R1=(5,0.3)$; $R2=(8,0.3)$; $R3=(5,1.35)$; $R4=(8,1.35)$.

The channel thus acts as an open waveguide. Its is called SOFAR channel (for SOund Fixing And Ranging) or underwater channel axis.

Johnson et al. (1963) have shown that seismic waves generated by underwater earthquakes or landslides can be converted into hydro-acoustic waves, and propagate in the SOFAR channel. Those waves are called tertiary waves, or T-waves. Several studies suggested that T-waves could add valuable information about underwater seismic events (Ewing et al., 1950; Okal et al., 2003). However, the conversion of seismic waves into T-waves is not fully understood yet. In particular, waves can propagate in the SOFAR channel only if they enter the channel with a relatively low grazing angle, namely the angle between the ray and the channel axis. This condition is hard to satisfy for configurations with a mild topography (Williams et al., 2006; Balanche, 2010). Several models were proposed, and in many of them the role of topography was stressed (De Groot-Hedlin and Orcutt, 1999, 2001).

The ray theory is often used for the study of the SOFAR channel. This theory is valid for high-frequency waves, namely with a wavelength much smaller than the physical scales of the problem (Jensen et al., 2011). However, acoustic waves generated by seismic event can be of relatively low frequency. Another widely used method is the normal mode decomposition: when considering a point source with a harmonic time dependancy, the acoustic pressure field can be obtained as a sum of normal modes (Brekhovskikh and Lysanov, 2003).

In this preliminary work, we present simulations of acoustic waves trapped in the SOFAR channel. The novelty of this work is that it provides illustrations for non point-wise, non-harmonic sources. We show first numerical simulations for a source located inside the channel axis with different sound speed profiles. Those simulations validate the numerical model for the wave trapping. Then, we present a simulation of T-waves. Waves are generated in the ocean near the seabed, and trapped in the SOFAR channel. This simulation also shows the influence of topography on T-wave propagation.

Sound speed profiles. We present two methods for computing the sound speed profile. The first method ensures that all background variables are compatible with the model. Moreover, it allows to freely choose a temperature profile. For the second method, a canonical profile is used.

Following the derivation of the model, the sound speed is computed as $c = (\partial\rho_0/\partial p_0)_{s_0}$, where the background pressure p_0 , density ρ_0 and entropy s_0 are related by an equation of state. We use the reference equation of state given in IAPWS-SR7 (2009). The starting point is the Gibbs function, which is expressed as a function of temperature T and pressure p ,

$$g(T_0, p_0)/g^* = \sum_{j=0}^7 \sum_{k=0}^6 g_{jk} \tau^j \pi^k, \quad \tau = \frac{T_0 - T_{\text{ref}}}{T^*}, \quad \pi = \frac{p_0 - p_{\text{ref}}}{p^*}. \quad (5.11)$$

Numerical values for the coefficients g_{jk} , the references temperatures T_{ref} , T^* and pressures p_{ref} , p^* are given. The density ρ is then expressed as functions of the Gibbs energy g ,

$$\rho(T, p) = \frac{1}{g_p}. \quad (5.12)$$

Moreover, since those variables are background quantities, they should satisfy the static equilibrium,

$$\frac{dp_0}{dz} = -\rho_0 g, \quad p_0(H) = 0. \quad (5.13)$$

Choosing a temperature profile T_0 and combining Equations (5.12) and (5.13) yields an ordinary differential equation for p_0 . The obtained pressure is used with the temperature to compute the

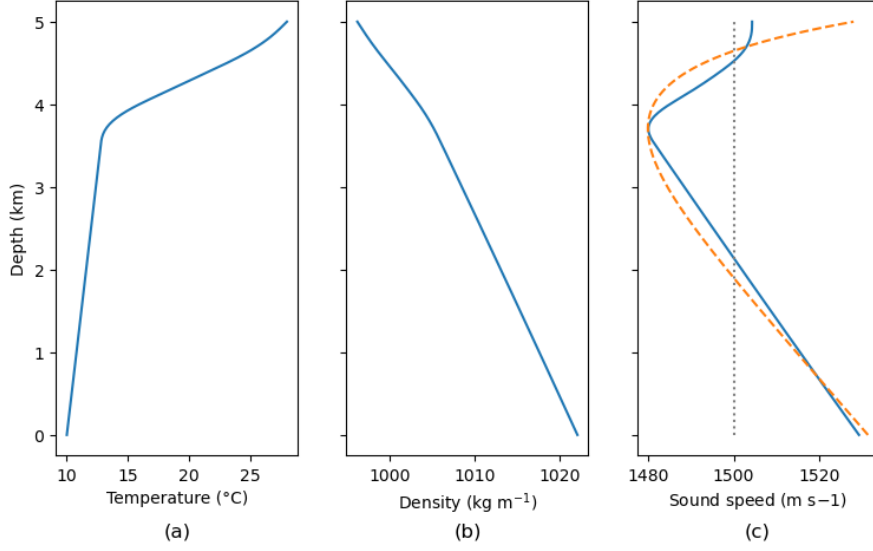


Figure 5.5: Background quantities for a variable temperature: (a) temperature; (b): density; (c): sound speed profiles. In panel (c), the Munk profile is in dashed line, the profile obtained from Equation (5.14) is in continuous line, and the constant profile is in dotted line. Here the vertical axis is oriented upwards, hence 5 km corresponds to the surface, and 0 km to the seabed.

sound speed profile, expressed as a function of the Gibbs energy,

$$c(T, p) = g_p \sqrt{\frac{g_{TT}}{(g_{Tp})^2 - g_{TT} g_{pp}}}. \quad (5.14)$$

Doing so ensures that the background quantity correspond to the static equilibrium used in the model (see Chapter 2). Figure 5.5 shows a typical temperature profile and the corresponding density and sound speed, computed using Equation (5.14).

Another way of computing the sound speed is to use the Munk profile (Munk, 1974; Brekhovskikh and Lysanov, 2003), where the sound speed can be explicitly computed as a function of depth. The expression depends on the minimal sound speed c_{\min} , reached at $z = z_0$, and the effective width of the sound channel B ,

$$c(z) = c_{\min}(1 + \varepsilon(e^\eta - \eta - 1)), \quad \eta = 2 \frac{z - z_0}{B}, \quad \varepsilon = \frac{B}{2} 1.14 \cdot 10^{-5}. \quad (5.15)$$

For example, for a channel axis with a minimum $c_{\min} = 1480 \text{ ms}^{-1}$ at $z_0 = 1.3 \text{ km}$ below the surface and an effective width of $B = 1.3 \text{ km}$, the sound speed profile is

$$c(z) = 1480(1 + \varepsilon(e^\eta - \eta - 1)), \quad \eta = 2 \frac{z - 1300}{1300}, \quad \varepsilon = 0.00737. \quad (5.16)$$

For comparison, both profiles are shown in Figure 5.5-(c). The constant sound speed profile $c \equiv 1500 \text{ ms}^{-1}$ is also plotted. The temperature profile for Equation (5.14) is chosen such that the sound speed has the same minimum and the channel axis is located at the same depth as the Munk profile, computed from Equation (5.16).

5.2.1 Simulation of trapped waves

In this first experiment, we show that the model for acoustic-gravity waves can reproduce the characteristics of the SOFAR channel. To show the effect of the velocity profile, we show results for the three different sound speed profiles shown in Figure 5.5-(c). We use the dual formulation presented in Chapter 3, with a volumic source term of the form $F_\phi = (f_\phi \ 0)^t$,

$$\begin{aligned} \frac{d^2}{dt^2} \int_{\Omega} \frac{\rho_0}{c_0^2} \varphi \tilde{\varphi} \, dx + \frac{d^2}{dt^2} \int_{\Omega} \rho_0 \psi \tilde{\psi} \, dx \\ + \int_{\Omega} \rho_0 \left(-\nabla \varphi + N \left(\psi + \frac{N}{g} \varphi \right) \mathbf{e}_z \right) \left(-\nabla \tilde{\varphi} + N \left(\tilde{\psi} + \frac{N}{g} \tilde{\varphi} \right) \mathbf{e}_z \right) \, dx \\ + \frac{d^2}{dt^2} \int_{\Gamma_s} \frac{\rho_0}{g} \varphi \tilde{\varphi} \, ds + \int_{\Omega} f_\phi \tilde{\varphi} \, dx = 0, \quad \forall \begin{pmatrix} \tilde{\varphi} \\ \tilde{\psi} \end{pmatrix} \in \mathcal{V}. \end{aligned} \quad (5.17)$$

The discretization of the formulation (5.17) is presented in Chapter 3. The pressure field is then computed from the velocity field \mathbf{U} using the equation

$$\frac{\partial p}{\partial t} = -\rho_0 c_0^2 \nabla \cdot \mathbf{U}. \quad (5.18)$$

We plot the acoustic energy \mathcal{E}_p , defined with the acoustic pressure p_a (see Chapter 2),

$$\mathcal{E}_p = \frac{p_a^2}{\rho_0 c_0^2}, \quad \text{with} \quad p_a = p - \nabla p_0 \cdot \mathbf{d} = p + \rho_0 g \mathbf{d} \cdot \mathbf{e}_z. \quad (5.19)$$

For the source term, we choose $f_\phi(x, z, t) = f(x, z)g(t)$, where f is a Gaussian beam with angle θ , and g is a Ricker function,

$$f(x, z) = f_0 \exp(-k(x - x_s)^2) \exp(-k(z - z_s)^2) \cos(2k_\theta \pi (\cos(\theta)x + \sin(\theta)z)), \quad (5.20)$$

$$g(t) = g_0(4s_0^2 t^2 - 2s_0) \exp(-(t - t_0)s_0). \quad (5.21)$$

The frequency k_θ represents the width of the beam. The higher k_θ , the narrower the beam is, and the limit $k_\theta \rightarrow \infty$ corresponds to a perfect ray. However, a higher frequency requires a larger number of degrees of freedoms. In the simulations we use $k = 50 \text{m}^{-2}$, $f_0 = 1 \text{m}^2$, $t_0 = 1.5 \text{s}$, $s_0 = 5 \text{s}^{-2}$, $g_0 = 1 \text{s}$ and $\theta = -0.17 \text{rad}$. The source is located at the sound minimum, namely $x_s = 0$, $z_s = 3.750 \text{km}$. The domain is 2D and rectangular. It is 5 km high, and 45 km long. Since the source is located in the middle to avoid reflections at the boundary, we show only the one half of the domain. We compare the same beam propagating in an ocean with three different speed profiles. The profiles described by Equation (5.14), Equation (5.16) and a constant profile $c \equiv 1500 \text{ms}^{-1}$ are compared. The obtained energy maps are shown in Figure 5.6.

The wave trapping is clearly seen in the energy map for the Munk profile (Figure 5.6-a). The beam is curved and does not reach the bottom. For the two other sound speed profiles, the beam reaches the bottom and is then reflected. The reflection is seen on the narrow bands near the bottom. In the case of the sound speed profile obtained from the temperature (Figure 5.6-b), the beam is curved but not as much as with the Munk profile. Finally, for a constant sound speed (Figure 5.6-c), the same beam is straight and reflects against the bottom. The Munk profile seems more adapted to illustrate the effects of the SOFAR channel.

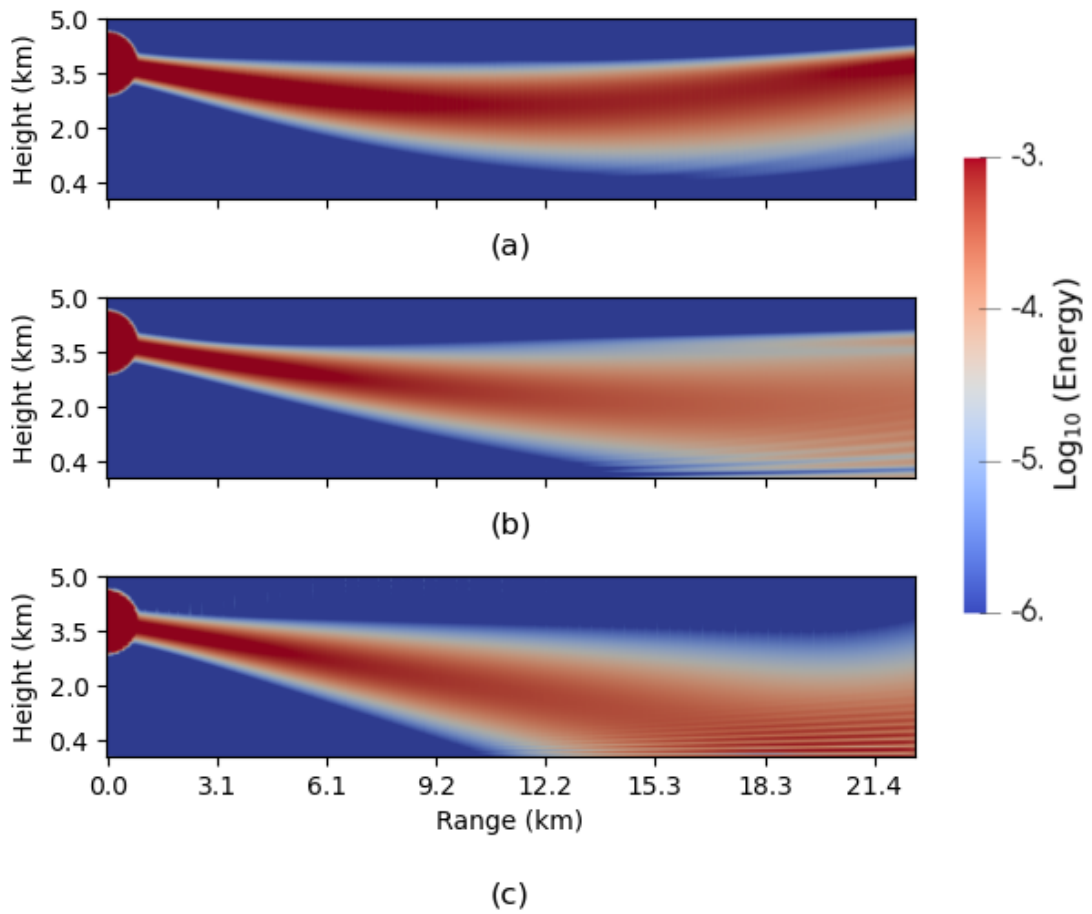


Figure 5.6: Logarithm of the acoustic energy $\log_{10} \mathcal{E}_p$ for different sound speed profiles: (a) with the Munk profile; (b) with the profile $c(p, T)$; (c) with the constant profile $c \equiv 1500 \text{ms}^{-1}$.

5.2.2 T-wave propagation from a beam located near the seabed

In this second experiment, we illustrate the fact that waves generated near the bottom can be trapped in the SOFAR channel. To be trapped in the channel, waves must satisfy two conditions: they should be emitted above a critical depth, and they have to reach the SOFAR axis with a sufficiently low grazing angle (Williams et al., 2006). The critical depth corresponds to the depth z_c such that the sound speed at this depth becomes greater than the sound speed at the surface. For the Munk profile shown in Figure 5.5-(c), the critical depth is $z_c = 0$. Here, we do not consider the conversion mechanism from seismic wave to hydro-acoustic wave, and assume that a hydro-acoustic wave with a low grazing angle is generated near the seabed.

In order for the source term to be above the critical depth, we consider a domain with a topography (see Figure 5.7). The domain has a mild slope (2%). We use the same formulation (5.17) and source term as in the previous section. The source term is described by Equation (5.20)-(5.21). The only difference is that the source is located at $x_s = 45$ km, $z_s = 1.8$ km, see Figure 5.7-(a). The Munk profile is used. For reference, the sound speed profile is plotted in Figure 5.7-(b) with the same z-axis than the domain.

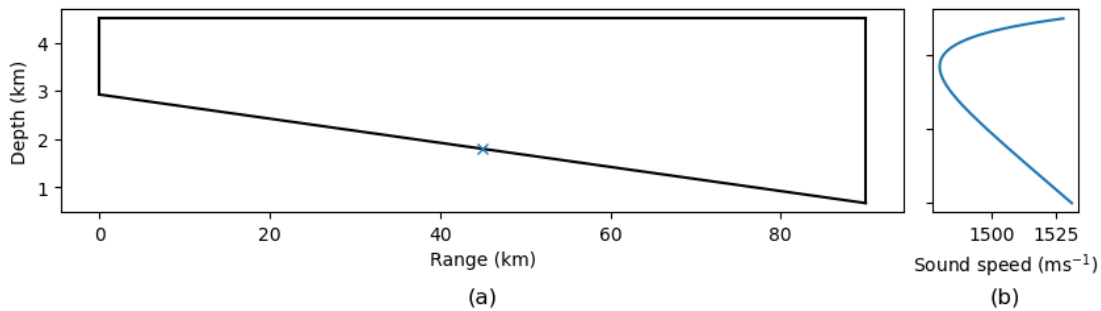


Figure 5.7: Data for the second simulation: (a) the domain; (b) the Munk sound speed profile, obtained from Equation (5.16). In panel (a), the cross indicates the center of the source.

The resulting energy map is shown in Figure 5.8. In the downwards slope, the waves reflect only mildly on the bottom and the surface. On the other hand, for the upwards slope several reflection both on the surface and the bottom can be seen. This simulation illustrates the strong influence of topography on the wave propagation.

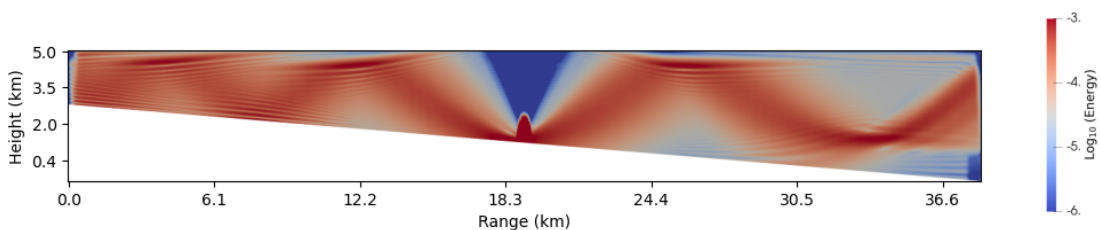


Figure 5.8: Acoustic energy density.

5.2.3 Perspectives

In this section, we have shown that the model can reproduce wave trapping in the SOFAR channel. The numerical model allows for a great variety of source terms. Moreover, the model developed in Chapter 4 provides equations for the coupling with an elastic seabed. Hence, those two models could be used to test the mechanisms proposed in the literature for the generation of T-waves, in particular concerning the conversion of seismic waves into acoustic waves. One of the mechanism that could be tested is the one proposed by Balanche (2010).

5.3 Conclusion and future work

In this chapter, we have presented preliminary results demonstrating the ability of the model developed in the thesis to reproduce simplified test cases for geophysical applications.

It should be noted that the presented model is not well suited for real-life applications: in particular, the 3D computations can become extremely costly. Running 3D simulations of wave propagating over dozens of kilometers would require significant modifications in the implementation, such as using parallel computing and adaptive meshes. Moreover, the derivation of the model assumes only a vertical stratification, which prevents the use of range-dependent parameters.

However, the implementation allows the use of various source terms, sound speed profiles and topography. The numerical model can hence be used to provide illustrations in some simplified (2D and range-independent) cases, which can help for a better understanding of the wave propagation. Moreover, since the model includes the effects of gravity, it can be used to simulate cases where the surface or internal gravity waves are of interest, e.g. for a landslide-generated tsunami.

We intend to continue this preliminary work with further simulations. For the first application, we plan to simulate a landslide and analyze the obtained pressure field. The model could also be used to investigate the influence of topography on the pressure field. For the second application, a possible work would be to use the fully coupled earth-ocean model developed in Chapter 4 to simulate T-waves generation. One possibility would be to test the model proposed by Balanche (2010). However, more information concerning the relevant scales for this application are required.

Perspectives

In this thesis, we have presented two models for the generation and propagation of acoustic and tsunami waves in a stratified, free-surface flow: one for the ocean alone, and one for the coupled earth-ocean system. The theoretical analysis of those models required the use of original formulations, in the first model due to the role of boundary conditions and in the second model due to the effect of a pre-stress. Moreover, the theoretical analysis led to a new formulation for the ocean model. Both models were numerically solved with a spectral element method. With those simulations, the models could be validated against the literature, and new illustration for some geophysical phenomena were obtained. The work presented in this thesis opens the way for several perspectives, both for theoretical and numerical aspects:

- **Influence of usual hypothesis on the propagation of hydro-acoustic waves.** One of the main advantages of the model developed in Chapter 2 is that it was obtained with very few modeling assumptions, hence it keeps many terms representing different physical phenomena. This could be used to quantify the magnitude of some terms usually neglected. For example, we could compute the magnitude of the gravity terms inside the domain. Moreover, the potential-based formulation provides a natural splitting between the rotational and the irrotational parts of the velocity. This decomposition could be used to test the hypothesis of an irrotational flow in different cases, e.g. when there is a bathymetry or when the source term is rotational.
- **Potential-based formulation for the Galbrun equation.** For the transient Galbrun equation, in the particular case of a vanishing mean flow, the potential-based formulation proved to be more advantageous from a computational and a theoretical point of view. This naturally raises the question of the existence of such formulation for the case with a mean flow. Obtaining the potential-based formulation was possible thanks to the symmetry of the problem, and the presence of a mean flow breaks this symmetry. For this reason, a potential-based formulation with a mean flow cannot be directly deduced from the case studied in this thesis, and the existence of such formulation is an open question. Another aspect concerns the harmonic problem, even without mean flow: for the velocity-based formulation, a naive discretization generates spurious modes. Those modes exist because of the lack of H^1 -coercivity for the velocity-based formulation. We have shown that the potential-based formulation is coercive

in $H^1 \times L^2$, hence one could expect that this formulation does not generate spurious modes in the harmonic case. This remains to be tested.

- **The static stress in the earth-ocean model.** The model developed in Chapter 4 has the novelty of taking a static stress in the solid Earth into account. The static stress is written in a very general form, meaning that the model can account for any static stress satisfying only two conditions: it should correspond to a static equilibrium, and for the analysis we require some bound in order to prove well-posedness. The model could then be used to assess the influence of this static stress on seismic waves, hydro-acoustic waves and tsunamis.
- **Geophysical simulations.** The work on geophysical application, presented in Chapter 5 also offers many possible continuations. For the first application, we plan to simulate a landslide and analyze the obtained pressure field. The model could also be used to investigate the influence of topography on the pressure field. For the second application, a possible study would be to use the fully coupled earth-ocean model developed in Chapter 4 to simulate T-waves generation. One possibility would be to test the model proposed by Balanche (2010). However, we would need to know which scales are relevant for this application.

Bibliography

- A. Abdolali, J. T. Kirby, and G. Bellotti. Depth-integrated equation for hydro-acoustic waves with bottom damping. *Journal of Fluid Mechanics*, 766:R1, 2015. ISSN 0022-1120, 1469-7645. doi: 10.1017/jfm.2015.37. URL https://www.cambridge.org/core/product/identifier/S0022112015000373/type/journal_article.
- A. Abdolali, J. T. Kirby, G. Bellotti, S. Grilli, and J. C. Harris. Hydro-Acoustic Wave Generation during the Tohoku-Oki 2011 Earthquake. In *Coastal Structures and Solutions to Coastal Disasters 2015*, pages 24–34, Boston, Massachusetts, July 2017. American Society of Civil Engineers. ISBN 978-0-7844-8031-1. doi: 10.1061/9780784480311.003. URL <http://ascelibrary.org/doi/10.1061/9780784480311.003>.
- A. Abdolali, U. Kadri, and J. T. Kirby. Effect of Water Compressibility, Sea-floor Elasticity, and Field Gravitational Potential on Tsunami Phase Speed. *Scientific Reports*, 9(1):16874, Nov. 2019. ISSN 2045-2322. doi: 10.1038/s41598-019-52475-0. URL <https://www.nature.com/articles/s41598-019-52475-0>.
- L. S. Abrahams, L. Krenz, E. M. Dunham, A.-A. Gabriel, and T. Saito. Comparison of methods for coupled earthquake and tsunami modelling. *Geophysical Journal International*, 234(1):404–426, Feb. 2023. ISSN 0956-540X, 1365-246X. doi: 10.1093/gji/ggad053. URL <https://academic.oup.com/gji/article/234/1/404/7036777>.
- G. Allaire. *Analyse numérique et optimisation, deuxième édition*. Les Éditions de l'École Polytechnique, 2015.
- K. E. Allstadt, R. S. Matoza, A. B. Lockhart, S. C. Moran, J. Caplan-Auerbach, M. M. Haney, W. A. Thelen, and S. D. Malone. Seismic and acoustic signatures of surficial mass movements at volcanoes. *Journal of Volcanology and Geothermal Research*, 364:76–106, Sept. 2018. ISSN 03770273. doi: 10.1016/j.jvolgeores.2018.09.007. URL <https://linkinghub.elsevier.com/retrieve/pii/S0377027317306261>.
- F. Auclair, L. Debreu, E. Duval, M. Hilt, P. Marchesiello, E. Blayo, F. Dumas, and Y. Morel. Theory and analysis of acoustic-gravity waves in a free-surface compressible and stratified ocean.

- Ocean Modelling*, 168:101900, 2021. ISSN 14635003. doi: 10.1016/j.ocemod.2021.101900. URL <https://linkinghub.elsevier.com/retrieve/pii/S1463500321001530>.
- N. Aïssiouene, M.-O. Bristeau, E. Godlewski, A. Mangeney, C. Parés Madroñal, and J. Sainte-Marie. A two-dimensional method for a family of dispersive shallow water models. *The SMAI journal of computational mathematics*, 6:187–226, Sept. 2020. ISSN 2426-8399. doi: 10.5802/smai-jcm.66. URL https://smai-jcm.centre-mersenne.org/item/SMAI-JCM_2020__6__187_0.
- A. Balanche. *Conversion sismo-acoustique au passage du fond océanique*. PhD thesis, Université de Brest, 2010.
- K. Berriri. *Approche analytique et numérique pour l'aéroacoustique en régime transitoire par le modèle de Galbrun*. PhD thesis, Université Paris Dauphine, 2006.
- L. Boittin. *Modeling, analysis and simulation of two geophysical flows*. Thèse de doctorat, Sorbonne Université, Inria, 2019.
- A.-S. Bonnet-Ben Dhia, E.-M. Duclairoir, G. Legendre, and J.-F. Mercier. Time-harmonic acoustic propagation in the presence of a shear flow. *Journal of Computational and Applied Mathematics*, 204(2):428–439, July 2007. ISSN 03770427. doi: 10.1016/j.cam.2006.02.048. URL <https://linkinghub.elsevier.com/retrieve/pii/S0377042706003700>.
- A. S. Bonnet-Bendhia, K. Berriri, and P. Joly. Régularisation de l'équation de Galbrun pour l'aéroacoustique en régime transitoire. *Revue Africaine de Recherche en Informatique et Mathématiques Appliquées*, Volume 5, Special Issue TAM...:1855, Sept. 2006. ISSN 1638-5713. doi: 10.46298/arima.1855. URL <https://arima.episciences.org/1855>.
- J.-P. Brazier. Derivation of an exact energy balance for Galbrun equation in linear acoustics. *Journal of Sound and Vibration*, 330(12):2848–2868, June 2011. ISSN 0022460X. doi: 10.1016/j.jsv.2011.01.009. URL <https://linkinghub.elsevier.com/retrieve/pii/S0022460X11000344>.
- L. M. Brekhovskikh and I. P. Lysanov. *Fundamentals of ocean acoustics*. AIP series in modern acoustics and signal processing. Springer, New York, 3rd ed edition, 2003. ISBN 978-0-387-95467-7.
- F. Brezzi and M. Fortin. *Mixed and hybrid finite element methods*. Number 15 in Springer series in computational mathematics. Springer, New York Berlin Heidelberg, 1991. ISBN 978-1-4612-3172-1 978-0-387-97582-5 978-3-540-97582-3 978-1-4612-7824-5. doi: 10.1007/978-1-4612-3172-1.
- E. E. Brodsky, E. Gordeev, and H. Kanamori. Landslide basal friction as measured by seismic waves: LANDSLIDE BASAL FRICTION. *Geophysical Research Letters*, 30(24), Dec. 2003. ISSN 00948276. doi: 10.1029/2003GL018485. URL <http://doi.wiley.com/10.1029/2003GL018485>.
- J. Caplan-Auerbach, C. G. Fox, and F. K. Duennebier. Hydroacoustic detection of submarine landslides on Kilauea Volcano. *Geophysical Research Letters*, 28(9):1811–1813, 2001. ISSN 00948276. doi: 10.1029/2000GL012545. URL <http://doi.wiley.com/10.1029/2000GL012545>.

- J. Caplan-Auerbach, R. P. Dziak, D. R. Bohnenstiehl, W. W. Chadwick, and T.-K. Lau. Hydroacoustic investigation of submarine landslides at West Mata volcano, Lau Basin: landslides at west mata volcano. *Geophysical Research Letters*, 41(16):5927–5934, Aug. 2014. ISSN 00948276. doi: 10.1002/2014GL060964. URL <http://doi.wiley.com/10.1002/2014GL060964>.
- C. Cecioni, G. Bellotti, A. Romano, A. Abdolali, P. Sammarco, and L. Franco. Tsunami Early Warning System based on Real-time Measurements of Hydro-acoustic Waves. *Procedia Engineering*, 70:311–320, 2014. ISSN 18777058. doi: 10.1016/j.proeng.2014.02.035. URL <https://linkinghub.elsevier.com/retrieve/pii/S187770581400037X>.
- J. Chabassier and M. Duruflé. Solving time-harmonic Galbrun’s equation with an arbitrary flow. Application to Helioseismology. Research Report 9192, 2018.
- F. Chierici, L. Pignagnoli, and D. Embriaco. Modeling of the hydroacoustic signal and tsunami wave generated by seafloor motion including a porous seabed. *Journal of Geophysical Research*, 115(C3):C03015, Mar. 2010. ISSN 0148-0227. doi: 10.1029/2009JC005522. URL <http://doi.wiley.com/10.1029/2009JC005522>.
- Ciarlet. *Mathematical elasticity. Vol. 1 : Three-dimensional elasticity / by Philippe G. Ciarlet*. North-Holland, 1988.
- G. C. Cohen. *Higher-Order Numerical Methods for Transient Wave Equations*. Scientific Computation. Springer Berlin, Heidelberg, 2001.
- A. Constantin. On the propagation of tsunami waves, with emphasis on the tsunami of 2004. *Discrete & Continuous Dynamical Systems - B*, 12(3):525–537, 2009. ISSN 1553-524X. doi: 10.3934/dcdsb.2009.12.525. URL <http://aimsciences.org//article/doi/10.3934/dcdsb.2009.12.525>.
- F. A. Dahlen and J. Tromp. *Theoretical Global Seismology*. Princeton University Press, 1998. ISBN 978-0-691-00124-1. doi: 10.2307/j.ctv131bvfd. URL <http://www.jstor.org/stable/j.ctv131bvfd>.
- R. Dautray and J.-L. Lions. *Mathematical analysis and numerical methods for science and technology. 5: Evolution problems*, volume 5. Springer, Berlin Heidelberg, nachdr. edition, 2000. ISBN 978-3-540-66101-6.
- C. D. De Groot-Hedlin and J. A. Orcutt. Synthesis of earthquake-generated T-waves. *Geophysical Research Letters*, 26(9):1227–1230, May 1999. ISSN 00948276. doi: 10.1029/1999GL900205. URL <http://doi.wiley.com/10.1029/1999GL900205>.
- C. D. De Groot-Hedlin and J. A. Orcutt. Excitation of T -phases by seafloor scattering. *The Journal of the Acoustical Society of America*, 109(5):1944–1954, May 2001. ISSN 0001-4966, 1520-8524. doi: 10.1121/1.1361057. URL <https://pubs.aip.org/jasa/article/109/5/1944/549151/Excitation-of-T-phases-by-seafloor-scattering>.
- M. V. de Hoop, S. Holman, and H. Pham. On the system of elastic-gravitational equations describing the oscillations of the earth, Apr. 2017. URL <http://arxiv.org/abs/1511.03200>. arXiv:1511.03200 [math-ph].
- J. Dubois, S. Imperiale, A. Mangeney, F. Bouchut, and J. Sainte-Marie. Acoustic and gravity waves in the ocean: a new derivation of a linear model from the compressible Euler equation. *Journal of Fluid Mechanics*, 970, 2023. doi: <https://doi.org/10.1017/jfm.2023.595>.

- J. K. Dukowicz. Evaluation of Various Approximations in Atmosphere and Ocean Modeling Based on an Exact Treatment of Gravity Wave Dispersion. *Monthly Weather Review*, 141(12):4487–4506, Dec. 2013. ISSN 0027-0644, 1520-0493. doi: 10.1175/MWR-D-13-00148.1. URL <http://journals.ametsoc.org/doi/10.1175/MWR-D-13-00148.1>.
- D. Dutykh and F. Dias. Water waves generated by a moving bottom. In *Tsunami and Non-linear Waves*, pages 65–95. Springer Berlin Heidelberg, Berlin, Heidelberg, 2007. ISBN 978-3-540-71255-8 978-3-540-71256-5. doi: 10.1007/978-3-540-71256-5_4. URL http://link.springer.com/10.1007/978-3-540-71256-5_4.
- D. Dutykh and F. Dias. Tsunami generation by dynamic displacement of sea bed due to dip-slip faulting. *Mathematics and Computers in Simulation*, 80(4):837–848, Dec. 2009. ISSN 03784754. doi: 10.1016/j.matcom.2009.08.036. URL <https://linkinghub.elsevier.com/retrieve/pii/S0378475409002821>.
- G. Duvaut and J. L. Lions. *Inequalities in Mechanics and Physics*, volume 219 of *Grundlehren der mathematischen Wissenschaften*. Springer Berlin Heidelberg, Berlin, Heidelberg, 1976. ISBN 978-3-642-66167-9 978-3-642-66165-5. doi: 10.1007/978-3-642-66165-5. URL <http://link.springer.com/10.1007/978-3-642-66165-5>.
- L. C. Evans. *Partial Differential Equations*. Graduate Studies in Mathematics. American Mathematical Society (AMS), 2004.
- M. Ewing, I. Tolstoy, and F. Press. Proposed use of the T phase in tsunami warning systems. *Bulletin of the Seismological Society of America*, 40(1):53–58, 1950. ISSN 1943-3573, 0037-1106. doi: 10.1785/BSSA0400010053. URL <https://pubs.geoscienceworld.org/ssa/bssa/article/40/1/53/115600/Proposed-use-of-the-T-phase-in-tsunami-warning>.
- E. Eyov, A. Klar, U. Kadri, and M. Stiasnie. Progressive waves in a compressible-ocean with an elastic bottom. *Wave Motion*, 50(5):929–939, July 2013. ISSN 01652125. doi: 10.1016/j.wavemoti.2013.03.003. URL <https://linkinghub.elsevier.com/retrieve/pii/S016521251300053X>.
- I. A. for the Properties of Water and Steam. IAPWS SR7-09, Supplementary Release on a Computationally Efficient Thermodynamic Formulation for Liquid Water for Oceanographic Use, 2009. URL <http://www.iapws.org/relguide/OceanLiquid.html>.
- J.-F. Gerbeau and B. t. Perthame. Derivation of Viscous Saint-Venant System for Laminar Shallow Water ; Numerical Validation. *HAL*, 2001.
- A. E. Gill. *Atmosphere-ocean dynamics*. International geophysics series. Academic Press, New York, 1982. ISBN 978-0-12-283522-3.
- V. Girault and P.-A. Raviart. *Finite element methods for Navier-Stokes equations: theory and algorithms*. Number 5 in Springer series in computational mathematics. Springer, Berlin Heidelberg, 1. ed. 1986. edition, 1986. ISBN 978-3-540-15796-0 978-3-642-64888-5 978-0-387-15796-2. doi: 10.1007/978-3-642-64888-5.
- O. A. Godin. An exact wave equation for sound in inhomogeneous, moving, and non-stationary fluids. In *OCEANS'11 MTS/IEEE KONA*, pages 1–5, Waikoloa, HI, Sept. 2011. IEEE. ISBN 978-1-4577-1427-6 978-0-933957-39-8. doi: 10.23919/OCEANS.2011.6106920. URL <http://ieeexplore.ieee.org/document/6106920/>.

- E. Godlewski, M. Olazabal, and P.-A. Raviart. On the linearization of systems of conservation laws for fluids at a material contact discontinuity. *Journal de Mathématiques Pures et Appliquées*, 78(10):1013–1042, 1999. ISSN 00217824. doi: 10.1016/S0021-7824(99)00136-1. URL <https://linkinghub.elsevier.com/retrieve/pii/S0021782499001361>.
- B. Gomez and U. Kadri. Near real-time calculation of submarine fault properties using an inverse model of acoustic signals. *Applied Ocean Research*, 109:102557, 2021. ISSN 01411187. doi: 10.1016/j.apor.2021.102557. URL <https://linkinghub.elsevier.com/retrieve/pii/S0141118721000341>.
- G. Grubb. *Distributions and operators*. Number 252 in Graduate texts in mathematics. Springer, New York, 2009. ISBN 978-0-387-84894-5. OCLC: ocn258078542.
- E. Guyon, editor. *Physical hydrodynamics*. Oxford University Press, Oxford ; New York, 2001. ISBN 978-0-19-851746-7 978-0-19-851745-0. OCLC: ocm47048231.
- C. Hibert, A. Mangeney, G. Grandjean, and N. M. Shapiro. Slope instabilities in Dolomieu crater, Réunion Island: From seismic signals to rockfall characteristics. *Journal of Geophysical Research*, 116(F4):F04032, Dec. 2011. ISSN 0148-0227. doi: 10.1029/2011JF002038. URL <http://doi.wiley.com/10.1029/2011JF002038>.
- L. Hägg and M. Berggren. On the well-posedness of Galbrun’s equation. *Journal de Mathématiques Pures et Appliquées*, 150:112–133, 2021. ISSN 00217824. doi: 10.1016/j.matpur.2021.04.004. URL <https://linkinghub.elsevier.com/retrieve/pii/S0021782421000593>.
- F. B. Jensen, W. A. Kuperman, M. B. Porter, and H. Schmidt. *Computational Ocean Acoustics*. Springer New York, New York, NY, 2011. ISBN 978-1-4419-8677-1 978-1-4419-8678-8. doi: 10.1007/978-1-4419-8678-8. URL <http://link.springer.com/10.1007/978-1-4419-8678-8>.
- R. H. Johnson, J. Northrop, and R. Eppley. Sources of Pacific *T* phases. *Journal of Geophysical Research*, 68(14):4251–4260, July 1963. ISSN 01480227. doi: 10.1029/JZ068i014p04251. URL <http://doi.wiley.com/10.1029/JZ068i014p04251>.
- P. Joly, C. Tsogka, G. Derveaux, and J. Rodriguez. *Effective Computational Methods for Wave Propagation, Part. 3 Numerical Methods for Elastic Wave Propagation*. Chapman and Hall/CRC, 1 edition, 2008.
- U. Kadri and M. Stiassnie. Generation of an acoustic-gravity wave by two gravity waves, and their subsequent mutual interaction. *Journal of Fluid Mechanics*, 735:R6, Nov. 2013. ISSN 0022-1120, 1469-7645. doi: 10.1017/jfm.2013.539. URL https://www.cambridge.org/core/product/identifier/S0022112013005399/type/journal_article.
- K. Kajiura. The leading wave of a tsunami. *Bulletin of the Earthquake Research Institute*, 41: 535–571, 1963.
- B. King, M. Stone, H. P. Zhang, T. Gerkema, M. Marder, R. B. Scott, and H. L. Swinney. Buoyancy frequency profiles and internal semidiurnal tide turning depths in the oceans. *Journal of Geophysical Research: Oceans*, 117, 2012. ISSN 01480227. doi: 10.1029/2011JC007681. URL <http://doi.wiley.com/10.1029/2011JC007681>.

- D. Komatitsch and J. Tromp. Introduction to the spectral element method for three-dimensional seismic wave propagation. *Geophysical Journal International*, 139(3):806–822, Dec. 1999. ISSN 0956540X, 1365246X. doi: 10.1046/j.1365-246x.1999.00967.x. URL <https://academic.oup.com/gji/article/139/3/806/587264>.
- D. Komatitsch and J.-P. Vilotte. The spectral element method: An efficient tool to simulate the seismic response of 2D and 3D geological structures. *Bulletin of the Seismological Society of America*, 88(2):368–392, Apr. 1998. ISSN 1943-3573, 0037-1106. doi: 10.1785/BSSA0880020368. URL <https://pubs.geoscienceworld.org/bssa/article/88/2/368/120304/The-spectral-element-method-An-efficient-tool-to>.
- L. Krenz, L. S. Abrahams, E. M. Dunham, C. Uphoff, T. Ulrich, A.-A. Gabriel, and M. Bader. 3D Acoustic-Elastic Coupling with Gravity: The Dynamics of the 2018 Palu, Sulawesi Earthquake and Tsunami. In *Proceedings of the International Conference for High Performance Computing, Networking, Storage and Analysis*, volume 63, page 14. Association for Computing Machinery, 2021. ISBN 978-1-4503-8442-1. doi: 10.1145/3458817.3476173.
- J. Kuehnert, A. Mangeney, Y. Capdeville, J. P. Métaxian, L. F. Bonilla, E. Stutzmann, E. Chaljub, P. Boissier, C. Brunet, P. Kowalski, F. Lauret, and C. Hibert. Simulation of Topography Effects on Rockfall-Generated Seismic Signals: Application to Piton de la Fournaise Volcano. *Journal of Geophysical Research: Solid Earth*, 125(10), Oct. 2020. ISSN 2169-9313, 2169-9356. doi: 10.1029/2020JB019874. URL <https://onlinelibrary.wiley.com/doi/10.1029/2020JB019874>.
- D. Lannes. *The water waves problem: mathematical analysis and asymptotics*. Number volume 188 in Mathematical surveys and monographs. American Mathematical Society, Providence, Rhode Island, 2013. ISBN 978-0-8218-9470-5.
- G. Legendre. *Rayonnement acoustique dans un fluide en écoulement: analyse mathématique et numérique de l'équation de Galbrun*. PhD thesis, Paris VI, 2003.
- J. Lighthill. *Waves in fluids*. Cambridge University Press, 1978.
- J. L. Lions and E. Magenes. *Non-Homogeneous Boundary Value Problems and Applications*. Springer Berlin Heidelberg, Berlin, Heidelberg, 1972. ISBN 978-3-642-65219-6 978-3-642-65217-2. doi: 10.1007/978-3-642-65217-2. URL <http://link.springer.com/10.1007/978-3-642-65217-2>.
- M. S. Longuet-Higgins. A Theory of the Origin of Microseisms. *Philosophical Transactions of the Royal Society of London. Series A, Mathematical and Physical Sciences*, 243(857):1–35, 1950. URL <http://www.jstor.org/stable/91470>.
- G. C. Lotto and E. M. Dunham. High-order finite difference modeling of tsunami generation in a compressible ocean from offshore earthquakes. *Computational Geosciences*, 19(2):327–340, 2015. ISSN 1420-0597, 1573-1499. doi: 10.1007/s10596-015-9472-0. URL <http://link.springer.com/10.1007/s10596-015-9472-0>.
- G. C. Lotto, T. N. Jeppson, and E. M. Dunham. Fully Coupled Simulations of Megathrust Earthquakes and Tsunamis in the Japan Trench, Nankai Trough, and Cascadia Subduction Zone. *Pure and Applied Geophysics*, 176(9):4009–4041, Sept. 2019. ISSN 0033-4553, 1420-9136. doi: 10.1007/s00024-018-1990-y. URL <http://link.springer.com/10.1007/s00024-018-1990-y>.

- T. Maeda and T. Furumura. FDM Simulation of Seismic Waves, Ocean Acoustic Waves, and Tsunamis Based on Tsunami-Coupled Equations of Motion. *Pure and Applied Geophysics*, 170 (1-2):109–127, Jan. 2013. ISSN 0033-4553, 1420-9136. doi: 10.1007/s00024-011-0430-z. URL <http://link.springer.com/10.1007/s00024-011-0430-z>.
- M. Maeder, G. Gabard, and S. Marburg. 90 Years of Galbrun's Equation: An Unusual Formulation for Aeroacoustics and Hydroacoustics in Terms of the Lagrangian Displacement. *Journal of Theoretical and Computational Acoustics*, 28(04):2050017, Dec. 2020. ISSN 2591-7285, 2591-7811. doi: 10.1142/S2591728520500176. URL <https://www.worldscientific.com/doi/abs/10.1142/S2591728520500176>.
- H. Matsumoto, S. Inoue, T. Ohmachi, Japan Agency for Marine-Earth Science and Technology, 2-15 Natsushima, Yokosuka 237-0061, Japan, Takenaka Research and Development Institute, 1-5-1 Ohtsuka, Inzai, Chiba 270-1395, Japan, and Japan Dam Engineering Center, Nissyoku Bld., 2-9-7 Ikenohata, Taito, Tokyo 110-0008, Japan. Dynamic Response of Bottom Water Pressure due to the 2011 Tohoku Earthquake. *Journal of Disaster Research*, 7(sp):468–475, Aug. 2012. ISSN 1883-8030, 1881-2473. doi: 10.20965/jdr.2012.p0468. URL <https://www.fujipress.jp/jdr/dr/dsstr000700070468>.
- L. Moretti, A. Mangeny, Y. Capdeville, E. Stutzmann, C. Huggel, D. Schneider, and F. Bouchut. Numerical modeling of the Mount Steller landslide flow history and of the generated long period seismic waves: LANDQUAKE MODELING. *Geophysical Research Letters*, 39(16):n/a–n/a, Aug. 2012. ISSN 00948276. doi: 10.1029/2012GL052511. URL <http://doi.wiley.com/10.1029/2012GL052511>.
- W. H. Munk. Sound channel in an exponentially stratified ocean, with application to SOFAR. *The Journal of the Acoustical Society of America*, 55(2):220–226, Feb. 1974. ISSN 0001-4966, 1520-8524. doi: 10.1121/1.1914492. URL <https://pubs.aip.org/jasa/article/55/2/220/686823/Sound-channel-in-an-exponentially-stratified-ocean>.
- M. Nosov. Tsunami generation in compressible ocean. *Physics and Chemistry of the Earth, Part B: Hydrology, Oceans and Atmosphere*, 24(5):437–441, 1999. ISSN 14641909. doi: 10.1016/S1464-1909(99)00025-8. URL <https://linkinghub.elsevier.com/retrieve/pii/S1464190999000258>.
- M. A. Nosov and S. V. Kolesov. Elastic oscillations of water column in the 2003 Tokachi-oki tsunami source: in-situ measurements and 3-D numerical modelling. *Natural Hazards and Earth System Sciences*, 7(2):243–249, 2007. ISSN 1684-9981. doi: 10.5194/nhess-7-243-2007. URL <https://nhess.copernicus.org/articles/7/243/2007/>.
- F. Noguier, B. Chapron, and C.-A. Guérin. Second-order Lagrangian description of tri-dimensional gravity wave interactions. *Journal of Fluid Mechanics*, 772:165–196, 2015. ISSN 0022-1120, 1469-7645. doi: 10.1017/jfm.2015.179. URL https://www.cambridge.org/core/product/identifier/S0022112015001792/type/journal_article.
- E. A. Okal, P.-J. Alasset, O. Hyvernaud, and F. Schindele. The deficient T waves of tsunami earthquakes. *Geophysical Journal International*, 152(2):416–432, 2003.
- G. Richard, K. Msheik, and A. Duran. A preliminary depth-integrated model for tsunamis propagation including water compressibility and seafloor elasticity. *European Journal of Mechanics -*

- B/Fluids*, 99:84–97, May 2023. ISSN 09977546. doi: 10.1016/j.euromechflu.2023.01.004. URL <https://linkinghub.elsevier.com/retrieve/pii/S0997754623000110>.
- T. Saito. *Tsunami Generation and Propagation*. Springer Geophysics. Springer Japan, Tokyo, 2019. ISBN 978-4-431-56848-3 978-4-431-56850-6. doi: 10.1007/978-4-431-56850-6. URL <http://link.springer.com/10.1007/978-4-431-56850-6>.
- T. Saito and H. Tsushima. Synthesizing ocean bottom pressure records including seismic wave and tsunami contributions: Toward realistic tests of monitoring systems. *Journal of Geophysical Research: Solid Earth*, 121(11):8175–8195, Nov. 2016. ISSN 2169-9313, 2169-9356. doi: 10.1002/2016JB013195. URL <https://onlinelibrary.wiley.com/doi/10.1002/2016JB013195>.
- P. Sammarco, C. Cecioni, G. Bellotti, and A. Abdolali. Depth-integrated equation for large-scale modelling of low-frequency hydroacoustic waves. *Journal of Fluid Mechanics*, 722:R6, 2013. ISSN 0022-1120, 1469-7645. doi: 10.1017/jfm.2013.153. URL https://www.cambridge.org/core/product/identifier/S0022112013001535/type/journal_article.
- M. Shams, M. Destrade, and R. W. Ogden. Initial stresses in elastic solids: Constitutive laws and acoustoelasticity. *Wave Motion*, 48(7):552–567, Nov. 2011. ISSN 01652125. doi: 10.1016/j.wavemoti.2011.04.004. URL <http://arxiv.org/abs/1302.1961>. arXiv:1302.1961 [cond-mat].
- J. A. Smith. Revisiting Oceanic Acoustic Gravity Surface Waves. *Journal of Physical Oceanography*, 45(12):2953–2958, 2015. ISSN 0022-3670, 1520-0485. doi: 10.1175/JPO-D-14-0256.1. URL <https://journals.ametsoc.org/view/journals/phoc/45/12/jpo-d-14-0256.1.xml>.
- M. Stiassnie. Tsunamis and acoustic-gravity waves from underwater earthquakes. *Journal of Engineering Mathematics*, 67(1-2):23–32, 2010. ISSN 0022-0833, 1573-2703. doi: 10.1007/s10665-009-9323-x. URL <http://link.springer.com/10.1007/s10665-009-9323-x>.
- E. Stutzmann, F. Ardhuin, M. Schimmel, A. Mangeney, and G. Patau. Modelling long-term seismic noise in various environments: *Modelling seismic noise*. *Geophysical Journal International*, 191(2):707–722, Nov. 2012. ISSN 0956540X. doi: 10.1111/j.1365-246X.2012.05638.x. URL <https://academic.oup.com/gji/article-lookup/doi/10.1111/j.1365-246X.2012.05638.x>.
- I. Tolstoy. The T Phase of Shallow-Focus Earthquakes. *Bulletin of the Seismological Society of America 1950*, 40(1):25–51, 1950.
- B. Valette. About the influence of pre-stress upon adiabatic perturbations of the Earth. *Geophysical Journal International*, 85(1):179–208, Apr. 1986. ISSN 0956-540X, 1365-246X. doi: 10.1111/j.1365-246X.1986.tb05177.x. URL <https://academic.oup.com/gji/article-lookup/doi/10.1111/j.1365-246X.1986.tb05177.x>.
- S. Watada. Tsunami speed variations in density-stratified compressible global oceans. *Geophysical Research Letters*, 40(15):4001–4006, Aug. 2013. ISSN 0094-8276, 1944-8007. doi: 10.1002/grl.50785. URL <https://onlinelibrary.wiley.com/doi/10.1002/grl.50785>.
- C. M. Williams, R. A. Stephen, and D. K. Smith. Hydroacoustic events located at the intersection of the Atlantis (30°N) and Kane (23°40'N) Transform Faults with the Mid-Atlantic Ridge: HYDROACOUSTIC EVENTS AT THE MAR. *Geochemistry, Geophysics, Geosystems*, 7(6):n/a–n/a, June 2006. ISSN 15252027. doi: 10.1029/2005GC001127. URL <http://doi.wiley.com/10.1029/2005GC001127>.

- M. Yamada, A. Mangeney, Y. Matsushi, and T. Matsuzawa. Estimation of dynamic friction and movement history of large landslides. *Landslides*, 15(10):1963–1974, Oct. 2018. ISSN 1612-510X, 1612-5118. doi: 10.1007/s10346-018-1002-4. URL <http://link.springer.com/10.1007/s10346-018-1002-4>.
- T. Yamamoto. Gravity waves and acoustic waves generated by submarine earthquakes. *International Journal of Soil Dynamics and Earthquake Engineering*, 1(2):75–82, 1982. ISSN 02617277. doi: 10.1016/0261-7277(82)90016-X. URL <https://linkinghub.elsevier.com/retrieve/pii/026172778290016X>.

Vagues et ondes hydro-acoustiques pour l'alerte précoce de tsunami : modélisation, analyse et simulation

Résumé

L'objectif de cette thèse est de proposer des modèles décrivant la génération et la propagation des ondes acoustiques et des ondes de tsunami générées par les mouvements du fond marin. Lors d'un tremblement de terre sous-marin générant un tsunami, les ondes acoustiques qui se propagent dans l'eau peuvent être considérées comme un précurseur du tsunami. L'étude de ces ondes acoustiques peut donc permettre d'améliorer les systèmes d'alerte précoce aux tsunamis. Nous commençons par un chapitre introductif décrivant l'état de l'art sur le sujet, ainsi que les principales notions qui seront abordées. Nous présentons ensuite un modèle permettant de décrire la propagation des ondes acoustiques et des ondes de gravité dans un fluide à surface libre. Les propriétés mathématiques du modèle sont ensuite étudiées, et une discrétisation par la méthode des éléments finis spectraux est proposée. En particulier, nous montrons que le même modèle physique peut être décrit à l'aide d'un autre système d'équations portant sur une nouvelle variable. Afin de mieux décrire les interactions des ondes avec le fond marin, le modèle est ensuite étendu pour étudier un système fluide-solide. Pour cette extension, nous présentons son étude mathématique ainsi qu'une simulation. Enfin, nous utilisons les équations développées au cours des précédents chapitres pour simuler des cas-tests appliqués à la géophysique.

Mots clés : Modélisation, analyse, simulation, fluide à surface libre, ondes acoustiques

Acoustic-gravity waves in free-surface flows: modeling, analysis and simulation towards tsunami early-warning systems

Abstract

The aim of the present thesis is to propose models describing the generation and propagation of acoustic and tsunami waves generated by movements of the seabed. In the event of an underwater earthquake generating a tsunami, acoustic waves propagating in water can be seen as a precursor of the tsunami wave. The study of these acoustic waves can therefore lead to improvements of tsunami early-warning systems. We start with an introductory chapter describing the state of the art on the subject, as well as the main concepts to be covered. Then, we present a model describing the propagation of acoustic-gravity waves in a free-surface flow. The mathematical properties of the model are then studied, and a discretization based on the spectral finite elements method is proposed. In particular, we show that the same physical model can be described by an alternative system of equations written for a new variable. In order to describe more accurately the ocean interaction with the seabed, the model is then extended so as to study a fluid-solid system. We present the mathematical study and the discretization of this new model. Finally, the equations that were introduced throughout the previous chapters are used to simulate test-cases with application to geophysics.

Keywords: Modeling, analysis, simulation, free-surface flow, acoustic waves
